UNIVERSITY OF CALIFORNIA,
IRVINE

Reconstructing rainfall variability in Northeast Mexico in the late-Pleistocene and Holocene using multiple speleothem geochemical proxies

DISSERTATION

Submitted in partial satisfaction of the requirements for the degree of

DOCTOR OF PHILOSOPHY

in Earth System Science

by
Kevin Timothy Wright

Dissertation Committee:
Prof. Kathleen Johnson (chair)
Prof. Claudia I. Czimczik
Prof. Jin-Yi Yu

2021

DEDICATION

To my father Randall Wright

Your words "Up and at em' son"

continued to serve as motivation and encouragement.

Thank you for always believing in me.

To my mother Patricia Tansey-Wright,

Thank you for always reminding me to

"Work hard, try your best, and don't worry about the rest"

Who knew helping me study at the kitchen table for a 2nd grade French spelling test,

would end up shaping my life philosophy.

To my wife Lindsay Wright,

Thank you for always supporting my lofty endeavors and having unreasonable faith in me.

I can't say the "long con" will ever end, but hope is on the horizon!

To my sister Christina Wright-Yee,

Thank you for always being my biggest source of inspiration,

But, as your little brother,

Good luck trying to get me to say these words out loud.

TABLE OF CONTENTS

LIST OF FIGURES

LIST OF TABLES

ACKNOWLEDGEMENTS

I would like to thank my beautiful wife, Lindsay Wright, for her incredible support, affection, and love throughout this process. I am incredibly grateful for your patience and care as we've traversed the perils of the PhD together. Thank you for bringing Penny into our lives, although she was quite a handful as a puppy, she always softens a bad day. I don't know what the future holds for us, but I'm so happy to embark on the next adventure with you both. Love you, babe.

I would like to thank my father, Dr. Randall Wright, who unfortunately passed away shortly before I began the PhD. Your courage, tenacity, and grace continue to inspire and motivate me. It's been an honor to share this journey in life with you.

I would like to thank my mother, Patricia Tansey-Wright, for your love and support. Thank you for always lending an ear for me to vent and for providing a haven from PhD life.

I would like to thank my sister and brother in-law, Christina Wright-Yee and Darrin Yee, for the humor and free food they have provided me with over the last ~ 5 years. Christina you can finally stop teasing me now, I will have a 'd' in my credentials!

I would like to thank my friends Ginger & Zack Martin, Austin Gardner, Dominic Amara, Louis Penna, Gabi Serrato Marks, Dillon Elsbury, Shawn Pedron and Zack Wolff. Thanks for the good times and the equally bad hangovers.

I would like to thank my official and unofficial mentors Dr. Peter Weber, Dr. Christopher Wood and Dr. Jessica Wang for their guidance.

Lastly, I would like to thank my advisor, Professor Kathleen Johnson, who has helped me immensely grow on both a professional and personal level. I immensely appreciated not only your guidance, advice, and expertise, but your philosophical approach to science, teaching, and mentorship. Thanks for putting up with me.

CURRICULUM VITA

Kevin Timothy Wright

EDUCATION

- **PhD, Earth System Science** — **University of California, Irvine, USA** — **2021**
- **MS, Earth System Science** — **University of California, Irvine, USA** — **2019**
- **BS, Geology** — **California State University, Bakersfield, USA** — **2016**
- **BA, Anthropology** — **University of California, Berkeley, USA** — **2013**

RESEARCH EXPERIENCE

Graduate Research Assistant 2016-*Present*
Department of Earth System Science, University of California – Irvine
Advisor: Kathleen Johnson
Caves, Climate and (Geo) Chemistry: Reconstructing past rainfall in Northern Mexico over the Holocene and Late-Pleistocene using stable isotopes and trace metals

Graduate Research Fellow 2019-*Present*
Nuclear and Chemical Sciences Division, Lawrence Livermore National Laboratory
Advisor: Peter Weber
Seasonal to sub-seasonal paleoclimate reconstruction using NanoSIMS and laser ablation inductively coupled plasma mass spectrometry (LA-ICP-MS)

Undergraduate Research Assistant 2016
Department of Geology, California State University – Bakersfield
Advisor: David Miller
Cenozoic evolution of the San Joaquin Basin, Bakersfield, California

PUBLICATIONS

Kevin T. Wright, Kathleen R. Johnson, Tripti Bhattacharya, Gabriela Serrato Marks, David McGee, Dillon Elsbury, Yannick Peings, Jean-Louis Lacaille-Muzquiz, Gianna Lum, Laura Beramendi-Orosco. *Northeast Mexico precipitation primarily controlled by Atlantic SSTs.* Science (*Submitted*).

Kevin T. Wright, Kathleen R. Johnson, Gabriela Serrato Marks, David McGee, Tripti Bhattacharya, Gregory R. Goldsmith, Clay R. Tabor, Jean-Louis Lacaille-Muzquiz, Gianna Lum, Laura Beramendi-Orosco. *Thermodynamics control prcipitation in NE Mexico on orbital to millennial timescales.* Nature Communications (*In Review*).

Kevin T. Wright, Kathleen R. Johnson, Gabriela Serrato Marks, David McGee, Tripti Bhattacharya, Gregory R. Goldsmith, Clay R. Tabor, Jean-Louis Lacaille-Muzquiz, Gianna Lum, Laura Beramendi-Orosco. *Determining the sensitivity of Cueva Bonita to record overlying hydrological changes* (*In Prep*).

PRESENTATIONS

Wright, K., Serrato-Marks, G., Johnson, K., McGee, D., Bhattacharya, T., Beramendi-Orosco, L., Lacaille-Múzquiz, JL., *Uncovering Spatial Patterns and Drivers of Droughts in NE Mexico with a New Stalagmite Record of the Last Millennium.* American Geophysical Union. Poster Presentation.

Wright, K., Serrato-Marks, G., Johnson, K., McGee, D., Bhattacharya, T., Beramendi-Orosco, L., Lacaille-Múzquiz, JL., *Mexico Precipitation Forced by the Atlantic or the Pacific?* Karst Record 9 (Summer 2020). Oral Presentation. – Cancelled due to COVID

Wood, C., Johnson, K., Lewis, L., Mason, A., **Wright, K.**, Wang, J., Griffiths, M., Borsato, A., Hig*h Resolution, Multiproxy Speleothem Record of the 8.2kya Event from Mainland Southeast Asia.* Karst Record 9 (Summer 2020). Oral Presentation. – Cancelled due to COVID

Wright, K., Serrato-Marks, G., Johnson, K., McGee, D., Bhattacharya, T., Goldsmith, G., *Did the Pacific Storm Track Reach Northeast Mexico During the Last Glacial Maximum?* Geological Society of America Cordilleran Section (Spring 2020). Oral presentation. – Cancelled due to COVID

Johnson, K., McCabe-Glynn, S., Cheng, H., **Wright, K.**, Coreas, C., White, A., *California Hydroclimate Variability Since the Last Glacial Maximum: Preliminary Stalagmite Results from Crystal Cave, Sequoia National Park, California*. Geological Society of America Cordilleran Section (Spring 2020). Oral presentation. – Cancelled due to COVID

Wright, K., Serrato-Marks, G., Johnson, K., McGee, D., Bhattacharya, T., Beramendi-Orosco, L., Lacaille-Múzquiz, JL., *What are the Dominant Drivers of Precipitation Change in NE Mexico? A 60,000 Year Precipitation Record Reconstructed through Multiple Speleothem Proxies*. American Geophysical Union (Fall 2019). Oral presentation.

Serrato-Marks, G., **Wright, K**., Johnson, K., McGee, D., Bhattacharya, T., Beramendi-Orosco, L., Lacaille-Múzquiz, JL., *Stalagmite records of northeast Mexican Hydroclimate in the first millennium of the Common Era.,* American Geophysical Union (Fall 2019). Oral Presentation.

Wright, K., Serrato-Marks, G., Johnson, K., McGee, D., Bhattacharya, T., Beramendi-Orosco, L., Lacaille-Múzquiz, JL., *Drying in NE Mexico in response to Heinrich Events inferred from a multi-proxy speleothem record.* Goldschmidt (Summer 2019). Poster Presentation.

Wright, K., Johnson, K., Lum, G., *Caves and Climate: Reconstructing the climate history of northeast Mexico through a geochemical analysis of cave deposits.* Environmental Research Symposium (Spring 2018). Poster presentation. -Awarded for best presentation

Wright, K., *Speleothem Reconstruction of Late-Pleistocene Holocene Precipitation in NE Mexico.* Summer Speleothem Summer School, Burgos, Spain (August 2017). Poster presentation. -Awarded for best presentation

Wright, K., History of Native American Archaeology. *Cal Day,* Berkeley, CA (Spring 2013). Oral presentation.

TEACHING EXPERIENCE

Graduate Student Instructor Assistant 2016-2019

- Earth System Science 1: Introduction to Earth Science
- Earth System Science 3: Oceanography
- Earth System Science 7: Physical Geology
- Earth System Science 21: On Thin Ice: Climate Change and the Cryosphere
- Earth System Science 132: Terrestrial Hydrology
- Earth System Science 134: Fundamentals of GIS in Environmental Sciences

SERVICE

Member of UCI's Climate, Literacy, Empowerment and iNquiry *2016-2020*
University of California, Irvine

Planning Committee for Summer Speleothem Science School (S4) *2017 – 2019*
Babesh-Boyai University, Cluj, Romania

Graduate and undergraduate student mentor *2018 - 2021*
University of California, Irvine

HONORS/AWARDS

UC Laboratory Research Fees, In-Residence Graduate Fellowship – $200,000 USD

Outstanding Contribution to the Earth System Science Department

NSF Graduate Research Fellowship Program Honorable Mention

Geological Society of America Graduate Student Grant - $2000 USD

L. Austin Weeks Undergraduate Grant Program - American Association of Petroleum Geologists

"Outstanding Geoscientist Student" -San Joaquin Geological Society/Pacific Section of the American

Victor & Virginia Church Scholarship for scoring highest in structural geology (1/50) – CSU Bakersfield

TECHNICAL SKILLS

Programming

- Python — statistical analysis, data visualization, time series analysis, climate data analysis
- R — comparison of time-series data sets and correcting for auto-correlation
- Matlab — age-depth modelling software
- NCL — manipulation of netcdf files
- ArcGIS — geospatial analysis, gridded datasets

Instrumentation

- Cameca NanoSIMS 50L
- Nu Instruments Attom High Resolution Inductively Coupled Mass Spectrometry
- Thermo Fisher Scientific Kiel Carbonate Device
- Thermo Fisher Scientific IV Isotope Ratio Mass Spectrometer
- Thermo Scientific Laser-Ablation Inductively Coupled Plasma Mass Spectrometer

ABSTRACT OF THE DISSERTATION

Reconstructing rainfall variability in Northeast Mexico in the late-Pleistocene and Holocene using multiple speleothem geochemical proxies

by

Kevin Timothy Wright

Doctor of Philosophy in Earth System Science

University of California, Irvine, 2021

Dr. Kathleen Johnson, Chair

Northeast Mexico is projected to become drier in the future, however, the timing, magnitude and spatial extent of precipitation is poorly constrained at present. Although paleoclimate records can help inform us about the range and mechanism of natural precipitation variability, few records are currently available. To address this, we have developed two multiproxy U-Th dated speleothem records of past hydroclimate variability from the northeast state of Tamaulipas, Mexico, with interpretations of speleothem geochemistry supported by cave monitoring data and geochemical modeling.

We utilize multiple geochemical proxies ($\delta^{18}O$, $\delta^{13}C$ and Mg/Ca) in a speleothem sample (CB2) that spans from 4.6 ka to 58.5 ka to provide one of the highest temporally resolved records of precipitation variability in Mexico over this time-period. This record demonstrates a dominant thermodynamic control on precipitation via changes in Atlantic SSTs during major paleoclimate events, including the interglacial-glacial transition, the Last Glacial Maximum, the Younger Dryas, and Heinrich Stadials 1-5, as well as on longer, orbital, timescales. Lastly, we demonstrate drying in response to cooler Atlantic SSTs is consistent across large parts of Mexico

and Central America, suggesting the entire region is likely to respond similarly to precipitation change in the future.

This thesis also presents the first speleothem record (CB4) from NE Mexico covering the last millennium, an essential time-period to evaluate the role of internal climate variability and for improving projections of future rainfall. While Pacific SST variability has consistently been suggested as the central influence of Northern Mexico precipitation, we instead demonstrate that mean annual rainfall in NE Mexico is more heavily influenced by Atlantic SST variability, which is further supported by forced-SST climate model simulations. We suggest previous interpretations have primarily utilized tree ring records, which tend to record winter or early summer precipitation. In contrast to future predictions of a drier climate, we demonstrate precipitation in NE Mexico has become wetter over the industrial period, and that this trend is likely to continue in the future.

Chapter 1: Introduction

1.1 Role of precipitation variability on past, present, and future inhabitants of Mexico

Records of past climate, or paleoclimate, have consistently linked socio-cultural changes in Mexico and Central America (Mesoamerica) to precipitation variability over the last few millennia. Previous comparisons of archaeological and paleoclimate records have tended to emphasize disaster, for instance, linking droughts to the abandonment of large city centers in Belize and Guatemala during the Maya Classic Period, or to the initiation of Aztec human sacrifice practices in Central Mexico (Gill *et al.*, 2007; Hoggarth *et al.*, 2017; Bierhorst, 1992; Kennett *et al.*, 2012; Medina-Elizalde & Rohling, 2012; Webster *et al.*, 2007). While previous work underemphasizes cases of resiliency, such as migration, a diversity in diet, and technological innovation as effective climate adaptation strategies (Dunning *et al.*, 2012; Kennett *et al.*, 2012; Lentz *et al.*, 2018), the amalgamation of archaeological and paleoclimate records have undoubtedly highlighted how precipitation variability can drive large disruptions to society. Unfortunately, under current climate change, rainfall variability continues to significantly influence social upheaval in the region.

In 2021, the southern United States border is currently experiencing the highest influx of immigrants over the last two decades (U.S. Customs and Border Protection, 2021). Many immigrants are seeking refuge from extreme climate events, such as droughts and hurricanes. For instance, Hurricane Eta was only one of five land-falling hurricanes in Mesoamerica during the 2020 season but this single event displaced hundreds of thousands of people, destroyed homes, devastated crops, and caused substantial loss of life (Shultz *et al.*, 2021). Additionally, surges in

northward migration, especially from Northern Mexico, have also been propelled by consecutive years of drought, which have led to failed harvests, crop abandonment and national food shortages in Mexico (Feng *et al.*, 2010; Johnson, 2011; Murray-Tortarolo & Salgado, 2021). Unfortunately, the crisis is amplified by national governments which often lack the economic and technological resources to respond to, and mitigate, these disasters. While migration and immigration can be effective responses to such catastrophes, the journey can be dangerous, costly, and may not result in success.

Given the past impact and current impact of precipitation on the Mesoamerican people, projections of future precipitation are crucial for future water management, heath, and immigration patterns. While climate models suggest drying will become more pronounced throughout Mesoamerica in the future, models currently exhibit significant discrepancies in terms of the spatial distribution and magnitude of drying (Knutti & Sedláček, 2013; Lewis *et al.*, 2010). This is especially true for Northeast (NE) Mexico, where the mechanisms and drivers of hydroclimate, including both external drivers (i.e. insolation, pCO_2) and internal ocean-atmospheric variability, have remained unexplored or inconsistent (Quiroz-Jiménez *et al.*, 2018; Roy *et al.*, 2016, 2020). In part, this is due to the scarcity of long-term historical rainfall records and/or high-resolution paleoclimate records from the region. Secondary cave mineral deposits, known as speleothems, contain multiple hydrological proxies, can be radiometrically dated, and can record climate on sub-seasonal to orbital timescales, potentially offering a solution to the lack of long-term observations of precipitation. Despite the growing use of speleothems and the prevalence of limestone karst in Northeast Mexico (Chen *et al.*, 2017), there are no previous speleothem records from the region (Fig. 1.1).

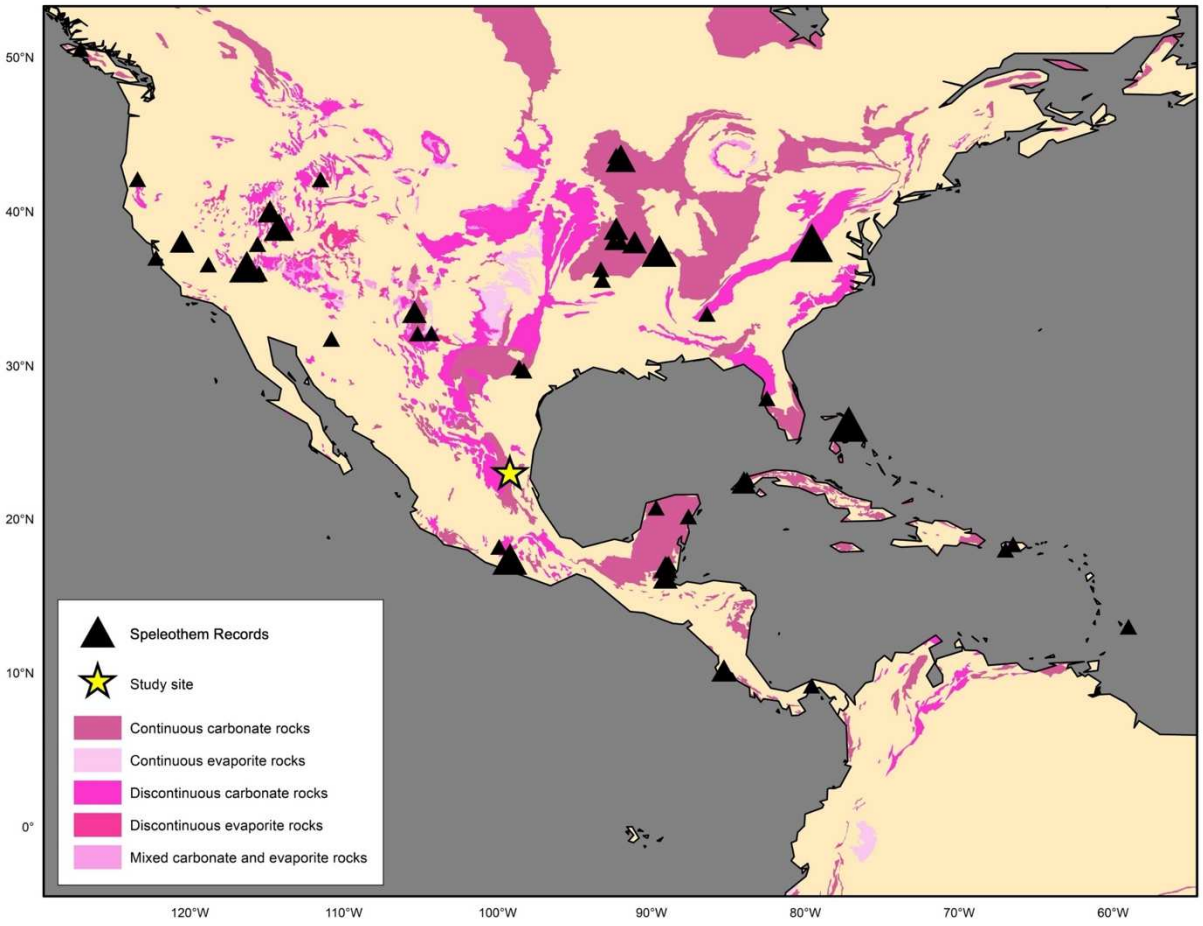

Fig. 1.1: Map of speleothem records in North and Central America. Various pinks indicate carbonate and evaporite rocks (Chen et al., 2017). Black triangles represent previous speleothem records with the size of the triangle proportional to the number of speleothem records from an individual cave (Oster et al., 2019). The star denotes the study site for this dissertation.

1.2 Speleothems as records of past precipitation

1.2.1 Speleothem formation

Speleothems are secondary cave deposits that form underground in limestone or dolomitic caves from overlying cave drip water. Speleothems are primarily composed of calcium carbonate ($CaCO_3$), and precipitate layer-by-layer as calcite minerals. Occasionally, and under certain hydrological and bedrock conditions, speleothems can also precipitate as the calcite polymorph aragonite (Frisia *et al.*, 2002). The growth of speleothem layers occur on a range of timescales and are sometimes annual due to seasonal fluctuations in cave air pCO_2 and/or drip

rate (Baker *et al.*, 2008), but this is highly dependent on the individual cave and hydrological routing to the sample.

Speleothem geochemical proxies are influenced by overlying changes in climate due to the various processes that control speleothem formation. Cave drip water, for instance, is generally sourced from overlying precipitation that has been subjected to and reacted with high pCO_2 in the soil zone from microbial and root respiration (Fairchild *et al.*, 2006; Fig. 1.2, *Eq. 1*). This forms a weak carbonic acid (H_2CO_3) which dissolves the cave bedrock introducing the Ca cations necessary for subsequent speleothem formation into solution (Fig. 1.2, *Eq. 2*). When the groundwater enters the cave, it is subjected to considerably lower pCO_2 levels, which causes bicarbonate supersaturation and the precipitation of calcium carbonate as a speleothem (Fig. 1.2, *Eq. 3*). Speleothems can precipitate in many different forms, but most paleoclimate work involves the use of stalagmites due their simple growth geometry, growing upwards from the cave floor with older layers at the bottom (Fairchild *et al.*, 2006). The chemical equations below describe the speleothem formation process (*Eq. 1-3)*:

$$CO_2 + H_2O \rightarrow H_2CO_3 \qquad \textit{(Eq. 1)}$$

$$H_2CO_3 + CaCO_3 \rightarrow Ca^{2+} + 2HCO_3^- \qquad \textit{(Eq. 2)}$$

$$Ca^{2+} + 2HCO_3^- \rightarrow CO_2 + CaCO_3 + H_2O \qquad \textit{(Eq. 3)}$$

Due to the interaction of water in the atmosphere, soil zone, bedrock and cave environment, the final speleothem geochemistry can reflect a myriad of processes (Fairchild *et al.*, 2006). Generally, oxygen stable isotopes ($\delta^{18}O$), carbon stable isotopes ($\delta^{13}C$), trace element variations (Mg/Ca) and radiocarbon (^{14}C) are interpreted to be reflective of overlying changes in hydrology. However, geochemical proxies often exhibit nuances in their dominant hydrological controls, with oxygen stable isotopes often reflecting larger more regional or mesoscale changes

in precipitation amount and rainout history, and the other proxies reflecting more localized changes, such as precipitation and evaporation above the cave (Fairchild *et al.*, 2006; Fairchild & Treble, 2009; Griffiths *et al.*, 2012, 2020; Johnson *et al.*, 2006). Additionally, while speleothem geochemistry is most frequently linked to changes in overlying hydrology, non-hydrological processes and have been documented within cave systems and can obscure the interpretation of past

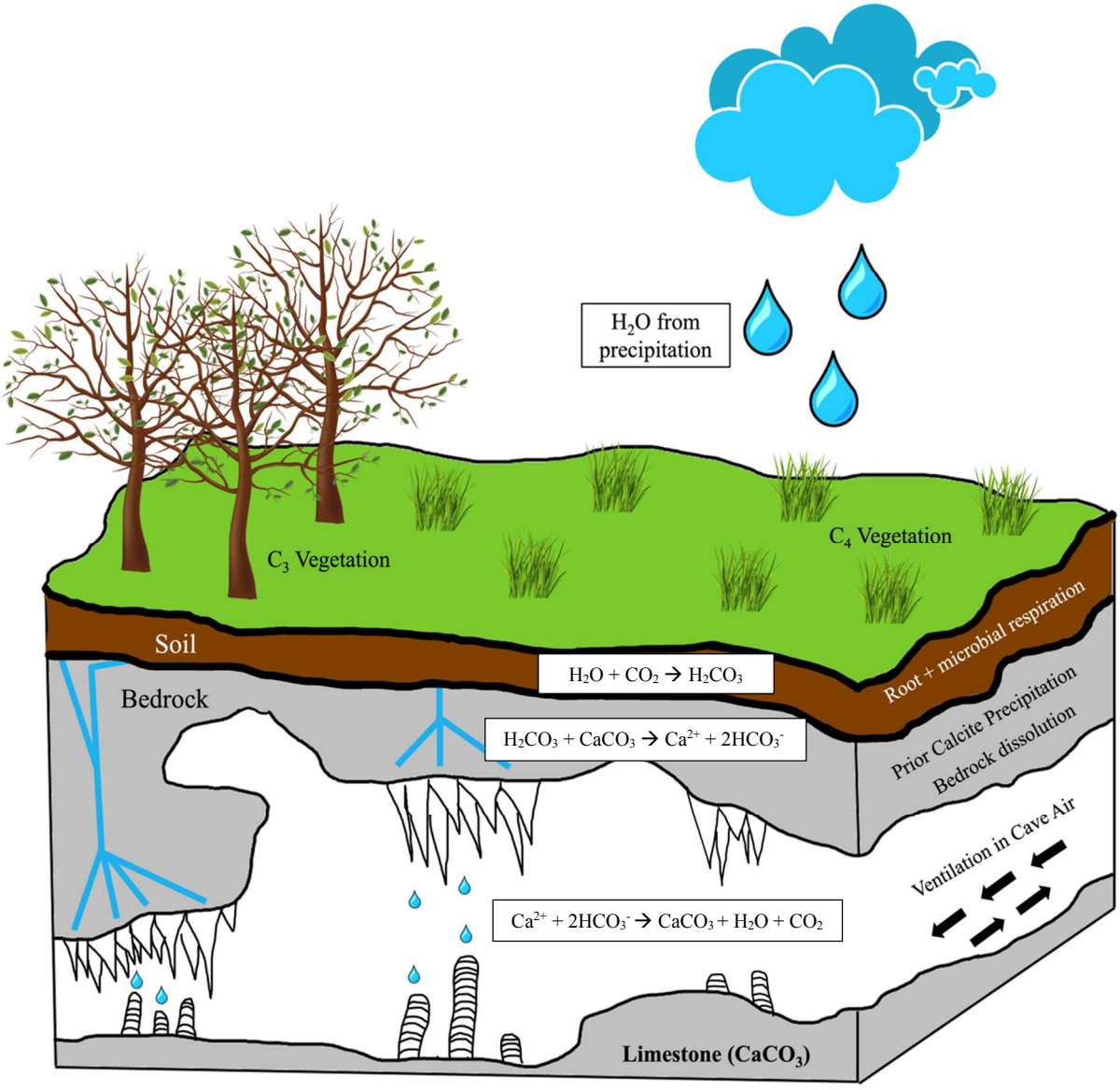

Fig. 1.2: Schematic demonstrating speleothem formation. Speleothem formation is shown in a limestone cave with some of the potential influences on geochemical proxies at various stages of speleothem formation.

rainfall (Feng *et al.*, 2012, 2013; Lyu *et al.*, 2020; Mickler *et al.*, 2004, 2019). In-situ studies of precipitation, drip water and the cave environment can help decipher the influence of these processes at various stages of speleothem formation (Wong *et al.*, 2011), but a multiproxy approach is more frequently applied due to the logistical constraints of fieldwork and ability to precisely decipher the mechanism of past rainfall variability.

1.2.2 The delta (δ) notation

Oxygen stable isotopes are frequently expressed by delta notation (δ) in units of per mil (‰), calculated by the subsequent equation:

$$\delta^{18}O = \left[\frac{R^{\text{Sample}} - R^{\text{Standard}}}{R^{\text{Standard}}} - 1 \right] \times 1000‰ \qquad \textit{(Eq. 4)}$$

Where $R = {}^{18}O/{}^{16}O$

This equation is the same for carbon stable isotopes, with the more isotopically abundant isotope always in the denominator and the more isotopically rare isotope in the numerator for R (i.e. $R = {}^{13}C/{}^{12}C$). The standard used to calculate δ for speleothem and other carbonate paleoclimate studies is Vienna Pee Dee Belemnite (VPDB). For water samples, the Vienna Standard Mean Ocean Water (VSMOW) is commonly used.

1.2.3 $\delta^{18}O$

The most common climate proxy utilized in speleothems is stable oxygen isotopes ($\delta^{18}O$). Under isotopic equilibrium, the $\delta^{18}O$ composition of speleothems reflects cave temperature, which represents the mean annual temperature of the overlying cave surface, and drip water $\delta^{18}O$ (Fairchild *et al.*, 2006; Hendy, 1971). Although a site-specific analysis of karst hydrology and groundwater mixing is preferred, it is commonly assumed the drip water $\delta^{18}O$

preserves the composition of local rainfall $\delta^{18}O$, or precipitation $\delta^{18}O$ ($\delta^{18}O_{precip}$) (Lachniet, 2009). While some studies have successfully used speleothem fluid inclusion $\delta^{18}O$ to reconstruct mean annual temperature (Griffiths *et al.*, 2010; Schwarcz *et al.*, 1976), observational and laboratory studies have demonstrated a relatively minor role of temperature on speleothem calcite $\delta^{18}O$ ($\delta^{18}O_{speleo}$), with a -0.23 per mil (‰) change per 1°C of warming (Kim & O'Neil, 1997). Although large amplitude temperature variations, such as during interglacial-glacial transitions, could significantly alter $\delta^{18}O_{speleo}$, the temperature dependence of calcite fractionation is well constrained thus major fluctuations in cave temperatures can be corrected for. Therefore, most of the variability in $\delta^{18}O_{speleo}$ is attributed to variability in $\delta^{18}O_{precip}$ (Lachniet, 2009).

Understanding the dominant drivers of variability in $\delta^{18}O_{precip}$ however still possess many challenges, as it can be controlled by a variety of processes (Lachniet, 2009). In some cases, such as in the Asian Monsoon region, uncertainties regarding the dominant control of $\delta^{18}O_{precip}$ have led to widespread disputes within the paleoclimate community (Cai *et al.*, 2015; Caley *et al.*, 2014; Clemens *et al.*, 2010; Dayem *et al.*, 2010; Lewis *et al.*, 2010; Pausata *et al.*, 2011; Yang *et al.*, 2016; Zhang *et al.*, 2018). In the tropics, $\delta^{18}O_{precip}$ is generally interpreted to reflect the amount of rainfall (Dansgaard, 1964), however, $\delta^{18}O_{precip}$ has also been shown to be sensitive to changes in moisture source (Araguás-Araguás *et al.*, 1998; Breitenbach *et al.*, 2010; Palmer & Palmer, 2012; Wagner *et al.*, 2010; Wong *et al.*, 2015), rainout history (Kurita *et al.*, 2009; Pausata *et al.*, 2011) and/or the monsoon intensity (Cheng *et al.*, 2016). Furthermore, variations in stratiform versus convective precipitation (Aggarwal *et al.*, 2016), microphysical cloud processes (Bony *et al.*, 2008; Risi *et al.*, 2008) and cloud-top height (Cai & Tian, 2016) are also

known to affect precipitation $\delta^{18}O$. Unfortunately, due to the paucity of both paleoclimate records and modern precipitation isotope systematic studies from NE Mexico, the dominant mechanisms driving precipitation $\delta^{18}O$ in the region have yet to be ascertained. Nearby records from Southern Mexico have consistently interpreted $\delta^{18}O_{precip}$ to reflect precipitation amount (Frappier *et al.*, 2014; Lachniet *et al.*, 2013, 2017; Lases-Hernández *et al.*, 2020; Medina-Elizalde *et al.*, 2016), but it is unclear if this mechanism also dominates in more northern regions. For instance, records from Texas, North Central Mexico (Chihuahua), Arizona and New Mexico have instead interpreted $\delta^{18}O_{precip}$ to be more reflective of shifting proportions of rainfall sourced from the Gulf of Mexico versus the Pacific, with precipitation amount playing a much more minor or inconsequential role (Palmer & Palmer, 2012; Rivera-Rivera *et al.*, 2021; Wagner *et al.*, 2010; Wong *et al.*, 2015). Thus, the use of additional geochemical proxies to reconstruct local rainfall are ideally utilized for a more robust interpretation, especially in relatively unexplored regions such as NE Mexico.

1.2.4 $\delta^{13}C$

Unlike speleothem $\delta^{18}O$, which is often a measure of large-scale atmospheric processes, speleothem $\delta^{13}C$ ($\delta^{13}C_{speleo}$) reflects more localized processes occurring directly above or within the cave (Fairchild *et al.*, 2006). Carbon incorporated in speleothems is dominantly sourced from the soil, epikarst and bedrock (Fairchild *et al.*, 2006; Hendy, 1971). Shifts in vegetation, both in vegetation type and abundance, can significantly alter the overall composition of $\delta^{13}C_{speleo}$. For instance, previous work has evoked that shifts from C3 vegetation, with an average $\delta^{13}C$ value of -28 ‰, to C4 vegetation, with an average value of -14‰, can increase the $\delta^{13}C_{speleo}$ composition and reflect drier conditions above the cave surface (Dorale, 1998; McDermott, 2004). However, changes in vegetation are not necessarily linked to hydroclimate changes, as the preference of C3

vegetation to utilize $C^{16}O_2$ gives the less preferential C4-vegetation a competitive edge during lower atmospheric CO_2 conditions, such as during the last glacial (Galy *et al.*, 2008). Other work has thus suggested $\delta^{13}C_{speleo}$ is better summarized as representing the amount of overlying soil activity, which emphasizes total vegetation abundance and microbial activity as the dominant driver of $\delta^{13}C_{speleo}$. For instance, Genty *et al.* (2001) demonstrated drier conditions drives a significant reduction in microbial activity, decreasing soil respiration and ultimately shifting $\delta^{13}C_{speleo}$ values towards higher atmospheric values (-8‰). More recent work has also provided evidence that during wetter conditions there are significant increases in soil respiration which drives higher soil pCO_2, more negative soil and groundwater $\delta^{13}C$, ultimately imparting a more negative $\delta^{13}C$ signal in the speleothem (Fohlmeister *et al.*, 2020).

In addition to $\delta^{13}C_{speleo}$ reflecting hydrological changes in the soil zone, $\delta^{13}C_{speleo}$ can also reflect hydrological changes within the epikarst and bedrock via prior calcite precipitation (PCP). PCP generally refers to the precipitation of calcite anywhere before the speleothem, which can occur on overhanging stalactite tips, on the cave ceiling, in the karst aquifer, in the epikarst and even in the soil zone (Johnson *et al.*, 2006). Prior calcite precipitation occurs when conditions are dry, leading to more air present in voids, fissures, and pore spaces of the bedrock (Fairchild *et al.*, 2006; Frisia *et al.*, 2011; Johnson *et al.*, 2006). All of which serve to increase the degree of CO_2 degassing, which drives degassing of the isotopically lighter $^{12}CO_2$, leaving the speleothem subsequently enriched in ^{13}C (Johnson *et al.*, 2006; Oster *et al.*, 2010; Treble *et al.*, 2015). It is important to mention that both soil activity and PCP drive changes in $\delta^{13}C_{speleo}$ in the same direction, with wetter conditions driving decreased $\delta^{13}C_{speleo}$ values and vice-versa for dry conditions.

In addition to soil activity and PCP, $\delta^{13}C_{speleo}$ can also be controlled by the degree to which bedrock dissolution occurs in an 'open' or 'closed' system in relation to the overlying soil zone and atmosphere (Hendy, 1971; Oster *et al.*, 2010). During wet conditions, the pore spaces and conduits of the bedrock are closed off from the overlying soil zone and atmosphere, leading to the dissolution of the limestone bedrock in a 'closed' system. Closed system dissolution shift dissolved inorganic carbon (DIC) towards bedrock $\delta^{13}C$ values, with stoichiometry dictating upwards of a 50% bedrock $\delta^{13}C$ contribution to DIC (Hendy, 1971). During dry conditions, open spaces in the pores, cavities and fissures of the bedrock allow for continual exchange of percolating waters with soil CO_2, which will almost always retain a lower $\delta^{13}C$ value than the bedrock due to microbial activity and root respiration in the soil zone (Hendy, 1971; Griffiths, 2012). Unfortunately, open versus closed-system dissolution drives a potential discrepancy in interpreting speleothem $\delta^{13}C$, where wetter conditions could lead to increased $\delta^{13}C$ values if closed system dissolution dominantly controls the speleothem carbon composition, or decreased $\delta^{13}C$ values if soil activity/PCP is the dominant driver of speleothem carbon composition. Paleoclimate interpretation is therefore aided by comparing $\delta^{13}C_{speleo}$ to other geochemical proxies.

In addition to processes affecting $\delta^{13}C_{speleo}$ in the soil and bedrock zone, CO_2 degassing driven by hydrological and non-hydrological processes within the cave environment can also drive variability in $\delta^{13}C_{speleo}$ (Deininger *et al.*, 2012; Deininger & Scholz, 2019; Frisia *et al.*, 2011). For instance, cave ventilation is driven by density differences between external surface and internal cave air and often takes place on seasonal to diurnal timescales (Baldini *et al.*, 2008; Freitas *et al.*, 1982; James *et al.*, 2015). Observational studies have demonstrated when cave

temperatures are lower than surface temperatures ($T_{cave} < T_{surface}$), cave air stagnation is induced (Freitas *et al.*, 1982). Stagnation serves to increase cave air pCO_2, decreasing the rate of CO_2 degassing, leading to less PCP and consequently lower speleothem $\delta^{13}C$ values (Baldini *et al.*, 2008; Lyu *et al.*, 2020). Ventilation occurs under opposite conditions ($T_{cave} > T_{surface}$), driving increased PCP and higher $\delta^{13}C_{speleo}$ values. However, cave air pCO_2 is also sourced from the overlying soil zone which can increase from more microbial activity due to wet conditions and/or warmer temperatures. This may amplify the role of ventilation if the wet season co-occurs with warmer cave air (Baldini *et al.*, 2008; Fohlmeister *et al.*, 2020; Lyu *et al.*, 2020). The signal-to-noise ratio caused by ventilation is expected to be quite low on interannual to decadal timescales but could impart a strong effect on $\delta^{13}C$ on shorter, seasonal to sub-seasonal timescales. Drip rates, through the same process of CO_2 degassing can also impact $\delta^{13}C_{speleo}$. Slower drip rates increase $\delta^{13}C_{speleo}$ by increasing the amount of time the water is subjected to CO_2 degassing (Deininger & Scholz, 2019; Mühlinghaus *et al.*, 2007, 2009), which can occur both before and while the water is in contact with the speleothem surface. Modelling studies demonstrate that PCP in the cave or above in the bedrock may amplify this process, but changes in drip rate alone can also alter $\delta^{13}C_{speleo}$ (Deininger & Scholz, 2019). Unlike changes in ventilation, drip rates often reflect local water balance above the cave (P-ET), driving changes in $\delta^{13}C_{speleo}$ in the same direction as PCP and soil activity (wetter = more negative $\delta^{13}C$), and can therefore amplify the hydroclimate signal recorded in $\delta^{13}C_{speleo}$.

Processes controlling $\delta^{13}C$ are abundant and decoupling climatic versus non-climatic controls can be an intricate process. While long-term cave monitoring studies can help illuminate the dominant controls of $\delta^{13}C$ (Meyer *et al.*, 2014; Osácar *et al.*, 2017; Riechelmann *et al.*, 2011;

Spötl *et al.*, 2005), it often requires several years and many field campaigns to collect the necessary data. Therefore, utilizing emerging speleothem proxies, such as trace elements (Mg/Ca) and radiocarbon (^{14}C) can offer additional evidence of past rainfall variability and help constrain whether $\delta^{13}C$ is more influenced by PCP or bedrock dissolution.

1.2.5 Trace Elements

Trace elements in speleothems are an emerging paleoclimate proxy. Trace elements are generally sourced from the overlying bedrock (Johnson *et al.*, 2006) and soil (Fairchild *et al.*, 2001; Hartland *et al.*, 2012; Treble *et al.*, 2003). Minor contributions from dust and sea-spray have also been recorded in speleothem samples, but this generally occurs only in samples retrieved close to cave entrances (Frumkin & Stein, 2004; Goede *et al.*, 1998; Sinclair *et al.*, 2012). The substitution of trace elements (Tr) for calcium (Ca) in the calcite matrix from solution is expressed by the partition coefficient (K_{Tr}) in the following equation (Fairchild & Treble, 2009):

$$(Tr/Ca_{CaCO_3}) = K_{Tr}\,(Tr/Ca)_{Solution} \qquad \textit{(Eq. 5)}$$

For paleoclimate analysis, Mg/Ca and Sr/Ca have traditionally been used for paleoclimate reconstruction when they are interpreted to reflect prior calcite precipitation (Fairchild & Treble, 2009; Johnson *et al.*, 2006; Smith *et al.*, 2009). In addition to increasing $\delta^{13}C_{speleo}$, PCP during drier conditions leads to the preferential uptake of Ca, leaving the solution subsequently enriched in trace metals (Mg, Sr) because the partition coefficient is much less than unity ($K_{Tr}<<1$) (Morse & Bender, 1990). Trace elements are also sensitive to CO_2 degassing and to other non-hydrological controls such as cave ventilation (Wong *et al.*, 2011), changes in water flow path through the bedrock (Fairchild & Treble, 2009), changes in growth rate (Gabitov & Watson,

2006), and groundwater mixing (Fairchild *et al.*, 2001; Huang *et al.*, 2001). Therefore, cave monitoring to evaluate the role of these processes on trace element concentration in drip waters, or comparison to $\delta^{13}C_{speleo}$ and $\delta^{18}O_{speleo}$ can provide evidence for a strong hydrologic or PCP control (Griffiths *et al.*, 2016).

While speleothem Mg and Sr are predominantly generated from bedrock dissolution and exchange for Ca directly in the crystal lattice, soil-derived trace elements can also be incorporated into speleothems. Previous studies have highlighted the chemical mobilization and infiltration of soil derived elements of Fe, P, Cd, Y and possibly U during heavy rainfall events and/or after vegetation die-back (Fairchild *et al.*, 2001; Hartland *et al.*, 2012; Treble *et al.*, 2003). Soil-derived trace elements have therefore been used to reconstruct past changes in rainfall, with higher ratios of soil derived trace metals associated with higher rainfall (Fairchild & Treble, 2009).

1.2.6 Dead Carbon Proportion

Speleothem radiocarbon ($^{14}C_{speleo}$) has been utilized in several areas of paleoclimate research, such as determining the source of speleothem carbon (Noronha *et al.*, 2015), the calibration of atmospheric ^{14}C (Southon *et al.*, 2012), and as an additional hydrological proxy (Griffiths *et al.*, 2012, 2020). Speleothem radiocarbon can reflect changes in local water balance via open versus closed system bedrock dissolution controlling the amount of the dead carbon proportion (Fohlmeister *et al.*, 2011; Griffiths *et al.*, 2012). Dead Carbon Proportion (DCP) is calculated by first solving for initial stalagmite activity ($a^{14}C_{initial}$) by correcting for radioactive decay in the measured activity ($a^{14}C_{measured}$) (Genty *et al.*, 1999):

$$a^{14}C_{initial} = \frac{a^{14}C_{measured}}{\exp[\frac{-\ln(2)}{5730} * t]} \qquad \textit{(Eq. 6)}$$

However, this produces an initial activity ratio which is not corrected for atmospheric activity, which can vary through time due to solar wind activity and the Earth's magnetic field (Kovaltsov *et al.*, 2012). Therefore, U-Th ages or U-Th based age model estimates are used to estimate the time of deposition at each depth and determine the atmospheric activity ($a^{14}C_{atmosphere}$) using a record of atmospheric radiocarbon such as IntCal3 (Reimer *et al.*, 2013). DCP can then be calculated using the subsequent equation (Genty & Massault, 1997; Reimer *et al.*., 2013):

$$DCP = \left[1 - \left(\frac{a^{14}C_{initial}}{a^{14}C_{atmosphere}}\right)\right] * 100\%$$

A fully open dissolution system occurs when conditions are dry and dissolved inorganic carbon in the epikarst is in complete isotopic equilibrium with modern ^{14}C values (1950). In this scenario, the DCP would be equal to 0% (Hendy, 1971). Alternatively, a completely closed system dissolution occurs when conditions are wet, and water in the voids and fractures of the epikarst are in isotopic exchange with both the atmosphere and the bedrock. Therefore, the upper limit of DCP in a completely closed system would be 50% (Bajo *et al.*, 2017; Hendy, 1971; Noronha *et al.*, 2015). Of course, most DCP values in natural cave systems are somewhere between these extremes, with caves demonstrating an average DCP of 15 ± 5% (Genty *et al.*, 1999). Including DCP can be particularly useful in helping to determine the effect of open-versus-closed system dissolution on $\delta^{13}C$.

1.3 Speleothem Chronologies

Speleothems are unique paleoclimate records in that they can be precisely dated using a suite of absolute dating methods and relative dating methods. While some rare samples record climate extending as far back as the Permian geologic period (47 - 299 Ma) (Woodhead *et al.*,

2010), most speleothems are much younger, covering the geologic epochs of the Holocene (< 0.012 Ma) or late-Pleistocene (0.012-0.5 Ma). Records covering longer timescales (10^4 years) are particularly crucial for understanding the response of climate to external forcings, such as orbitally induced changes in incoming solar radiation, changes in atmospheric pCO_2 and fluctuations in global ice sheet/sea level volume while records covering the Common Era (last 2,000 years) are more useful for the tuning of climate models.

Speleothems are primarily dated using uranium series methods (Cheng *et al.*, 2016; Dykoski *et al.*, 2005; Wang *et al.*, 2008, 2001), which utilizes the alpha decay of the parent nuclide ^{234}U to daughter nuclide ^{230}Th. Uranium is generally sourced from the overlying bedrock, is soluble under oxidizing conditions, and co-precipitates with calcite from water during speleothem formation (Fairchild *et al.*, 2006). Natural waters typically have very little Th, because it is highly insoluble, and therefore most of the ^{230}Th in calcite is generally interpreted to be sourced from the decay of uranium (Fairchild *et al.*, 2006). However, Th can adhere to the surface of clay minerals which can be incorporated during speleothem formation. This is often referred to as initial thorium and it can increase the amount of measured ^{230}Th, producing an inaccurate and older-than-true date. Therefore, correction for initial thorium is necessary and is achieved by measuring ^{232}Th and assuming an bulk Earth average $^{230}Th/^{232}Th$ atomic ratio of 4.4 ppm (Hellstrom, 2006). However, significant deviations from this average have been recorded (0.2-18 ppm) and a site-specific analysis is often required (Beck *et al.*, 2001; Drysdale *et al.*, 2006; Hellstrom, 2006).

Radiocarbon (^{14}C) dating of speleothem samples is not common, but has been used to build age-depth models in select cases typically with younger speleothem samples that have a high initial Th (Hua *et al.*, 2017; Yadava & Ramesh, 2005). However, compared to U-Th methods,

radiocarbon usually provides larger age uncertainties, is limited to only dating more recent samples (< 50,000 years), and the amount of ^{14}C in the speleothem can be affected by overlying hydrology (Griffiths *et al.*, 2012, 2020). For instance, to correct for the contribution of ^{14}C from the aged soil organic matter and bedrock, also known as the speleothem ^{14}C reservoir effect, accurate radiocarbon dates require the dead carbon proportion to be known and that it remains constant throughout the sample (Hua *et al.*, 2017). If DCP is not measured and the ages corrected, radiocarbon dates will always over-estimate the age of the sample compared to U-Th methods. However, the assumption of a constant DCP over time is often incorrect, adding further uncertainty to radiocarbon age models, given DCP often varies in response to changes in local water as described previously. Speleothem radiocarbon dating is therefore more useful to determine if samples are 'modern' or formed after 1950 due to the atmospheric spike in ^{14}C in the 1960s from nuclear bomb development and testing (Hodge *et al.*, 2011). If precise sampling is conducted, finding the location of the bomb peak within the sample can also serve as an additional chronological marker.

In addition to radiometric dating methods, speleothems can also be dated using visible or geochemical laminae that are seasonal or annual in nature. Seasonal or annual laminae may form as a direct response to a change in hydrology (i.e. shifts in rainfall amount), vegetation dye-back, and within cave processes (i.e. ventilation), which can be amplified when these events combine (Baker *et al.*, 2008). However, layer counting is almost always used to complement U-Th dates, not as a standalone dating method. This is due to layers not always being annual in nature, whereby individual heavy rainfall events can create multiple layers per year, sometimes referred to as 'false' layers, and/or dry conditions can cause micro-hiatuses and 'missing' layers due to inhibited growth of the speleothem (Shen *et al.*, 2013). To combine U-Th and layer counting data

for a more robust age model, a depth-age model such as Constructing Proxy Records from Age Models (COPRA) is typically employed (Breitenbach *et al.*, 2012). Other, less complex, relative dating methods can also be employed typically during fieldwork to determine if the speleothem was actively growing when collected, such as if the speleothem has drip water actively falling from above or if new calcite growth is detected at the site of collection.

1.4 Regional Climatology

Regional rainfall amount in NE Mexico is highly sensitive to orography. On the windward side of the Sierra Madre Oriental, orographic precipitation combined with precipitation from tropical storms and hurricanes provide considerable moisture to create a tropical wet climate (Fig. 1.3; Landsea & Franklin, 2013; Pérez Quezadas *et al.*, 2015; Wang *et al.*, 2006, 2011). The lee-ward side of the Sierra Madre Occidental is considered a semi-arid climate, with aridity increasing westward and eventually transitioning into a completely arid environment as part of the Chihuahua desert plateau (Salinas-Rodríguez *et al.*, 2017). Despite regional differences in precipitation amount, precipitation in NE Mexico has been shown to respond similarly on seasonal to interannnual timescales.

NE Mexico precipitation is dominated by a warm wet summers and cool dry winters (Chávez-Lara *et al.*, 2019; Roy *et al.*, 2016, 2020). Precipitation during the warm summer months is driven by an intensification of the northerly branch of the Caribbean Low-Level Jet (CLLJ) increasing the southeasterly airflow bringing moisture from the Caribbean Sea and Gulf of Mexico to NE Mexico (Fig. 1.3; Mestas-Nuñez *et al.*, 2007). The CLLJ is strengthened by the intensification and westward expansion of the North Atlantic Subtropical High (NASH), increasing easterly trade winds which directly feed into the CLLJ (Fig. 1.3; Mestas-Nuñez *et al.*, 2007). Precipitation during summer is further amplified by warmer Tropical North Atlantic, Gulf

of Mexico, and Caribbean Sea SSTs, which serve to increase boundary layer moisture and regional precipitation (Bhattacharya & Coats, 2020). Anomalously warm SSTs are also known to increase the frequency and magnitude of tropical storms and hurricanes, which can lead to dangerous amounts of precipitation. For instance, Hurricane Ingrid (2013) brought heavy rainfall (>502 mm) that caused rapid flooding, 1.5 billion dollars (USD) in damage and 32 deaths (Kovacs *et al.*, 2017). During the winter, precipitation is significantly reduced compared to the summer season. Decreased precipitation is attributed to a weakening of the northerly branch of the CLLJ, cutting off the flow of moisture to NE Mexico and cooler regional SSTs (Mestas-Nuñez *et al.*, 2007). However, short, and infrequent low-level winds carrying moisture from the north (Fig. 1.3), known as *nortes*, are known to pass through the region and provide precipitation during the dry season (Kurczyn *et al.*, 2021; Osorio-Osorio *et al.*, 2020; Villanueva-Diaz *et al.*, 2007).

On interannual timescales, the climatology of Northern Mexico is influenced by Pacific coupled ocean-atmospheric climate modes, such as the El Niño Southern Oscillation (ENSO). During El Niño years, increased precipitation during boreal winter is driven by a shift in the subtropical jet, and an increase in the frequency and magnitude of *nortes* (Magaña *et al.*, 2003). However, the effects of ENSO on precipitation are poorly constrained in both time and space. For example, El Niño has been shown in instrumental records to consistently increase precipitation in NW Mexico and decrease precipitation in Southern Mexico (Magaña *et al.*, 2003; Méndez & Magaña, 2010; Stahle *et al.*, 2012, 2016). However, tree rings suggest the correlation to El Niño is temporally inconsistent in NE Mexico (Gutiérrez-García *et al.*, 2020), limiting our confidence in the role of the Pacific on regional precipitation variability. Modeling studies (Bhattacharya & Chiang, 2014; Seager *et al.*, 2009) suggest El Niño drives a divergence

in the seasonal response of precipitation, with increased winter moisture and decreased summer moisture. Drying during summer is attributed to El Niño-driven tropospheric heating which enhances evapotranspiration in NE Mexico from warmer temperatures and decreased cloud cover (Bhattacharya *et al.*, 2017). Drying is further amplified by warmer SSTs and anomalous SLP changes over the Atlantic in response to the tropospheric heating, which leads to decreased precipitation from a weakening of the CLLJ (Bhattacharya and Chiang 2014). The Pacific Decadal Oscillation is thought to also drive the same climatological response, but on longer timescales and to a weaker extent (Pavia *et al.*, 2006; Stahle *et al.*, 2016). Current interpretations of the Pacific's role on precipitation in Northern Mexico, however, are limited by the paucity of paleoclimate records, inconsistency of pre-existing records, and uncertainties in model-performance. High-resolution rainfall reconstructions would significantly aid in interpreting the role of the Pacific in this region.

While a lot of attention has been given to the role of ENSO on regional rainfall, Atlantic driven ocean-atmospheric variability has also been suggested as a driver of climate in the region on longer multidecadal timescales (Bhattacharya *et al.*, 2017; Stahle *et al.*, 2016). Tree ring reconstructions, for instance, have suggested a positive phase of Atlantic Multidecadal Oscillation (AMO) drives a weak but spatially broad reduction in precipitation over much of Mexico (Stahle *et al.*, 2016). However, instrumental records combined with climate model simulations, suggest the spatial response of precipitation is more complex. For instance, Bhattacharya *et al.* (2017) suggests a positive phase of the AMO drives a dipole, out-of-phase, precipitation pattern in Mesoamerica, with wetter conditions in Northern Mesoamerica and drier conditions in Southern Mesoamerica. The bimodal precipitation pattern is attributed to a westward expansion of the North Atlantic Subtropical High which strengthens the CLLJ and

carries moisture away from southern Mesoamerica, thereby increasing the moisture flux to Northern Mexico (Bhattacharya *et al.*, 2017; Bhattacharya & Coats, 2020). While this response has been verified using speleothems, tree-ring and lake-sediments from southern Mesoamerica (Bhattacharya & Coats 2020), this response remains untested in Northern Mexico due to the dearth of paleoclimate records.

1.5 Study Site

All samples discussed in this thesis were retrieved from Cueva Bonita (23°N, 99°W; 1071 m above sea level), which resides within the highlands of the windward side of the Sierra Madre Oriental in the northeast Mexican state of Tamaulipas. The cave is located within the El Cielo Biosphere Reserve, the northernmost tropical rainforest in Mexico (Gram & Faaborg, 1997). The cave has a relatively narrow entrance, approximately 5 m in diameter, followed by a steep (>70°) vertical drop of approximately 15 m to the first floor of the cave (see Chapter 2, Fig. 2.2). The first floor is well ventilated, dry, and does not have any easily assessable stalagmite formations, at least those suitable for paleoclimate reconstruction. A second, less intense vertical drop (~45°) approximately 10 m in length leads to the second floor of the cave. The second floor of the cave is wet, has many stalagmite formations, and is separated by a wall with a narrow passage forming a front and rear room (see Chapter 2, Fig. 2.2). Regional geology is dominated by thick (>2000 m) Lower Cretaceous limestone (Gary, 2006), uplifted by normal and thrust faults (Ford, 2000). The cave has ~50 m of overburden, a single relatively narrow entrance, and a shallow soil profile with 30 cm of dark brown clay loam soil. The vegetation above the cave is dominated by C_3 plants, including the *podocarpus reichei*, *liquidambar styraciflua*, *quercus sartorii*, *quercus germana*, *clethra pringlei*, *magnolia tamaulipana*, *acer skutchii, cercis canadensis*, and diverse epiphytic orchid species.

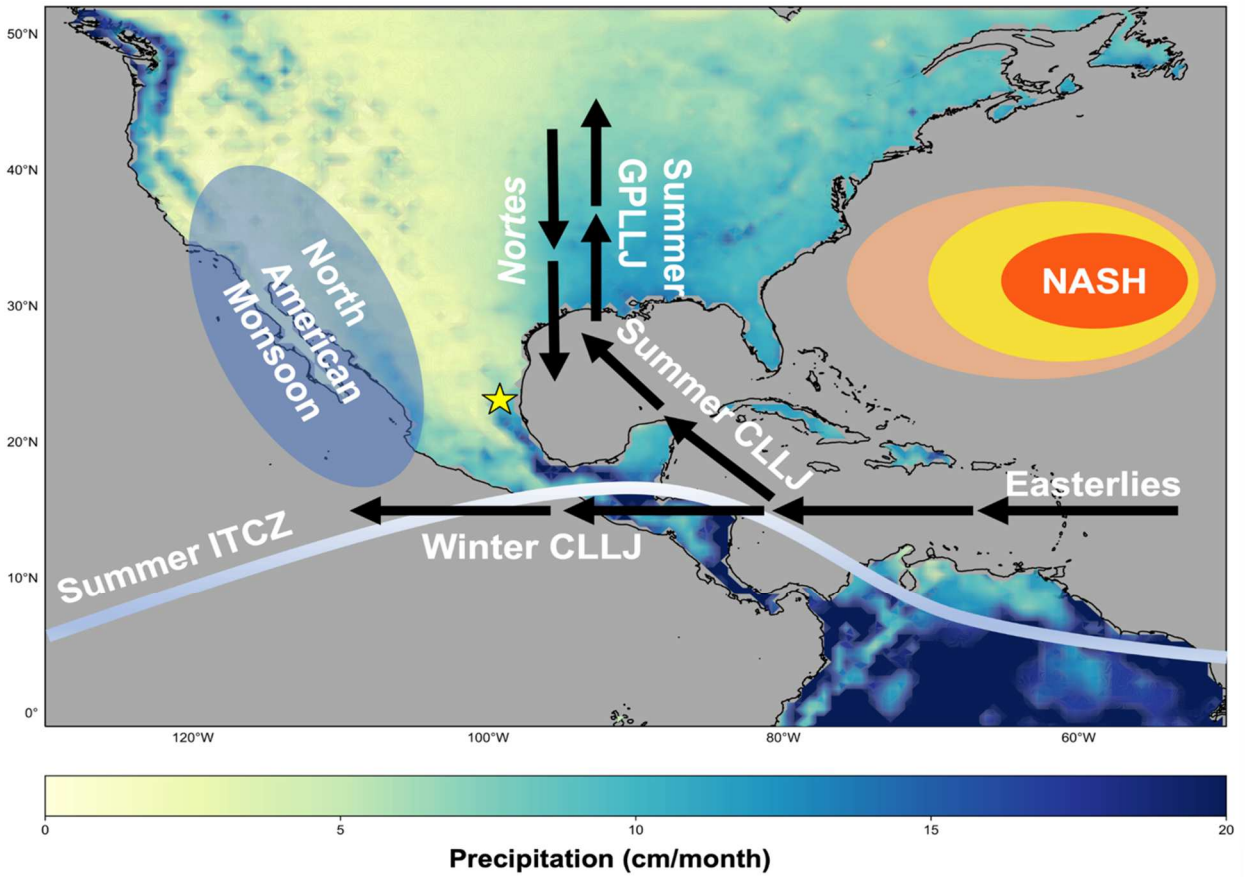

Fig. 1.3: Conceptual model of modern climate dynamics. Precipitation in NE Mexico is linked to a westward expansion and intensification of the North Atlantic Subtropical High which drives an intensification of the easterlies and the bifurcation of the CLLJ during the summer months. Winds from the north (*nortes)* during winter can also provide some additional precipitation. NE Mexico rainfall is not directly affected by the ITCZ or strength of the North American Monsoon.

1.6 Research Objectives

The overarching goal of this thesis to use speleothems to better constrain precipitation variability in NE Mexico, to accomplish this goal, my thesis focuses on the following research questions:

1. What are the dominant controls of speleothem geochemical proxies at Cueva Bonita?
2. What the main drivers of precipitation variability in Northeast Mexico on orbital to millennial timescales over the Holocene and Late-Pleistocene?
3. What is the role of Atlantic versus Pacific in driving hydroclimate in NE Mexico on multi-decadal timescales over the Common Era?

1.7 Outline of Chapters

Chapter 2: Testing climatic and environmental controls on speleothem geochemical proxies from Cueva Bonita

While initial paleoclimate work from the tropics generally assumed precipitation $\delta^{18}O$, and thus speleothem $\delta^{18}O$, was dominantly controlled by a rainfall amount effect, many studies have shown that precipitation $\delta^{18}O$ is affected by a range of factors. Previous work identified shifts in moisture source, monsoon intensity, and seasonality of precipitation to be equally dominant controls of precipitation $\delta^{18}O$. Furthermore, as previously mentioned, the controls of $\delta^{13}C$ and trace metals in speleothems can be vast, including PCP, cave ventilation, and bedrock dissolution. Therefore, having a site-specific study of the geochemical proxies is crucial for their proper hydrological interpretation.

In this chapter, I will demonstrate geochemical proxies are reflective of both hydrological and non-hydrological processes utilizing a combination of observational, cave monitoring and modeling data. Precipitation samples collected from Alta Cima, located approximately ~1 km from Cueva Bonita, were analyzed for $\delta^{18}O$ and D and compared to local precipitation records, which revealed a strong precipitation amount effect. Additionally, using air parcel trajectories and moisture uptake analyses, we demonstrate that almost all moisture at Cueva Bonita is

sourced from the Gulf of Mexico and Caribbean Sea. This suggests that precipitation $\delta^{18}O$ is not reflective of shifting moisture sources, as it is nearby Arizona, Chihuahua, New Mexico, or Texas. This work will provide validation of isotope-enabled climate models, which indicate a strong amount effect on precipitation $\delta^{18}O$ in the region.

Additionally, in this chapter I will utilize a suite of cave monitoring data (drip water $\delta^{18}O$ and $\delta^{2}H$, pCO_2, relative humidity, temperature, glass grown calcite, drip rate) collected over a 4-year period, combined with isotope enabled models, to demonstrate the precipitation $\delta^{18}O$ signal is successfully transferred to the speleothem. Cave monitoring data also reveals significant intra-cave variability in trace elements concentrations at various drip sites, not all of which appear to be controlled by hydrology. Ultimately, this work suggests Cueva Bonita is suitable for $\delta^{18}O$ on sub-seasonal to orbital timescales, but seasonal controls on trace elements may inhibit the use of trace elements for seasonal to sub-seasonal reconstruction, at least at certain locations within the cave.

Chapter 3: Thermodynamics control precipitation in NE Mexico on orbital to millennial timescales

Pre-existing records from NE Mexico have suggested changes in dynamics, namely the strength of the Caribbean Low-Level Jet (CLLJ), drive the pacing and amount of regional rainfall. This mechanism has been suggested on both longer timescales in response to external, orbital-induced changes in earth's incoming solar radiation (higher insolation = stronger jet) and on shorter timescales, such as during cold ice-sheet rafting events known as Heinrich Stadials (Heinrich Stadials = weaker jet). However, previous records disagree on the season of insolation driving rainfall variability on orbital timescales, with some records suggesting spring or autumn

insolation as the more dominant forcing (Quiroz-Jiménez *et al.*, 2018; Roy *et al.*, 2016). Furthermore, many records do not extend beyond the interglacial-glacial transition (Chávez-Lara *et al.*, 2019; Roy *et al.*, 2013a, 2013b, 2016), making it difficult to determine if hydrological changes are truly driven by insolation or, if hydroclimate is more sensitive to other external drivers of climate variability known to also vary during this time-period. Furthermore, previous records covering Heinrich Stadials demonstrate an inconsistent hydrological response, with different proxies within a single record exhibiting both wet and dry conditions (Roy *et al.*, 2020). To confront these discrepancies, we provide a new U-Th dated speleothem sample (CB2) with multiple geochemical proxies ($\delta^{18}O$, $\delta^{13}C$, Mg/Ca) of past hydroclimate variability.

Sample CB2 grew continuously from 4.6 to 58.5 ka, covers Heinrich Stadials 1-5, and extends 28.5 ka further back than previous paleoclimate records from NE Mexico. With over 1600 stable isotope ($\delta^{18}O$, $\delta^{13}C$) and 800 trace element (Mg/Ca) measurements, we demonstrate precipitation does not increase with a strengthening of the CLLJ on orbital timescales as previously thought. Instead, we demonstrate a strong thermodynamic control on hydroclimate, primarily through regional SSTs, changes in atmospheric pCO_2 and/or Northern Hemisphere land temperatures. We also demonstrate that SSTs are the most important drivers of regional rainfall on millennial timescales during major paleoclimate events, including Heinrich Stadials 1, 3, 4, 5, and the Younger Dryas. We combine our results with a state-of-the-art climate model to demonstrate cool Atlantic SSTs, and a strengthening of the CLLJ, is the dominant mechanism of drying. Through model simulations and comparison to other records, we demonstrate Mesoamerica responds similarly (dry) to cool Atlantic SSTs. This suggests future drying, or wetting, may be more spatially ubiquitous than models currently predict. The supplementary material for this chapter can be found in Appendix A.

Chapter 4: Atlantic SSTs drive hydroclimate in NE Mexico over the Common Era

Paleoclimate records covering the Common Era are incredibly important for the tuning of climate models and elucidating the dominant ocean-atmospheric climate modes altering precipitation on multi-decadal timescales. However, producing continuous records covering the Common Era in the tropics can be difficult. For instance, tree rings can provide annual resolution but typically only cover the last few centuries and may preferentially record winter or early-spring moisture. This poses a particularly big problem for NE Mexico, which receives most of its precipitation during summer and late-autumn. Similarly, lake-sediment studies can occasionally contain annual laminae, but more frequently have centennial to millennial temporal resolution with relatively large age uncertainties.

In this chapter, I will present the first speleothem reconstruction of hydroclimate in NE Mexico covering the last 1,100 years. This record has an annual resolution of 2.8 years and an age-depth model with very low uncertainty ($\mu < 9$ years). Reduced uncertainty was achieved due to the use of multiple dating methods, including 14 U-series dates and annual microscopic fluorescent layer counting, combined with 2000 Monte Carlo simulations using the age-depth modeling software COPRA. This study utilizes multiple proxies to reconstruct overlying rainfall and local water balance, including stable isotopes ($\delta^{18}O$, $\delta^{13}C$), trace elements (Mg/Ca) and radiocarbon (DCP). While previous tree ring records from Northern Mexico have consistently linked a stronger Caribbean Low-Level Jet and warm Pacific SSTs to increased precipitation, our new speleothem data, which is reflective of total annual rainfall, combined with forced SST climate model simulations suggest a stronger jet leads to regional drying. We highlight, again in contrast to tree ring reconstructions, that warmer Atlantic SSTs drive increased precipitation in the region, with warmer Pacific SSTs leading to decreased annual rainfall. We suggest previous

interpretations may have more strongly biased winter and early-summer precipitation dynamics. Most importantly, our record demonstrates increased precipitation over the industrial period (last ~200 years) in response to warming SSTs. This suggests the region may become wetter under future climate change, in contrast to many model predictions.

Summary

Results from this dissertation help constrain the dominant mechanisms of precipitation change in NE Mexico, a region where advancements in climatology are currently constrained by a lack of long-term observational records and high model uncertainty. This work assists our understanding of the hydrological controls of geochemical proxies, both locally in NE Mexico and more broadly in speleothems. Utilizing a speleothem sample covering the Holocene and Late-Pleistocene, we demonstrate regional precipitation has a strong thermodynamic response that is spatially ubiquitous across most of Mesoamerica. Additionally, this dissertation provides the first speleothem sample covering the last millennium in Northern Mexico. In contrast to previous work, we demonstrate precipitation throughout Mexico is dominantly influenced by changes in Atlantic SSTs and suggest precipitation may increase in the future. We hope this work will assist in the tuning of climate models, improving projections of future rainfall and, overall, to a better our understanding of the Earth System.

1.8 References

Aggarwal, P. K., Fröhlich, K., Kulkarni, K. M., & Gourcy, L. L. (2004). Stable isotope evidence for moisture sources in the asian summer monsoon under present and past climate regimes. *Geophysical Research Letters*, *31*(8). doi: 10.1029/2004GL019911

Aggarwal, P. K., Romatschke, U., Araguas-Araguas, L., Belachew, D., Longstaae, F. J., Berg, P., … Funk, A. (2016). *Proportions of convective and stratiform precipitation revealed in water isotope ratios*. doi: 10.1038/NGEO2739

Araguás-Araguás, L., Froehlich, K., & Rozanski, K. (1998). Stable isotope composition of precipitation over southeast Asia. *Journal of Geophysical Research: Atmospheres*, *103*(D22), 28721–28742. doi: 10.1029/98JD02582

Ashouri, H., Hsu, K.-L., Sorooshian, S., Braithwaite, D. K., Knapp, K. R., Cecil, L. D., … Prat, O. P. (2015). PERSIANN-CDR: Daily Precipitation Climate Data Record from Multisatellite Observations for Hydrological and Climate Studies. *Bulletin of the American Meteorological Society*, *96*(1), 69–83. doi: 10.1175/BAMS-D-13-00068.1

Ayalon, A., Bar-Matthews, M., & Sass, E. (1998). Rainfall-recharge relationships within a karstic terrain in the Eastern Mediterranean semi-arid region, Israel: δ 18O and δD characteristics. *Journal of Hydrology*, *207*(1–2), 18–31. doi: 10.1016/S0022-1694(98)00119-X

Bajo, P., Borsato, A., Drysdale, R., Hua, Q., Frisia, S., Zanchetta, G., … Woodhead, J. (2017). Stalagmite carbon isotopes and dead carbon proportion (DCP) in a near-closed-system situation: An interplay between sulphuric and carbonic acid dissolution. *Geochimica et Cosmochimica Acta*, *210*, 208–227. doi: 10.1016/j.gca.2017.04.038

Baker, A., & Bradley, C. (2009). *Modern stalagmite δ 18 O: Instrumental calibration and forward modelling*. doi: 10.1016/j.gloplacha.2009.05.002

Baker, A., Ito, E., Smart, P. L., & McEwan, R. F. (1997). Elevated and variable values of 13C in speleothems in a British cave system. *Chemical Geology*, *136*(3–4), 263–270. doi: 10.1016/S0009-2541(96)00129-5

Baker, A., Smith, C., Jex, C., Fairchild, I., Genty, D., & Fuller, L. (2008). Annually laminated speleothems: a review. *International Journal of Speleology*, *37*(3), 4. doi: http://dx.doi.org/10.5038/1827-806X.37.3.4

Baldini, J. U. L., McDermott, F., Hoffmann, D. L., Richards, D. A., & Clipson, N. (2008). Very high-frequency and seasonal cave atmosphere PCO2 variability: Implications for stalagmite growth and oxygen isotope-based paleoclimate records. *Earth and Planetary Science Letters*, *272*(1–2), 118–129. doi: 10.1016/J.EPSL.2008.04.031

Beck, J. W., Richards, D. A., Edwards, R. L., Silverman, B. W., Smart, P. L., Donahue, D. J., … Biddulph, D. (2001). Extremely large variations of atmospheric 14C concentration during the last glacial period. *Science*, *292*(5526), 2453–2458. doi: 10.1126/science.1056649

Bereiter, B., Eggleston, S., Schmitt, J., Nehrbass-Ahles, C., Stocker, T. F., Fischer, H., … Chappellaz, J. (2015). Revision of the EPICA Dome C CO2 record from 800 to 600-kyr before present. *Geophysical Research Letters*, *42*(2), 542–549. doi: 10.1002/2014GL061957

Bernal, J. P., Lachniet, M., McCulloch, M., Mortimer, G., Morales, P., & Cienfuegos, E. (2011).

A speleothem record of Holocene climate variability from southwestern Mexico. *Quaternary Research*, *75*(01), 104–113. doi: 10.1016/j.yqres.2010.09.002

Bhattacharya, T., & Chiang, J. C. H. (2014). Spatial variability and mechanisms underlying El Niño-induced droughts in Mexico. *Climate Dynamics*, *43*(12), 3309–3326. doi: 10.1007/s00382-014-2106-8

Bhattacharya, T., Chiang, J. C. H., & Cheng, W. (2017). Ocean-atmosphere dynamics linked to 800–1050 CE drying in mesoamerica. *Quaternary Science Reviews*, *169*, 263–277. doi: 10.1016/j.quascirev.2017.06.005

Bhattacharya, T., & Coats, S. (2020). Atlantic-Pacific Gradients Drive Last Millennium Hydroclimate Variability in Mesoamerica. *Geophysical Research Letters*, *47*(13), e2020GL088061. doi: 10.1029/2020GL088061

Bony, S., Risi, C., & Vimeux, F. (2008). Influence of convective processes on the isotopic composition (δ18O and δD) of precipitation and water vapor in the tropics: 1. Radiative-convective equilibrium and Tropical Ocean–Global Atmosphere–Coupled Ocean-Atmosphere Response Experiment (TOGA-COARE) simulations. *Journal of Geophysical Research: Atmospheres*, *113*(D19), 19305. doi: 10.1029/2008JD009942

Borsato, A., Johnston, V. E., Frisia, S., Miorandi, R., Corradini, F., Au, (A, & Borsato,). (2016). Temperature and altitudinal influence on karst dripwater chemistry: Implications for regional-scale palaeoclimate reconstructions from speleothems Cosmogenic Cl-36 in speleothems as a potential solar proxy View project OLOAMBIENT View project Temperature and altitudinal influence on karst dripwater chemistry: Implications for regional-scale palaeoclimate reconstructions from speleothems. *Geochimica et Cosmochimica Acta*, *177*, 275–297. doi: 10.1016/j.gca.2015.11.043

Bradley, C., Baker, A., Jex, C. N., & Leng, M. J. (2010). Hydrological uncertainties in the modelling of cave drip-water δ18O and the implications for stalagmite palaeoclimate reconstructions. *Quaternary Science Reviews*, *29*(17–18), 2201–2214. doi: 10.1016/j.quascirev.2010.05.017

Breitenbach, S. F. M., Adkins, J. F., Meyer, H., Marwan, N., Kumar, K. K., & Haug, G. H. (2010). Strong influence of water vapor source dynamics on stable isotopes in precipitation observed in Southern Meghalaya, NE India. *Earth and Planetary Science Letters*, *292*(1–2), 212–220. doi: 10.1016/j.epsl.2010.01.038

Breitenbach, S. F. M., Rehfeld, K., Goswami, B., Baldini, J. U. L., Ridley, H. E., Kennett, D. J., … Marwan, N. (2012). Constructing proxy records from age models (COPRA). *Climate of the Past*, *8*(5), 1765–1779. doi: 10.5194/cp-8-1765-2012

Burns, S. J., Godfrey, L. R., Faina, P., Mcgee, D., Hardt, B., Ranivoharimanana, L., & Randrianasy, J. (2016). *Rapid human-induced landscape transformation in Madagascar at the end of the first millennium of the Common Era*. doi: 10.1016/j.quascirev.2016.01.007

Cai, Y., Fung, I. Y., Edwards, R. L., An, Z., Cheng, H., Lee, J. E., … Chiang, J. C. H. (2015). Variability of stalagmite-inferred Indian monsoon precipitation over the past 252,000 y. *Proceedings of the National Academy of Sciences of the United States of America*, *112*(10), 2954–2959. doi: 10.1073/pnas.1424035112

Cai, Z., & Tian, L. (2016). Atmospheric controls on seasonal and interannual variations in the precipitation isotope in the East Asian Monsoon region. *Journal of Climate*, *29*(4), 1339–1352. doi: 10.1175/JCLI-D-15-0363.1

Caley, T., Roche, D. M., & Renssen, H. (2014). Orbital Asian summer monsoon dynamics revealed using an isotope-enabled global climate model. *Nature Communications*, *5*(1), 1–6.

doi: 10.1038/ncomms6371
Chávez-Lara, C. M., Holtvoeth, J., Roy, P. D., & Pancost, R. D. (2019). Lipid biomarkers in lacustrine sediments of subtropical northeastern Mexico and inferred ecosystem changes during the late Pleistocene and Holocene. *Palaeogeography, Palaeoclimatology, Palaeoecology*, *535*. doi: 10.1016/j.palaeo.2019.109343
Chen, Z., Auler, A. S., Bakalowicz, M., Drew, D., Griger, F., Hartmann, J., … Goldscheider, N. (2017). The World Karst Aquifer Mapping project: concept, mapping procedure and map of Europe. *Hydrogeology Journal 2017 25:3*, *25*(3), 771–785. doi: 10.1007/S10040-016-1519-3
Cheng, H., Edwards, R. L., Sinha, A., Spötl, C., Yi, L., Chen, S., … Zhang, H. (2016). The Asian monsoon over the past 640,000 years and ice age terminations. *Nature*, *534*(7609), 640–646. doi: 10.1038/nature18591
Cheng, H., Lawrence Edwards, R., Shen, C. C., Polyak, V. J., Asmerom, Y., Woodhead, J., … Calvin Alexander, E. (2013). Improvements in 230Th dating, 230Th and 234U half-life values, and U-Th isotopic measurements by multi-collector inductively coupled plasma mass spectrometry. *Earth and Planetary Science Letters*, *371–372*, 82–91. doi: 10.1016/j.epsl.2013.04.006
Clemens, S. C., Prell, W. L., & Sun, Y. (2010). Orbital-scale timing and mechanisms driving Late Pleistocene Indo-Asian summer monsoons: Reinterpreting cave speleothem δ18O. *Paleoceanography*, *25*(4). doi: 10.1029/2010PA001926
Cross, M. (2015). PySPLIT: Package for the Generation, Analysis, and Visualization of HYSPLIT Air Parcel Trajectories. In *PROC*. Retrieved from https://www.youtube.com/watch?v=2mzhTC4Kp-Y
Cuthbert, M. O., Baker, A., Jex, C. N., Graham, P. W., Treble, P. C., Andersen, M. S., & Ian Acworth, R. (2014). Drip water isotopes in semi-arid karst: Implications for speleothem paleoclimatology. *Earth and Planetary Science Letters*, *395*, 194–204. doi: 10.1016/j.epsl.2014.03.034
Daëron, M., Drysdale, R. N., Peral, M., Huyghe, D., Blamart, D., Coplen, T. B., … Zanchetta, G. (2019). Most Earth-surface calcites precipitate out of isotopic equilibrium. *Nature Communications*, *10*(1), 1–7. doi: 10.1038/s41467-019-08336-5
Dansgaard, W. (1964). Stable isotopes in precipitation. *Tellus*, *16*(4), 436–468. doi: 10.3402/tellusa.v16i4.8993
Day, C. C., & Henderson, G. M. (2013). Controls on trace-element partitioning in cave-analogue calcite. *Geochimica et Cosmochimica Acta*, *120*, 612–627. doi: 10.1016/j.gca.2013.05.044
Dayem, K. E., Molnar, P., Battisti, D. S., & Roe, G. H. (2010). Lessons learned from oxygen isotopes in modern precipitation applied to interpretation of speleothem records of paleoclimate from eastern Asia. *Earth and Planetary Science Letters*, *295*(1–2), 219–230. doi: 10.1016/j.epsl.2010.04.003
Dee, S., Emile-Geay, J., Evans, M. N., Allam, A., Steig, E. J., & Thompson, D. M. (2015). PRYSM: An open-source framework for PRoxY System Modeling, with applications to oxygen-isotope systems. *Journal of Advances in Modeling Earth Systems*, *7*(3), 1220–1247. doi: 10.1002/2015MS000447
Deininger, M., Fohlmeister, J., Scholz, D., & Mangini, A. (2012). Isotope disequilibrium effects: The influence of evaporation and ventilation effects on the carbon and oxygen isotope composition of speleothems - A model approach. *Geochimica et Cosmochimica Acta*, *96*, 57–79. doi: 10.1016/j.gca.2012.08.013

Deininger, M., & Scholz, D. (2019). ISOLUTION 1.0: an ISOtope evoLUTION model describing the stable oxygen (δ18O) and carbon (δ13C) isotope values of speleothems. *International Journal of Speleology*, *48*(1), 21–32. doi: 10.5038/1827-806X.48.1.2219

Denniston, R. F., Houts, A. N., Asmerom, Y., Wanamaker, A. D., Haws, J. A., Polyak, V. J., … Bicho, N. F. (2018). A stalagmite test of North Atlantic SST and Iberian hydroclimate linkages over the last two glacial cycles. *Climate of the Past*, *14*(12), 1893–1913. doi: 10.5194/cp-14-1893-2018

Deplazes, G., Lückge, A., Peterson, L. C., Timmermann, A., Hamann, Y., Hughen, K. A., … Haug, G. H. (2013). Links between tropical rainfall and North Atlantic climate during the last glacial period. *Nature Geoscience*, *6*(3), 213–217. doi: 10.1038/ngeo1712

Dietzel, M., Tang, J., Leis, A., & Köhler, S. J. (2009). Oxygen isotopic fractionation during inorganic calcite precipitation - Effects of temperature, precipitation rate and pH. *Chemical Geology*, *268*(1–2), 107–115. doi: 10.1016/j.chemgeo.2009.07.015

Dorale, J. A. (1998). Climate and Vegetation History of the Midcontinent from 75 kyr to 25 kyr. A Speleothem Record from Crevice Cave, Missouri, USA. *Science*, *282*(5395), 1871–1874. doi: 10.1126/science.282.5395.1871

Dorale, J. A., & Liu, Z. (2009). Limitations of hendy test criteria in judging the paleoclimatic suitability of speleothems and the need for replication. In *Journal of Cave and Karst Studies* (Vol. 71). doi: PNR61

Dreybrodt, W., & Deininger, M. (2014). The impact of evaporation to the isotope composition of DIC in calcite precipitating water films in equilibrium and kinetic fractionation models. *Geochimica et Cosmochimica Acta*, *125*, 433–439. doi: 10.1016/j.gca.2013.10.004

Drysdale, R., Zanchetta, G., Hellstrom, J., Maas, R., Fallick, A., Pickett, M., … Piccini, L. (2006). Late Holocene drought responsible for the collapse of Old World civilizations is recorded in an Italian cave flowstone. *Geology*, *34*(2), 101–104. doi: 10.1130/G22103.1

Dubois, N., Kienast, M., Kienast, S., Normandeau, C., Calvert, S. E., Herbert, T. D., & Mix, A. (2011). Millennial-scale variations in hydrography and biogeochemistry in the Eastern Equatorial Pacific over the last 100 kyr. *Quaternary Science Reviews*, *30*(1–2), 210–223. doi: 10.1016/j.quascirev.2010.10.012

Dunning, N. P., Beach, T. P., & Luzzadder-Beach, S. (2012). Kax and kol: Collapse and resilience in lowland Maya civilization. *Proceedings of the National Academy of Sciences*, *109*(10), 3652–3657. doi: 10.1073/PNAS.1114838109

Dykoski, C. A., Lawrence Edwards, R., Cheng, H., Yuan, D., Cai, Y., Zhang, M., … Boyle, E. (2005). *A high-resolution, absolute-dated Holocene and deglacial Asian monsoon record from Dongge Cave, China*. doi: 10.1016/j.epsl.2005.01.036

Escobar, J., Hodell, D. A., Brenner, M., Curtis, J. H., Gilli, A., Mueller, A. D., … Guilderson, T. P. (2012). A ~43-ka record of paleoenvironmental change in the Central American lowlands inferred from stable isotopes of lacustrine ostracods. *Quaternary Science Reviews*, *37*, 92–104. doi: 10.1016/j.quascirev.2012.01.020

Fairchild, I., Baker, A., Borsato, A., & Frisia, S. (2001). Annual to sub-annual resolution of multiple trace-element trends in speleothems. *Article in Journal of the Geological Society*. doi: 10.1144/jgs.158.5.831

Fairchild, I. J., Smith, C. L., Baker, A., Fuller, L., Spötl, C., Mattey, D., … E.I.M.F. (2006). Modification and preservation of environmental signals in speleothems. *Earth-Science Reviews*, *75*(1–4), 105–153. doi: 10.1016/J.EARSCIREV.2005.08.003

Fairchild, I. J., & Treble, P. C. (2009). Trace elements in speleothems as recorders of

environmental change. *Quaternary Science Reviews*, *28*(5–6), 449–468. doi: 10.1016/j.quascirev.2008.11.007

Feng, S., Krueger, A. B., & Oppenheimer, M. (2010). Linkages among climate change, crop yields and Mexico-US cross-border migration. *Proceedings of the National Academy of Sciences of the United States of America*, *107*(32), 14257–14262. doi: 10.1073/pnas.1002632107

Feng, W., Banner, J. L., Guilfoyle, A. L., Musgrove, M. L., & James, E. W. (2012). Oxygen isotopic fractionation between drip water and speleothem calcite: A 10-year monitoring study, central Texas, USA. *Chemical Geology*, *304–305*, 53–67. doi: 10.1016/j.chemgeo.2012.02.004

Feng, W., Casteel, R. C., Banner, J. L., & Heinze-Fry, A. (2013). *Oxygen isotope variations in rainfall, drip-water and speleothem calcite from a well-ventilated cave in Texas, USA: Assessing a new speleothem temperature proxy*. doi: 10.1016/j.gca.2013.11.039

Fetter, C. W. (2014). Applied hydrogeology. 4th. In *Pearson*. Retrieved from http://sutlib2.sut.ac.th/sut_contents/H109081.pdf

Fohlmeister, J., Kromer, B., & Mangini, A. (2011). The influence of soil organic matter age spectrum on the reconstruction of atmospheric 14C levels via stalagmites. *Radiocarbon*, *53*(1), 99–115. doi: 10.1017/S003382220003438X

Fohlmeister, J., Voarintsoa, N. R. G., Lechleitner, F. A., Boyd, M., Brandtstätter, S., Jacobson, M. J., & Oster, J. L. (2020). Main controls on the stable carbon isotope composition of speleothems. *Geochimica et Cosmochimica Acta*, *279*, 67–87. doi: 10.1016/j.gca.2020.03.042

Ford, D. C. (2000). Deep phreatic caves and groundwater systems of the Sierra de El Abra, Mexico. *Speleogenesis: Evolution of Karst Aquifers: Huntsville, Alabama, National Speleological*, 325–331.

Frappier, A. B., Pyburn, J., Pinkey-Drobnis, A. D., Wang, X., Corbett, D. R., & Dahlin, B. H. (2014). Two millennia of tropical cyclone-induced mud layers in a northern Yucatán stalagmite: Multiple overlapping climatic hazards during the Maya Terminal Classic "megadroughts." *Geophysical Research Letters*, *41*(14), 5148–5157. doi: 10.1002/2014GL059882

Frappier, A. B., Sahagian, D., Carpenter, S. J., González, L. A., & Frappier, B. R. (2007). Stalagmite stable isotope record of recent tropic cyclone events. *Geology*, *35*(2), 111–114. doi: 10.1130/G23145A.1

Freitas, C. R. De, Littlbjohn, R. N., Clarkson, T. S., & Kristament, I. S. (1982). Cave climate: Assessment of airflow and ventilation. *Journal of Climatology*, *2*(4), 383–397. doi: 10.1002/JOC.3370020408

Frisia, S., Borsato, A., Fairchild, I. J., McDermott, F., & Selmo, E. M. (2002). Aragonite-calcite relationships in speleothems (Grotte de Clamouse, France): Environment, fabrics, and carbonate geochemistry. *Journal of Sedimentary Research*, *72*(5), 687–699. doi: 10.1306/020702720687

Frisia, S., Fairchild, I. J., Fohlmeister, J., Miorandi, R., Spötl, C., & Borsato, A. (2011). Carbon mass-balance modelling and carbon isotope exchange processes in dynamic caves. *Geochimica et Cosmochimica Acta*, *75*(2), 380–400. doi: 10.1016/J.GCA.2010.10.021

Frumkin, A., & Stein, M. (2004). The Sahara–East Mediterranean dust and climate connection revealed by strontium and uranium isotopes in a Jerusalem speleothem. *Earth and Planetary Science Letters*, *217*(3–4), 451–464. doi: 10.1016/S0012-821X(03)00589-2

Gabitov, R. I., & Watson, E. B. (2006). Partitioning of strontium between calcite and fluid. *Geochemistry, Geophysics, Geosystems*, *7*(11). doi: 10.1029/2005GC001216

Galy, V., François, L., France-Lanord, C., Faure, P., Kudrass, H., Palhol, F., & Singh, S. K. (2008). C4 plants decline in the Himalayan basin since the Last Glacial Maximum. *Quaternary Science Reviews*, *27*(13–14), 1396–1409. doi: 10.1016/J.QUASCIREV.2008.04.005

Gary, M. S. J. (2006). *Volcanogenic karstification of Sistema Zacatón, Mexico*. 79–89. doi: 10.1130/2006.2404(08)

Genty, D., & Massault, M. (1997). Bomb14C recorded in laminated speleothems: Calculation of dead carbon proportion. *Radiocarbon*, *39*(1), 33–48. doi: 10.1017/S0033822200040881

Genty, D., Massault, M., Gilmour, M., Baker, A., Verheyden, S., & Kepens, E. (1999). Calculation of past dead carbon proportion and variability by the comparison of AMS 14C and TIMS U/Th ages on two Holocene stalagmites. *Radiocarbon*, *41*(3), 251–270. doi: 10.1017/S003382220005712X

Gill, R. B., Mayewski, P. A., Nyberg, J., Haug, G. H., & Peterson, L. C. (2007). Drought and the maya collapse. *Ancient Mesoamerica*, *18*(2), 283–302. doi: 10.1017/S0956536107000193

Giorgetta, M. A., Jungclaus, J., Reick, C. H., Legutke, S., Bader, J., Böttinger, M., … Stevens, B. (2013). Climate and carbon cycle changes from 1850 to 2100 in MPI-ESM simulations for the Coupled Model Intercomparison Project phase 5. *Journal of Advances in Modeling Earth Systems*, *5*(3), 572–597. doi: 10.1002/jame.20038

Goede, A., McCulloch, M., McDermott, F., & Hawkesworth, C. (1998). Aeolian contribution to strontium and strontium isotope variations in a Tasmanian speleothem. *Chemical Geology*, *149*(1–2), 37–50. doi: 10.1016/S0009-2541(98)00035-7

Goldsmith, G. R., Allen, S. T., Braun, S., Engbersen, N., González-Quijano, C. R., Kirchner, J. W., & Siegwolf, R. T. W. (2019). Spatial variation in throughfall, soil, and plant water isotopes in a temperate forest. *Ecohydrology*, *12*(2), e2059. doi: 10.1002/ECO.2059

Gram, W. K., & Faaborg, J. (1997). The Distribution of Neotropical Migrant Birds Wintering in the El Cielo Biosphere Reserve, Tamaulipas, Mexico. *The Condor*, *99*(3), 658–670. doi: 10.2307/1370478

Griffiths, M. L., Drysdale, R. N., Vonhof, H. B., Gagan, M. K., Zhao, J. xin, Ayliffe, L. K., … Suwargadi, B. W. (2010). Younger Dryas-Holocene temperature and rainfall history of southern Indonesia from δ18O in speleothem calcite and fluid inclusions. *Earth and Planetary Science Letters*, *295*(1–2), 30–36. doi: 10.1016/j.epsl.2010.03.018

Griffiths, M. L., Fohlmeister, J., Drysdale, R. N., Hua, Q., Johnson, K. R., Hellstrom, J. C., … Zhao, J. x. (2012). Hydrological control of the dead carbon fraction in a Holocene tropical speleothem. *Quaternary Geochronology*, *14*, 81–93. doi: 10.1016/J.QUAGEO.2012.04.001

Griffiths, M. L., Johnson, K. R., Pausata, F. S. R., White, J. C., Henderson, G. M., Wood, C. T., … Sekhon, N. (2020). End of Green Sahara amplified mid- to late Holocene megadroughts in mainland Southeast Asia. *Nature Communications*, *11*(1), 4204. doi: 10.1038/s41467-020-17927-6

Griffiths, M. L., Kimbrough, A. K., Gagan, M. K., Drysdale, R. N., Cole, J. E., Johnson, K. R., … Hantoro, W. S. (2016). Western Pacific hydroclimate linked to global climate variability over the past two millennia. *Nature Communications*, *7*. doi: 10.1038/ncomms11719

Gutiérrez-García, G., Beramendi-Orosco, L. E., & Johnson, K. R. (2020). Climate-growth relationships of Pinus pseudostrobus from a tropical mountain cloud forest in northeast Mexico. *Dendrochronologia*, *64*, 125749. doi: 10.1016/j.dendro.2020.125749

Harman, C. J. (2015). Time-variable transit time distributions and transport: Theory and application to storage-dependent transport of chloride in a watershed. *Water Resources Research*, *51*(1), 1–30. doi: 10.1002/2014WR015707

Hartland, A., Fairchild, I. J., Lead, J. R., Borsato, A., Baker, A., Frisia, S., & Baalousha, M. (2012). From soil to cave: Transport of trace metals by natural organic matter in karst dripwaters. *Chemical Geology*, *304–305*, 68–82. doi: 10.1016/J.CHEMGEO.2012.01.032

Hartland, A., & Zitoun, R. (2018). Transition metal availability to speleothems controlled by organic binding ligands. *Geochem. Persp. Let*, *8*, 22–25. doi: 10.7185/geochemlet.1824

Hellstrom, J. (2006). U–Th dating of speleothems with high initial 230Th using stratigraphical constraint. *Quaternary Geochronology*, *1*(4), 289–295. doi: 10.1016/J.QUAGEO.2007.01.004

Hendy, C. H. (1971). *The isotopic geochemistry of speleothems-I. The calculation of the effects of different modes of formation on the isotopic composition of speleothems and their applicability as palaeoclimatic indicators* * (Vol. 35). Pergamon Press. Printed in Northern Ireland. Retrieved from Pergamon Press. Printed in Northern Ireland website: https://ac.els-cdn.com/001670377190127X/1-s2.0-001670377190127X-main.pdf?_tid=9d24d077-1c6a-4651-b253-c15525034ea9&acdnat=1549696557_a9657fa3d144aca8ac631b95b8603c45

Hodge, E., McDonald, J., Fischer, M., Redwood, D., Hual, Q., Levchenko, V., … Fink, D. (2011). Using the 14C bomb pulse to date young speleothems. In *Radiocarbon* (Vol. 53). doi: 10.1017/S0033822200056605

Hoggarth, J. A., Restall, M., Wood, J. W., & Kennett, D. J. (2017). Drought and its demographic effects in the maya lowlands. *Current Anthropology*, *58*(1), 82–113. doi: 10.1086/690046

Hu, C., Henderson, G. M., Huang, J., Xie, S., Sun, Y., & Johnson, K. R. (2008). Quantification of Holocene Asian monsoon rainfall from spatially separated cave records. *Earth and Planetary Science Letters*, *266*(3–4), 221–232. doi: 10.1016/j.epsl.2007.10.015

Hua, Q., Cook, D., Fohlmeister, J., Penny, D., Bishop, P., & Buckman, S. (2017). Radiocarbon Dating of a Speleothem Record of Paleoclimate for Angkor, Cambodia. *Radiocarbon*, *59*(6), 1873–1890. doi: 10.1017/RDC.2017.115

Huang, Y., Fairchild, I. J., Borsato, A., Frisia, S., Cassidy, N. J., McDermott, F., & Hawkesworth, C. J. (2001). Seasonal variations in Sr, Mg and P in modern speleothems (Grotta di Ernesto, Italy). *Chemical Geology*, *175*(3–4), 429–448. doi: 10.1016/S0009-2541(00)00337-5

Jaffey, A. H., Flynn, K. F., Glendenin, L. E., Bentley, W. C., & Essling, A. M. (1971). Precision measurement of half-lives and specific activities of U235 and U238. *Physical Review C*, *4*(5), 1889–1906. doi: 10.1103/PhysRevC.4.1889

James, E. W., Banner, J. L., & Hardt, B. (2015). A global model for cave ventilation and seasonal bias in speleothem paleoclimate records. *Geochemistry, Geophysics, Geosystems*, *16*(4), 1044–1051. doi: 10.1002/2014GC005658

John Bierhorst. (1992). *History and Mythology of the Aztecs: The Codex Chimalpopoca - Google Books*. Retrieved from https://books.google.com/books?hl=en&lr=&id=xErlvmBuakoC&oi=fnd&pg=PA1&dq=Bierhorst,+J.,+Ed.,+Trans.,+1992:+History+and+Mythology+of+the+Aztecs:+The+Codex+Chimalpopoca.+University+of+Arizona+Press,+238+pp.&ots=BuLIKOxdw9&sig=mGh1x__1DElEzd_sP_U_UY0BStU#v=

Johnson, K. R., Hu, C., Belshaw, N. S., & Henderson, G. M. (2006). Seasonal trace-element and stable-isotope variations in a Chinese speleothem: The potential for high-resolution

paleomonsoon reconstruction. *Earth and Planetary Science Letters*, *244*(1–2), 394–407. doi: 10.1016/j.epsl.2006.01.064
Johnson, R. (2011). Immigration as a Response Variable to Climate Change from Mexico into the United States. In *Journal of Alternative Perspectives in the Social Sciences* (Vol. 3).
Kennett, D. J., Breitenbach, S. F. M., Aquino, V. V., Asmerom, Y., Awe, J., Baldini, J. U. L., … Haug, G. H. (2012). Development and disintegration of maya political systems in response to climate change. *Science*, *338*(6108), 788–791. doi: 10.1126/science.1226299
Kim, S. T., & O'Neil, J. R. (1997). Equilibrium and nonequilibrium oxygen isotope effects in synthetic carbonates. *Geochimica et Cosmochimica Acta*, *61*(16), 3461–3475. doi: 10.1016/S0016-7037(97)00169-5
Knutti, R., & Sedláček, J. (2013). Robustness and uncertainties in the new CMIP5 climate model projections. *Nature Climate Change*, *3*(4), 369–373. doi: 10.1038/nclimate1716
Konecky, B. L., Noone, D. C., & Cobb, K. M. (2019). The Influence of Competing Hydroclimate Processes on Stable Isotope Ratios in Tropical Rainfall. *Geophysical Research Letters*, *46*(3), 1622–1633. doi: 10.1029/2018GL080188
Kovacs, S. E., Reinhardt, E. G., Stastna, M., Coutino, A., Werner, C., Collins, S. V., … Le Maillot, C. (2017). Hurricane Ingrid and Tropical Storm Hanna's effects on the salinity of the coastal aquifer, Quintana Roo, Mexico. *Journal of Hydrology*, *551*, 703–714. doi: 10.1016/J.JHYDROL.2017.02.024
Kovaltsov, G. A., Mishev, A., & Usoskin, I. G. (2012). A new model of cosmogenic production of radiocarbon 14C in the atmosphere. *Earth and Planetary Science Letters*, *337–338*, 114–120. doi: 10.1016/j.epsl.2012.05.036
Kurczyn, J. A., Appendini, C. M., Beier, E., Sosa-López, A., López-González, J., & Posada-Vanegas, G. (2021). Oceanic and atmospheric impact of central American cold surges (Nortes) in the Gulf of Mexico. *International Journal of Climatology*, *41*(S1), E1450–E1468. doi: 10.1002/joc.6779
Kurita, N., Ichiyanagi, K., Matsumoto, J., Yamanaka, M. D., & Ohata, T. (2009). The relationship between the isotopic content of precipitation and the precipitation amount in tropical regions. *Journal of Geochemical Exploration*, *102*(3), 113–122. doi: 10.1016/J.GEXPLO.2009.03.002
Lachniet, M. S. (2009). Climatic and environmental controls on speleothem oxygen-isotope values. *Quaternary Science Reviews*, *28*(5–6), 412–432. doi: 10.1016/j.quascirev.2008.10.021
Lachniet, M. S., Asmerom, Y., Bernal, J. P., Polyak, V. J., & Vazquez-Selem, L. (2013). Orbital pacing and ocean circulation-induced collapses of the Mesoamerican monsoon over the past 22,000 y. *Proceedings of the National Academy of Sciences of the United States of America*, *110*(23), 9255–9260. doi: 10.1073/pnas.1222804110
Lachniet, M. S., Asmerom, Y., Polyak, V., & Bernal, J. P. (2017). Two millennia of Mesoamerican monsoon variability driven by Pacific and Atlantic synergistic forcing. *Quaternary Science Reviews*, *155*, 100–113. doi: 10.1016/j.quascirev.2016.11.012
Lachniet, M. S., Bernal, J. P., Asmerom, Y., Polyak, V., & Piperno, D. (2012). A 2400 yr Mesoamerican rainfall reconstruction links climate and cultural change. *Geology*, *40*(3), 259–262. doi: 10.1130/G32471.1
Lachniet, M. S., Burns, S. J., Piperno, D. R., Asmerom, Y., Polyak, V. J., Moy, C. M., & Christenson, K. (2004). A 1500-year El Niño/Southern Oscillation and rainfall history for the Isthmus of Panama from speleothem calcite. *Journal of Geophysical Research D:*

Atmospheres, *109*(20), 20117. doi: 10.1029/2004JD004694
Lachniet, M. S., & Patterson, W. P. (2009). Oxygen isotope values of precipitation and surface waters in northern Central America (Belize and Guatemala) are dominated by temperature and amount effects. *Earth and Planetary Science Letters*, *284*(3–4), 435–446. doi: 10.1016/J.EPSL.2009.05.010
Lachniet, M. S., Patterson, W. P., Burns, S., Asmerom, Y., & Polyak, V. (2007). Caribbean and Pacific moisture sources on the Isthmus of Panama revealed from stalagmite and surface water δ18O gradients. *Geophysical Research Letters*, *34*(1). doi: 10.1029/2006GL028469
Landsea, C. W., & Franklin, J. L. (2013). Atlantic Hurricane Database Uncertainty and Presentation of a New Database Format. *Monthly Weather Review*, *141*(10), 3576–3592. doi: 10.1175/MWR-D-12-00254.1
Lases-Hernández, F., Medina-Elizalde, M., & Benoit Frappier, A. (2020). Drip water δ18O variability in the northeastern Yucatán Peninsula, Mexico: Implications for tropical cyclone detection and rainfall reconstruction from speleothems. *Geochimica et Cosmochimica Acta*, *285*, 237–256. doi: 10.1016/J.GCA.2020.07.008
Lawrence Edwards, R., Chen, J. H., & Wasserburg, G. J. (1987). 238U234U230Th232Th systematics and the precise measurement of time over the past 500,000 years. *Earth and Planetary Science Letters*, *81*(2–3), 175–192. doi: 10.1016/0012-821X(87)90154-3
Lea, D. W., Pak, D. K., Peterson, L. C., & Hughen, K. A. (2003). Synchroneity of tropical and high-latitude Atlantic temperatures over the last glacial termination. *Science*, *301*(5638), 1361–1364. doi: 10.1126/science.1088470
Lentz, D. L., Dunning, N. P., Scarborough, V. L., & Grazioso, L. (2018). Imperial resource management at the ancient Maya city of Tikal: A resilience model of sustainability and collapse. *Journal of Anthropological Archaeology*, *52*, 113–122. doi: 10.1016/J.JAA.2018.08.005
Lewis, S. C., LeGrande, A. N., Kelley, M., & Schmidt, G. A. (2010). Water vapour source impacts on oxygen isotope variability in tropical precipitation during Heinrich events. *Climate of the Past* , 87–133. doi: 10.5194/cpd-6-87-2010
Liu, W. J., Li, P. J., Li, H. M., & Duan, W. P. (2006). Estimation of evaporation rate from soil surface using stable isotopic composition of throughfall and stream water in a tropical seasonal rain forest in Xishuangbanna, China. *Acta Ecologica Sinica*, *26*(5), 1303–1311. doi: 10.1016/s1872-2032(06)60022-x
Lynch-Stieglitz, J., Schmidt, M. W., Gene Henry, L., Curry, W. B., Skinner, L. C., Mulitza, S., … Chang, P. (2014). Muted change in Atlantic overturning circulation over some glacial-aged Heinrich events. *Nature Geoscience*, *7*(2), 144–150. doi: 10.1038/ngeo2045
Lyu, Y., Luo, W., Wang, Y., Zeng, G., Wang, Y., Cheng, A., … Wang, S. (2020). *Impacts of cave ventilation on drip water δ 13 C DIC and its paleoclimate implication*. doi: 10.1016/j.quaint.2020.03.050
Magaña, V. O., Vázquez, J. L., Pérez, J. L., & Pérez, J. B. (2003). Impact of El Niño on precipitation in Mexico . *Geofísica Internacional* , *42*(3), 313–330. Retrieved from http://www.redalyc.org/articulo.oa?id=56842304
Marks, G. S. (2020). Investigating Mexican paleoclimate with precisely dated speleothems. In *Investigating Mexican paleoclimate with precisely dated speleothems*. Massachusetts Institute of Technology. doi: 10.1575/1912/26101
Martín-Chivelet, J., Belén Muñoz-García, M., Cruz, J. A., Ortega, A. I., Turrero, M. J., & Jones, B. (2017). *Speleothem Architectural Analysis: Integrated approach for stalagmite-based*

paleoclimate research. doi: 10.1016/j.sedgeo.2017.03.003
McDermott, F. (2004). Palaeo-climate reconstruction from stable isotope variations in speleothems: a review. *Quaternary Science Reviews*, *23*(7–8), 901–918. doi: 10.1016/J.QUASCIREV.2003.06.021
Medina-Elizalde, M., Burns, S. J., Lea, D. W., Asmerom, Y., von Gunten, L., Polyak, V., … Karmalkar, A. (2010a). High resolution stalagmite climate record from the Yucatán Peninsula spanning the Maya terminal classic period. *Earth and Planetary Science Letters*, *298*(1–2), 255–262. doi: 10.1016/J.EPSL.2010.08.016
Medina-Elizalde, M., Burns, S. J., Lea, D. W., Asmerom, Y., von Gunten, L., Polyak, V., … Karmalkar, A. (2010b). High resolution stalagmite climate record from the Yucatán Peninsula spanning the Maya terminal classic period. *Earth and Planetary Science Letters*, *298*(1–2), 255–262. doi: 10.1016/j.epsl.2010.08.016
Medina-Elizalde, M., Burns, S. J., Polanco-Martínez, J. M., Beach, T., Lases-Hernández, F., Shen, C. C., & Wang, H. C. (2016). High-resolution speleothem record of precipitation from the Yucatan Peninsula spanning the Maya Preclassic Period. *Global and Planetary Change*, *138*, 93–102. doi: 10.1016/j.gloplacha.2015.10.003
Medina-Elizalde, M., & Rohling, E. J. (2012). Collapse of Classic Maya Civilization Related to Modest Reduction in Precipitation. *Science* . doi: 10.1126/science.1216629
Méndez, M., & Magaña, V. (2010). Regional aspects of prolonged meteorological droughts over Mexico and central America. *Journal of Climate*, *23*(5), 1175–1188. doi: 10.1175/2009JCLI3080.1
Mestas-Nuñez, A. M., Enfield, D. B., & Zhang, C. (2007). Water vapor fluxes over the Intra-Americas Sea: Seasonal and interannual variability and associations with rainfall. *Journal of Climate*, *20*(9), 1910–1922. doi: 10.1175/JCLI4096.1
Meyer, K. W., Feng, W., Breecker, D. O., Banner, J. L., & Guilfoyle, A. (2014). Interpretation of speleothem calcite δ13C variations: Evidence from monitoring soil CO2, drip water, and modern speleothem calcite in central Texas. *Geochimica et Cosmochimica Acta*, *142*, 281–298. doi: 10.1016/j.gca.2014.07.027
Mickler, P. J., Banner, J. L., Stern, L., Asmerom, Y., Edwards, R. L., & Ito, E. (2004). Stable isotope variations in modern tropical speleothems: Evaluating equilibrium vs. kinetic isotope effects. *Geochimica et Cosmochimica Acta*, *68*(21), 4381–4393. doi: 10.1016/j.gca.2004.02.012
Mickler, P. J., Carlson, P., Banner, J. L., Breecker, D. O., Stern, L., & Guilfoyle, A. (2019). Quantifying carbon isotope disequilibrium during in-cave evolution of drip water along discreet flow paths. *Geochimica et Cosmochimica Acta*, *244*, 182–196. doi: 10.1016/j.gca.2018.09.027
Mickler, P. J., Stern, L. A., & Banner, J. L. (2006). Large kinetic isotope effects in modern speleothems. *GSA Bulletin*, *118*(1–2), 65–81. doi: 10.1130/B25698.1
Mischel, S. A., Scholz, D., & Spötl, C. (2015). δ18O values of cave drip water: a promising proxy for the reconstruction of the North Atlantic Oscillation? *Climate Dynamics*, *45*(11–12), 3035–3050. doi: 10.1007/s00382-015-2521-5
Moreau-Le Golvan, Y., Michelot, J. L., & Boisson, J. Y. (1997). Stable isotope contents of porewater in a claystone formation (Tournemire, France): Assessment of the extraction technique and preliminary results. *Applied Geochemistry*, *12*(6), 739–745. doi: 10.1016/S0883-2927(97)00044-9
Morse, J. W., & Bender, M. L. (1990). Partition coefficients in calcite: Examination of factors

influencing the validity of experimental results and their application to natural systems. *Chemical Geology*, *82*(C), 265–277. doi: 10.1016/0009-2541(90)90085-L

Mühlinghaus, C., Scholz, D., & Mangini, A. (2007). Modelling stalagmite growth and δ13C as a function of drip interval and temperature>. *Geochimica et Cosmochimica Acta*, *71*(11), 2780–2790. doi: 10.1016/j.gca.2007.03.018

Mühlinghaus, C., Scholz, D., & Mangini, A. (2009). Modelling fractionation of stable isotopes in stalagmites. *Geochimica et Cosmochimica Acta*, *73*(24), 7275–7289. doi: 10.1016/j.gca.2009.09.010

Murray-Tortarolo, G. N., & Salgado, M. M. (2021). Drought as a driver of Mexico-US migration. *Climatic Change*, *164*(3–4), 1–11. doi: 10.1007/s10584-021-03030-2

Nguyen, P., Shearer, E. J., Tran, H., Ombadi, M., Hayatbini, N., Palacios, T., … Sorooshian, S. (2019). The CHRS data portal, an easily accessible public repository for PERSIANN global satellite precipitation data. *Scientific Data*, *6*(1), 1–10. doi: 10.1038/sdata.2018.296

Noronha, A. L., Johnson, K. R., Southon, J. R., Hu, C., Ruan, J., & McCabe-Glynn, S. (2015). Radiocarbon evidence for decomposition of aged organic matter in the vadose zone as the main source of speleothem carbon. *Quaternary Science Reviews*, *127*, 37–47. doi: 10.1016/J.QUASCIREV.2015.05.021

Oerter, E., Finstad, K., Schaefer, J., Goldsmith, G. R., Dawson, T., & Amundson, R. (2014). Oxygen isotope fractionation effects in soil water via interaction with cations (Mg, Ca, K, Na) adsorbed to phyllosilicate clay minerals. *Journal of Hydrology*, *515*, 1–9. doi: 10.1016/j.jhydrol.2014.04.029

Osácar, M. C., Sancho, C., Muñoz, A., Moreno, A., Bartolomé, M., Pérez, C., … Stoll, H. (2017). δ13C and Mg/Ca dripwater response to environmental conditions in the Ortigosa caves (La Rioja, Spain). *Geogaceta*, *61*, 175–178.

Osorio-Osorio, J. A., Astudillo-Sánchez, C. C., Villanueva-Díaz, J., Soria-Díaz, L., & Vargas-Tristán, V. (2020). Historical precipitation reconstruction of el cielo biosphere reserve, Mexico, using taxodium mucronatum (Cupressaceae) annual growth rings. *Revista de Biologia Tropical*, *68*(3), 818–832. doi: 10.15517/RBT.V68I3.39624

Oster, J. L., Montañez, I. P., Guilderson, T. P., Sharp, W. D., & Banner, J. L. (2010). Modeling speleothem δ13C variability in a central Sierra Nevada cave using 14C and 87Sr/86Sr. *Geochimica et Cosmochimica Acta*, *74*(18), 5228–5242. doi: 10.1016/j.gca.2010.06.030

Palmer, M. V., & Palmer, A. N. (2012). Petrographic and isotopic evidence for late-stage processes in sulfuric acid caves of the Guadalupe Mountains, New Mexico, USA. *International Journal of Speleology*, *41*(2), 231–250. doi: 10.5038/1827-806X.41.2.10

Pausata, F. S. R., Battisti, D. S., Nisancioglu, K. H., & Bitz, C. M. (2011). Chinese stalagmite δ 18 O controlled by changes in the indian monsoon during a simulated heinrich event. *Nature Geoscience*, *4*(7), 474–480. doi: 10.1038/ngeo1169

Pavia, E. G., Graef, F., & Reyes, J. (2006). PDO–ENSO Effects in the Climate of Mexico. *Journal of Climate*, *19*(24), 6433–6438. doi: 10.1175/JCLI4045.1

Pérez Quezadas, J., Cortés Silva, A., Inguaggiato, S., del Rocío Salas Ortega, M., Cervantes Pérez, J., & Heilweil, V. M. (2015). Meteoric isotopic gradient on the windward side of the sierra madre oriental area, Veracruz - Mexico. *Geofisica Internacional*, *54*(3), 267–276. doi: 10.1016/j.gi.2015.04.021

Quezadas, J. P., Adams, D., Sánchez Murillo, R., Lagunes, A. J., & Rodríguez Castañeda, J. L. (2021). Isotopic variability (δ18O, δ2H and d-excess) during rainfall events of the north American monsoon across the Sonora River Basin, Mexico. *Journal of South American*

Earth Sciences, *105*, 102928. doi: 10.1016/j.jsames.2020.102928
Quiroz-Jiménez, J. D., Roy, P. D., Beramendi-Orosco, L. E., Lozano-García, S., & Vázquez-Selem, L. (2018). Orbital-scale droughts in central-northern Mexico during the late Quaternary and comparison with other subtropical and tropical records. *Geological Journal*, *53*(1), 230–242. doi: 10.1002/gj.2888
Rasmussen, S. O., Andersen, K. K., Svensson, A. M., Steffensen, J. P., Vinther, B. M., Clausen, H. B., … Ruth, U. (2006). A new Greenland ice core chronology for the last glacial termination. *Journal of Geophysical Research Atmospheres*, *111*(6), D06102. doi: 10.1029/2005JD006079
Reimer, P. J., Bard, E., Bayliss, A., Beck, J. W., Blackwell, P. G., Ramsey, C. B., … van der Plicht, J. (2013). Selection and Treatment of Data for Radiocarbon Calibration: An Update to the International Calibration (IntCal) Criteria. *Radiocarbon*, *55*(4), 1923–1945. doi: 10.2458/azu_js_rc.55.16955
Riechelmann, D. F. C., Deininger, M., Scholz, D., Riechelmann, S., Schröder-Ritzrau, A., Spötl, C., … Immenhauser, A. (2013). Disequilibrium carbon and oxygen isotope fractionation in recent cave calcite: Comparison of cave precipitates and model data. *Geochimica et Cosmochimica Acta*, *103*, 232–244. doi: 10.1016/j.gca.2012.11.002
Riechelmann, D. F. C., Schröder-Ritzrau, A., Scholz, D., Fohlmeister, J., Spötl, C., Richter, D. K., & Mangini, A. (2011). Monitoring Bunker Cave (NW Germany): A prerequisite to interpret geochemical proxy data of speleothems from this site. *Journal of Hydrology*, *409*(3–4), 682–695. doi: 10.1016/J.JHYDROL.2011.08.068
Risi, C., Bony, S., & Vimeux, F. (2008). Influence of convective processes on the isotopic composition (δ^{18} O and δ D) of precipitation and water vapor in the tropics: 2. Physical interpretation of the amount effect. *Journal of Geophysical Research*, *113*(D19), D19306. doi: 10.1029/2008JD009943
Rivera-Rivera, D. M., Chidambaram, S., Tirumalesh, K., Escobedo-Urias, D. C., Sujitha, S. B., Rodriguez-Espinosa, P. F., … Jonathan, M. P. (2021). Stable isotopic (δ2H, δ18O) monograms of winter precipitation events and hydro-climatic dynamics in Central Mexico. *Atmospheric Research*, *261*, 105744. doi: 10.1016/j.atmosres.2021.105744
Roy, P. D., Quiroz-Jiménez, J. D., Pérez-Cruz, L. L., Lozano-García, S., Metcalfe, S. E., Lozano-Santacruz, R., … Romero, F. M. (2013a). Late Quaternary paleohydrological conditions in the drylands of northern Mexico: A summer precipitation proxy record of the last 80 cal ka BP. *Quaternary Science Reviews*, *78*, 342–354. doi: 10.1016/j.quascirev.2012.11.020
Roy, P. D., Rivero-Navarette, A., Lopez-Balbiaux, N., Pérez-Cruz, L. L., Metcalfe, S. E., Sankar, G. M., & Sánchez-Zavala, J. L. (2013b). A record of Holocene summer-season palaeohydrological changes from the southern margin of Chihuahua Desert (Mexico) and possible forcings. *The Holocene*, *23*(8), 1105–1114. doi: 10.1177/0959683613483619
Roy, P. D., Rivero-Navarrete, A., Sánchez-Zavala, J. L., Beramendi-Orosco, L. E., Muthu-Sankar, G., & Lozano-Santacruz, R. (2016). Atlantic Ocean modulated hydroclimate of the subtropical northeastern Mexico since the last glacial maximum and comparison with the southern US. *Earth and Planetary Science Letters*, *434*, 141–150. doi: 10.1016/j.epsl.2015.11.048
Roy, P. D., Vera-Vera, G., Sánchez-Zavala, J. L., Shanahan, T. M., Quiroz-Jiménez, J. D., Curtis, J. H., … Muthusankar, G. (2020). Depositional histories of vegetation and rainfall intensity in Sierra Madre Oriental Mountains (northeast Mexico) since the late Last Glacial.

Global and Planetary Change, *187*(July 2019), 103136. doi: 10.1016/j.gloplacha.2020.103136

Rudzka, D., McDermott, F., Baldini, L. M., Fleitmann, D., Moreno, A., & Stoll, H. (2011). The coupled δ13C-radiocarbon systematics of three Late Glacial/early Holocene speleothems; insights into soil and cave processes at climatic transitions. *Geochimica et Cosmochimica Acta*, *75*(15), 4321–4339. doi: 10.1016/j.gca.2011.05.022

Salinas-Rodríguez, M. M., Estrada-Castillón, E., & Illarreal-Quintanilla, J. A. (2017). Endemic vascular plants of the sierra madre oriental, Mexico. *Phytotaxa*, *328*(1), 1–52. doi: 10.11646/PHYTOTAXA.328.1.1

Sánchez-Murillo, R., Birkel, C., Welsh, K., Esquivel-Hernández, G., Corrales-Salazar, J., Boll, J., … Araguás-Araguás, L. J. (2016). Key drivers controlling stable isotope variations in daily precipitation of Costa Rica: Caribbean Sea versus Eastern Pacific Ocean moisture sources. *Quaternary Science Reviews*, *131*, 250–261. doi: 10.1016/J.QUASCIREV.2015.08.028

Sánchez-Murillo, R., Esquivel-Hernández, G., Welsh, K., Brooks, E. S., Boll, J., Alfaro-Solís, R., … Valdés-González, J. (2013). Spatial and Temporal Variation of Stable Isotopes in Precipitation across Costa Rica: An Analysis of Historic GNIP Records. *Open Journal of Modern Hydrology*, *3*(4), 226–240. doi: 10.4236/OJMH.2013.34027

Schmidt, M. W., Spero, H. J., & Lea, D. W. (2004). Links between salinity variation in the Caribbean and North Atlantic thermohaline circulation. *Nature*, *428*(6979), 160–163. doi: 10.1038/nature02346

Schwarcz, H. P., Harmon, R. S., Thompson, P., & Ford, D. C. (1976). Stable isotope studies of fluid inclusions in speleothems and their paleoclimatic significance. *Geochimica et Cosmochimica Acta*, *40*(6), 657–665. doi: 10.1016/0016-7037(76)90111-3

Seager, R., Ting, M., Davis, M., & Stahle, D. W. (2009). Mexican drought: an observational modeling and tree ring study of variability and climate change. In *Atmósfera* (Vol. 22). Retrieved from http://ingrid.ldeo.columbia.edu/SOURCES/UNAM/

Shen, C.-C., Lin, K., Duan, W., Jiang, X., Partin, J. W., Edwards, R. L., … Tan, M. (2013). Testing the annual nature of speleothem banding. *Scientific Reports 2013 3:1*, *3*(1), 1–5. doi: 10.1038/srep02633

Shultz, J. M., Berg, R. C., Kossin, J. P., Burkle Jr, F., Maggioni, A., Pinilla Escobar, V. A., … Galea, S. (2021). Convergence of climate-driven hurricanes and COVID-19: The impact of 2020 hurricanes Eta and Iota on Nicaragua. *The Journal of Climate Change and Health*, *3*, 100019. doi: 10.1016/j.joclim.2021.100019

Sinclair, D. J., Banner, J. L., Taylor, F. W., Partin, J., Jenson, J., Mylroie, J., … Miklavič, B. (2012). Magnesium and strontium systematics in tropical speleothems from the Western Pacific. *Chemical Geology*, *294–295*, 1–17. doi: 10.1016/J.CHEMGEO.2011.10.008

Smith, C. L., Fairchild, I. J., Spötl, C., Frisia, S., Borsato, A., Moreton, S. G., & Wynn, P. M. (2009). Chronology building using objective identification of annual signals in trace element profiles of stalagmites. *Quaternary Geochronology*, *4*(1), 11–21. doi: 10.1016/j.quageo.2008.06.005

Southon, J., Noronha, A. L., Cheng, H., Edwards, R. L., & Wang, Y. (2012). A high-resolution record of atmospheric 14C based on Hulu Cave speleothem H82. *Quaternary Science Reviews*, *33*, 32–41. doi: 10.1016/j.quascirev.2011.11.022

Spötl, C., Fairchild, I. J., & Tooth, A. F. (2005). Cave air control on dripwater geochemistry, Obir Caves (Austria): Implications for speleothem deposition in dynamically ventilated

caves. *Geochimica et Cosmochimica Acta*, *69*(10), 2451–2468. doi: 10.1016/J.GCA.2004.12.009

Spötl, C., Mangini, A., & Richards, D. A. (2006). Chronology and paleoenvironment of Marine Isotope Stage 3 from two high-elevation speleothems, Austrian Alps. *Quaternary Science Reviews*, *25*(9–10), 1127–1136. doi: 10.1016/j.quascirev.2005.10.006

Sprenger, M., Leistert, H., Gimbel, K., & Weiler, M. (2016). Illuminating hydrological processes at the soil-vegetation-atmosphere interface with water stable isotopes. *Reviews of Geophysics*, *54*(3), 674–704. doi: 10.1002/2015RG000515

Sprenger, M., Tetzlaff, D., Buttle, J., Laudon, H., Leistert, H., Mitchell, C. P. J., … Soulsby, C. (2018). Measuring and Modeling Stable Isotopes of Mobile and Bulk Soil Water. *Vadose Zone Journal*, *17*(1), 170149. doi: 10.2136/vzj2017.08.0149

Stahle, D. W., Burnette, D. J., Villanueva, J., Cerano, J., Fye, F. K., Griffin, R. D., … Wolff, K. P. (2012). Tree-ring analysis of ancient baldcypress trees and subfossil wood. *Quaternary Science Reviews*, *34*, 1–15. doi: 10.1016/J.QUASCIREV.2011.11.005

Stahle, D. W., Cook, E. R., Burnette, D. J., Villanueva, J., Cerano, J., Burns, J. N., … Howard, I. M. (2016, October 1). The Mexican Drought Atlas: Tree-ring reconstructions of the soil moisture balance during the late pre-Hispanic, colonial, and modern eras. *Quaternary Science Reviews*, Vol. 149, pp. 34–60. Pergamon. doi: 10.1016/j.quascirev.2016.06.018

Stein, A. F., Draxler, R. R., Rolph, G. D., Stunder, B. J. B., Cohen, M. D., & Ngan, F. (2015, December 1). Noaa's hysplit atmospheric transport and dispersion modeling system. *Bulletin of the American Meteorological Society*, Vol. 96, pp. 2059–2077. American Meteorological Society. doi: 10.1175/BAMS-D-14-00110.1

Stoll, H. M., Müller, W., & Prieto, M. (2012). I-STAL, a model for interpretation of Mg/Ca, Sr/Ca and Ba/Ca variations in speleothems and its forward and inverse application on seasonal to millennial scales. *Geochemistry, Geophysics, Geosystems*, *13*(9). doi: 10.1029/2012GC004183

Tooth, A. F., & Fairchild, I. J. (2003). Soil and karst aquifer hydrological controls on the geochemical evolution of speleothem-forming drip waters, Crag Cave, southwest Ireland. *Journal of Hydrology*, *273*(1–4), 51–68. doi: 10.1016/S0022-1694(02)00349-9

Treble, P. C., Fairchild, I. J., Griffiths, A., Baker, A., Meredith, K. T., Wood, A., & McGuire, E. (2015). Impacts of cave air ventilation and in-cave prior calcite precipitation on Golgotha Cave dripwater chemistry, southwest Australia. *Quaternary Science Reviews*, *127*, 61–72. doi: 10.1016/j.quascirev.2015.06.001

Treble, P., Shelley, J. M. G., & Chappell, J. (2003). Comparison of high resolution sub-annual records of trace elements in a modern (1911–1992) speleothem with instrumental climate data from southwest Australia. *Earth and Planetary Science Letters*, *216*(1–2), 141–153. doi: 10.1016/S0012-821X(03)00504-1

U.S. Customs and Border Protection. (2021). US Border Patrol Apprehensions Southwest land Border Encounters per year. *U.S. Customs and Border ProtectionU.S. Customs and Border Protection*. Retrieved from https://www.cbp.gov/newsroom/stats/southwest-land-border-encounters

Villanueva-Diaz, J., Stahle, D. W., Luckman, B. H., Cerano-Paredes, J., Therrell, M. D., Cleaveland, M. K., & Cornejo-Oviedo, E. (2007). Winter-spring precipitation reconstructions from tree rings for northeast Mexico. *Climatic Change*, *83*(1–2), 117–131. doi: 10.1007/s10584-006-9144-0

Vuille, M., & Werner, M. (2005). Stable isotopes in precipitation recording South American

summer monsoon and ENSO variability: Observations and model results. *Climate Dynamics*, *25*(4), 401–413. doi: 10.1007/s00382-005-0049-9
Waelbroeck, C., Labeyrie, L., Michel, E., Duplessy, J. C., Mcmanus, J. F., Lambeck, K., … Labracherie, M. (2002). Sea-level and deep water temperature changes derived from benthic foraminifera isotopic records. In *Quaternary Science Reviews* (Vol. 21).
Wagner, J. D. M., Cole, J. E., Beck, J. W., Patchett, P. J., Henderson, G. M., & Barnett, H. R. (2010). Moisture variability in the southwestern United States linked to abrupt glacial climate change. *Nature Geoscience*, *3*(2), 110–113. doi: 10.1038/ngeo707
Wang, C., Enfield, D. B., Lee, S. K., & Landsea, C. W. (2006). Influences of the Atlantic warm pool on western hemisphere summer rainfall and Atlantic hurricanes. *Journal of Climate*, *19*(12), 3011–3028. doi: 10.1175/JCLI3770.1
Wang, C., Liu, H., Lee, S. K., & Atlas, R. (2011). Impact of the Atlantic warm pool on United States landfalling hurricanes. *Geophysical Research Letters*, *38*(19), n/a-n/a. doi: 10.1029/2011GL049265
Wang, Y., Cheng, H., Edwards, R. L., Kong, X., Shao, X., Chen, S., … An, Z. (2008). Millennial- and orbital-scale changes in the East Asian monsoon over the past 224,000 years. *Nature*, *451*(7182), 1090–1093. doi: 10.1038/nature06692
Wang, Y. J., Cheng, H., Edwards, R. L., An, Z. S., Wu, J. Y., Shen, C. C., & Dorale, J. A. (2001). A high-resolution absolute-dated late Pleistocene Monsoon record from Hulu Cave, China. *Science (New York, N.Y.)*, *294*(5550), 2345–2348. doi: 10.1126/science.1064618
Warken, S. F., Scholz, D., Spötl, C., Jochum, K. P., Pajón, J. M., Bahr, A., & Mangini, A. (2019). Caribbean hydroclimate and vegetation history across the last glacial period. *Quaternary Science Reviews*, *218*, 75–90. doi: 10.1016/j.quascirev.2019.06.019
Webster, J. W., Brook, G. A., Railsback, L. B., Cheng, H., Edwards, R. L., Alexander, C., & Reeder, P. P. (2007). Stalagmite evidence from Belize indicating significant droughts at the time of Preclassic Abandonment, the Maya Hiatus, and the Classic Maya collapse. *Palaeogeography, Palaeoclimatology, Palaeoecology*, *250*(1–4), 1–17. doi: 10.1016/j.palaeo.2007.02.022
Williams, P. W., King, D. N. T., Zhao, J. X., & Collerson, K. D. (2005). Late Pleistocene to Holocene composite speleothem 18O and 13C chronologies from South Island, New Zealand - Did a global Younger Dryas really exist? *Earth and Planetary Science Letters*, *230*(3–4), 301–317. doi: 10.1016/j.epsl.2004.10.024
Wong, C. I., Banner, J. L., & Musgrove, M. L. (2011). Seasonal dripwater Mg/Ca and Sr/Ca variations driven by cave ventilation: Implications for and modeling of speleothem paleoclimate records. *Geochimica et Cosmochimica Acta*, *75*(12), 3514–3529. doi: 10.1016/j.gca.2011.03.025
Wong, C. I., Banner, J. L., & Musgrove, M. L. (2015). Holocene climate variability in Texas, USA: An integration of existing paleoclimate data and modeling with a new, high-resolution speleothem record. *Quaternary Science Reviews*, *127*, 155–173. doi: 10.1016/j.quascirev.2015.06.023
Woodhead, J., Reisz, R., Fox, D., Drysdale, R., Hellstrom, J., Maas, R., … Edwards, R. L. (2010). Speleothem climate records from deep time? Exploring the potential with an example from the Permian. *Geology*, *38*(5), 455–458. doi: 10.1130/G30354.1
Yadava, M. G., & Ramesh, R. (2005). Monsoon reconstruction from radiocarbon dated tropical Indian speleothems. *Holocene*, *15*(1), 48–59. doi: 10.1191/0959683605h1783rp
Yang, H., Johnson, K. R., Griffiths, M. L., & Yoshimura, K. (2016). Interannual controls on

oxygen isotope variability in Asian monsoon precipitation and implications for paleoclimate reconstructions. *Journal of Geophysical Research*, *121*(14), 8410–8428. doi: 10.1002/2015JD024683

Zhang, H., Griffiths, M. L., Chiang, J. C. H., Kong, W., Wu, S., Atwood, A., … Xie, S. (2018). East Asian hydroclimate modulated by the position of the westerlies during Termination I. *Science*, *362*(6414), 580–583. doi: 10.1126/science.aat9393

Zhang, P., Cheng, H., Edwards, R. L., Chen, F., Wang, Y., Yang, X., … Johnson, K. R. (2008). A test of climate, sun, and culture relationships from an 1810-year Chinese cave record. *Science*, *322*(5903), 940–942. doi: 10.1126/science.1163965

Ziegler, M., Nürnberg, D., Karas, C., Tiedemann, R., & Lourens, L. J. (2008). Persistent summer expansion of the Atlantic Warm Pool during glacial abrupt cold events. *Nature Geoscience*, *1*(9), 601–605. doi: 10.1038/ngeo277

Chapter 2: Testing climatic and environmental controls on speleothem geochemical proxies from Cueva Bonita

2.1 Introduction

Secondary cave calcite deposits known as speleothems are becoming increasingly used as a terrestrial paleoclimate archive due to their ability to be precisely dated and record climate on orbital to sub-seasonal timescales. Hydroclimate reconstructions spanning these timescales are incredibly important for improving our understanding of regional climate dynamics and constraining the role of both internal naturally driven ocean-atmospheric climate variability and externally-driven changes in solar radiation and greenhouse gases. The growing use of speleothems over the last two decades, however, has highlighted a myriad of climatic and non-climatic processes that can affect speleothem geochemical proxies, potentially hindering our ability to interpret past hydroclimate (Deininger *et al.*, 2012; Deininger & Scholz, 2019; Dietzel *et al.*, 2009; Dreybrodt & Deininger, 2014; Fohlmeister *et al.*, 2011; Riechelmann *et al.*, 2013). Therefore, a comprehensive understanding of precipitation isotope systematics and the cave system is needed to determine the sensitivity of speleothem geochemical proxies to changes in overlying rainfall. This chapter will specifically focus on evaluating the controls of speleothem $\delta^{18}O$ and trace elements (Mg, Ba, Sr) at Cueva Bonita.

Speleothem $\delta^{18}O$ ($\delta^{18}O_{speleo}$) is commonly used for reconstructing past changes in precipitation and is controlled by precipitation $\delta^{18}O$ ($\delta^{18}O_{precip}$) and cave temperature when calcite is deposited in isotopic equilibrium (Fairchild *et al.*, 2006; Hendy, 1971; Lachniet, 2009). The dominant controls of $\delta^{18}O_{precip}$, however, can vary greatly in both time and space. In the tropics, $\delta^{18}O_{precip}$ has historically reflected the 'amount effect' (Dansgaard, 1964), with more

precipitation leading to more negative $\delta^{18}O$ values. However, recent analyses have suggested rainfall $\delta^{18}O$ is highly dependent on a wide range of processes taking place on more regional spatial scales. For instance, temperature (Lachniet & Patterson, 2009), shifting moisture sources (Aggarwal *et al.*, 2004; Vuille & Werner, 2005), local moisture recycling (Sánchez-Murillo *et al.*, 2016), orographic effects (Sánchez-Murillo *et al.*, 2013), rainout history (Lachniet *et al.*, 2007), microphysical cloud processes (Bony *et al.*, 2008; Konecky *et al.*, 2019; Risi *et al.*, 2008), and storm type (Frappier *et al.*, 2007) have all been suggested to influence the oxygen isotope composition. Interpretation of isotopes in modern rainfall can help elucidate the most important processes controlling $\delta^{18}O_{precip}$, therefore, improving the interpretation of $\delta^{18}O$ of past rainfall preserved in the speleothem. Isotopic monitoring stations of rainfall, however, are relatively limited with only two GNIP stations in Mexico.

In addition to processes controlling $\delta^{18}O_{precip,}$ previous studies have demonstrated canopy interception and the rate of infiltrating water in the soil zone can also alter the oxygen isotope composition of cave drip water, thereby altering $\delta^{18}O_{speleo}$ (Fetter, 2014; Lachniet, 2009; Sprenger *et al.*, 2016, 2018). For instance, a dense canopy and slow rate of infiltrating water would lead to an ^{18}O-enrichment of drip waters, due to increased interception of precipitation and increased evaporation. Furthermore, karst hydrology has also been attributed to the smoothing of climate signals on seasonal to timescales in the bedrock zone, primarily driven by the degree of groundwater mixing and speed of water transit (Bradley *et al.*, 2010). Within the cave, non-hydrological processes such as changes in cave temperatures, ventilation, relative humidity, and fluctuations in cave air pCO_2 can also affect $\delta^{18}O_{speleo}$ (Daëron *et al.*, 2019; Deininger & Scholz, 2019; Feng *et al.*, 2012; Mickler *et al.*, 2004, 2006). Cave monitoring can help identify the degree of hydrological smoothing and potentially provide direct evidence for

calcite deposited in (or near) isotopic equilibrium (Cuthbert *et al.*, 2014; Frisia *et al.*, 2011; Lases-Hernández *et al.*, 2020; Spötl *et al.*, 2005). However, the synchronous variability of cave conditions can pose a challenge in isolating the dominant driver(s) of non-equilibrium effects on $\delta^{18}O_{speleo}$ (Deininger *et al.*, 2012; Deininger & Scholz, 2019). To elucidate how changes in the cave environment influence $\delta^{18}O_{speleo}$, proxy system models initialized with observational measurements can be used to predict $\delta^{18}O_{speleo}$ values, potentially illuminating both the magnitude and driver(s) of disequilibrium isotope fractionation effects (Dee *et al.*, 2015; Deininger & Scholz, 2019; Harman, 2015). Isotope evolution models can therefore help quantify uncertainty in speleothem $\delta^{18}O$ records, and demonstrate how closely $\delta^{18}O_{speleo}$ reflects overlying changes in rainfall.

In addition to speleothem $\delta^{18}O$, there is a growing effort within the speleothem community to utilize trace element abundances to provide a more localized reconstruction of precipitation variability. Trace elements sourced from the bedrock (Mg, Sr, Ba) are generally interpreted to reflect the amount of prior calcite precipitation (PCP). PCP is a process in which calcite precipitation in the soil and epikarst preferentially uptakes Ca^{2+}, leaving the subsequent solution (and speleothem) with a higher relative concentration of trace metals (Tr/Ca) (Fairchild & Treble, 2009; Johnson *et al.*, 2006). During wetter conditions, PCP and the Tr/Ca ratio decreases, providing a record of local water balance (P-ET). However, similar to $\delta^{18}O$, variability in trace elements is also sensitive to non-climatic controls, especially on shorter, seasonal to sub-seasonal timescales. For instance, cave ventilation, groundwater mixing and vegetation die-back can also influence speleothem trace element ratios (Day & Henderson, 2013; Hartland *et al.*, 2012; Hartland & Zitoun, 2018; Wong *et al.*, 2011). Measuring trace element

concentrations in cave drip waters on seasonal to interannual timescales can therefore deepen our understanding of the sensitivity of trace elements to overlying changes in hydroclimate.

Here we present precipitation, drip water, and modern glass-grown calcite stable isotope ratios and trace elemental abundances from Cueva Bonita in Northeast Mexico (Fig 2.1) over a multi-year period (2017-2020). We combine isotopic precipitation sample analysis with models of wind trajectories to determine a strong influence of precipitation amount on $\delta^{18}O_{precip.}$ We demonstrate the oxygen and deuterium composition of cave drip waters are reflective of amount-weighted precipitation. We also demonstrate using modern glass-grown calcite samples,

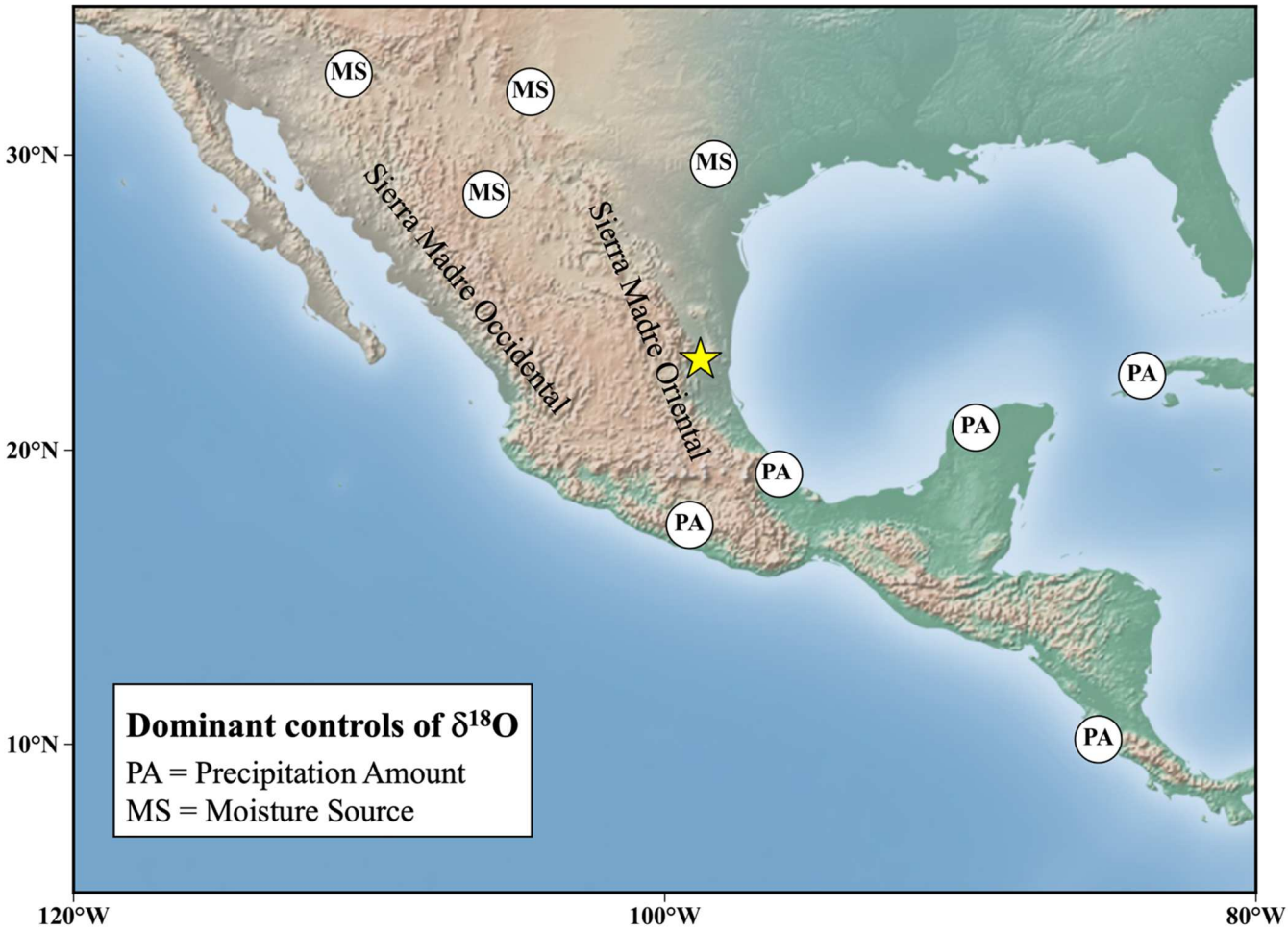

Fig. 2.1: Map of field site. Cueva Bonita is indicated by the star. Previous studies of oxygen isotopes in precipitation from Mexico and United States are plotted as white circles with their interpretation indicated by either MS for a dominant moisture source effect or PA for a dominant precipitation amount effect.

monitoring data, and isotope evolution models that Cueva Bonita speleothem $\delta^{18}O$ is a not strongly affected by kinetic or disequilibrium fractionation, and therefore is a suitable proxy for precipitation $\delta^{18}O$. Additionally, we demonstrate on seasonal to interannual timescales that the control of trace element ratios (Mg, Sr, U) in drip waters vary by drip site, mostly responding to changes in ventilation or hydrology (drip rate), suggesting trace elements in speleothem can potentially be used as additional paleoclimate proxies, especially if they co-vary with other geochemical proxies.

2.2 Study Site

Cueva Bonita (23°N, 99°W; 1071 m above sea level) is located in the highlands of the Sierra Madre Oriental in the northeast Mexican state of Tamaulipas (Fig. 2.1). The region is thought to be influenced by the synergistic forcing of the Atlantic and the Pacific, altering precipitation patterns on interannual to multi-decadal timescales (Stahle et al., 2016). The climate surrounding Cueva Bonita is classified as a tropical cloud forest, and the nearest weather station suggests an annual mean precipitation of 1800 mm/yr and an annual mean exterior temperature of 23.3°C (Gram & Faaborg, 1997). Summer precipitation accounts for a large majority of annual rainfall (70%) but occasional cold fronts from the north (nortes) provide some additional winter moisture (Chávez-Lara et al., 2019; Roy et al., 2016, 2020). The cave is situated within a thick deposit of Lower Cretaceous limestone (Gary, 2006), uplifted by normal and thrust faults (Ford, 2000) with about 50 m of overburden. Soil above the cave is relatively shallow (30 cm) composed of dark brown clay loam. Vegetation above the cave is dominantly trees (C3) and include diverse epiphytic orchid species. The cave can only be accessed via a dirt road and a ~5 km steep hike, there is no major anthropogenic disturbances nearby and the cave is not open to tourists.

Within the cave there are 3 major rooms (Fig 2.2). The first room sits at the bottom of the 30 m shear vertical entrance to the cave, is relatively dry and well ventilated by the cave's 3 m diameter entrance. The second room is located deeper within the cave, approximately 20 m lower than the first room, is less ventilated, and contains many active drips but few actively growing speleothems. The third room is farthest from the cave entrance, is slightly elevated (~5 m) than the second room, is poorly ventilated, contains many active drips, seasonally floods, and has many actively growing speleothems. In total, we present data from 9 drip sites, labeled D1-8 and CB4-scar (Fig. 2.2).

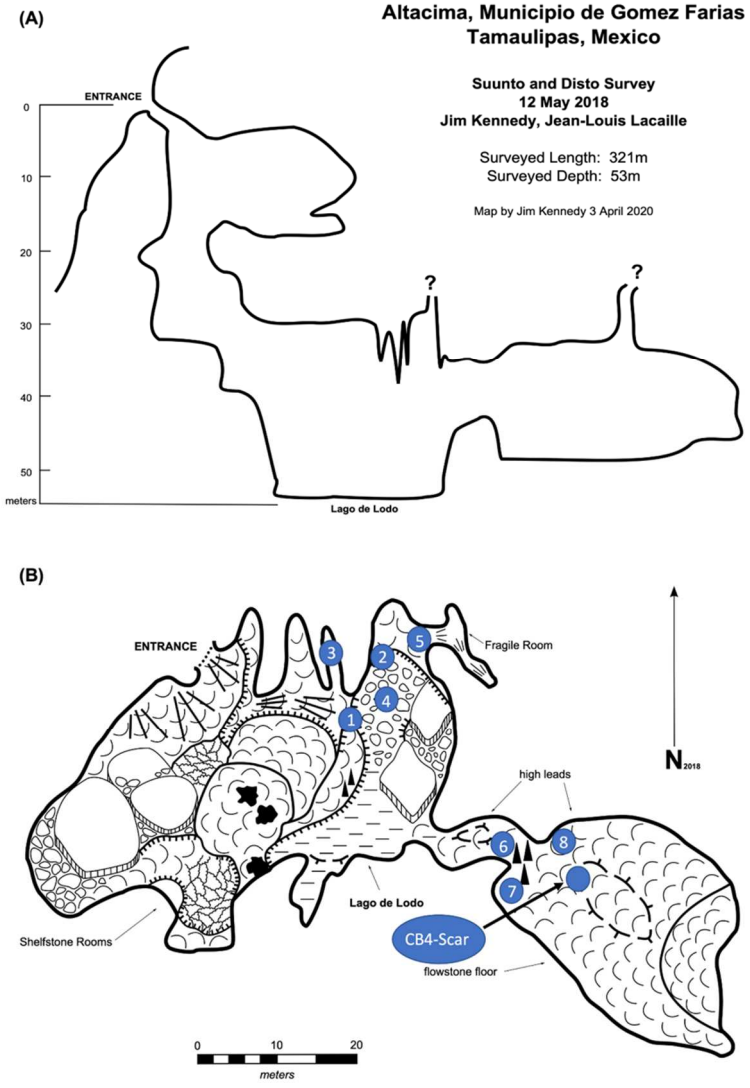

Fig. 2.2: Map of Cueva Bonita. (A) Idealized profile of Cueva Bonita. (B) Plan view of Cueva Bonita with the location of the 9 drip sites plotted.

2.3 Methods

2.3.1 Wind-trajectory analysis

Moisture source analysis at Cueva Bonita was conducted using air parcel back-trajectory simulations using the NOAA HYSPIT model (Stein *et al.*, 2015) combined with the Python package PYSPLIT (Cross, 2015) for increased computational efficiency. Air parcel trajectories were launched every 6 hours at an elevation of 1500 m over a 13-year period between 2005 and 2018 using GDAS weekly data. Each trajectory evaluated the air parcel's location over the previous 72 hours from launch. We chose to select only wind-trajectories that yielded precipitation at our field site. In total, 3600 rain-bearing trajectories were produced for the combined summer (JJAS) and winter (DJFM) months, only rain-bearing trajectories were included in analysis.

2.3.2 Precipitation samples

There are two precipitation stations of the International Atomic Energy Agency in Mexico (Veracruz and Chihuahua), unfortunately, they are over 600 km from our field site, are located at different altitudes and may not be representative of $\delta^{18}O_{precip}$ at Cueva Bonita (Fig. 2.1). Therefore, we established a local precipitation collection station approximately 1 km from Cueva Bonita in a small township (Alta Cima). To reduce kinetic effects on precipitation $\delta^{18}O$ due to evaporation, evaporation-limiting precipitation collectors were

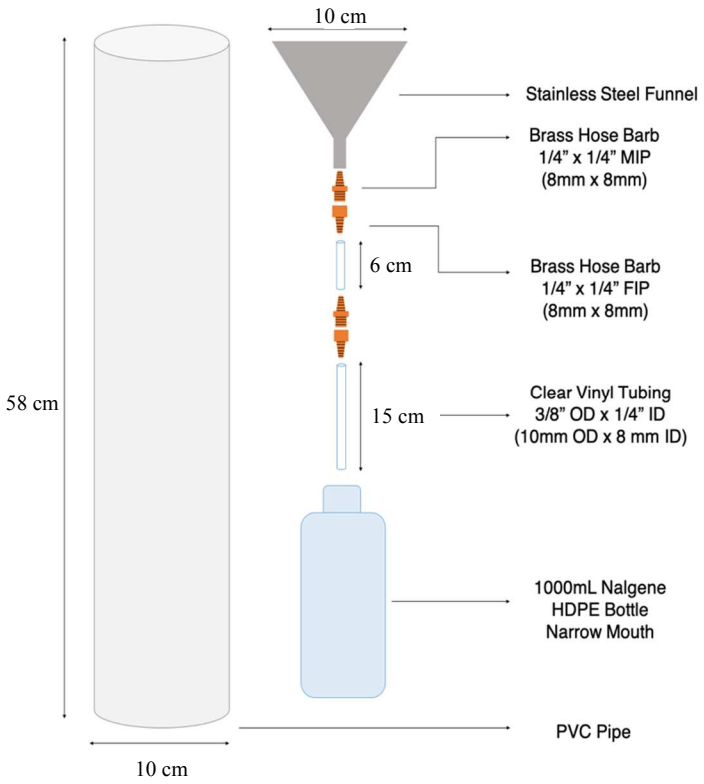

Fig. 2.3: Design of evaporation-limiting precipitation collectors. These were built at UC Irvine and deployed May 2018 in NE Mexico.

built and deployed during fieldwork (Fig. 2.3). Samples were collected after rainfall events in 1.5 ml glass vials with conical inserts, sealed with parafilm and refrigerated to limit evaporation. In total, 80 precipitation samples were collected from June 2018 to May 2019 and analyzed for δ^2D and $\delta^{18}O$ via a Picarro L2130i Cavity Ringdown Spectrometer at Chapman University. The analytical precision for δ^2D and $\delta^{18}O$ is 0.1‰ and 0.03‰, respectively.

2.3.3 Cave monitoring

An cave monitoring campaign from 2017 to 2020 was conducted to determine the degree of seasonal and interannual variability. Relative humidity and temperature fluctuations have been recorded using an Onset HOBO Relative Humidity-Temperature logger, every 2 hours, over a 27-month period. Daily CO_2 measurements were made using a handheld Vaisala GM-70 CO_2 monitor attached to a 12 Volt lantern battery, which typically lasted 1-3 months. Drip rate monitors (Driptych Stalagmates) were placed at various drip sites and recorded the number of drips per 30-minute period. Acid-washed frosted glass plates were also placed under various drip sites to capture new calcite growth for stable isotope analysis. We attempted fieldwork during different months between years to capture the full amplitude of seasonal variability.

Although we established 9 drip sites, some sites were dry depending on the season of fieldwork and thus could not be collected. Drip waters were collected from 4 drip sites in 2017, 6 drip sites in 2018 and, 7 drip sites in 2019, and 8 drip sites in 2020. Drip waters from 2017-2019 were analyzed using Cavity Ring Down Spectroscopy (CRDS) at either the University of Utah's Stable Isotope Ratio Facility for Environmental Research (SIRFER) or at Chapman University. Drip waters stable isotope analysis of 2019 and 2020 samples have yet to be analyzed. Drip waters from 2017-2020 from up to 9 drip sites were diluted (10x and 100x) using double distilled 2% nitric acid solution and analyzed using a Nu Instruments Attom High Resolution Inductively

Coupled Plasma Mass Spectrometer (HR-ICP-MS) at the Center for Isotope Tracers in Earth Sciences laboratory (CITIES) at UC Irvine. Trace element ratios were calculated using five standards of known concentration and an internal standard (Ge) added to samples to correct for instrumental drift.

Calcite samples captured on glass plates were analyzed for stable isotopes from three drip sites between 2017-2019. The calcite powder was generated from scraping the calcite off the glass plate using a hardness pick, weighed out to 40 - 80 μg and analyzed on a Kiel IV Carbonate Preparation Device coupled to a Thermo Scientific Delta V-IRMS at the UC Irvine CITIES laboratory utilizing methods described by McCabe-Glynn *et al.* (2013) to determine $\delta^{18}O$ and $\delta^{13}C$. For every 32 samples of unknown composition analyzed, we utilized 14 standards that included a mix of NBS-18, IAEA-CO-1, and an in-house standard. The analytical precision for $\delta^{18}O$ and $\delta^{13}C$ is 0.08‰ and 0.05‰, respectively.

2.3.4 Proxy System Modelling

Data collected from cave monitoring, including temperature, relative humidity, pCO_2 of cave air, $\delta^{18}O$ of drip waters and drip rate were to initialize the calcite isotope evolution model ISOLUTION 1.0 (Deininger & Scholz, 2019). Additional parameters not measured during fieldwork but required to run ISOLUTION include cave wind velocity and pCO_2 of drip water (Deininger & Scholz, 2019). The pCO_2 of cave drip water was estimated using the ISOLUTION CALCPCO2.m function Ca^{2+} concentration measured in drip waters and cave temperature as input parameters. We used ISOLUTION to evaluate the role of drip rate, temperature, pCO_2 of cave air, and evaporation rate (relative humidity) on calcite $\delta^{18}O$ and compared modelled $\delta^{18}O_{calcite}$ values to observational $\delta^{18}O_{calcite}$. All isotope modelling is based off measurements at

drip site CB-D6 because glass-grown calcite at this location could be constrained by drip water $\delta^{18}O$ measurements from samples collected before and after calcite precipitated.

2.4 Results

2.4.1 Hysplit

Results from HYSPLIT analyses demonstrate summer moisture is almost entirely sourced from the Tropical North Atlantic (Fig 2.4), specifically from the Gulf of Mexico and Caribbean Sea, with significant moisture fluxes upwards of 250 g/kg m/s associated with individual storms. During boreal winter, although back-trajectory analysis demonstrates the Pacific can contribute moisture to the region, the amount of moisture is relatively insignificant, often providing < 5 g/kg m/s. The Gulf of Mexico and Caribbean Sea also appear to be the predominant source of precipitation during the winter season, with trajectories yielding up to 200 g/kg m/s.

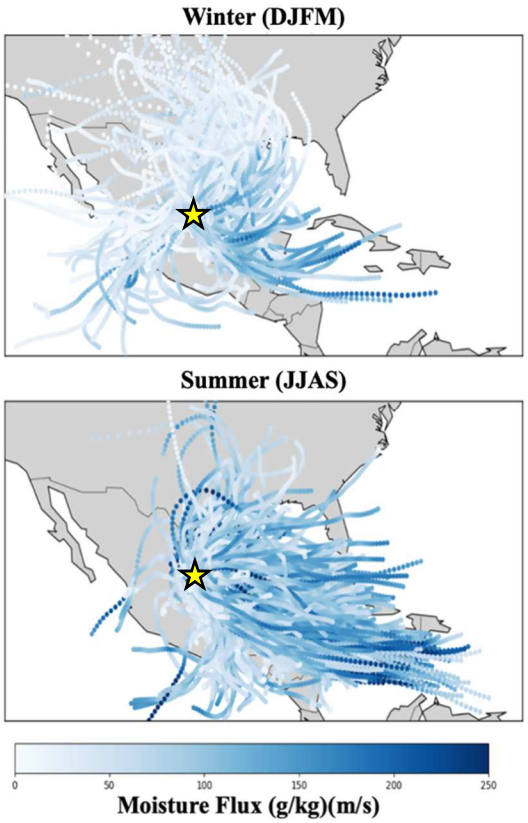

Fig. 2.4: Moisture bearing wind trajectories. Results of 3600 trajectories show most of the moisture is sourced from the Gulf of Mexico during summer and winter at Cueva Bonita.

2.4.2 Precipitation, drip water and modern calcite

All precipitation samples collected from June 2018 to May 2019 fall on the Global Meteoric Water Line (GMWL) with $\delta^{18}O$ values ranging from -14.03‰ to 0.22‰ and δD values ranging from -98.3‰ to 6.7‰ (VSMOW) (Fig. 2.5). In total 48 samples were collected and the mean amount-weighted $\delta^{18}O_{precip}$ is -4.84 ± 2.81‰. Precipitation samples have increased Deuterium excess (d-excess) in comparison to the GMWL. Interpreting d-excess in precipitation

is often ambiguous, but likely reflects changes in moisture source, wind speed and other processes taking place during vapor transport (Bershaw, 2018). In comparison to averaged GNIP data from Veracruz and Chihuahua, $\delta^{18}O_{precip}$ from Alta Cima exhibits its own unique pattern throughout the year. It is evident, however, $\delta^{18}O_{precip}$ is significantly more negative during the historically wetter months of July and September (Fig. 2.5). Monthly-averaged precipitation amount from a nearby weather station and $\delta^{18}O$ values demonstrate a relatively strong correlation (r^2 = 0.88), with a dependency of 2‰ per every 100 mm change in precipitation amount (Fig. 2.5). While our data has the potential to exhibit a potential seasonal bias due to the temporal limitation of data, the spatial correlation of annual weighted mean precipitation $\delta^{18}O$ from IsoGSM and annual GPCC v7 precipitation over a 36-year period reinforces our results, demonstrating a negative correlation between precipitation oxygen isotope ratios and regional precipitation amount (Fig. 2.6).

The 18 drip water samples collected from 2017 to 2019 deviate from the Global Meteoric Water Line,

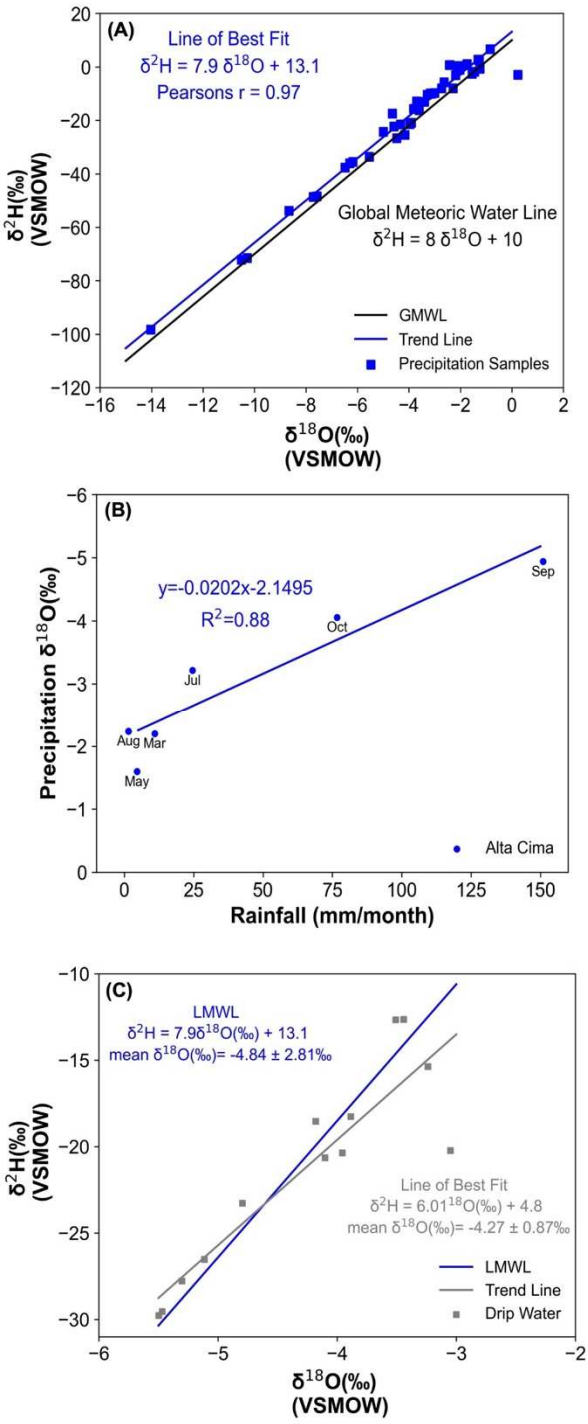

Fig. 2.5: Isotopic composition of rainfall and drip waters. (A) Almost all precipitation samples fall on the global meteoric water line suggesting little evaporation during collection. (B) Precipitation $\delta^{18}O$ shows a strong negative correlation to monthly precipitation amount. (C) Drip waters fall closely to the LMWL but show some evidence of evaporation.

suggesting some degree of evaporation (Fig. 2.6). Drip water $\delta^{18}O$ values range from -3.05‰ to -5.50‰ and $\delta^{2}D$ values range from -12.6‰ to 29.8‰ (VSMOW) (Fig. 2.6). Variability of drip water $\delta^{18}O$ within Cueva Bonita is relatively small ($2\sigma = 0.87$), although some samples with low drip rates have significantly higher $\delta^{18}O$ values (Table 2.1). The mean of all drip water samples is -4.27 ± 0.87‰, well within the standard deviation of mean amount-weighted precipitation -4.84 ± 2.81‰.

We collected 3 modern calcite samples, two from room 2 (CB2-glass and CB3-glass) and the third from room 3 (CB-D6). CB2-glass and CB3-glass were placed during a previous, but incomplete, study of Cueva Bonita in 2012 and collected in April 2016. CB-D6 was placed after collecting speleothem CB-D5 in November 2019. All three samples exhibited similar $\delta^{18}O$

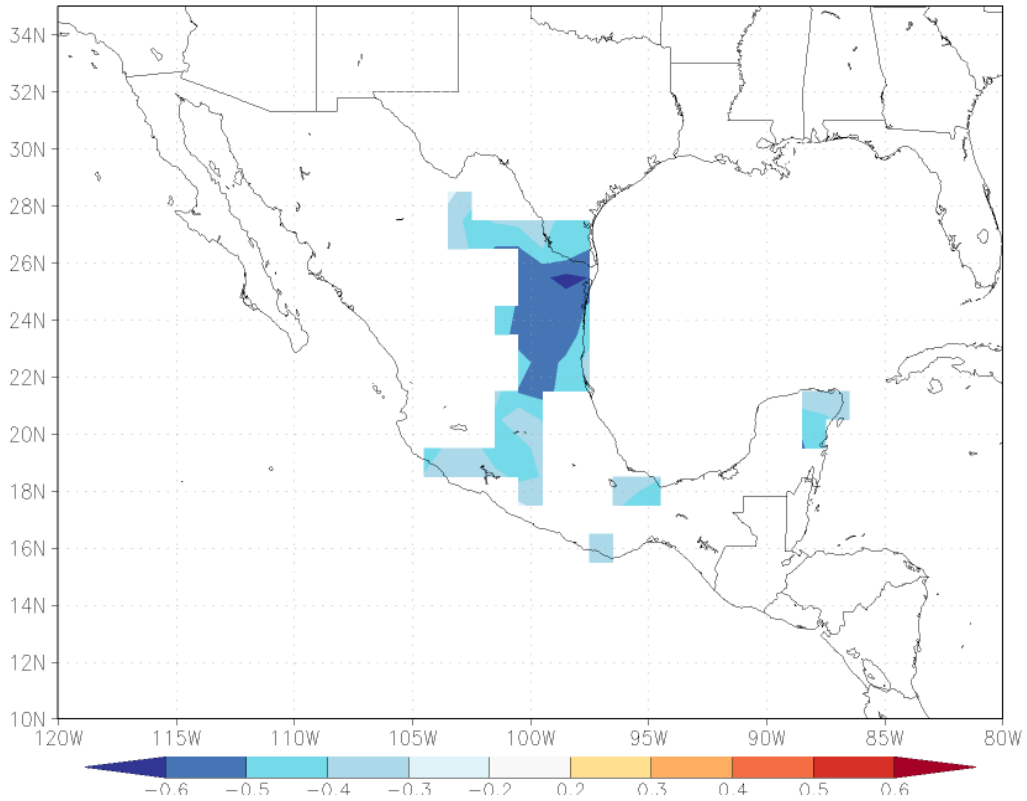

Fig. 2.6: Spatial correlation of annual weighted mean precipitation $\delta^{18}O$. Data compares IsoGSM gridpoints nearest Cueva Bonita with annual GPCC v7 precipitation (1979-2015), illustrating a negative correlation between precipitation oxygen isotope ratios and regional precipitation amount in our study area.

values, ranging from -3.95‰ to -4.78‰ and exhibited more variability in $\delta^{13}C$, from -5.57‰ to -9.92‰ (Table 2.1). The more negative $\delta^{13}C$ and $\delta^{18}O$ values in CB-D6 compared to other samples is likely attributed to CB-D6 location in a wetter part of the cave.

2.4.3 Cave Monitoring

Daily mean CO_2 for Cueva Bonita recorded every 3-12 hours from April 2017 to February 2020 demonstrates higher pCO_2 levels during summer, reaching upwards of 1200 ppm, compared to relatively low winter levels of 400 ppm (Fig. 2.7). The variability in cave air pCO_2 juxtaposes the stability of temperature and relative humidity. HOBO loggers recording conditions every 2 hours demonstrates temperature remains relatively constant at 17°C and relative humidity remains 100% year-round (Fig. 2.7). However, measurements during fieldwork suggest relative humidity may be overestimated by HOBO loggers, with field measurements of relative humidity ranging from 60-80%. Drip rate was recorded at each drip site from 2017 to 2020 during fieldwork and exhibits significant within cave and interannual variability, ranging from completely dry (<1 drips/min) to small steady streams (>300 drips/min)

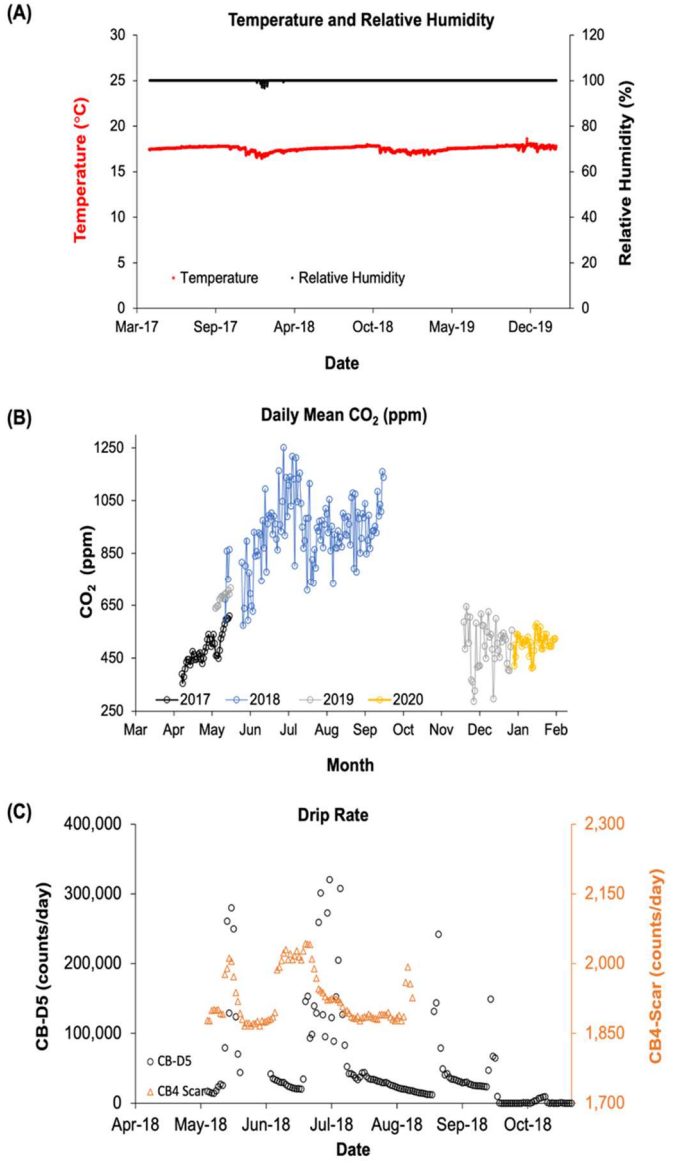

Fig. 2.7: Cave monitoring results. (A) Temperature and relative humidity. (B) Daily mean cave air pCO_2. (C) Drip rate at two drip locations within Cueva Bonita.

(Table 2.1). Additionally, Stalagmates placed within the cave demonstrate seasonal variability in drip rate (Fig. 2.6). Comparison to local rainfall events suggest a roughly 2-month transit time, although this may vary at other drip sites due to individual flow paths.

Table 2.1: Results of cave monitoring and drip water chemistry

Site	Date	pCO_2	Drip Rate	Precipitation	$\delta^{18}O_{drip}$	$\delta^{18}O_{speleo}$	$\delta^{13}C_{speleo}$	Mg/Ca	Sr/Ca	U/Ca
(D#)	(mon year)	(ppm)	(drips/min)	(mm)	(‰)	(‰)	(‰)	(mmol/mol)	(mmol/mol)	(mmol/mol)
D1	April 2017	400	109	166	-5.20	-4.19	-6.81	280	3.64	0.894
D1	May 2018	680	300	201	-4.10			193	2.19	0.740
D1	May 2019	600	66	105	-5.30			261	2.33	0.824
D1	Nov 2019	570	100	127				197	1.63	0.776
D1	Feb 2020	450	123	65				229	1.63	0.842
D2	April 2017	400	58	166	-4.50			226	3.60	0.686
D2	May 2018	680	126	201	-3.96			288	2.14	0.622
D2	May 2019	600	1	105	-3.51			300	4.50	0.980
D2	Nov 2019	570	61	127				275	2.88	0.735
D2	Feb 2020	450	12	65				264	4.09	0.865
D4	April 2017	400	12	166	-4.90	-3.95	-5.57	258	3.64	0.726
D4	May 2018	680	10	201	-3.05			208	1.72	0.819
D4	May 2019	600	5	105	-5.11			275	1.87	1.365
D4	Nov 2019	570	13	127				264	1.73	0.836
D4	Feb 2020	450	10	65				233	1.68	0.566
D5	April 2017	700	14	201				281	3.36	0.823
D5	May 2018	600	1	105	-4.80			302	4.96	0.518
D5	Nov 2019	570	18	127	-3.44			271	3.23	0.542
D5	Feb 2020	450	4	65				252	4.93	0.721
D6	May 2018	700	7	201	-5.50				2.39	0.797
D6	May 2019	840	6	105	-4.18	-4.78	-9.92	403	4.40	0.977
D6	Nov 2019	570	4	127				285	1.94	0.759
D6	Feb 2020	450	7	65				281	1.80	0.725
D7	May 2019	840	6	105	-5.47			350	3.76	0.848
D7	Nov 2019	570	6	127				349	1.70	0.627
D7	Feb 2020	450	7	65				307	1.29	0.832
D8	Nov 2019	570	1	127				422	5.41	0.660
D8	Feb 2020	450	2	65				387	12.39	0.634
D9	Nov 2019	570	1	127				352	2.37	1.237
D9	Feb 2020	450	1	65				287	1.61	0.534

2.4.4 Drip Water Trace Elements

Trace element ratios from Cueva Bonita Drip water samples (n = 30) collected between May 2017 and February 2020 are shown in Table 2.1. The magnesium concentration is relatively high in the waters, with Mg/Ca ratios ranging from 194-422 mmol/mol. Strontium and Uranium concentrations are considerably lower with ratios ranging from 1.29 to 12.4 mmol/mol and 0.52 to 1.37 mmol/mol, respectively. There is a moderate positive correlation of Mg/Ca and Sr/Ca throughout the cave ($r = 0.50$, $p < 0.01$). U/Ca does not correlate to Mg/Ca throughout Cueva Bonita ($r = 0.08$ $p < 0.01$) which could be driven by the different sourcing of U from both the soil and bedrock, or contamination since U concentrations are so low. For instance, U/Ca and Mg/Ca positively correlate at D1 ($r = 0.89$, $P < 0.01$), D3 ($r = 0.40$, $p < 0.01$), D4 ($r = 0.55$, $p < 0.01$), D6 ($r = 0.99$, $p < 0.02$), D8 ($r = 1$, $p < 0.03$) and CB4-Scar ($r = 1$, $p > 0.05$) and negatively correlate at D5 ($r = -0.41$, $p < 0.01$) and D7 ($r = -0.44$, $p < 0.01$).

To evaluate controls of Cueva Bonita trace elements in drip waters, trace element ratios were compared to drip rate (Fig. 2.8) and cave air pCO_2 (Fig. 2.9) recorded during fieldwork (Table 2.1). Trend lines plotted are for the combined response of Mg and Sr, U was not included due to its inconsistent response at various drip sites. The negative trendline is evident for changing drip rates (Fig. 2.8) at D1 ($R^2 = 0.02$), D2 ($R^2 = 0.02$), D4 ($R^2 = 0.21$), and D5 ($R^2 = 0.44$) but not the other sites. We suggest the limited number of samples likely restricts the statistical significance of this correlation. D1 is the only site that shows a negative response to rising pCO_2 ($R^2 = 0.41$).

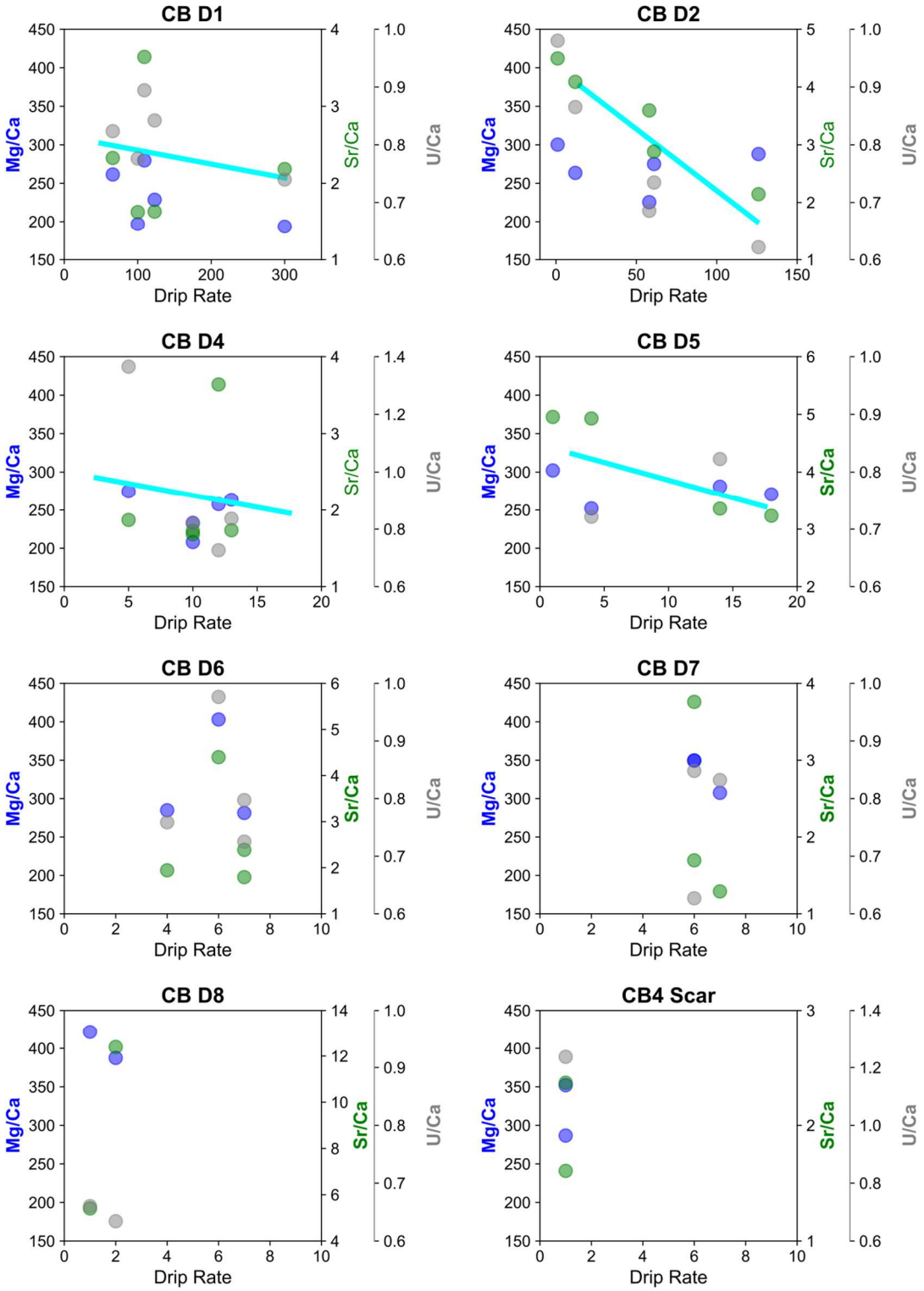

Fig. 2.8: Trace element ratios compared to drip rate. The drip rate and trace element ratios are compared at each individual drip site. D1-2 and D4-5 exhibit a negative trend, while D6-D8 and CB4-Scar do not. All values reported are in mmol/mol.

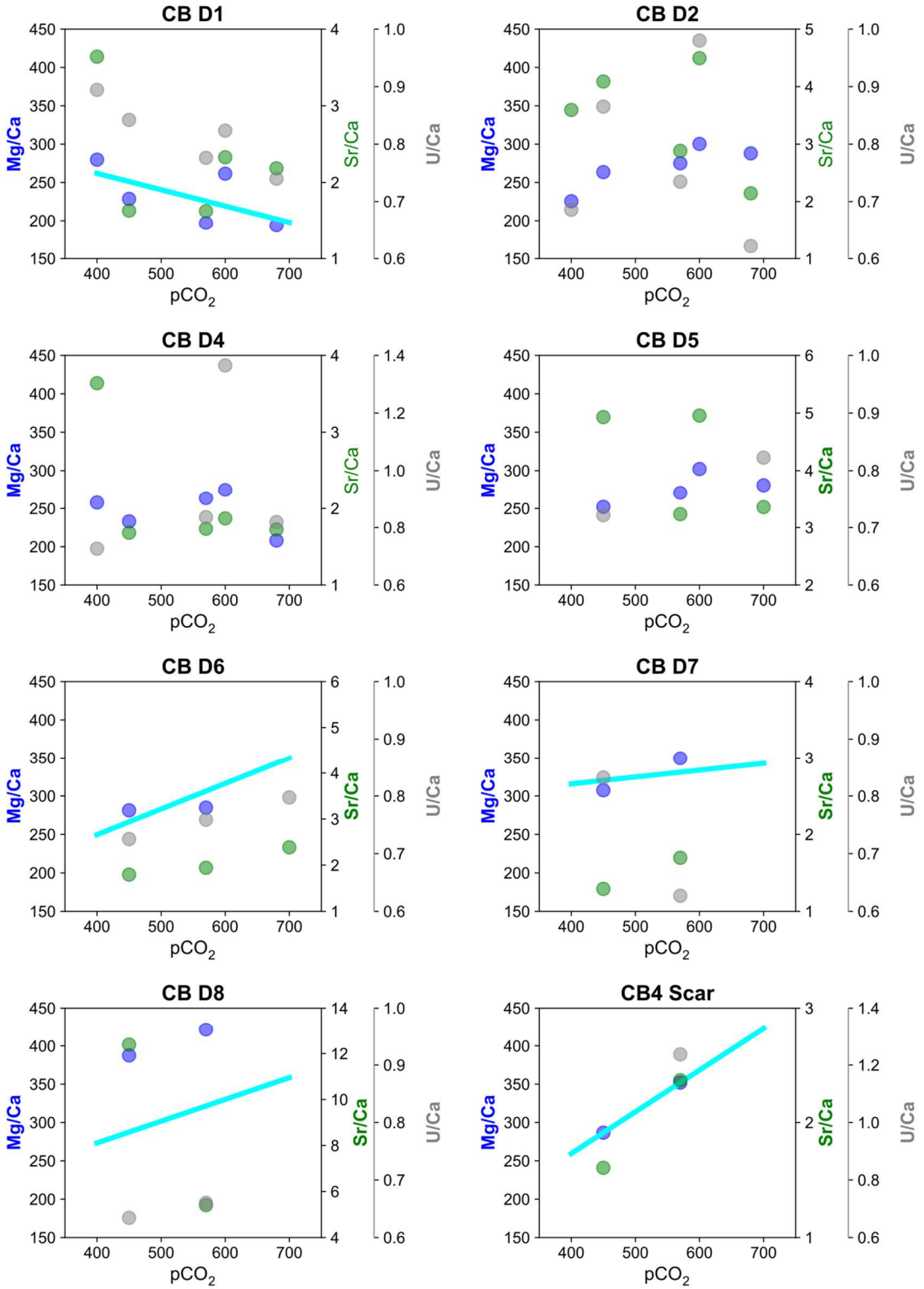

Fig. 2.9: Trace element ratios compared to *p*CO₂. The drip rate and trace element ratios are compared at each individual drip site. D1-2 and D4-5 exhibit a negative trend, while D6-D8 and CB4-Scar do not. All values reported are in mmol/mol.

2.4.5 Proxy System Modelling

Isotope modelling results suggest the strongest driver of calcite $\delta^{18}O$ is the drip interval, with the drip interval driving upwards of a 0.3 per mil change in calcite $\delta^{18}O$ (Fig 2.10). Given the oxygen isotope composition of glass grown calcite at CB-D6, Figure 2.9 demonstrates the average drip interval is less than 100s, consistent with field measurements from 2018 to 2020 (Table 2.1). Comparatively, other cave processes appear to impart a relatively minor change on speleothem $\delta^{18}O$. For instance, the seasonal variability in cave air pCO_2 determined the upper (1250 ppm) and lower (400 ppm) limits initialized by the model. Model predictions demonstrate an insignificant change (< 0.02‰) in calcite $\delta^{18}O$ (Fig. 2.10). Changes in relative humidity were also insignificant where a 50% change in humidity barely caused a change in the oxygen isotope composition of calcite (Fig. 2.9). It's possible changes in

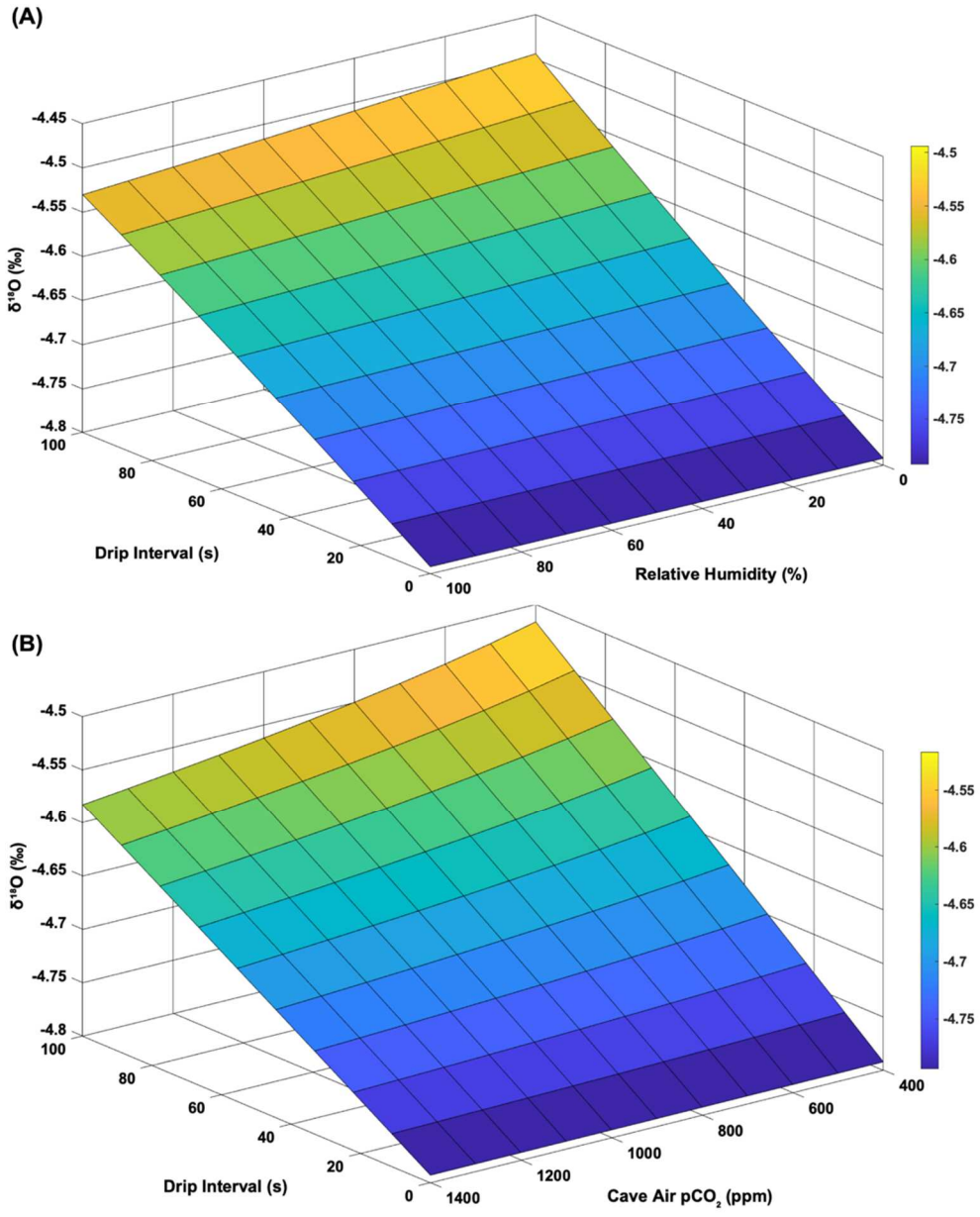

Fig. 2.10: Modelled response of $\delta^{18}O$ to cave variability. (A) Demonstrates the response of $\delta^{18}O$ at CB-D6 to changes in relative humidity and drip interval. (B) Demonstrates the response of $\delta^{18}O$ to changes in cave air pCO_2 and drip interval.

relative humidity, drip interval and especially cave air pCO_2 could have a larger kinetic fractionation effect on $\delta^{13}C$ than $\delta^{18}O$, but drip water $\delta^{13}C$ have not yet been analyzed and were therefore excluded from simulations.

2.5 Discussion

2.5.1 Precipitation $\delta^{18}O$

Previous work from Southern Mexico and Central America has highlighted how the 'amount effect' strongly controls $\delta^{18}O_{precip}$ (Fig. 2.1; Bernal *et al.*, 2011; Lachniet *et al.*, 2017, 2012; Lases-Hernández *et al.*, 2020; Medina-Elizalde *et al.*, 2010; Pérez Quezadas *et al.*, 2015), consistent with the classical interpretation of oxygen isotopes in tropical rainfall (Dansgaard, 1964). However, studies from Northern Mexico suggest the amount effect may play a much more minuscule role. Precipitation $\delta^{18}O$ in the Northwestern state of Sonora, for instance, is more heavily influenced by the amount of upstream rainout in relation to the intensity of the North American Monsoon (Quezadas *et al.*, 2021), which is not necessarily correlated to changes in the amount of precipitation locally. In the North Central state of Chihuahua, precipitation is not reflective of precipitation amount or upstream rainout, and is instead reflective of shifting proportions of moisture sourced from either the Gulf of Mexico or the Pacific (Rivera-Rivera *et al.*, 2021). Shifting moisture sources has also been suggested as the prevalent driver of precipitation $\delta^{18}O$ in nearby Texas and New Mexico as well (Palmer & Palmer, 2012; Wong *et al.*, 2015), suggesting $\delta^{18}O_{precip}$ in NE Mexico may also be more sensitive to shifting moisture sources.

Wind trajectory analysis demonstrates precipitation above Cueva Bonita, however, is dominantly sourced from the Gulf of Mexico and Caribbean Sea (Fig. 2.4). We suggest given the similar oxygen isotope composition of Caribbean Sea and Gulf of Mexico seawater, the short

proximity between uptake locations and, relatively high humidity in the region, that variation between these two sources would exhibit negligible influence on precipitation $\delta^{18}O$ at Cueva Bonita. Although we provide evidence that individual storms could provide Pacific-sourced moisture, HYSPLIT results demonstrate these events are infrequent, and tend to lead to considerably less precipitation at the study site. This is likely to impart a trivial impact on amount-weighted or monthly-averaged $\delta^{18}O_{precip}$, let alone annual-averaged $\delta^{18}O_{precip,}$ with the latter often reflected in speleothem $\delta^{18}O$ due to mixing of infiltrating waters in the soil zone and bedrock (Baker & Bradley, 2009).

Overall, the HYSPLIT analysis presented here demonstrates $\delta^{18}O_{precip}$ does not strongly reflect a moisture source effect, in contrast to interpretations from Chihuahua, New Mexico, and Texas (Palmer & Palmer, 2012; Rivera-Rivera *et al.*, 2021; Wong *et al.*, 2011). We suggest the topography of NE Mexico shields the region from Pacific-derived storms, as Pacific-sourced precipitation would have to traverse over both the Sierra Madre Occidental and through the dry Mexican highlands before reaching the study site (Fig. 2.1). With a minimal role of shifting precipitation source identified at Cueva Bonita, the precipitation amount effect observed in southern Mexico may also extend to this region (Lachniet *et al.*, 2013; Lases-Hernández *et al.*, 2020; Medina-Elizalde *et al.*, 2010b).

Precipitation Samples collected over a ~1 year period demonstrate precipitation at Cueva Bonita exhibits seasonal isotopic variability, with precipitation $\delta^{18}O_{precip}$ shifting from negative values during the warm-wet Summer (JJAS) season to considerably more positive values during late-Spring and late-Autumn (Fig 2.5). Due to the shift towards negative values during the wet season, precipitation $\delta^{18}O$ is likely influenced by a precipitation amount effect. To test this, we compared monthly-averaged $\delta^{18}O_{precip}$ to monthly-averaged precipitation amount from satellite-

based PERSIANN data (Nguyen *et al.*, 2019), which demonstrates a strong precipitation amount effect on rainfall above Cueva Bonita (Fig. 2.5). The dependency of 2‰ per every 100 mm change in precipitation amount is similar to values reported from Southern Mexico (3‰), Costa Rica (3.‰) and Cuba (2‰), which have also interpreted $\delta^{18}O_{precip}$ to reflect rainfall amount (IAEA-GNIP, 2002–2015; Lachniet *et al.*, 2004; Lases-Hernández *et al.*, 2020). Furthermore, precipitation samples collected ~100 km west of Cueva Bonita as part of this project but not included in this dissertation also show a strong dependence on precipitation amount (Marks, 2020), suggesting precipitation in the entire region of NE Mexico may be dominated by a precipitation amount effect. While additional studies are needed to further test this hypothesis, we provide robust evidence that precipitation $\delta^{18}O$ directly above Cueva Bonita is reflective of precipitation amount. However, the degree to which the oxygen isotope composition of precipitation is successfully transferred to the underlying speleothem is dependent upon additional processes within the Critical Zone.

2.5.2 Drip Water $\delta^{18}O$

Drip water $\delta^{18}O$ ($\delta^{18}O_{drip}$) is sensitive to processes occurring in the overlying soil and bedrock zone, which can significantly alter the isotopic composition of precipitation. For instance, the oxygen composition of soil water can be enriched in ^{18}O due to canopy and litter interception (Liu *et al.*, 2006; Sprenger *et al.*, 2016), which in select cases has been shown to drive upwards of a 4.8‰ disparity between precipitation and soil water $\delta^{18}O$ (Goldsmith *et al.*, 2019). However, cave drip waters are more reflective of infiltrating water, which is not likely to be significantly affected by fractionated soil waters in the upper soil zone. Furthermore, soil texture and porosity can alter the surface area of soil water and the rate of infiltration, ultimately tempering the amount of evaporation occurring at the soil surface (Moreau-Le Golvan *et al.*,

1997). Even variations in soil chemistry have also been shown to alter the $\delta^{18}O$ of soil water via cation exchange with clay minerals (Oerter *et al.*, 2014). Processes affecting the oxygen isotope composition of drip water in the soil zone are compounded further by groundwater mixing, variations in groundwater flow path, and residence time in the epikarst and bedrock (Ayalon *et al.*, 1998; Baker & Bradley, 2009; Cuthbert *et al.*, 2014; Mischel *et al.*, 2015). By directly comparing drip water to precipitation $\delta^{18}O$, we can evaluate to what extent these processes are relevant at Cueva Bonita.

Drip water samples collected between 2018 and 2019 exhibit significant variability between drip sites with a range of 1.96‰ (Fig 2.5, Table 2.1). This is likely reflective of different transit times, transport and mixing of groundwater, with certain drip sites exhibiting characteristics of a more fracture-dominated (higher drip rate with a faster transit time; D1, D5), or a matrix-dominated (lower drip rate site with a slower transit time; D2-4, D6-D8, CB4-Scar) flow path. All drip water $\delta^{2}D$ and $\delta^{18}O$ samples from Cueva Bonita plot relatively closely to local precipitation samples (Fig 2.5), with the mean $\delta^{18}O_{drip}$ of -4.27 ± 0.87‰ well within the standard deviation of the amount-weighted mean precipitation (-4.84 ± 2.81‰). This suggests mean cave drip water $\delta^{18}O$ retains the majority of the $\delta^{18}O$ signal from overlying precipitation. The 1.96 per mil range in drip water $\delta^{18}O$ could potentially reflect varying degrees of hydrological smoothing or seasonal bias at each drip location. While future field work can help determine which drip sites capture seasonal or sub-seasonal variability in $\delta^{18}O$, available data suggests drip water samples from Cueva Bonita are overall reflective of annual overlying precipitation $\delta^{18}O$, and therefore reflective of precipitation amount on annual timescales. The small 0.57 per mil observed difference between precipitation and drip water $\delta^{18}O$ could be attributed to many of the previously discussed processes (evaporation, groundwater mixing or

soil chemistry), but the slope of drip water $\delta^{18}O$ and $\delta^{2}D$ suggests evaporation is the most likely culprit. Evaporation is evident with a shift in slope from 7.9 in the local meteoric water line (LMWL) to 6.1 in the trendline of the drip waters (Fig 2.5). However, the deviation from the LMWL is minor, could be driven by a single data point, and does not inhibit the use of precipitation $\delta^{18}O$ to reconstruct past changes in relative precipitation amount (wetter/drier) assuming calcite is deposited near isotopic equilibrium.

2.5.3 Drip water trace elements

Mg and Sr in drip waters are generally interpreted to be sourced from the bedrock and epikarst (Fairchild & Treble, 2009). However, trace elements can also be sourced from the soil zone, flushed down to the cave during intense periods of rainfall or during the onset of the wet season (Fairchild *et al.*, 2001; Hartland *et al.*, 2012; Treble *et al.*, 2003). Uranium, for instance, has been shown to be sourced from both the bedrock and soil zone, which may explain why it behaves similarly to Mg/Ca ratios in some instances (Fig. 2.8; D1, D2, D4, D6, D8, CB4-Scar) but not others (D5, D7) (Johnson *et al.*, 2006). The moderate correlation between Mg and Sr at different drip sites and locations within the cave, however, suggest these elements are influenced by a similar control (Fairchild & Treble, 2009; Johnson *et al.*, 2006). While previous work has suggested the co-variation is likely driven by changes in local water balance, frequently evoking prior calcite precipitation as the dominant driver during drier conditions, seasonal ventilation driving fluctuations in cave air pCO_2 can also control the concentration of Mg and Sr via enhanced CO_2 degassing at lower cave air pCO_2 concentrations (Wong *et al.*, 2011). Therefore, by comparing local water balance and pCO_2 variability in the cave, we can determine to what extent PCP (and trace element concentrations) is controlled by ventilation or hydrology.

In this analysis, we use the drip rate measured during fieldwork as an indicator of local water balance. We therefore presume when the local water balance (P-E) is higher, the drip rate is faster and PCP is weaker, resulting in a decrease in the Mg/Ca and Sr/Ca ratios. Figure 2.8 demonstrates this process occurs at select drip site locations, including D1, D2, D4, D5. However, at locations in which there was considerably less variability in drip rate (D6, D7, D8, CB4-Scar), the response is more stochastic and appears to have no correlation to changing drip rate. This could potentially provide evidence these drip sites are more dominantly controlled by seasonal changes in pCO_2. However, a reduction in cave air pCO_2 would theoretically increase trace element ratios via enhanced CO_2 degassing and PCP on stalactite tips and on the cave ceiling. CB D6-8 and CB4-Scar do not respond in this manner, and in fact, exhibit a positive trend in response to increasing CO_2. The only drip site that appears to respond in this manner is D1, which is located near the cave entrance and is likely subjected to enhanced ventilation (Fig. 2.2 and 2.9). Due to the poor correlation to pCO_2 we suggest drip sites D6-8 and CB4-Scar are also potentially sensitive to changes in overlying hydrology. Although these sites do not correlate well with drip rate, which often responds synchronously with rainfall (Cuthbert *et al.*, 2014; Tooth & Fairchild, 2003), PCP can take place over a several year period as the water travels through the epikarst. Although the transit time is unknown at these locations, the slower drip rate indicates an extended transit time. We suggest the slower response time of these drip sites are not reliably captured by our limited fieldwork. Conducting additional fieldwork during September and/or October, and in future years, would be ideal to test if there is a decrease in trace element concentrations in response to hydrology.

Ultimately, we present evidence that trace elements in Cueva Bonita drip waters are weakly or moderately influenced by local water balance at certain locations, with ventilation

seemingly playing a relatively minor role. Unfortunately, the dominant control of trace elements at many drip site locations remains elusive at least on seasonal timescales. We therefore suggest trace elements have the potential to record PCP in response to changes in hydroclimate, however, this should be verified utilizing additional speleothem geochemical proxies for PCP, such as $\delta^{13}C$.

2.5.4 Modern Speleothem $\delta^{18}O$ and $\delta^{13}C$

Although drip water and precipitation $\delta^{18}O$ are reflective of precipitation amount, the kinetic fractionation and disequilibrium isotope fractionation between dissolved carbonate phases and solid $CaCO_3$ can potentially blur the climate signal recorded in speleothem $\delta^{18}O$. Kinetic fractionation is primarily driven by evaporation, rapid CO_2 degassing and/or calcite precipitation and is amplified by variations in the cave environment that can cause further disequilibrium (Deininger *et al.*, 2012; Deininger & Scholz, 2019; Hendy, 1971; Mickler *et al.*, 2004, 2006). Previous studies have employed the 'Hendy Test' to evaluate the degree of kinetic fractionation present in speleothems, which considers a positive correlation between $\delta^{18}O$ and $\delta^{13}C$ along a single speleothem growth layer or along the central growth axis as evidence for kinetic fractionation (Denniston *et al.*, 2018; Hu *et al.*, 2008; Spötl *et al.*, 2006; Williams *et al.*, 2005; Zhang *et al.*, 2008). However, sampling along an individual growth layer can be extremely challenging and a positive correlation between $\delta^{18}O$ and $\delta^{13}C$ along the central growth axis can occur if both stable isotopes are reflective of overlying hydroclimate, which is often the case (Dorale & Liu, 2009). Therefore, to determine if speleothems precipitated close to isotopic equilibrium we compare direct measurements of modern precipitated calcite $\delta^{18}O$ at CB-D6 to predicted calcite $\delta^{18}O$ deposited in isotopic equilibrium, using a fractionation factor determined by robust laboratory experiments (Kim & O'Neil, 1997).

Calcite from drip site CB-D6 which grew from 2018 to 2019 demonstrates an oxygen isotope composition of -4.78 ± 0.08‰. Utilizing the mean (n = 2) $\delta^{18}O_{drip}$ from 2018 and 2019 (-4.84 ± 0.93‰) and the average drip interval (11s), cave air pCO_2 (800 ppm), water pCO_2 (16,000 ppm), temperature (17.3°C), relative humidity (100%), and ventilation (0 m/s), the predicted $\delta^{18}O$ of calcite deposited in isotopic equilibrium is -4.77‰, very close to the measured value of cave calcite (-4.78 ± 0.08‰). This suggests calcite from CB-D6 is deposited very close to isotopic equilibrium and is therefore reflective of precipitation $\delta^{18}O$ and cave temperature. However, there are several caveats to this analysis. Primarily, the range of drip waters is quite large (-5.50‰ to -4.18‰) and the minimal number of drip water samples collected from CB-D6 (n = 2) provides a large standard deviation. Furthermore, cave monitoring demonstrates seasonal to interannual variability in parameters known to drive disequilibrium isotope fractionation. For instance, relative humidity levels potentially reach as low as 67% (if HOBO measurements are incorrect) and the drip interval can be highly variable (Fig. 2.7), both of which could drive evaporation on the speleothem surface. Also, a ~900 ppm change in seasonal cave air pCO_2 could also potentially cause rapid CO_2 degassing, further increasing fractionation. We therefore utilized an isotope evolution model (Deininger & Scholz, 2019) to quantitively evaluate the impact of the individual and combined influences of these parameters on speleothem isotope chemistry at Cueva Bonita.

Surprisingly, model results suggest the role of relative humidity on speleothem $\delta^{18}O$ is very minor (Fig. 2.10). Even at 0% relative humidity there is only a 0.05% change in $\delta^{18}O$ at the longest drip interval (100s). Changes in the drip interval appear to drive a more noticeable, but still relatively small, change in $\delta^{18}O$ with up to 0.25‰ at 100% relative humidity. While previous studies have shown relative humidity (RH) can drive a large magnitude shifts in $\delta^{18}O$

(Deininger *et al.*, 2012; Deininger & Scholz, 2019; Mühlinghaus *et al.*, 2009), results presented here, which include changes RH considerably larger than those observed at any drip site at Cueva Bonita, suggest the oxygen isotopic composition of speleothems at this cave are not particularly sensitive to changes in RH. We suggest this insensitivity is driven by the sufficient replenishment of water on the speleothem surface (low drip interval), inhibiting significant evaporation. Lastly, changes in cave air pCO_2 could also alter the oxygen isotope composition during deposition observed to vary seasonally. However, Figure 2.10 demonstrates cave air pCO_2 drives less than a 0.1‰ change in speleothem $\delta^{18}O$ at a 100s drip interval. Cumulatively, model results demonstrate that cave variability does not have a significant impact on speleothem $\delta^{18}O$, reinforcing the interpretation that speleothem $\delta^{18}O$ at CB-D6 and Cueva Bonita is deposited very close to isotopic equilibrium and is reflective of cave temperature and precipitation $\delta^{18}O$.

One of the more poignant discoveries of model results is the muted response of $\delta^{18}O$ to changes in relative humidity, drip interval and pCO_2, even when models were initialized by excessively different values than identified by cave monitoring. For instance, using significantly lower relative humidity values did not appear to strongly affect the speleothem $\delta^{18}O$. This is important for highlighting how past variations in the cave environment, such as possible decreased relative humidity, drip rates and pCO_2 during the drier Pleistocene, is still not likely to drive strong disequilibrium isotope fractionation during calcite precipitation. Furthermore, seasonal variability in the cave has been shown to impart a relatively minor role on speleothem $\delta^{18}O$ (~0.3‰), especially considering the 4‰ variability observed in rainfall which is likely also observed in drip water at least at some drip locations. Cumulatively, this suggests speleothem $\delta^{18}O$ is suitable to reconstruct past changes in precipitation on seasonal to orbital timescales.

Although the analysis of this study has predominantly focused on $\delta^{18}O$ variability, the $\delta^{13}C$ values of modern cave calcite provide preliminary evidence of some of the hydrologic processes influencing the stable carbon isotope composition of Cueva Bonita speleothems. For instance, speleothem $\delta^{13}C$ values are predominantly reflective of soil $\delta^{13}C$, and bedrock $\delta^{13}C$, depending on the degree of open-versus-closed system dissolution (Hendy, 1971; Noronha *et al.*, 2015). Given the surface immediately around the cave is dominated by C3 vegetation, we would expect the $\delta^{13}C$ of soil CO_2 to be roughly between -26 to -20‰ (Baker *et al.*, 1997), and while the limestone bedrock $\delta^{13}C$ can vary between sites, is generally assumed to be close to ~ 0 to 1‰ (Noronha *et al.*, 2015; Rudzka *et al.*, 2011). Therefore, the carbon isotope composition of modern calcite should be somewhere in the range of -13.5 to -9.5‰(Baker *et al.*, 1997). However, $\delta^{13}C$ of glass grown calcite appears to be slightly enriched in ^{13}C, with values ranging from -5.57 to 9.92‰ (Table 2.1). We suggest this may reflect the preferential CO_2 degassing of the lighter Carbon-12 in air-filled fractures within the epikarst or on the cave ceiling, or more simply described, be driven by PCP. Future work utilizing proxy system models and additional measurements should confirm this hypothesis and especially rule out the role of ^{13}C enrichment by kinetic effects.

2.6 Conclusion

Precipitation and cave monitoring at Cueva Bonita has focused on understanding the controls of $\delta^{18}O$ and trace elements to determine their suitability for paleoclimate reconstruction. Through a combination of modeling and observational data, we demonstrate precipitation in Northeast Mexico, specifically above Cueva Bonita, is not controlled by a moisture source effect and instead exhibits a strong precipitation amount effect consistent with precipitation in Southern Mexico. Analysis of Cueva Bonita drip waters suggest $\delta^{18}O$ is slightly modified by evaporation

but is still dominantly reflective of amount-weighted mean precipitation, and trace element variations are potentially controlled by PCP. We demonstrate that modern calcite at Cueva Bonita is deposited very close to or in isotopic equilibrium and is not particularly sensitive to seasonal or interannual variability in cave air pCO_2, drip interval, or relative humidity, known to drive isotopic disequilibrium in other cave systems. This suggests speleothems from Cueva Bonita preserve the oxygen isotopic composition of precipitation. Collectively, these results demonstrate trace elements have the potential to record past local water balance if validated by other speleothem geochemical proxies such as $\delta^{18}O$, which is a suitable proxy for reconstructing past precipitation change on a range of timescales.

2.7 References

Aggarwal, P. K., Fröhlich, K., Kulkarni, K. M., & Gourcy, L. L. (2004). Stable isotope evidence for moisture sources in the asian summer monsoon under present and past climate regimes. *Geophysical Research Letters*, *31*(8). doi: 10.1029/2004GL019911

Aggarwal, P. K., Romatschke, U., Araguas-Araguas, L., Belachew, D., Longstaae, F. J., Berg, P., … Funk, A. (2016). *Proportions of convective and stratiform precipitation revealed in water isotope ratios*. doi: 10.1038/NGEO2739

Araguás-Araguás, L., Froehlich, K., & Rozanski, K. (1998). Stable isotope composition of precipitation over southeast Asia. *Journal of Geophysical Research: Atmospheres*, *103*(D22), 28721–28742. doi: 10.1029/98JD02582

Ashouri, H., Hsu, K.-L., Sorooshian, S., Braithwaite, D. K., Knapp, K. R., Cecil, L. D., … Prat, O. P. (2015). PERSIANN-CDR: Daily Precipitation Climate Data Record from Multisatellite Observations for Hydrological and Climate Studies. *Bulletin of the American Meteorological Society*, *96*(1), 69–83. doi: 10.1175/BAMS-D-13-00068.1

Ayalon, A., Bar-Matthews, M., & Sass, E. (1998). Rainfall-recharge relationships within a karstic terrain in the Eastern Mediterranean semi-arid region, Israel: δ 18O and δD characteristics. *Journal of Hydrology*, *207*(1–2), 18–31. doi: 10.1016/S0022-1694(98)00119-X

Bajo, P., Borsato, A., Drysdale, R., Hua, Q., Frisia, S., Zanchetta, G., … Woodhead, J. (2017). Stalagmite carbon isotopes and dead carbon proportion (DCP) in a near-closed-system situation: An interplay between sulphuric and carbonic acid dissolution. *Geochimica et Cosmochimica Acta*, *210*, 208–227. doi: 10.1016/j.gca.2017.04.038

Baker, A., & Bradley, C. (2009). *Modern stalagmite δ 18 O: Instrumental calibration and forward modelling*. doi: 10.1016/j.gloplacha.2009.05.002

Baker, A., Ito, E., Smart, P. L., & McEwan, R. F. (1997). Elevated and variable values of 13C in speleothems in a British cave system. *Chemical Geology*, *136*(3–4), 263–270. doi: 10.1016/S0009-2541(96)00129-5

Baker, A., Smith, C., Jex, C., Fairchild, I., Genty, D., & Fuller, L. (2008). Annually laminated speleothems: a review. *International Journal of Speleology*, *37*(3), 4. doi: http://dx.doi.org/10.5038/1827-806X.37.3.4

Baldini, J. U. L., McDermott, F., Hoffmann, D. L., Richards, D. A., & Clipson, N. (2008). Very high-frequency and seasonal cave atmosphere PCO2 variability: Implications for stalagmite growth and oxygen isotope-based paleoclimate records. *Earth and Planetary Science Letters*, *272*(1–2), 118–129. doi: 10.1016/J.EPSL.2008.04.031

Beck, J. W., Richards, D. A., Edwards, R. L., Silverman, B. W., Smart, P. L., Donahue, D. J., … Biddulph, D. (2001). Extremely large variations of atmospheric 14C concentration during the last glacial period. *Science*, *292*(5526), 2453–2458. doi: 10.1126/science.1056649

Bereiter, B., Eggleston, S., Schmitt, J., Nehrbass-Ahles, C., Stocker, T. F., Fischer, H., … Chappellaz, J. (2015). Revision of the EPICA Dome C CO2 record from 800 to 600-kyr before present. *Geophysical Research Letters*, *42*(2), 542–549. doi: 10.1002/2014GL061957

Bernal, J. P., Lachniet, M., McCulloch, M., Mortimer, G., Morales, P., & Cienfuegos, E. (2011). A speleothem record of Holocene climate variability from southwestern Mexico. *Quaternary Research*, *75*(01), 104–113. doi: 10.1016/j.yqres.2010.09.002

Bhattacharya, T., & Chiang, J. C. H. (2014). Spatial variability and mechanisms underlying El

Niño-induced droughts in Mexico. *Climate Dynamics*, *43*(12), 3309–3326. doi: 10.1007/s00382-014-2106-8

Bhattacharya, T., Chiang, J. C. H., & Cheng, W. (2017). Ocean-atmosphere dynamics linked to 800–1050 CE drying in mesoamerica. *Quaternary Science Reviews*, *169*, 263–277. doi: 10.1016/j.quascirev.2017.06.005

Bhattacharya, T., & Coats, S. (2020). Atlantic-Pacific Gradients Drive Last Millennium Hydroclimate Variability in Mesoamerica. *Geophysical Research Letters*, *47*(13), e2020GL088061. doi: 10.1029/2020GL088061

Bony, S., Risi, C., & Vimeux, F. (2008). Influence of convective processes on the isotopic composition (δ18O and δD) of precipitation and water vapor in the tropics: 1. Radiative-convective equilibrium and Tropical Ocean–Global Atmosphere–Coupled Ocean-Atmosphere Response Experiment (TOGA-COARE) simulations. *Journal of Geophysical Research: Atmospheres*, *113*(D19), 19305. doi: 10.1029/2008JD009942

Borsato, A., Johnston, V. E., Frisia, S., Miorandi, R., Corradini, F., Au, (A, & Borsato,). (2016). Temperature and altitudinal influence on karst dripwater chemistry: Implications for regional-scale palaeoclimate reconstructions from speleothems Cosmogenic Cl-36 in speleothems as a potential solar proxy View project OLOAMBIENT View project Temperature and altitudinal influence on karst dripwater chemistry: Implications for regional-scale palaeoclimate reconstructions from speleothems. *Geochimica et Cosmochimica Acta*, *177*, 275–297. doi: 10.1016/j.gca.2015.11.043

Bradley, C., Baker, A., Jex, C. N., & Leng, M. J. (2010). Hydrological uncertainties in the modelling of cave drip-water δ18O and the implications for stalagmite palaeoclimate reconstructions. *Quaternary Science Reviews*, *29*(17–18), 2201–2214. doi: 10.1016/j.quascirev.2010.05.017

Breitenbach, S. F. M., Adkins, J. F., Meyer, H., Marwan, N., Kumar, K. K., & Haug, G. H. (2010). Strong influence of water vapor source dynamics on stable isotopes in precipitation observed in Southern Meghalaya, NE India. *Earth and Planetary Science Letters*, *292*(1–2), 212–220. doi: 10.1016/j.epsl.2010.01.038

Breitenbach, S. F. M., Rehfeld, K., Goswami, B., Baldini, J. U. L., Ridley, H. E., Kennett, D. J., … Marwan, N. (2012). Constructing proxy records from age models (COPRA). *Climate of the Past*, *8*(5), 1765–1779. doi: 10.5194/cp-8-1765-2012

Burns, S. J., Godfrey, L. R., Faina, P., Mcgee, D., Hardt, B., Ranivoharimanana, L., & Randrianasy, J. (2016). *Rapid human-induced landscape transformation in Madagascar at the end of the first millennium of the Common Era*. doi: 10.1016/j.quascirev.2016.01.007

Cai, Y., Fung, I. Y., Edwards, R. L., An, Z., Cheng, H., Lee, J. E., … Chiang, J. C. H. (2015). Variability of stalagmite-inferred Indian monsoon precipitation over the past 252,000 y. *Proceedings of the National Academy of Sciences of the United States of America*, *112*(10), 2954–2959. doi: 10.1073/pnas.1424035112

Cai, Z., & Tian, L. (2016). Atmospheric controls on seasonal and interannual variations in the precipitation isotope in the East Asian Monsoon region. *Journal of Climate*, *29*(4), 1339–1352. doi: 10.1175/JCLI-D-15-0363.1

Caley, T., Roche, D. M., & Renssen, H. (2014). Orbital Asian summer monsoon dynamics revealed using an isotope-enabled global climate model. *Nature Communications*, *5*(1), 1–6. doi: 10.1038/ncomms6371

Chávez-Lara, C. M., Holtvoeth, J., Roy, P. D., & Pancost, R. D. (2019). Lipid biomarkers in lacustrine sediments of subtropical northeastern Mexico and inferred ecosystem changes

during the late Pleistocene and Holocene. *Palaeogeography, Palaeoclimatology, Palaeoecology*, *535*. doi: 10.1016/j.palaeo.2019.109343

Chen, Z., Auler, A. S., Bakalowicz, M., Drew, D., Griger, F., Hartmann, J., … Goldscheider, N. (2017). The World Karst Aquifer Mapping project: concept, mapping procedure and map of Europe. *Hydrogeology Journal 2017 25:3*, *25*(3), 771–785. doi: 10.1007/S10040-016-1519-3

Cheng, H., Edwards, R. L., Sinha, A., Spötl, C., Yi, L., Chen, S., … Zhang, H. (2016). The Asian monsoon over the past 640,000 years and ice age terminations. *Nature*, *534*(7609), 640–646. doi: 10.1038/nature18591

Cheng, H., Lawrence Edwards, R., Shen, C. C., Polyak, V. J., Asmerom, Y., Woodhead, J., … Calvin Alexander, E. (2013). Improvements in 230Th dating, 230Th and 234U half-life values, and U-Th isotopic measurements by multi-collector inductively coupled plasma mass spectrometry. *Earth and Planetary Science Letters*, *371–372*, 82–91. doi: 10.1016/j.epsl.2013.04.006

Clemens, S. C., Prell, W. L., & Sun, Y. (2010). Orbital-scale timing and mechanisms driving Late Pleistocene Indo-Asian summer monsoons: Reinterpreting cave speleothem δ18O. *Paleoceanography*, *25*(4). doi: 10.1029/2010PA001926

Cross, M. (2015). PySPLIT: Package for the Generation, Analysis, and Visualization of HYSPLIT Air Parcel Trajectories. In *PROC*. Retrieved from https://www.youtube.com/watch?v=2mzhTC4Kp-Y

Cuthbert, M. O., Baker, A., Jex, C. N., Graham, P. W., Treble, P. C., Andersen, M. S., & Ian Acworth, R. (2014). Drip water isotopes in semi-arid karst: Implications for speleothem paleoclimatology. *Earth and Planetary Science Letters*, *395*, 194–204. doi: 10.1016/j.epsl.2014.03.034

Daëron, M., Drysdale, R. N., Peral, M., Huyghe, D., Blamart, D., Coplen, T. B., … Zanchetta, G. (2019). Most Earth-surface calcites precipitate out of isotopic equilibrium. *Nature Communications*, *10*(1), 1–7. doi: 10.1038/s41467-019-08336-5

Dansgaard, W. (1964). Stable isotopes in precipitation. *Tellus*, *16*(4), 436–468. doi: 10.3402/tellusa.v16i4.8993

Day, C. C., & Henderson, G. M. (2013). Controls on trace-element partitioning in cave-analogue calcite. *Geochimica et Cosmochimica Acta*, *120*, 612–627. doi: 10.1016/j.gca.2013.05.044

Dayem, K. E., Molnar, P., Battisti, D. S., & Roe, G. H. (2010). Lessons learned from oxygen isotopes in modern precipitation applied to interpretation of speleothem records of paleoclimate from eastern Asia. *Earth and Planetary Science Letters*, *295*(1–2), 219–230. doi: 10.1016/j.epsl.2010.04.003

Dee, S., Emile-Geay, J., Evans, M. N., Allam, A., Steig, E. J., & Thompson, D. M. (2015). PRYSM: An open-source framework for PRoxY System Modeling, with applications to oxygen-isotope systems. *Journal of Advances in Modeling Earth Systems*, *7*(3), 1220–1247. doi: 10.1002/2015MS000447

Deininger, M., Fohlmeister, J., Scholz, D., & Mangini, A. (2012). Isotope disequilibrium effects: The influence of evaporation and ventilation effects on the carbon and oxygen isotope composition of speleothems - A model approach. *Geochimica et Cosmochimica Acta*, *96*, 57–79. doi: 10.1016/j.gca.2012.08.013

Deininger, M., & Scholz, D. (2019). ISOLUTION 1.0: an ISOtope evoLUTION model describing the stable oxygen (δ18O) and carbon (δ13C) isotope values of speleothems. *International Journal of Speleology*, *48*(1), 21–32. doi: 10.5038/1827-806X.48.1.2219

Denniston, R. F., Houts, A. N., Asmerom, Y., Wanamaker, A. D., Haws, J. A., Polyak, V. J., … Bicho, N. F. (2018). A stalagmite test of North Atlantic SST and Iberian hydroclimate linkages over the last two glacial cycles. *Climate of the Past*, *14*(12), 1893–1913. doi: 10.5194/cp-14-1893-2018

Deplazes, G., Lückge, A., Peterson, L. C., Timmermann, A., Hamann, Y., Hughen, K. A., … Haug, G. H. (2013). Links between tropical rainfall and North Atlantic climate during the last glacial period. *Nature Geoscience*, *6*(3), 213–217. doi: 10.1038/ngeo1712

Dietzel, M., Tang, J., Leis, A., & Köhler, S. J. (2009). Oxygen isotopic fractionation during inorganic calcite precipitation - Effects of temperature, precipitation rate and pH. *Chemical Geology*, *268*(1–2), 107–115. doi: 10.1016/j.chemgeo.2009.07.015

Dorale, J. A. (1998). Climate and Vegetation History of the Midcontinent from 75 kyr to 25 kyr. A Speleothem Record from Crevice Cave, Missouri, USA. *Science*, *282*(5395), 1871–1874. doi: 10.1126/science.282.5395.1871

Dorale, J. A., & Liu, Z. (2009). Limitations of hendy test criteria in judging the paleoclimatic suitability of speleothems and the need for replication. In *Journal of Cave and Karst Studies* (Vol. 71). doi: PNR61

Dreybrodt, W., & Deininger, M. (2014). The impact of evaporation to the isotope composition of DIC in calcite precipitating water films in equilibrium and kinetic fractionation models. *Geochimica et Cosmochimica Acta*, *125*, 433–439. doi: 10.1016/j.gca.2013.10.004

Drysdale, R., Zanchetta, G., Hellstrom, J., Maas, R., Fallick, A., Pickett, M., … Piccini, L. (2006). Late Holocene drought responsible for the collapse of Old World civilizations is recorded in an Italian cave flowstone. *Geology*, *34*(2), 101–104. doi: 10.1130/G22103.1

Dubois, N., Kienast, M., Kienast, S., Normandeau, C., Calvert, S. E., Herbert, T. D., & Mix, A. (2011). Millennial-scale variations in hydrography and biogeochemistry in the Eastern Equatorial Pacific over the last 100 kyr. *Quaternary Science Reviews*, *30*(1–2), 210–223. doi: 10.1016/j.quascirev.2010.10.012

Dunning, N. P., Beach, T. P., & Luzzadder-Beach, S. (2012). Kax and kol: Collapse and resilience in lowland Maya civilization. *Proceedings of the National Academy of Sciences*, *109*(10), 3652–3657. doi: 10.1073/PNAS.1114838109

Dykoski, C. A., Lawrence Edwards, R., Cheng, H., Yuan, D., Cai, Y., Zhang, M., … Boyle, E. (2005). *A high-resolution, absolute-dated Holocene and deglacial Asian monsoon record from Dongge Cave, China*. doi: 10.1016/j.epsl.2005.01.036

Escobar, J., Hodell, D. A., Brenner, M., Curtis, J. H., Gilli, A., Mueller, A. D., … Guilderson, T. P. (2012). A ~43-ka record of paleoenvironmental change in the Central American lowlands inferred from stable isotopes of lacustrine ostracods. *Quaternary Science Reviews*, *37*, 92–104. doi: 10.1016/j.quascirev.2012.01.020

Fairchild, I., Baker, A., Borsato, A., & Frisia, S. (2001). Annual to sub-annual resolution of multiple trace-element trends in speleothems. *Article in Journal of the Geological Society*. doi: 10.1144/jgs.158.5.831

Fairchild, I. J., Smith, C. L., Baker, A., Fuller, L., Spötl, C., Mattey, D., … E.I.M.F. (2006). Modification and preservation of environmental signals in speleothems. *Earth-Science Reviews*, *75*(1–4), 105–153. doi: 10.1016/J.EARSCIREV.2005.08.003

Fairchild, I. J., & Treble, P. C. (2009). Trace elements in speleothems as recorders of environmental change. *Quaternary Science Reviews*, *28*(5–6), 449–468. doi: 10.1016/j.quascirev.2008.11.007

Feng, S., Krueger, A. B., & Oppenheimer, M. (2010). Linkages among climate change, crop

yields and Mexico-US cross-border migration. *Proceedings of the National Academy of Sciences of the United States of America*, *107*(32), 14257–14262. doi: 10.1073/pnas.1002632107

Feng, W., Banner, J. L., Guilfoyle, A. L., Musgrove, M. L., & James, E. W. (2012). Oxygen isotopic fractionation between drip water and speleothem calcite: A 10-year monitoring study, central Texas, USA. *Chemical Geology*, *304–305*, 53–67. doi: 10.1016/j.chemgeo.2012.02.004

Feng, W., Casteel, R. C., Banner, J. L., & Heinze-Fry, A. (2013). *Oxygen isotope variations in rainfall, drip-water and speleothem calcite from a well-ventilated cave in Texas, USA: Assessing a new speleothem temperature proxy*. doi: 10.1016/j.gca.2013.11.039

Fetter, C. W. (2014). Applied hydrogeology. 4th. In *Pearson*. Retrieved from http://sutlib2.sut.ac.th/sut_contents/H109081.pdf

Fohlmeister, J., Kromer, B., & Mangini, A. (2011). The influence of soil organic matter age spectrum on the reconstruction of atmospheric 14C levels via stalagmites. *Radiocarbon*, *53*(1), 99–115. doi: 10.1017/S003382220003438X

Fohlmeister, J., Voarintsoa, N. R. G., Lechleitner, F. A., Boyd, M., Brandtstätter, S., Jacobson, M. J., & Oster, J. L. (2020). Main controls on the stable carbon isotope composition of speleothems. *Geochimica et Cosmochimica Acta*, *279*, 67–87. doi: 10.1016/j.gca.2020.03.042

Ford, D. C. (2000). Deep phreatic caves and groundwater systems of the Sierra de El Abra, Mexico. *Speleogenesis: Evolution of Karst Aquifers: Huntsville, Alabama, National Speleological*, 325–331.

Frappier, A. B., Pyburn, J., Pinkey-Drobnis, A. D., Wang, X., Corbett, D. R., & Dahlin, B. H. (2014). Two millennia of tropical cyclone-induced mud layers in a northern Yucatán stalagmite: Multiple overlapping climatic hazards during the Maya Terminal Classic "megadroughts." *Geophysical Research Letters*, *41*(14), 5148–5157. doi: 10.1002/2014GL059882

Frappier, A. B., Sahagian, D., Carpenter, S. J., González, L. A., & Frappier, B. R. (2007). Stalagmite stable isotope record of recent tropic cyclone events. *Geology*, *35*(2), 111–114. doi: 10.1130/G23145A.1

Freitas, C. R. De, Littlbjohn, R. N., Clarkson, T. S., & Kristament, I. S. (1982). Cave climate: Assessment of airflow and ventilation. *Journal of Climatology*, *2*(4), 383–397. doi: 10.1002/JOC.3370020408

Frisia, S., Borsato, A., Fairchild, I. J., McDermott, F., & Selmo, E. M. (2002). Aragonite-calcite relationships in speleothems (Grotte de Clamouse, France): Environment, fabrics, and carbonate geochemistry. *Journal of Sedimentary Research*, *72*(5), 687–699. doi: 10.1306/020702720687

Frisia, S., Fairchild, I. J., Fohlmeister, J., Miorandi, R., Spötl, C., & Borsato, A. (2011). Carbon mass-balance modelling and carbon isotope exchange processes in dynamic caves. *Geochimica et Cosmochimica Acta*, *75*(2), 380–400. doi: 10.1016/J.GCA.2010.10.021

Frumkin, A., & Stein, M. (2004). The Sahara–East Mediterranean dust and climate connection revealed by strontium and uranium isotopes in a Jerusalem speleothem. *Earth and Planetary Science Letters*, *217*(3–4), 451–464. doi: 10.1016/S0012-821X(03)00589-2

Gabitov, R. I., & Watson, E. B. (2006). Partitioning of strontium between calcite and fluid. *Geochemistry, Geophysics, Geosystems*, *7*(11). doi: 10.1029/2005GC001216

Galy, V., François, L., France-Lanord, C., Faure, P., Kudrass, H., Palhol, F., & Singh, S. K.

(2008). C4 plants decline in the Himalayan basin since the Last Glacial Maximum. *Quaternary Science Reviews*, *27*(13–14), 1396–1409. doi: 10.1016/J.QUASCIREV.2008.04.005

Gary, M. S. J. (2006). *Volcanogenic karstification of Sistema Zacatón, Mexico*. 79–89. doi: 10.1130/2006.2404(08)

Genty, D., & Massault, M. (1997). Bomb14C recorded in laminated speleothems: Calculation of dead carbon proportion. *Radiocarbon*, *39*(1), 33–48. doi: 10.1017/S0033822200040881

Genty, D., Massault, M., Gilmour, M., Baker, A., Verheyden, S., & Kepens, E. (1999). Calculation of past dead carbon proportion and variability by the comparison of AMS 14C and TIMS U/Th ages on two Holocene stalagmites. *Radiocarbon*, *41*(3), 251–270. doi: 10.1017/S003382220005712X

Gill, R. B., Mayewski, P. A., Nyberg, J., Haug, G. H., & Peterson, L. C. (2007). Drought and the maya collapse. *Ancient Mesoamerica*, *18*(2), 283–302. doi: 10.1017/S0956536107000193

Giorgetta, M. A., Jungclaus, J., Reick, C. H., Legutke, S., Bader, J., Böttinger, M., … Stevens, B. (2013). Climate and carbon cycle changes from 1850 to 2100 in MPI-ESM simulations for the Coupled Model Intercomparison Project phase 5. *Journal of Advances in Modeling Earth Systems*, *5*(3), 572–597. doi: 10.1002/jame.20038

Goede, A., McCulloch, M., McDermott, F., & Hawkesworth, C. (1998). Aeolian contribution to strontium and strontium isotope variations in a Tasmanian speleothem. *Chemical Geology*, *149*(1–2), 37–50. doi: 10.1016/S0009-2541(98)00035-7

Goldsmith, G. R., Allen, S. T., Braun, S., Engbersen, N., González-Quijano, C. R., Kirchner, J. W., & Siegwolf, R. T. W. (2019). Spatial variation in throughfall, soil, and plant water isotopes in a temperate forest. *Ecohydrology*, *12*(2), e2059. doi: 10.1002/ECO.2059

Gram, W. K., & Faaborg, J. (1997). The Distribution of Neotropical Migrant Birds Wintering in the El Cielo Biosphere Reserve, Tamaulipas, Mexico. *The Condor*, *99*(3), 658–670. doi: 10.2307/1370478

Griffiths, M. L., Drysdale, R. N., Vonhof, H. B., Gagan, M. K., Zhao, J. xin, Ayliffe, L. K., … Suwargadi, B. W. (2010). Younger Dryas-Holocene temperature and rainfall history of southern Indonesia from δ18O in speleothem calcite and fluid inclusions. *Earth and Planetary Science Letters*, *295*(1–2), 30–36. doi: 10.1016/j.epsl.2010.03.018

Griffiths, M. L., Fohlmeister, J., Drysdale, R. N., Hua, Q., Johnson, K. R., Hellstrom, J. C., … Zhao, J. x. (2012). Hydrological control of the dead carbon fraction in a Holocene tropical speleothem. *Quaternary Geochronology*, *14*, 81–93. doi: 10.1016/J.QUAGEO.2012.04.001

Griffiths, M. L., Johnson, K. R., Pausata, F. S. R., White, J. C., Henderson, G. M., Wood, C. T., … Sekhon, N. (2020). End of Green Sahara amplified mid- to late Holocene megadroughts in mainland Southeast Asia. *Nature Communications*, *11*(1), 4204. doi: 10.1038/s41467-020-17927-6

Griffiths, M. L., Kimbrough, A. K., Gagan, M. K., Drysdale, R. N., Cole, J. E., Johnson, K. R., … Hantoro, W. S. (2016). Western Pacific hydroclimate linked to global climate variability over the past two millennia. *Nature Communications*, *7*. doi: 10.1038/ncomms11719

Gutiérrez-García, G., Beramendi-Orosco, L. E., & Johnson, K. R. (2020). Climate-growth relationships of Pinus pseudostrobus from a tropical mountain cloud forest in northeast Mexico. *Dendrochronologia*, *64*, 125749. doi: 10.1016/j.dendro.2020.125749

Harman, C. J. (2015). Time-variable transit time distributions and transport: Theory and application to storage-dependent transport of chloride in a watershed. *Water Resources Research*, *51*(1), 1–30. doi: 10.1002/2014WR015707

Hartland, A., Fairchild, I. J., Lead, J. R., Borsato, A., Baker, A., Frisia, S., & Baalousha, M. (2012). From soil to cave: Transport of trace metals by natural organic matter in karst dripwaters. *Chemical Geology*, *304–305*, 68–82. doi: 10.1016/J.CHEMGEO.2012.01.032

Hartland, A., & Zitoun, R. (2018). Transition metal availability to speleothems controlled by organic binding ligands. *Geochem. Persp. Let*, *8*, 22–25. doi: 10.7185/geochemlet.1824

Hellstrom, J. (2006). U–Th dating of speleothems with high initial 230Th using stratigraphical constraint. *Quaternary Geochronology*, *1*(4), 289–295. doi: 10.1016/J.QUAGEO.2007.01.004

Hendy, C. H. (1971). *The isotopic geochemistry of speleothems-I. The calculation of the effects of different modes of formation on the isotopic composition of speleothems and their applicability as palaeoclimatic indicators* * (Vol. 35). Pergamon Press. Printed in Northern Ireland. Retrieved from Pergamon Press. Printed in Northern Ireland website: https://ac.els-cdn.com/001670377190127X/1-s2.0-001670377190127X-main.pdf?_tid=9d24d077-1c6a-4651-b253-c15525034ea9&acdnat=1549696557_a9657fa3d144aca8ac631b95b8603c45

Hodge, E., McDonald, J., Fischer, M., Redwood, D., Hual, Q., Levchenko, V., … Fink, D. (2011). Using the 14C bomb pulse to date young speleothems. In *Radiocarbon* (Vol. 53). doi: 10.1017/S0033822200056605

Hoggarth, J. A., Restall, M., Wood, J. W., & Kennett, D. J. (2017). Drought and its demographic effects in the maya lowlands. *Current Anthropology*, *58*(1), 82–113. doi: 10.1086/690046

Hu, C., Henderson, G. M., Huang, J., Xie, S., Sun, Y., & Johnson, K. R. (2008). Quantification of Holocene Asian monsoon rainfall from spatially separated cave records. *Earth and Planetary Science Letters*, *266*(3–4), 221–232. doi: 10.1016/j.epsl.2007.10.015

Hua, Q., Cook, D., Fohlmeister, J., Penny, D., Bishop, P., & Buckman, S. (2017). Radiocarbon Dating of a Speleothem Record of Paleoclimate for Angkor, Cambodia. *Radiocarbon*, *59*(6), 1873–1890. doi: 10.1017/RDC.2017.115

Huang, Y., Fairchild, I. J., Borsato, A., Frisia, S., Cassidy, N. J., McDermott, F., & Hawkesworth, C. J. (2001). Seasonal variations in Sr, Mg and P in modern speleothems (Grotta di Ernesto, Italy). *Chemical Geology*, *175*(3–4), 429–448. doi: 10.1016/S0009-2541(00)00337-5

Jaffey, A. H., Flynn, K. F., Glendenin, L. E., Bentley, W. C., & Essling, A. M. (1971). Precision measurement of half-lives and specific activities of U235 and U238. *Physical Review C*, *4*(5), 1889–1906. doi: 10.1103/PhysRevC.4.1889

James, E. W., Banner, J. L., & Hardt, B. (2015). A global model for cave ventilation and seasonal bias in speleothem paleoclimate records. *Geochemistry, Geophysics, Geosystems*, *16*(4), 1044–1051. doi: 10.1002/2014GC005658

John Bierhorst. (1992). *History and Mythology of the Aztecs: The Codex Chimalpopoca - Google Books*. Retrieved from https://books.google.com/books?hl=en&lr=&id=xErlvmBuakoC&oi=fnd&pg=PA1&dq=Bierhorst,+J.,+Ed.,+Trans.,+1992:+History+and+Mythology+of+the+Aztecs:+The+Codex+Chimalpopoca.+University+of+Arizona+Press,+238+pp.&ots=BuLIKOxdw9&sig=mGh1x__1DElEzd_sP_U_UY0BStU#v=

Johnson, K. R., Hu, C., Belshaw, N. S., & Henderson, G. M. (2006). Seasonal trace-element and stable-isotope variations in a Chinese speleothem: The potential for high-resolution paleomonsoon reconstruction. *Earth and Planetary Science Letters*, *244*(1–2), 394–407. doi: 10.1016/j.epsl.2006.01.064

Johnson, R. (2011). Immigration as a Response Variable to Climate Change from Mexico into

the United States. In *Journal of Alternative Perspectives in the Social Sciences* (Vol. 3).
Kennett, D. J., Breitenbach, S. F. M., Aquino, V. V., Asmerom, Y., Awe, J., Baldini, J. U. L., … Haug, G. H. (2012). Development and disintegration of maya political systems in response to climate change. *Science*, *338*(6108), 788–791. doi: 10.1126/science.1226299
Kim, S. T., & O'Neil, J. R. (1997). Equilibrium and nonequilibrium oxygen isotope effects in synthetic carbonates. *Geochimica et Cosmochimica Acta*, *61*(16), 3461–3475. doi: 10.1016/S0016-7037(97)00169-5
Knutti, R., & Sedláček, J. (2013). Robustness and uncertainties in the new CMIP5 climate model projections. *Nature Climate Change*, *3*(4), 369–373. doi: 10.1038/nclimate1716
Konecky, B. L., Noone, D. C., & Cobb, K. M. (2019). The Influence of Competing Hydroclimate Processes on Stable Isotope Ratios in Tropical Rainfall. *Geophysical Research Letters*, *46*(3), 1622–1633. doi: 10.1029/2018GL080188
Kovacs, S. E., Reinhardt, E. G., Stastna, M., Coutino, A., Werner, C., Collins, S. V., … Le Maillot, C. (2017). Hurricane Ingrid and Tropical Storm Hanna's effects on the salinity of the coastal aquifer, Quintana Roo, Mexico. *Journal of Hydrology*, *551*, 703–714. doi: 10.1016/J.JHYDROL.2017.02.024
Kovaltsov, G. A., Mishev, A., & Usoskin, I. G. (2012). A new model of cosmogenic production of radiocarbon 14C in the atmosphere. *Earth and Planetary Science Letters*, *337–338*, 114–120. doi: 10.1016/j.epsl.2012.05.036
Kurczyn, J. A., Appendini, C. M., Beier, E., Sosa-López, A., López-González, J., & Posada-Vanegas, G. (2021). Oceanic and atmospheric impact of central American cold surges (Nortes) in the Gulf of Mexico. *International Journal of Climatology*, *41*(S1), E1450–E1468. doi: 10.1002/joc.6779
Kurita, N., Ichiyanagi, K., Matsumoto, J., Yamanaka, M. D., & Ohata, T. (2009). The relationship between the isotopic content of precipitation and the precipitation amount in tropical regions. *Journal of Geochemical Exploration*, *102*(3), 113–122. doi: 10.1016/J.GEXPLO.2009.03.002
Lachniet, M. S. (2009). Climatic and environmental controls on speleothem oxygen-isotope values. *Quaternary Science Reviews*, *28*(5–6), 412–432. doi: 10.1016/j.quascirev.2008.10.021
Lachniet, M. S., Asmerom, Y., Bernal, J. P., Polyak, V. J., & Vazquez-Selem, L. (2013). Orbital pacing and ocean circulation-induced collapses of the Mesoamerican monsoon over the past 22,000 y. *Proceedings of the National Academy of Sciences of the United States of America*, *110*(23), 9255–9260. doi: 10.1073/pnas.1222804110
Lachniet, M. S., Asmerom, Y., Polyak, V., & Bernal, J. P. (2017). Two millennia of Mesoamerican monsoon variability driven by Pacific and Atlantic synergistic forcing. *Quaternary Science Reviews*, *155*, 100–113. doi: 10.1016/j.quascirev.2016.11.012
Lachniet, M. S., Bernal, J. P., Asmerom, Y., Polyak, V., & Piperno, D. (2012). A 2400 yr Mesoamerican rainfall reconstruction links climate and cultural change. *Geology*, *40*(3), 259–262. doi: 10.1130/G32471.1
Lachniet, M. S., Burns, S. J., Piperno, D. R., Asmerom, Y., Polyak, V. J., Moy, C. M., & Christenson, K. (2004). A 1500-year El Niño/Southern Oscillation and rainfall history for the Isthmus of Panama from speleothem calcite. *Journal of Geophysical Research D: Atmospheres*, *109*(20), 20117. doi: 10.1029/2004JD004694
Lachniet, M. S., & Patterson, W. P. (2009). Oxygen isotope values of precipitation and surface waters in northern Central America (Belize and Guatemala) are dominated by temperature

and amount effects. *Earth and Planetary Science Letters*, *284*(3–4), 435–446. doi: 10.1016/J.EPSL.2009.05.010

Lachniet, M. S., Patterson, W. P., Burns, S., Asmerom, Y., & Polyak, V. (2007). Caribbean and Pacific moisture sources on the Isthmus of Panama revealed from stalagmite and surface water δ18O gradients. *Geophysical Research Letters*, *34*(1). doi: 10.1029/2006GL028469

Landsea, C. W., & Franklin, J. L. (2013). Atlantic Hurricane Database Uncertainty and Presentation of a New Database Format. *Monthly Weather Review*, *141*(10), 3576–3592. doi: 10.1175/MWR-D-12-00254.1

Lases-Hernández, F., Medina-Elizalde, M., & Benoit Frappier, A. (2020). Drip water δ18O variability in the northeastern Yucatán Peninsula, Mexico: Implications for tropical cyclone detection and rainfall reconstruction from speleothems. *Geochimica et Cosmochimica Acta*, *285*, 237–256. doi: 10.1016/J.GCA.2020.07.008

Lawrence Edwards, R., Chen, J. H., & Wasserburg, G. J. (1987). 238U234U230Th232Th systematics and the precise measurement of time over the past 500,000 years. *Earth and Planetary Science Letters*, *81*(2–3), 175–192. doi: 10.1016/0012-821X(87)90154-3

Lea, D. W., Pak, D. K., Peterson, L. C., & Hughen, K. A. (2003). Synchroneity of tropical and high-latitude Atlantic temperatures over the last glacial termination. *Science*, *301*(5638), 1361–1364. doi: 10.1126/science.1088470

Lentz, D. L., Dunning, N. P., Scarborough, V. L., & Grazioso, L. (2018). Imperial resource management at the ancient Maya city of Tikal: A resilience model of sustainability and collapse. *Journal of Anthropological Archaeology*, *52*, 113–122. doi: 10.1016/J.JAA.2018.08.005

Lewis, S. C., LeGrande, A. N., Kelley, M., & Schmidt, G. A. (2010). Water vapour source impacts on oxygen isotope variability in tropical precipitation during Heinrich events. *Climate of the Past* , 87–133. doi: 10.5194/cpd-6-87-2010

Liu, W. J., Li, P. J., Li, H. M., & Duan, W. P. (2006). Estimation of evaporation rate from soil surface using stable isotopic composition of throughfall and stream water in a tropical seasonal rain forest in Xishuangbanna, China. *Acta Ecologica Sinica*, *26*(5), 1303–1311. doi: 10.1016/s1872-2032(06)60022-x

Lynch-Stieglitz, J., Schmidt, M. W., Gene Henry, L., Curry, W. B., Skinner, L. C., Mulitza, S., … Chang, P. (2014). Muted change in Atlantic overturning circulation over some glacial-aged Heinrich events. *Nature Geoscience*, *7*(2), 144–150. doi: 10.1038/ngeo2045

Lyu, Y., Luo, W., Wang, Y., Zeng, G., Wang, Y., Cheng, A., … Wang, S. (2020). *Impacts of cave ventilation on drip water δ 13 C DIC and its paleoclimate implication*. doi: 10.1016/j.quaint.2020.03.050

Magaña, V. O., Vázquez, J. L., Pérez, J. L., & Pérez, J. B. (2003). Impact of El Niño on precipitation in Mexico . *Geofísica Internacional* , *42*(3), 313–330. Retrieved from http://www.redalyc.org/articulo.oa?id=56842304

Marks, G. S. (2020). Investigating Mexican paleoclimate with precisely dated speleothems. In *Investigating Mexican paleoclimate with precisely dated speleothems*. Massachusetts Institute of Technology. doi: 10.1575/1912/26101

Martín-Chivelet, J., Belén Muñoz-García, M., Cruz, J. A., Ortega, A. I., Turrero, M. J., & Jones, B. (2017). *Speleothem Architectural Analysis: Integrated approach for stalagmite-based paleoclimate research*. doi: 10.1016/j.sedgeo.2017.03.003

McDermott, F. (2004). Palaeo-climate reconstruction from stable isotope variations in speleothems: a review. *Quaternary Science Reviews*, *23*(7–8), 901–918. doi:

10.1016/J.QUASCIREV.2003.06.021
Medina-Elizalde, M., Burns, S. J., Lea, D. W., Asmerom, Y., von Gunten, L., Polyak, V., … Karmalkar, A. (2010a). High resolution stalagmite climate record from the Yucatán Peninsula spanning the Maya terminal classic period. *Earth and Planetary Science Letters*, *298*(1–2), 255–262. doi: 10.1016/J.EPSL.2010.08.016
Medina-Elizalde, M., Burns, S. J., Lea, D. W., Asmerom, Y., von Gunten, L., Polyak, V., … Karmalkar, A. (2010b). High resolution stalagmite climate record from the Yucatán Peninsula spanning the Maya terminal classic period. *Earth and Planetary Science Letters*, *298*(1–2), 255–262. doi: 10.1016/j.epsl.2010.08.016
Medina-Elizalde, M., Burns, S. J., Polanco-Martínez, J. M., Beach, T., Lases-Hernández, F., Shen, C. C., & Wang, H. C. (2016). High-resolution speleothem record of precipitation from the Yucatan Peninsula spanning the Maya Preclassic Period. *Global and Planetary Change*, *138*, 93–102. doi: 10.1016/j.gloplacha.2015.10.003
Medina-Elizalde, M., & Rohling, E. J. (2012). Collapse of Classic Maya Civilization Related to Modest Reduction in Precipitation. *Science* . doi: 10.1126/science.1216629
Méndez, M., & Magaña, V. (2010). Regional aspects of prolonged meteorological droughts over Mexico and central America. *Journal of Climate*, *23*(5), 1175–1188. doi: 10.1175/2009JCLI3080.1
Mestas-Nuñez, A. M., Enfield, D. B., & Zhang, C. (2007). Water vapor fluxes over the Intra-Americas Sea: Seasonal and interannual variability and associations with rainfall. *Journal of Climate*, *20*(9), 1910–1922. doi: 10.1175/JCLI4096.1
Meyer, K. W., Feng, W., Breecker, D. O., Banner, J. L., & Guilfoyle, A. (2014). Interpretation of speleothem calcite δ13C variations: Evidence from monitoring soil CO2, drip water, and modern speleothem calcite in central Texas. *Geochimica et Cosmochimica Acta*, *142*, 281–298. doi: 10.1016/j.gca.2014.07.027
Mickler, P. J., Banner, J. L., Stern, L., Asmerom, Y., Edwards, R. L., & Ito, E. (2004). Stable isotope variations in modern tropical speleothems: Evaluating equilibrium vs. kinetic isotope effects. *Geochimica et Cosmochimica Acta*, *68*(21), 4381–4393. doi: 10.1016/j.gca.2004.02.012
Mickler, P. J., Carlson, P., Banner, J. L., Breecker, D. O., Stern, L., & Guilfoyle, A. (2019). Quantifying carbon isotope disequilibrium during in-cave evolution of drip water along discreet flow paths. *Geochimica et Cosmochimica Acta*, *244*, 182–196. doi: 10.1016/j.gca.2018.09.027
Mickler, P. J., Stern, L. A., & Banner, J. L. (2006). Large kinetic isotope effects in modern speleothems. *GSA Bulletin*, *118*(1–2), 65–81. doi: 10.1130/B25698.1
Mischel, S. A., Scholz, D., & Spötl, C. (2015). δ18O values of cave drip water: a promising proxy for the reconstruction of the North Atlantic Oscillation? *Climate Dynamics*, *45*(11–12), 3035–3050. doi: 10.1007/s00382-015-2521-5
Moreau-Le Golvan, Y., Michelot, J. L., & Boisson, J. Y. (1997). Stable isotope contents of porewater in a claystone formation (Tournemire, France): Assessment of the extraction technique and preliminary results. *Applied Geochemistry*, *12*(6), 739–745. doi: 10.1016/S0883-2927(97)00044-9
Morse, J. W., & Bender, M. L. (1990). Partition coefficients in calcite: Examination of factors influencing the validity of experimental results and their application to natural systems. *Chemical Geology*, *82*(C), 265–277. doi: 10.1016/0009-2541(90)90085-L
Mühlinghaus, C., Scholz, D., & Mangini, A. (2007). Modelling stalagmite growth and δ13C as a

function of drip interval and temperature>. *Geochimica et Cosmochimica Acta*, *71*(11), 2780–2790. doi: 10.1016/j.gca.2007.03.018

Mühlinghaus, C., Scholz, D., & Mangini, A. (2009). Modelling fractionation of stable isotopes in stalagmites. *Geochimica et Cosmochimica Acta*, *73*(24), 7275–7289. doi: 10.1016/j.gca.2009.09.010

Murray-Tortarolo, G. N., & Salgado, M. M. (2021). Drought as a driver of Mexico-US migration. *Climatic Change*, *164*(3–4), 1–11. doi: 10.1007/s10584-021-03030-2

Nguyen, P., Shearer, E. J., Tran, H., Ombadi, M., Hayatbini, N., Palacios, T., … Sorooshian, S. (2019). The CHRS data portal, an easily accessible public repository for PERSIANN global satellite precipitation data. *Scientific Data*, *6*(1), 1–10. doi: 10.1038/sdata.2018.296

Noronha, A. L., Johnson, K. R., Southon, J. R., Hu, C., Ruan, J., & McCabe-Glynn, S. (2015). Radiocarbon evidence for decomposition of aged organic matter in the vadose zone as the main source of speleothem carbon. *Quaternary Science Reviews*, *127*, 37–47. doi: 10.1016/J.QUASCIREV.2015.05.021

Oerter, E., Finstad, K., Schaefer, J., Goldsmith, G. R., Dawson, T., & Amundson, R. (2014). Oxygen isotope fractionation effects in soil water via interaction with cations (Mg, Ca, K, Na) adsorbed to phyllosilicate clay minerals. *Journal of Hydrology*, *515*, 1–9. doi: 10.1016/j.jhydrol.2014.04.029

Osácar, M. C., Sancho, C., Muñoz, A., Moreno, A., Bartolomé, M., Pérez, C., … Stoll, H. (2017). δ13C and Mg/Ca dripwater response to environmental conditions in the Ortigosa caves (La Rioja, Spain). *Geogaceta*, *61*, 175–178.

Osorio-Osorio, J. A., Astudillo-Sánchez, C. C., Villanueva-Díaz, J., Soria-Díaz, L., & Vargas-Tristán, V. (2020). Historical precipitation reconstruction of el cielo biosphere reserve, Mexico, using taxodium mucronatum (Cupressaceae) annual growth rings. *Revista de Biologia Tropical*, *68*(3), 818–832. doi: 10.15517/RBT.V68I3.39624

Oster, J. L., Montañez, I. P., Guilderson, T. P., Sharp, W. D., & Banner, J. L. (2010). Modeling speleothem δ13C variability in a central Sierra Nevada cave using 14C and 87Sr/86Sr. *Geochimica et Cosmochimica Acta*, *74*(18), 5228–5242. doi: 10.1016/j.gca.2010.06.030

Palmer, M. V., & Palmer, A. N. (2012). Petrographic and isotopic evidence for late-stage processes in sulfuric acid caves of the Guadalupe Mountains, New Mexico, USA. *International Journal of Speleology*, *41*(2), 231–250. doi: 10.5038/1827-806X.41.2.10

Pausata, F. S. R., Battisti, D. S., Nisancioglu, K. H., & Bitz, C. M. (2011). Chinese stalagmite δ 18 O controlled by changes in the indian monsoon during a simulated heinrich event. *Nature Geoscience*, *4*(7), 474–480. doi: 10.1038/ngeo1169

Pavia, E. G., Graef, F., & Reyes, J. (2006). PDO–ENSO Effects in the Climate of Mexico. *Journal of Climate*, *19*(24), 6433–6438. doi: 10.1175/JCLI4045.1

Pérez Quezadas, J., Cortés Silva, A., Inguaggiato, S., del Rocío Salas Ortega, M., Cervantes Pérez, J., & Heilweil, V. M. (2015). Meteoric isotopic gradient on the windward side of the sierra madre oriental area, Veracruz - Mexico. *Geofisica Internacional*, *54*(3), 267–276. doi: 10.1016/j.gi.2015.04.021

Quezadas, J. P., Adams, D., Sánchez Murillo, R., Lagunes, A. J., & Rodríguez Castañeda, J. L. (2021). Isotopic variability (δ18O, δ2H and d-excess) during rainfall events of the north American monsoon across the Sonora River Basin, Mexico. *Journal of South American Earth Sciences*, *105*, 102928. doi: 10.1016/j.jsames.2020.102928

Quiroz-Jiménez, J. D., Roy, P. D., Beramendi-Orosco, L. E., Lozano-García, S., & Vázquez-Selem, L. (2018). Orbital-scale droughts in central-northern Mexico during the late

Quaternary and comparison with other subtropical and tropical records. *Geological Journal*, *53*(1), 230–242. doi: 10.1002/gj.2888

Rasmussen, S. O., Andersen, K. K., Svensson, A. M., Steffensen, J. P., Vinther, B. M., Clausen, H. B., … Ruth, U. (2006). A new Greenland ice core chronology for the last glacial termination. *Journal of Geophysical Research Atmospheres*, *111*(6), D06102. doi: 10.1029/2005JD006079

Reimer, P. J., Bard, E., Bayliss, A., Beck, J. W., Blackwell, P. G., Ramsey, C. B., … van der Plicht, J. (2013). Selection and Treatment of Data for Radiocarbon Calibration: An Update to the International Calibration (IntCal) Criteria. *Radiocarbon*, *55*(4), 1923–1945. doi: 10.2458/azu_js_rc.55.16955

Riechelmann, D. F. C., Deininger, M., Scholz, D., Riechelmann, S., Schröder-Ritzrau, A., Spötl, C., … Immenhauser, A. (2013). Disequilibrium carbon and oxygen isotope fractionation in recent cave calcite: Comparison of cave precipitates and model data. *Geochimica et Cosmochimica Acta*, *103*, 232–244. doi: 10.1016/j.gca.2012.11.002

Riechelmann, D. F. C., Schröder-Ritzrau, A., Scholz, D., Fohlmeister, J., Spötl, C., Richter, D. K., & Mangini, A. (2011). Monitoring Bunker Cave (NW Germany): A prerequisite to interpret geochemical proxy data of speleothems from this site. *Journal of Hydrology*, *409*(3–4), 682–695. doi: 10.1016/J.JHYDROL.2011.08.068

Risi, C., Bony, S., & Vimeux, F. (2008). Influence of convective processes on the isotopic composition (δ^{18} O and δ D) of precipitation and water vapor in the tropics: 2. Physical interpretation of the amount effect. *Journal of Geophysical Research*, *113*(D19), D19306. doi: 10.1029/2008JD009943

Rivera-Rivera, D. M., Chidambaram, S., Tirumalesh, K., Escobedo-Urias, D. C., Sujitha, S. B., Rodriguez-Espinosa, P. F., … Jonathan, M. P. (2021). Stable isotopic (δ2H, δ18O) monograms of winter precipitation events and hydro-climatic dynamics in Central Mexico. *Atmospheric Research*, *261*, 105744. doi: 10.1016/j.atmosres.2021.105744

Roy, P. D., Quiroz-Jiménez, J. D., Pérez-Cruz, L. L., Lozano-García, S., Metcalfe, S. E., Lozano-Santacruz, R., … Romero, F. M. (2013a). Late Quaternary paleohydrological conditions in the drylands of northern Mexico: A summer precipitation proxy record of the last 80 cal ka BP. *Quaternary Science Reviews*, *78*, 342–354. doi: 10.1016/j.quascirev.2012.11.020

Roy, P. D., Rivero-Navarette, A., Lopez-Balbiaux, N., Pérez-Cruz, L. L., Metcalfe, S. E., Sankar, G. M., & Sánchez-Zavala, J. L. (2013b). A record of Holocene summer-season palaeohydrological changes from the southern margin of Chihuahua Desert (Mexico) and possible forcings. *The Holocene*, *23*(8), 1105–1114. doi: 10.1177/0959683613483619

Roy, P. D., Rivero-Navarrete, A., Sánchez-Zavala, J. L., Beramendi-Orosco, L. E., Muthu-Sankar, G., & Lozano-Santacruz, R. (2016). Atlantic Ocean modulated hydroclimate of the subtropical northeastern Mexico since the last glacial maximum and comparison with the southern US. *Earth and Planetary Science Letters*, *434*, 141–150. doi: 10.1016/j.epsl.2015.11.048

Roy, P. D., Vera-Vera, G., Sánchez-Zavala, J. L., Shanahan, T. M., Quiroz-Jiménez, J. D., Curtis, J. H., … Muthusankar, G. (2020). Depositional histories of vegetation and rainfall intensity in Sierra Madre Oriental Mountains (northeast Mexico) since the late Last Glacial. *Global and Planetary Change*, *187*(July 2019), 103136. doi: 10.1016/j.gloplacha.2020.103136

Rudzka, D., McDermott, F., Baldini, L. M., Fleitmann, D., Moreno, A., & Stoll, H. (2011). The

coupled δ13C-radiocarbon systematics of three Late Glacial/early Holocene speleothems; insights into soil and cave processes at climatic transitions. *Geochimica et Cosmochimica Acta*, *75*(15), 4321–4339. doi: 10.1016/j.gca.2011.05.022

Salinas-Rodríguez, M. M., Estrada-Castillón, E., & Illarreal-Quintanilla, J. A. (2017). Endemic vascular plants of the sierra madre oriental, Mexico. *Phytotaxa*, *328*(1), 1–52. doi: 10.11646/PHYTOTAXA.328.1.1

Sánchez-Murillo, R., Birkel, C., Welsh, K., Esquivel-Hernández, G., Corrales-Salazar, J., Boll, J., … Araguás-Araguás, L. J. (2016). Key drivers controlling stable isotope variations in daily precipitation of Costa Rica: Caribbean Sea versus Eastern Pacific Ocean moisture sources. *Quaternary Science Reviews*, *131*, 250–261. doi: 10.1016/J.QUASCIREV.2015.08.028

Sánchez-Murillo, R., Esquivel-Hernández, G., Welsh, K., Brooks, E. S., Boll, J., Alfaro-Solís, R., … Valdés-González, J. (2013). Spatial and Temporal Variation of Stable Isotopes in Precipitation across Costa Rica: An Analysis of Historic GNIP Records. *Open Journal of Modern Hydrology*, *3*(4), 226–240. doi: 10.4236/OJMH.2013.34027

Schmidt, M. W., Spero, H. J., & Lea, D. W. (2004). Links between salinity variation in the Caribbean and North Atlantic thermohaline circulation. *Nature*, *428*(6979), 160–163. doi: 10.1038/nature02346

Schwarcz, H. P., Harmon, R. S., Thompson, P., & Ford, D. C. (1976). Stable isotope studies of fluid inclusions in speleothems and their paleoclimatic significance. *Geochimica et Cosmochimica Acta*, *40*(6), 657–665. doi: 10.1016/0016-7037(76)90111-3

Seager, R., Ting, M., Davis, M., & Stahle, D. W. (2009). Mexican drought: an observational modeling and tree ring study of variability and climate change. In *Atmósfera* (Vol. 22). Retrieved from http://ingrid.ldeo.columbia.edu/SOURCES/UNAM/

Shen, C.-C., Lin, K., Duan, W., Jiang, X., Partin, J. W., Edwards, R. L., … Tan, M. (2013). Testing the annual nature of speleothem banding. *Scientific Reports 2013 3:1*, *3*(1), 1–5. doi: 10.1038/srep02633

Shultz, J. M., Berg, R. C., Kossin, J. P., Burkle Jr, F., Maggioni, A., Pinilla Escobar, V. A., … Galea, S. (2021). Convergence of climate-driven hurricanes and COVID-19: The impact of 2020 hurricanes Eta and Iota on Nicaragua. *The Journal of Climate Change and Health*, *3*, 100019. doi: 10.1016/j.joclim.2021.100019

Sinclair, D. J., Banner, J. L., Taylor, F. W., Partin, J., Jenson, J., Mylroie, J., … Miklavič, B. (2012). Magnesium and strontium systematics in tropical speleothems from the Western Pacific. *Chemical Geology*, *294–295*, 1–17. doi: 10.1016/J.CHEMGEO.2011.10.008

Smith, C. L., Fairchild, I. J., Spötl, C., Frisia, S., Borsato, A., Moreton, S. G., & Wynn, P. M. (2009). Chronology building using objective identification of annual signals in trace element profiles of stalagmites. *Quaternary Geochronology*, *4*(1), 11–21. doi: 10.1016/j.quageo.2008.06.005

Southon, J., Noronha, A. L., Cheng, H., Edwards, R. L., & Wang, Y. (2012). A high-resolution record of atmospheric 14C based on Hulu Cave speleothem H82. *Quaternary Science Reviews*, *33*, 32–41. doi: 10.1016/j.quascirev.2011.11.022

Spötl, C., Fairchild, I. J., & Tooth, A. F. (2005). Cave air control on dripwater geochemistry, Obir Caves (Austria): Implications for speleothem deposition in dynamically ventilated caves. *Geochimica et Cosmochimica Acta*, *69*(10), 2451–2468. doi: 10.1016/J.GCA.2004.12.009

Spötl, C., Mangini, A., & Richards, D. A. (2006). Chronology and paleoenvironment of Marine

Isotope Stage 3 from two high-elevation speleothems, Austrian Alps. *Quaternary Science Reviews*, *25*(9–10), 1127–1136. doi: 10.1016/j.quascirev.2005.10.006

Sprenger, M., Leistert, H., Gimbel, K., & Weiler, M. (2016). Illuminating hydrological processes at the soil-vegetation-atmosphere interface with water stable isotopes. *Reviews of Geophysics*, *54*(3), 674–704. doi: 10.1002/2015RG000515

Sprenger, M., Tetzlaff, D., Buttle, J., Laudon, H., Leistert, H., Mitchell, C. P. J., … Soulsby, C. (2018). Measuring and Modeling Stable Isotopes of Mobile and Bulk Soil Water. *Vadose Zone Journal*, *17*(1), 170149. doi: 10.2136/vzj2017.08.0149

Stahle, D. W., Burnette, D. J., Villanueva, J., Cerano, J., Fye, F. K., Griffin, R. D., … Wolff, K. P. (2012). Tree-ring analysis of ancient baldcypress trees and subfossil wood. *Quaternary Science Reviews*, *34*, 1–15. doi: 10.1016/J.QUASCIREV.2011.11.005

Stahle, D. W., Cook, E. R., Burnette, D. J., Villanueva, J., Cerano, J., Burns, J. N., … Howard, I. M. (2016, October 1). The Mexican Drought Atlas: Tree-ring reconstructions of the soil moisture balance during the late pre-Hispanic, colonial, and modern eras. *Quaternary Science Reviews*, Vol. 149, pp. 34–60. Pergamon. doi: 10.1016/j.quascirev.2016.06.018

Stein, A. F., Draxler, R. R., Rolph, G. D., Stunder, B. J. B., Cohen, M. D., & Ngan, F. (2015, December 1). Noaa's hysplit atmospheric transport and dispersion modeling system. *Bulletin of the American Meteorological Society*, Vol. 96, pp. 2059–2077. American Meteorological Society. doi: 10.1175/BAMS-D-14-00110.1

Stoll, H. M., Müller, W., & Prieto, M. (2012). I-STAL, a model for interpretation of Mg/Ca, Sr/Ca and Ba/Ca variations in speleothems and its forward and inverse application on seasonal to millennial scales. *Geochemistry, Geophysics, Geosystems*, *13*(9). doi: 10.1029/2012GC004183

Tooth, A. F., & Fairchild, I. J. (2003). Soil and karst aquifer hydrological controls on the geochemical evolution of speleothem-forming drip waters, Crag Cave, southwest Ireland. *Journal of Hydrology*, *273*(1–4), 51–68. doi: 10.1016/S0022-1694(02)00349-9

Treble, P. C., Fairchild, I. J., Griffiths, A., Baker, A., Meredith, K. T., Wood, A., & McGuire, E. (2015). Impacts of cave air ventilation and in-cave prior calcite precipitation on Golgotha Cave dripwater chemistry, southwest Australia. *Quaternary Science Reviews*, *127*, 61–72. doi: 10.1016/j.quascirev.2015.06.001

Treble, P., Shelley, J. M. G., & Chappell, J. (2003). Comparison of high resolution sub-annual records of trace elements in a modern (1911–1992) speleothem with instrumental climate data from southwest Australia. *Earth and Planetary Science Letters*, *216*(1–2), 141–153. doi: 10.1016/S0012-821X(03)00504-1

U.S. Customs and Border Protection. (2021). US Border Patrol Apprehensions Southwest land Border Encounters per year. *U.S. Customs and Border ProtectionU.S. Customs and Border Protection*. Retrieved from https://www.cbp.gov/newsroom/stats/southwest-land-border-encounters

Villanueva-Diaz, J., Stahle, D. W., Luckman, B. H., Cerano-Paredes, J., Therrell, M. D., Cleaveland, M. K., & Cornejo-Oviedo, E. (2007). Winter-spring precipitation reconstructions from tree rings for northeast Mexico. *Climatic Change*, *83*(1–2), 117–131. doi: 10.1007/s10584-006-9144-0

Vuille, M., & Werner, M. (2005). Stable isotopes in precipitation recording South American summer monsoon and ENSO variability: Observations and model results. *Climate Dynamics*, *25*(4), 401–413. doi: 10.1007/s00382-005-0049-9

Waelbroeck, C., Labeyrie, L., Michel, E., Duplessy, J. C., Mcmanus, J. F., Lambeck, K., …

Labracherie, M. (2002). Sea-level and deep water temperature changes derived from benthic foraminifera isotopic records. In *Quaternary Science Reviews* (Vol. 21).

Wagner, J. D. M., Cole, J. E., Beck, J. W., Patchett, P. J., Henderson, G. M., & Barnett, H. R. (2010). Moisture variability in the southwestern United States linked to abrupt glacial climate change. *Nature Geoscience*, *3*(2), 110–113. doi: 10.1038/ngeo707

Wang, C., Enfield, D. B., Lee, S. K., & Landsea, C. W. (2006). Influences of the Atlantic warm pool on western hemisphere summer rainfall and Atlantic hurricanes. *Journal of Climate*, *19*(12), 3011–3028. doi: 10.1175/JCLI3770.1

Wang, C., Liu, H., Lee, S. K., & Atlas, R. (2011). Impact of the Atlantic warm pool on United States landfalling hurricanes. *Geophysical Research Letters*, *38*(19), n/a-n/a. doi: 10.1029/2011GL049265

Wang, Y., Cheng, H., Edwards, R. L., Kong, X., Shao, X., Chen, S., … An, Z. (2008). Millennial- and orbital-scale changes in the East Asian monsoon over the past 224,000 years. *Nature*, *451*(7182), 1090–1093. doi: 10.1038/nature06692

Wang, Y. J., Cheng, H., Edwards, R. L., An, Z. S., Wu, J. Y., Shen, C. C., & Dorale, J. A. (2001). A high-resolution absolute-dated late Pleistocene Monsoon record from Hulu Cave, China. *Science (New York, N.Y.)*, *294*(5550), 2345–2348. doi: 10.1126/science.1064618

Warken, S. F., Scholz, D., Spötl, C., Jochum, K. P., Pajón, J. M., Bahr, A., & Mangini, A. (2019). Caribbean hydroclimate and vegetation history across the last glacial period. *Quaternary Science Reviews*, *218*, 75–90. doi: 10.1016/j.quascirev.2019.06.019

Webster, J. W., Brook, G. A., Railsback, L. B., Cheng, H., Edwards, R. L., Alexander, C., & Reeder, P. P. (2007). Stalagmite evidence from Belize indicating significant droughts at the time of Preclassic Abandonment, the Maya Hiatus, and the Classic Maya collapse. *Palaeogeography, Palaeoclimatology, Palaeoecology*, *250*(1–4), 1–17. doi: 10.1016/j.palaeo.2007.02.022

Williams, P. W., King, D. N. T., Zhao, J. X., & Collerson, K. D. (2005). Late Pleistocene to Holocene composite speleothem 18O and 13C chronologies from South Island, New Zealand - Did a global Younger Dryas really exist? *Earth and Planetary Science Letters*, *230*(3–4), 301–317. doi: 10.1016/j.epsl.2004.10.024

Wong, C. I., Banner, J. L., & Musgrove, M. L. (2011). Seasonal dripwater Mg/Ca and Sr/Ca variations driven by cave ventilation: Implications for and modeling of speleothem paleoclimate records. *Geochimica et Cosmochimica Acta*, *75*(12), 3514–3529. doi: 10.1016/j.gca.2011.03.025

Wong, C. I., Banner, J. L., & Musgrove, M. L. (2015). Holocene climate variability in Texas, USA: An integration of existing paleoclimate data and modeling with a new, high-resolution speleothem record. *Quaternary Science Reviews*, *127*, 155–173. doi: 10.1016/j.quascirev.2015.06.023

Woodhead, J., Reisz, R., Fox, D., Drysdale, R., Hellstrom, J., Maas, R., … Edwards, R. L. (2010). Speleothem climate records from deep time? Exploring the potential with an example from the Permian. *Geology*, *38*(5), 455–458. doi: 10.1130/G30354.1

Yadava, M. G., & Ramesh, R. (2005). Monsoon reconstruction from radiocarbon dated tropical Indian speleothems. *Holocene*, *15*(1), 48–59. doi: 10.1191/0959683605h1783rp

Yang, H., Johnson, K. R., Griffiths, M. L., & Yoshimura, K. (2016). Interannual controls on oxygen isotope variability in Asian monsoon precipitation and implications for paleoclimate reconstructions. *Journal of Geophysical Research*, *121*(14), 8410–8428. doi: 10.1002/2015JD024683

Zhang, H., Griffiths, M. L., Chiang, J. C. H., Kong, W., Wu, S., Atwood, A., … Xie, S. (2018). East Asian hydroclimate modulated by the position of the westerlies during Termination I. *Science*, *362*(6414), 580–583. doi: 10.1126/science.aat9393

Zhang, P., Cheng, H., Edwards, R. L., Chen, F., Wang, Y., Yang, X., … Johnson, K. R. (2008). A test of climate, sun, and culture relationships from an 1810-year Chinese cave record. *Science*, *322*(5903), 940–942. doi: 10.1126/science.1163965

Ziegler, M., Nürnberg, D., Karas, C., Tiedemann, R., & Lourens, L. J. (2008). Persistent summer expansion of the Atlantic Warm Pool during glacial abrupt cold events. *Nature Geoscience*, *1*(9), 601–605. doi: 10.1038/ngeo277

Chapter 3: Thermodynamics control precipitation in NE Mexico on orbital to millennial timescales

Adapted from:

Kevin T. Wright, Kathleen R. Johnson, Gabriela Serrato Marks, David McGee, Tripti Bhattacharya, Gregory R. Goldsmith, Clay R. Tabor, Jean-Louis Lacaille-Muzquiz, Gianna Lum, Laura Beramendi-Orosco, Thermodynamics control precipitation in NE Mexico on orbital to millennial timescales, Nature Communications. *In Review.* DOI: 10.21203/rs.3.rs-611282/v1

3.1 Abstract

Northern Mexico is projected to become more arid in the future, however the magnitude, timing and spatial extent of precipitation change is presently poorly constrained. To address this, we have developed a multiproxy ($\delta^{18}O$, $\delta^{13}C$, Mg/Ca) U-Th dated speleothem record of past hydroclimate variability spanning 4.6 to 58.5 ka from Tamaulipas, Mexico. Our results demonstrate a dominant thermodynamic control on precipitation via changes in Atlantic SSTs. Our record robustly demonstrates this response during major paleoclimate events including the Last Glacial Maximum, the Younger Dryas and Heinrich Stadials 1, 3, 4, and 5. While previous work has suggested a strengthening of the Caribbean Low-Level Jet (CLLJ) increases regional rainfall, we utilize a state-of-the-art climate model to isolate cool Atlantic SSTs and a weakening of the CLLJ as the dominant mechanism increased rainfall. We also demonstrate this response is consistent across large parts of Mesoamerica, suggesting drying in the future may be more spatially homogenous than currently predicted.

3.2 Introduction

Records of past hydroclimate are critical for evaluating how precipitation patterns respond to internal ocean-atmospheric variability and external forcings over a range of timescales (100-105 years). Northern Mexico is a water-stressed region that is expected to become drier in the

future, but the spatial distribution and magnitude of this drying is poorly constrained at present due to significant discrepancies between climate model projections (Knutti & Sedláček, 2013; Lewis *et al.*, 2010). Improving hydroclimate projections for Northern Mexico is critical given the substantial social, economic, and ecological impacts that shifts in mean precipitation or precipitation extremes can have in the region. For instance, severe droughts in the past have led to agriculture collapse (Liverman, 1990), national food shortages, and surges in international immigration (Johnson, 2011). Although paleoclimate records can contribute to improved understanding of the range and mechanisms of natural precipitation variability in this sensitive region, thus providing a critical test for climate models, few records are currently available. Speleothems are ideally suited for addressing this gap in the paleoclimate record due to their robust U-Th based age models and the multiple hydrologically sensitive proxies they contain. Despite the prevalence of limestone karst landscapes in Northeast (NE) Mexico, they have not yet been studied in this region.

The modern climatology of NE Mexico is dominated by the Caribbean Low-Level Jet (CLLJ), which transports moisture from the Atlantic Ocean and Caribbean Sea to most of Mexico and Central America (Mesoamerica) during boreal summer. On seasonal timescales, the CLLJ strength exhibits a maxima in July, driven by increased solar heating and northward migration of the Intertropical Convergent Zone (ITCZ) (Muñoz *et al.*, 2008). The CLLJ exhibits another maxima in February, driven by intensified meridional pressure gradient linked to heating over South America. It is important to note, however, only the CLLJ maxima in Boreal summer is associated with increased precipitation over Mexico. On longer timescales, this suggests that insolation variations dominated by orbital precession could impact the CLLJ strength and regional hydroclimate in similar ways, with strengthening of the CLLJ and precipitation

increases during Northern Hemisphere insolation maxima, and a strengthening of the CLLJ without a corresponding precipitation increase during insolation minima.

Previous paleoclimate studies have invoked a strong role for insolation driven CLLJ variations in driving moisture variability across Mesoamerica, but most studies have focused on Southern Mexico and Northwest Mexico. The role insolation plays on longer timescales in NE Mexico is less clear. While a sediment record from the El Potosi Basin in NE Mexico demonstrates a strong correlation of runoff to Northern Hemisphere Summer Insolation (NHSI) through a strengthening of the CLLJ (Roy *et al.*, 2016), other paleoclimate studies have found a limited role for NHSI and have suggested other seasons of insolation as more important drivers of hydroclimate (Quiroz-Jiménez *et al.*, 2018; Roy *et al.*, 2015, 2019, 2020). In contrast, the role of insolation in NW Mexico and Southern Mexico is much better understood, with multiple records demonstrating a strong positive correlation between NHSI and precipitation via alteration of the North American Monsoon (Barron *et al.*, 2012; Kirby *et al.*, 2006; Metcalfe *et al.*, 2015; Roy *et al.*, 2012, 2013) and northward shifts in the ITCZ (Lachniet *et al.*, 2013). Unfortunately, records from NE Mexico do not span multiple orbital cycles, inhibiting our ability to fully constrain the response of precipitation to insolation, and limiting our understanding of the role of external forcing on future regional hydroclimate variability.

On millennial timescales, existing paleoclimate records from NE Mexico have linked decreased precipitation during Heinrich Stadials (HS) to a weakening of the CLLJ. For instance, Roy *et al.* (2016) found decreased Ti concentration in lake sediments from El Potosi Basin, which were interpreted as reflecting reduced precipitation during HS 1. The dry HS1 conditions were assumed to reflect a weakening of the CLLJ as the ITCZ shifted southward in response to a shutdown in the Atlantic Meridional Overturning Circulation (AMOC). However, this

interpretation may be inconsistent with modern dynamics of the CLLJ, which actually strengthens during Boreal winter (February) when the ITCZ migrates south and temperatures in northern South America warm (Cook & Vizy, 2010; Mestas-Nuñez *et al.*, 2007). Using the seasonal ITCZ migration as an analogue, this suggests the CLLJ could theoretically strengthen during HS events in response to a southward ITCZ shift. This highlights a potential discrepancy, wherein a strengthened CLLJ may be associated with increased precipitation during interstadial events and decreased precipitation during stadial events, suggesting some other factor may play a more important role in driving regional hydroclimate of NE Mexico. While previous records have not shown a strong SST control on mean precipitation in NE Mexico on orbital or millennial timescales, we hypothesize that decreased CLLJ strength alone cannot explain drying during Heinrich Stadials

Unlike most previous work reconstructing climate on millennial and orbital timescales in NE Mexico that have alluded to a strong control of CLLJ on precipitation, previous paleoclimate reconstructions and modeling studies focused on interannual to multi-decadal timescales have linked hydroclimate variations across Mesoamerica to changes in SSTs. For instance, elevated SSTs in the Gulf of Mexico (GOM) and North Atlantic are known to increase the intensity and frequency of tropical storms and hurricanes on seasonal timescales. Tree ring (Stahle *et al.*, 2007, 2016; Villanueva-Diaz *et al.*, 2007) and climate model studies have also shown that both Pacific and Atlantic (Bhattacharya *et al.*, 2017; Bhattacharya & Coats, 2020) SSTs exert a strong precipitation control across Mesoamerica on interannual to multidecadal timescales. Over the Common Era (last 2,000 years), changes in Atlantic SSTs are particularly associated with a strong, out-of-phase, dipole precipitation pattern between northern and southern Mesoamerica (Bhattacharya *et al.*, 2017). The impact of SST variations on Mesoamerican hydroclimate

patterns on millennial and orbital timescales is more poorly constrained, largely due to the paucity of records spanning long time periods. For instance, whether the north-south dipole response also dominates on longer timescales is still an open question. While records from southern Mesoamerica consistently show drying during HS events (Lachniet *et al.*, 2013; Medina-Elizalde *et al.*, 2017), lake sediment records from northern Mexico demonstrate a range of responses (Roy *et al.*, 2012, 2014, 2020). While the inconsistency of the northern Mexico records may simply be driven by uncertainties in the age models (Roy *et al.*, 2020), or the influence of tropical Pacific cyclones (Roy *et al.*, 2014), the sparse paleoclimate record from NE Mexico hinders our ability to assess whether the dipole precipitation pattern dominates on longer timescales.

More recent studies have begun to investigate the link between NE Mexico hydroclimate and SSTs on orbital and millennial timescales. For example, increased clay mineral concentration (Al+Si+K+Fe/Ca), interpreted to reflect increased watershed erosion from high intensity rainfall, in lake sediments from the Cieneguilla Basin and the Sandia Basin in NE Mexico have linked periods of increased tropical storm and hurricanes to warm Gulf of Mexico SSTs during the mid-Holocene and Bolling-Allerod (Roy *et al.*, 2019, 2020). However, notably these shifts in precipitation extremes were not clearly associated with shifts in mean precipitation. Overall, the correlation between Gulf of Mexico SSTs and NE Mexico precipitation on orbital and millennial timescales has been shown to be inconsistent (Roy *et al.*, 2016). Despite some evidence for SST influence on NE Mexican hydroclimate, most previous paleoclimate studies have concluded that changes in CLLJ strength are more significant than SSTs in driving regional hydroclimate. Resolving this issue and improving our understanding of the dynamic and thermodynamic response of precipitation across Mesoamerica to external

forcing and internal climate variability is incredibly important under future climate change (Lim *et al.*, 2018).

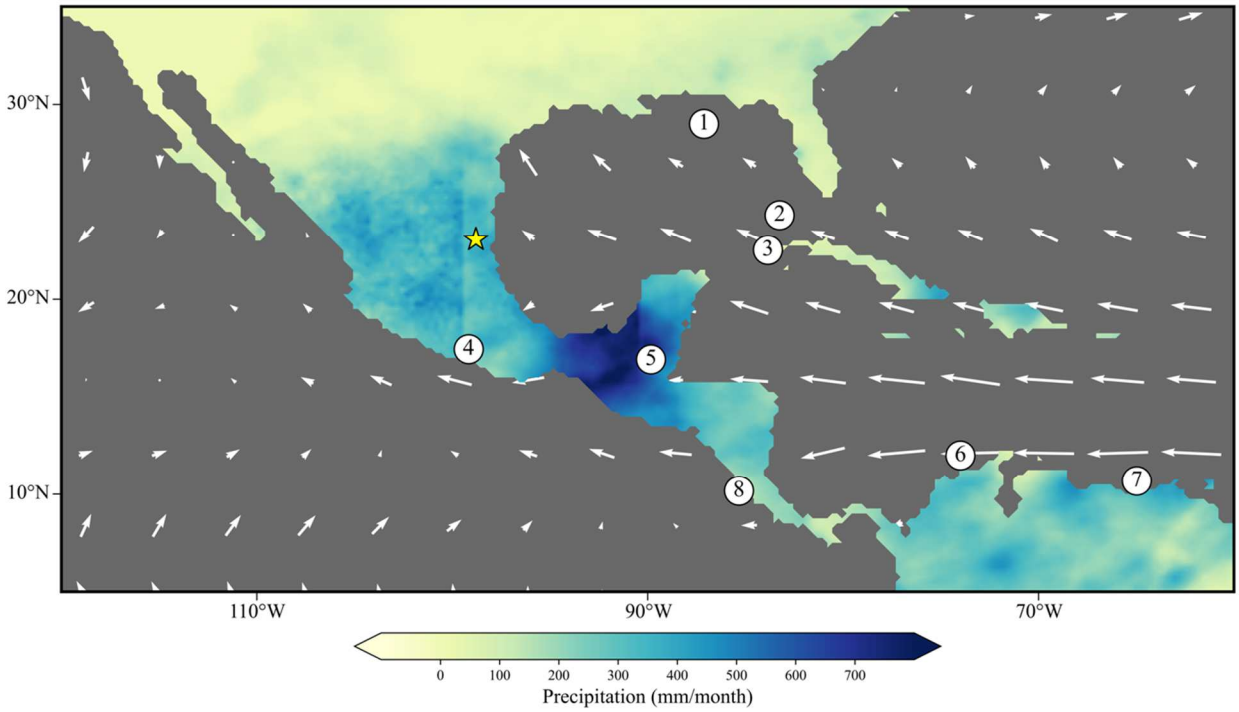

Fig. 3.1: Summer (JJAS) climatology and nearby paleoclimate records. Contour map of regional precipitation and magnitude of low-level (850mb) winds using PERSIANN precipitation data (Ashouri *et al.*, 2015) and winds from MPI-ESM-Historical (Giorgetta *et al.*, 2013). Nearby records include (1) an ocean sediment core from the Gulf of Mexico (Ziegler *et al.*, 2008) and the (2) Florida Straight (Lynch-Stieglitz *et al.*, 2014), speleothem records from (3) Cuba (Warken *et al.*, 2019), (4) Southern Mexico (Lachniet *et al.*, 2013) and (8) Costa Rica (Lachniet, 2009), additional ocean sediment cores from the (6) Caribbean Sea (Schmidt *et al.*, 2004), and (7) Cariaco Basin (Deplazes *et al.*, 2013), and a lake sediment core (5) from Guatemala (Escobar *et al.*, 2012).

To evaluate the timing and underlying dynamics of NE Mexico hydroclimate variability more fully, we present a new decadal-resolution, multi-proxy ($\delta^{18}O$, $\delta^{13}C$, Mg/Ca) speleothem record from Tamaulipas, Mexico that spans 58.5 to 4.6 ka (Fig. 3.1). Our results show strong hydrologic responses to key millennial-scale events including the Younger Dryas and Heinrich Stadials 1 through 5, and a muted response to NHSI. We utilize results of a freshwater-forcing experiment conducted with a state-of-the-art climate model to investigate the relative importance of dynamic and thermodynamic controls on NE Mexico precipitation. Our results suggest a dominant role for cool SSTs in driving decreased moisture transport to the region during these

millennial-scale cold events. This reduction in precipitation occurs despite the strengthening of the Caribbean Low-Level Jet, further highlighting the relative importance of thermodynamics. Finally, our model results combined with a comparison to other high-resolution precipitation records demonstrate that weakened AMOC leads to a spatially uniform drying across Mesoamerica, rather than the dipole response observed on shorter timescales.

3.3 Methods

3.3.1 Chronology

The CB2 stalagmite was cut, polished and sampled for 33 U-Th dates at 2.5 cm intervals along its vertical growth axis using a Dremel hand drill with a diamond dental bur. The CB2 sample has uranium concentrations ranging from 18 to 63 ng/g (Appendix A, Table S3.1). Calcite powder samples weighing 250-300 mg were prepared at Massachusetts Institute of Technology following methods similar to Edwards *et al.*, 1987. Powders were dissolved in nitric acid and spiked with a $^{229}Th - ^{233}U - ^{236}U$ tracer, followed by isolation of U and Th by iron co-precipitation and elution in columns with AG1-X8 resin. The isolated U and Th fractions were analyzed using a Nu Plasma II-ES multi-collector inductively coupled plasma mass spectrometer (MC-ICP-MS) equipped with an Aridus 2 desolvating nebulizer, following methods described in Burns *et al.*, 2016. The corrected ages were calculated using an initial $^{230}Th/^{232}Th$ value of 10.5 ± 2 ppm to correct for detrital ^{230}Th. This value and its uncertainty were determined by testing dates corrected with different initial ^{230}Th corrections for stratigraphic order (Appendix A, Table S3.1). U-Th ages range from 5550 ± 1400 to 58200 ± 1600 years before present (where present is 1950 CE), and all 33 dates fall in stratigraphic order within 2σ uncertainty (Table S3.1). The 95% confidence interval for the age-depth model was constructed using 2000 Monte-Carlo simulations through the age-depth modeling software COPRA (Breitenbach *et al.*, 2012).

3.3.2 Stable Isotope and Trace Element Analysis

CB2 was micro-sampled for both stable isotope and trace element analyses using a Sherline micromill at 500 μm increments to a depth of 1 mm, producing 1578 samples. The powder for CB2 was collected, weighed out to 40 - 80 μg and analyzed on a Kiel IV Carbonate Preparation Device coupled to a Thermo Scientific Delta V-IRMS at the UC Irvine Center for Isotope Tracers in Earth Sciences (CITIES) following methods described by McCabe-Glynn *et al.* (2013) to determine $\delta^{18}O$ and $\delta^{13}C$. Every 32 samples of unknown composition were analyzed with 14 standards which included a mix of NBS-18, IAEA-CO-1, and an in-house standard. The analytical precision for $\delta^{18}O$ and $\delta^{13}C$ is 0.08‰ and 0.05‰, respectively. Speleothem $\delta^{18}O$ values were ice-volume corrected using mean ocean $\delta^{18}O$ values (Appendix A, Fig. S3.1). In total, 1578 samples were analyzed.

For trace element analysis, 20 - 60 μg calcite powder samples were dissolved in 500 μL of a double distilled 2% nitric acid solution. The samples were analyzed using a Nu Instruments Attom High Resolution Inductively Coupled Plasma Mass Spectrometer (HR-ICP-MS) at the CITIES laboratory. Mg/Ca ratios were calculated from the intensity ratios using a bracketing technique with five standards of known concentration and an internal standard (Ge) added to all samples to correct for instrumental drift. Trace element analysis of CB2 serves to complement the interpretation of speleothem $\delta^{18}O$ and $\delta^{13}C$; therefore, a lower-resolution (multi-decadal to centennial) analysis was conducted over the complete record by analyzing every other sample (789 total). For plotting/aesthetic purposes, CB2 Mg/Ca, $\delta^{18}O$ and $\delta^{13}C$ were smoothed using a moving average. The pandas function DataFrame.rolling().mean()was utilized to smooth the data, with the size of the moving window set to 2.

3.3.3 Earth System Model Simulations

We use a water isotope tracer enabled version of the Community Earth System Model, iCESM1 (Brady *et al.*, 2019). Model physics are consistent with CESM1, which simulates present-day and historical climate change quite well (Hurrell *et al.*, 2013). Here, we run a fully-coupled configuration of iCESM1 with 1.9 x 2.5° atmosphere (CAM5) and land (CLM4), and nominal 1° ocean (POP2) and sea ice (CICE4). The model tracks stable water isotopes of oxygen and hydrogen through all model components. Previous studies demonstrate that the water isotope tracer components of iCESM1 can accurately simulate the $\delta^{18}O$ distribution of both present (Wong *et al.*, 2017) and past climates (Zhang *et al.*, 2017).

We configured our 21 ka simulation with period-appropriate orbital parameters and greenhouse gas concentrations, as in the PMIP3 protocol (Abe-Ouchi *et al.*, 2015), and ICE-6G ice sheets (Peltier *et al.*, 2015). Initial isotopic distribution in the ocean comes from the GISS interpolated ocean $\delta^{18}O$ dataset (LeGrande & Schmidt, 2006) with globally uniform enrichment of +1 ‰ for $\delta^{18}O$ (Duplessy *et al.*, 2002). All other ocean initial conditions come from a previously performed LGM simulation (Di Nezio *et al.*, 2016). We run this model configuration for 500 years to reach quasi-equilibrium, with our analyses coming from the final 50 years of simulation. We then branch this simulation to explore the effects of melt water flux in the North Atlantic at the LGM. Starting from year-500 of the 21 ka simulation, we add 0.50 Sv of freshwater with a $\delta^{18}O$ of -30‰ into the North Atlantic (50°N – 70°N), sufficient to rapidly and substantially weaken AMOC (Zhu *et al.*, 2017). After 100 years, we shutoff the freshwater flux and extend the simulation for another 50 years. Analyses come from the final 50 years of the 150-year simulation.

3.4 Results

We present a ~55,000 year record of hydroclimate utilizing oxygen isotopes ($\delta^{18}O$), carbon isotopes ($\delta^{13}C$) and trace elements (Mg/Ca) from speleothem sample CB2. CB2 is a 78 cm-long, candle-shaped, translucent grey and beige colored stalagmite composed of 100% calcite (Fig. 3.2). CB2 was retrieved from Cueva Bonita (23°N, 99°W; 1071 m above sea level), located in the highlands of the Sierra Madre Oriental in the northeastern Mexico state of Tamaulipas (Fig. 3.1). The climate of this region is characterized by cool-dry winters and warm-wet summers (Wang & Lee, 2007b) (Appendix A, Fig. S3.2), with a precipitation maximum in summer (July) driven by warm North Atlantic SSTs and an intensification of the Caribbean Low-Level Jet (Wang & Lee, 2007b) (Appendix A, Fig. S3.2). The stable isotope and trace element speleothem records are tied to a U-series age-depth model, produced by 33 ^{230}Th-^{234}U ages and

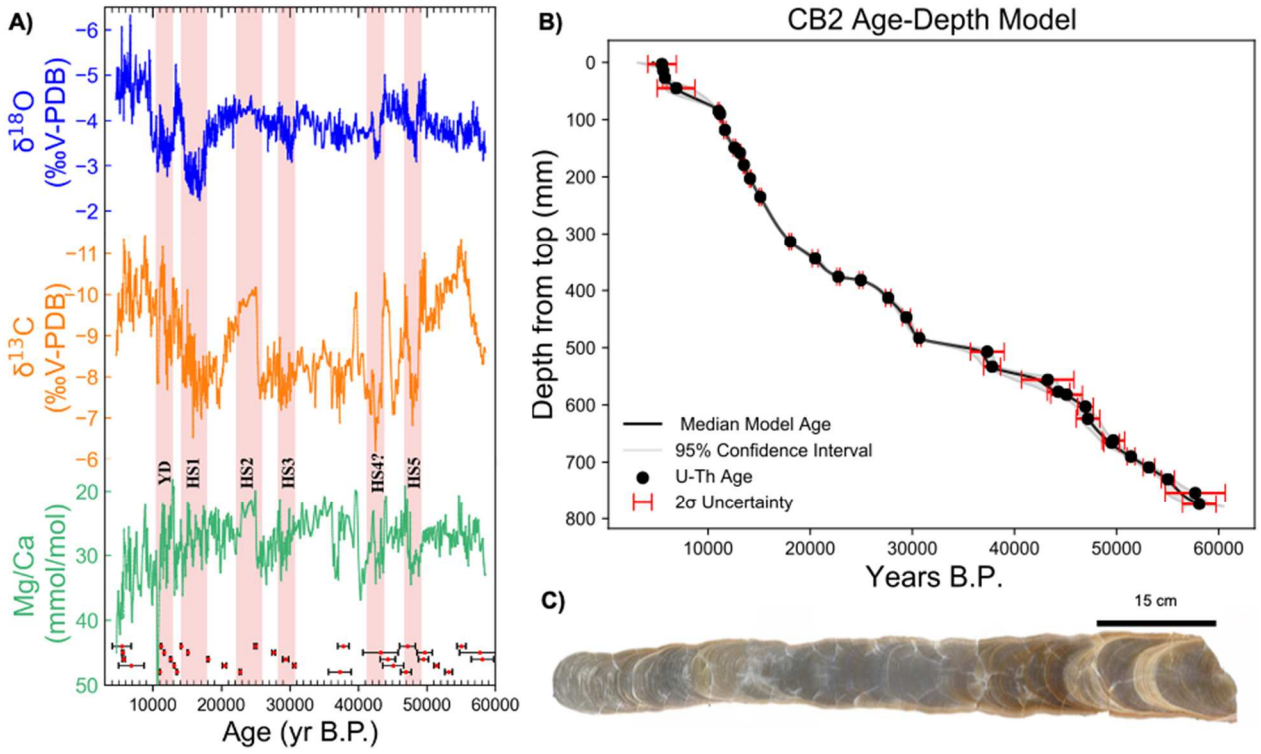

Fig. 3.2: Stalagmite CB2, Age-Depth Model and Mg/Ca, $\delta^{18}O$ and $\delta^{13}C$ results. A) Results of 1578 stable isotope and 789 trace element measurements. $\delta^{18}O$ is top and blue, $\delta^{13}C$ is central and in orange, Mg/Ca is in bottom and green. Dates with associated uncertainties are below Mg/Ca. Heinrich Stadials highlighted in light red. **B)** CB2 Age-Depth Model constructed using 2000 Monte-Carlo simulations via the age-depth modeling software COPRA and 33 U-Th ages. Uncertainty in age-depth model indicated by grey shading, uncertainty in U-Th ages indicated by red error bars. **C)** Sample CB2 after being cut and polished.

the mean of 2000 Monte-Carlo simulations using the age-modeling software COPRA (Breitenbach *et al.*, 2012). The age model indicates the sample formed continuously from 58.5 ± 3.8 ka to 4.6 ± 2.4 ka, with a relatively constant growth rate and an average temporal resolution of 34 years (Fig. 3.2). This represents the highest resolution continuous paleoclimate proxy record in Mexico over this time period.

Previous work in Southern Mexico has consistently interpreted $\delta^{18}O_p$ to be reflective of precipitation amount (Frappier *et al.*, 2014; Lachniet *et al.*, 2013, 2017; Medina-Elizalde *et al.*, 2016), with greater amounts of rainfall associated with more negative $\delta^{18}O_p$ values. (Risi *et al.*, 2008) argues the amount effect dominates in the tropics due to high rainfall rates, which limits isotopic exchange with near-surface moisture. However, in nearby Texas, $\delta^{18}O_p$ has been interpreted to reflect shifting moisture source, temperature, seasonality and shifts in thunderstorm size and duration (Maupin *et al.*, 2021; Wong *et al.*, 2015). However, given the modeling and observational data presented in Chapter 2, including an analysis of moisture bearing air trajectories (Fig. 2.4), observational records of precipitation and drip water $\delta^{18}O$ (Fig. 2.5), as well as proxy system model results (Fig. 2.10), we suggest speleothem $\delta^{18}O$ at Cueva Bonita is dominantly influenced by precipitation amount.

While $\delta^{18}O$ is often a proxy for previously mentioned larger scale atmospheric processes, the controls of $\delta^{13}C$ are often more localized and record changes in overlying vegetation (amount and type), soil respiration and CO_2 degassing (Fohlmeister *et al.*, 2020). We suggest the most likely driver of $\delta^{13}C$ in CB2 is prior calcite precipitation (PCP), which occurs when there is reduced local water balance and is the result of enhanced CO_2 degassing in the epikarst (Johnson *et al.*, 2006). As a further constraint on the mechanisms of CB2 $\delta^{13}C$ variability, we conducted Mg/Ca analyses to test for covariation of $\delta^{13}C$ and Mg/Ca, which is a robust indicator of PCP. In

addition to the preferential loss of ^{12}C from the drip water dissolved inorganic carbon pool during CO_2 degassing, PCP leads to the preferential uptake of Ca^{2+} leaving the remaining drip waters, and speleothem, enriched in trace elements (Mg^{2+}). CB2 $\delta^{13}C$ and Mg/Ca ratios strongly moderately correlate on orbital timescales (r = 0.31) and strongly correlate on millennial timescales, especially during Heinrich Stadials (r = 0.69), suggesting they are both dominantly controlled by PCP.

The CB2 $\delta^{18}O$ record is dominated by millennial scale variations during the glacial and deglacial periods, and there is a clear ~1‰ decrease from the last glacial maximum to the Holocene (after correcting for global ice volume). In contrast to speleothem records from Asia and South America (Cheng *et al.*, 2012, 2016), the CB2 $\delta^{18}O$ record shows no clear precessional signal on orbital timescales, likely reinforcing the notion that this location is not impacted by monsoon dynamics. While increased precipitation in the early-Holocene has been recorded elsewhere in Mesoamerica (Lachniet *et al.*, 2013; Warken *et al.*, 2019), the effects of changing glacial-interglacial cave temperatures could easily explain the 1‰ glacial-interglacial shift observed in our $\delta^{18}O$ record (see Appendix A). The lack or orbital variability provides a relatively stable and un-varying background to which large amplitude millennial scale variability is superimposed on. The $\delta^{18}O$ time series consistently exhibits large positive excursions during Heinrich Stadials, indicating shifts towards drier conditions. Speleothem $\delta^{18}O$ values (n = 1578) range from -1.29‰ to -6.30‰ (VPDB) with the most ^{18}O-enriched samples occurring during Heinrich Stadial 1 (HS 1) at ~16.8 ka (Fig. 2). However, excursions toward higher $\delta^{18}O$ values are also noted during 50-47 ka, 43-42 ka, 31-28 ka, 18-15 ka, and 12-10 ka, corresponding to HS 5, 4, 3, 1 and the Younger Dryas (YD), respectively (Fig. 2). While the timing of HS 4 in our

record is slightly older than the expected age (~40-38 ka) (Hemming, 2004), the offset can be attributed to a relatively large uncertainty in our age model around this time.

The CB2 $\delta^{13}C$ data co-varies with $\delta^{18}O$ (Pearson's r = 0.52) and is similarly dominated by large amplitude millennial variations during the glacial, and a ~3‰ decrease across the deglaciation (Fig. 3.2). A lake sediment record from the region suggests the decrease in $\delta^{13}C$ could reflect a shift from C_4 to C_3 dominant vegetation (Roy *et al.*, 2019), but this shift could also potentially reflect some combination of decreased PCP, increased soil respiration or vegetation intensity, and/or decreased water-rock interaction during the Holocene (Fohlmeister *et al.*, 2020b). Millennial-scale shifts in $\delta^{18}O$ are reproduced in the $\delta^{13}C$ record, consistent with decreased local water balance during the Younger Dryas and Heinrich Stadials. Increases in $\delta^{13}C$ were as large as 3.94‰ during HS 5. However, not all changes in $\delta^{13}C$ were as dramatic, such as during HS 3 the shift in $\delta^{13}C$ was as subtle as 1.04‰. We suggest the varying responses recorded by CB2 proxies may reflect real differences between individual Heinrich Stadials (Lynch-Stieglitz *et al.*, 2014).

The CB2 Mg/Ca values exhibit similar variations on millennial timescales as the stable isotopes, but diverge from them during the glacial-interglacial transition, with an increase from mean glacial concentrations of 30 mmol/mol to Holocene concentrations of ~40 mmol/mol (Fig. 3.2). We suggest this could potentially reflect the influence of temperatures on Mg partitioning into calcite (See Appendix A; Stoll *et al.*, 2012). During the glacial period, Mg/Ca data is consistent with a PCP control, especially during HS 3, 4 and 5, as evidenced by a significant positive correlation between $\delta^{13}C$ and Mg/Ca (Pearson's r = 0.8, r = 0.61, r = 0.66, respectively). We therefore interpret higher Mg/Ca ratios and enriched ^{13}C to reflect enhanced PCP during

periods of reduced local water balance (Appendix A), which is influenced by both precipitation amount and evapotranspiration.

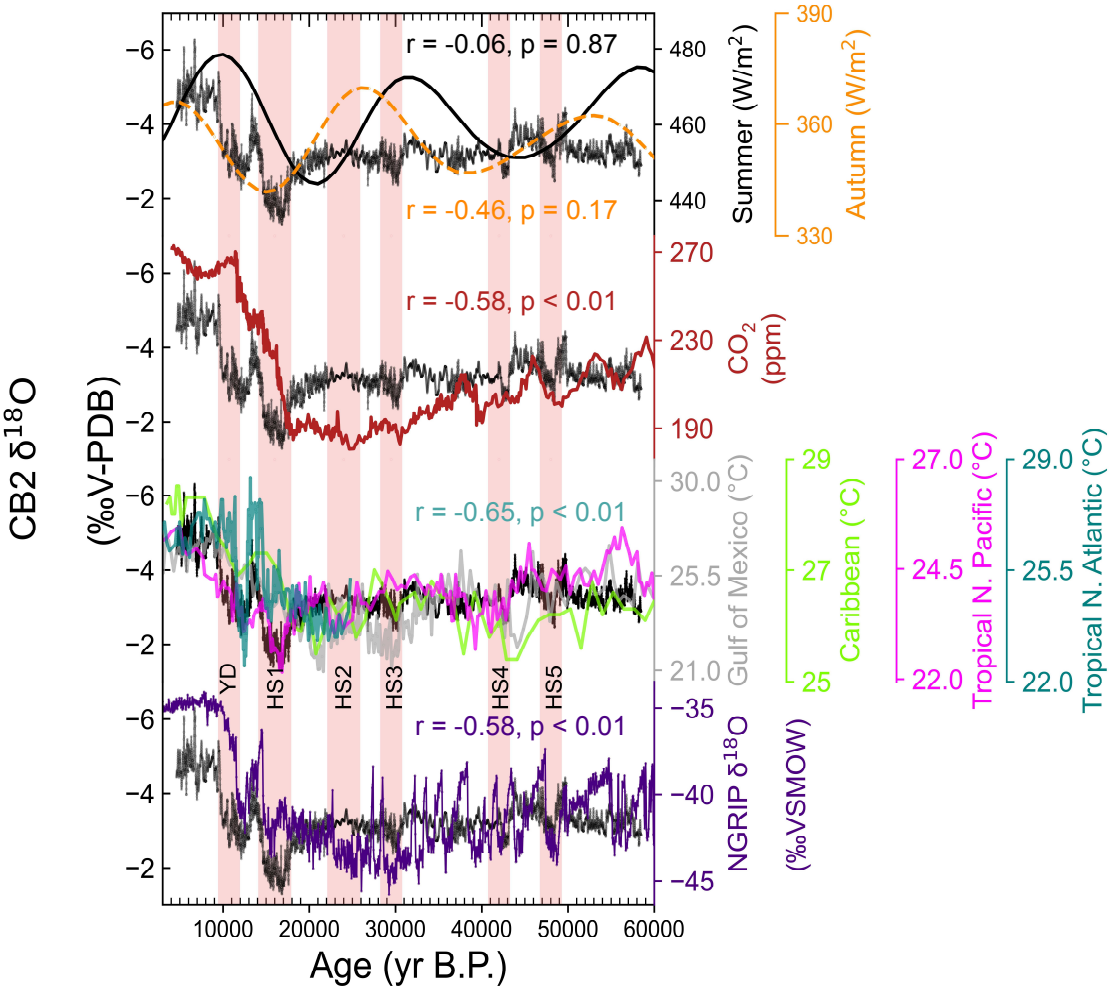

Fig. 3.3: Comparison of CB2 $\delta^{18}O$ to various forcings. a) Autumn (SON; orange) and Summer (JJA; black) insolation. b) Atmospheric pCO_2 (maroon; Bereiter et al., 2015). c) SSTs from Gulf of Mexico (r = -0.59, p < 0.01, silver, Ziegler et al., 2008), Caribbean (r = -0.59, p < 0.04, lime green, Schmidt et al., 2004), Tropical N. Pacific (r = -0.62, p < 0.01, magenta, Dubois et al., 2011) and Tropical N. Atlantic (r = -0.65, p < 0.01, teal, Lea et al., 2003). d) Greenland temperatures (indigo; Rasmussen et al., 2006).

3.5 Discussion

3.5.1 SST forcing of precipitation on orbital timescales

While orbital-driven variations in insolation have been invoked to explain widespread moisture variations in the broader region of Mesoamerica (Lachniet *et al.*, 2013), as well in NE

Mexico (Roy *et al.*, 2016), most of these records only span one precession cycle. The CB2 record, which spans ~2.5 precession cycles and extends ~25,000 years beyond the oldest lake record from NE Mexico (Roy *et al.*, 2020), thus offers a unique opportunity to further constrain the impacts of insolation on precipitation and local water balance. While summer insolation has been proposed to drive precipitation in NE Mexico via a northward shift in the ITCZ and a strengthening of the CLLJ (Roy *et al.*, 2016), and in NW Mexico via an intensified NAM (Barron *et al.*, 2012b; Metcalfe *et al.*, 2015), our record does not demonstrate a strong correlation to summer insolation. However, our record is not alone in that a growing number of records across Mesoamerica have also found a weak correlation to NHSI, suggesting the influence of autumn, winter or spring insolation as the dominant driver of hydroclimate variability on orbital timescales. For instance, Roy *et al.*, (2015, 2019, 2020) has attributed a strong correlation between increased watershed erosion and/or runoff in northern Mexico to autumn insolation through increased tropical cyclone and hurricane activity. Furthermore, water scarcity in North Central Mexico recorded by increased authigenic calcite precipitation in a sediment core from ephemeral Lake Santiaguillo, has been linked to peaks in spring insolation (Quiroz-Jiménez *et al.*, 2018). Even winter insolation has been linked to an extended wet season in speleothem $\delta^{18}O$ records from Santo Tomás Cave in Cuba and Terciopelo Cave in Costa Rica (Lachniet *et al.*, 2009; Warken *et al.*, 2019). However, comparison of CB2 $\delta^{18}O$ to Northern Hemisphere insolation from different seasons demonstrates consistently weak correlations over the last ~55 ka (Appendix A, Fig. S3.3). While CB2 $\delta^{18}O$ seemingly changes with insolation over the last 20,000 years (Fig. 3.3, Fig. S3.3), exhibiting an in-phase response with autumn insolation or a lagged response to summer insolation, this relationship doesn't continue throughout the late-Pleistocene. This lack of a consistent insolation pattern suggests that other boundary conditions

such as global ice volume, atmospheric pCO_2, or SSTs may play a more direct role in explaining glacial-interglacial hydroclimate variability in NE Mexico than insolation.

The CB2 $\delta^{18}O$ time series shows much more similarity with regional and global temperature records, indicating that precipitation at our study site may be more sensitive to thermodynamic controls on orbital timescales. Comparison with the Greenland ice core temperature record (Andersen *et al.*, 2004), shows the CB2 record is dominated by relatively cool and/or dry glacial conditions, as evidenced by relatively positive $\delta^{18}O$ values from 58.5 to 20 ka, with a shift towards warmer and/or wetter conditions during the deglacial and Holocene. Superimposed on this orbital-scale trend are millennial scale shifts towards more positive $\delta^{18}O$ values, indicating even drier conditions during Heinrich Stadials and the Younger Dryas. These trends are reproduced by the CB2 $\delta^{13}C$ and Mg/Ca records. Compared with insolation, CB2 $\delta^{18}O$ exhibits a much better correlation ($r = -0.59$ to -0.65) with regional SSTs, including the Tropical North Atlantic, the Gulf of Mexico, the Caribbean Sea, and the Eastern Equatorial Pacific (Fig. 3.3c; (Dubois *et al.*, 2011; Lea *et al.*, 2003; Schmidt *et al.*, 2004; Ziegler *et al.*, 2008). Similarly, the CB2 record also exhibits a closer relationship with atmospheric pCO_2 than with insolation ($r = -0.58$, $p < 0.05$, Fig. 3.3b). Other records from the region have also shown a strong correlation to changes in local SSTs. For instance, increased rainfall in SE USA indicated by increased Mississippi River discharge into the Gulf of Mexico has been attributed to warmer SSTs (Tripsanas *et al.*, 2013). Also, a stalagmite record from Cuba has attributed variability in $\delta^{18}O$ to be driven by Gulf of Mexico and Caribbean Sea SSTs on glacial-interglacial timescales (Warken *et al.*, 2019). Even lake sediment records from NE Mexico have identified SSTs as an important driver of climate on orbital timescales, but this record did not maintain a strong correlation to

SSTs into the Holocene, consequently, more emphasis was placed on insolation, shifts in the ITCZ, and a stronger CLLJ (Roy *et al.*, 2016).

The CB2 record does not support a direct insolation control on NE Mexico precipitation, but rather suggests that glacial-interglacial variations in sea surface temperatures, indirectly reflecting orbital forcing and associated feedbacks, are more important. This suggests SST variations may be the dominant control on long timescales and future water availability may be more sensitive to SST changes than local atmospheric circulation patterns.

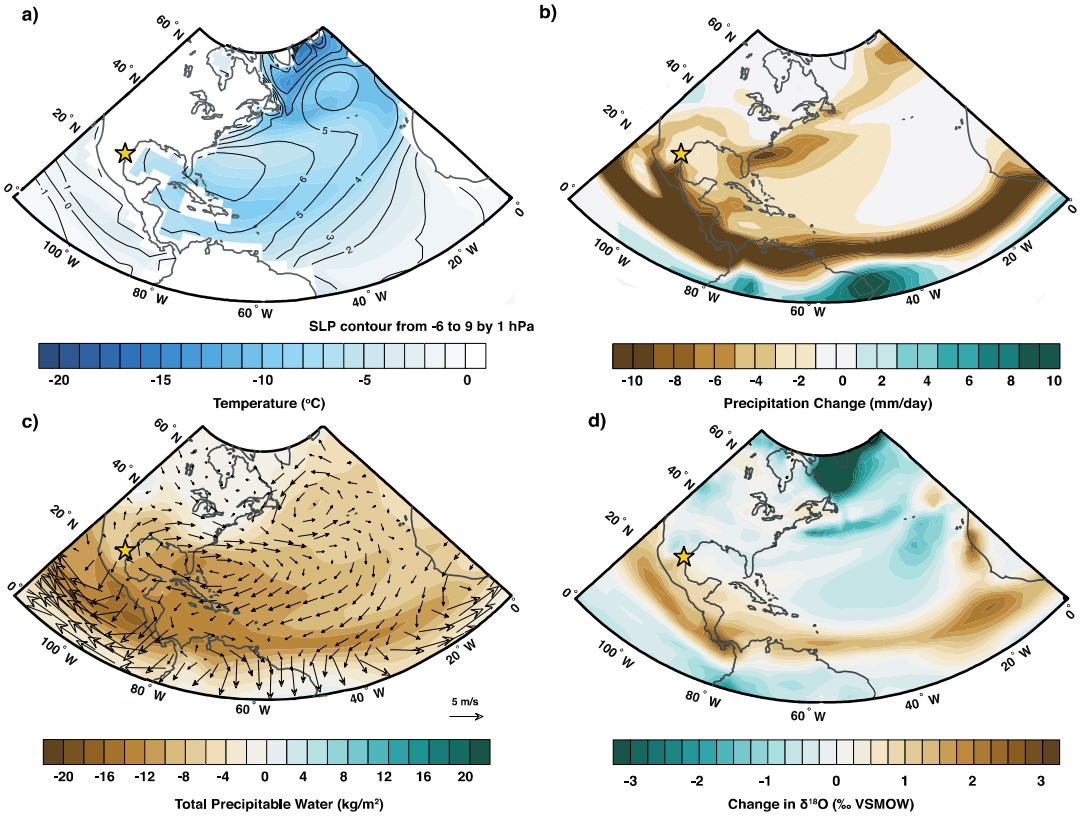

Fig. 3.4: Earth System Model simulations of Heinrich Stadials. Summary dynamical changes associated with high latitude freshwater input under glacial boundary conditions. **a)** Temperature and Sea Level Pressure changes; **b)** Changes in precipitation; **c)** Changes in total column precipitable water and 850 mb winds; **d)** Changes in the stable oxygen isotope ratio of precipitation.

3.5.2 Millennial-scale droughts linked to strengthened CLLJ and lower SSTs

While previous records have suggested a variable response of Northern Mexico precipitation to millennial-scale AMOC changes (Quiroz-Jimenez *et al.*, 2017; Roy *et al.*, 2020),

CB2 proxies consistently record drying in northeast Mexico during Heinrich Stadials, with the exception of HS 2 (Fig. 3.2). Roy *et al.* (2016) proposed that a southward shift of the ITCZ drove a weakening of the CLLJ during Heinrich Events, thus leading to dry conditions in NE Mexico. While the seasonal ITCZ migration may not be a perfect analogue for ITCZ shifts during Heinrich Stadials, the CLLJ also strengthens during boreal winter when the ITCZ is positioned farther south, highlighting the need for a better dynamical understanding of hydroclimate variations during Heinrich Stadials.

To evaluate the underlying climate dynamics associated with drying during Heinrich Stadials, we analyzed results of an isotope-enabled Earth System Model simulation (iCESM1;(Brady *et al.*, 2019) forced with freshwater added to the North Atlantic (see methods). Model results show 10°C (or more) of cooling across the Atlantic Basin (Fig. 3.4a). Cooling is simultaneously driven by a decrease in the warm western Gulf Stream and the positive wind-evaporation-SST feedback via an enhanced Bermuda High (Xie & Philander, 1994). This results in an intensification of the easterlies which funnel into the Caribbean Sea to feed the CLLJ (Fig. 3.4c). As the jet intensifies, it bifurcates across Mexico, increasing the magnitude of both the southern branch of the CLLJ across the Isthmus of Mexico and the southeasterly branch towards the United States (Fig. 3.4c). However, unlike the seasonal intensification of the CLLJ leading to increased rainfall, the resulting wind anomalies produce the opposite response. Strong winds combine with considerable SST cooling to reduce the vertically integrated moisture flux and precipitation over much of Mexico (Fig. 3.4b and 3.4c). Model results suggest moisture divergence can cause a 1 - 2 mm/day reduction in precipitation (Fig. 3.4b) and a 2‰ increase in precipitation $\delta^{18}O$ (Fig. 3.4d). This very closely matches the 1.5‰ increase we see in speleothem $\delta^{18}O$ during HS 1 (Fig. 3.2). The freshwater added to the model experiment (0.5 Sv for 100

years) is most similar to the freshwater released during HS 1 (Hemming, 2004), upwards of 66% more than during other Heinrich Stadials and explains why we see a stronger drying during HS1 than during other stadials. Although through different mechanisms, the Younger Dryas is estimated to exhibit similar SST cooling as Heinrich Stadials, explaining the similar magnitude of drying indicated by our proxies. It is important to note, the CB2 record suggests that changes in AMOC work in both directions, with increased precipitation leading to a -2‰ excursion in $\delta^{18}O$, a -3‰ shift in $\delta^{13}C$ and, a decrease of 15 mmol/mol of Mg/Ca during the Bølling-Allerød when AMOC was strengthened and SSTs are warmer (Thiagarajan *et al.*, 2014).

In juxtaposition to previous work from Northern Mexico which has suggested a weakening of CLLJ in response to Heinrich Stadials and SST cooling, we demonstrate the jet strengthened during shutdowns in AMOC. These new results demonstrate precipitation in Northeast Mexico precipitation is potentially inversely correlated to jet strength via enhanced moisture divergence and a positive wind-evaporation-SST. The main mechanism driving decreased precipitation is ambiguous at present, but we suggest, decreases in relative humidity, a reduction in orographic cooling and/or decreased vertical convection as potential processes driving decreased rainfall. Overall, our interpretation opposes modern climatology which suggests a stronger summer CLLJ leads to increased moisture availability in Northern Mexico and regions of the United States (Wang, 2007). The contrasting response of a strengthening jet in modern climatology and paleoclimate records suggest the precipitation is not necessarily linked to the variability of the CLLJ. Changes in thermodynamics, particular over the ocean, appear to be much more important drivers of hydroclimate variability. The modeling results demonstrated here are consistent with the similarities between CB2 $\delta^{18}O$ and regional SSTs on orbital timescales.

Our work also contradicts previous studies proposing that cooler SSTs drive an out-of-phase North-South precipitation pattern throughout Mesoamerica, at least on millennial timescales. We find CB2 exhibits similar patterns of variability to proxy records from farther south, including speleothem $\delta^{18}O$ records in Costa Rica (Lachniet *et al.*, 2009) and Cuba (Warken *et al.*, 2019), Cariaco Basin sediment records (Deplazes *et al.*, 2013), and magnetic susceptibility records from Guatemala (Escobar *et al.*, 2012) (Fig. 3.5). This comparison to

regional records suggests changes in regional SSTs and the CLLJ significantly and uniformly lead to drying across North and Central America and, will likely do so in the future.

3.5.3 Wet conditions in NE Mexico during the Last Glacial Maximum (or HS 2)

In contrast to the other Heinrich Stadials, the CB2 $\delta^{13}C$ and Mg/Ca records suggest an extended period of wetter conditions at our study site during HS 2 (~24 ka; Fig. 3.2). This is in

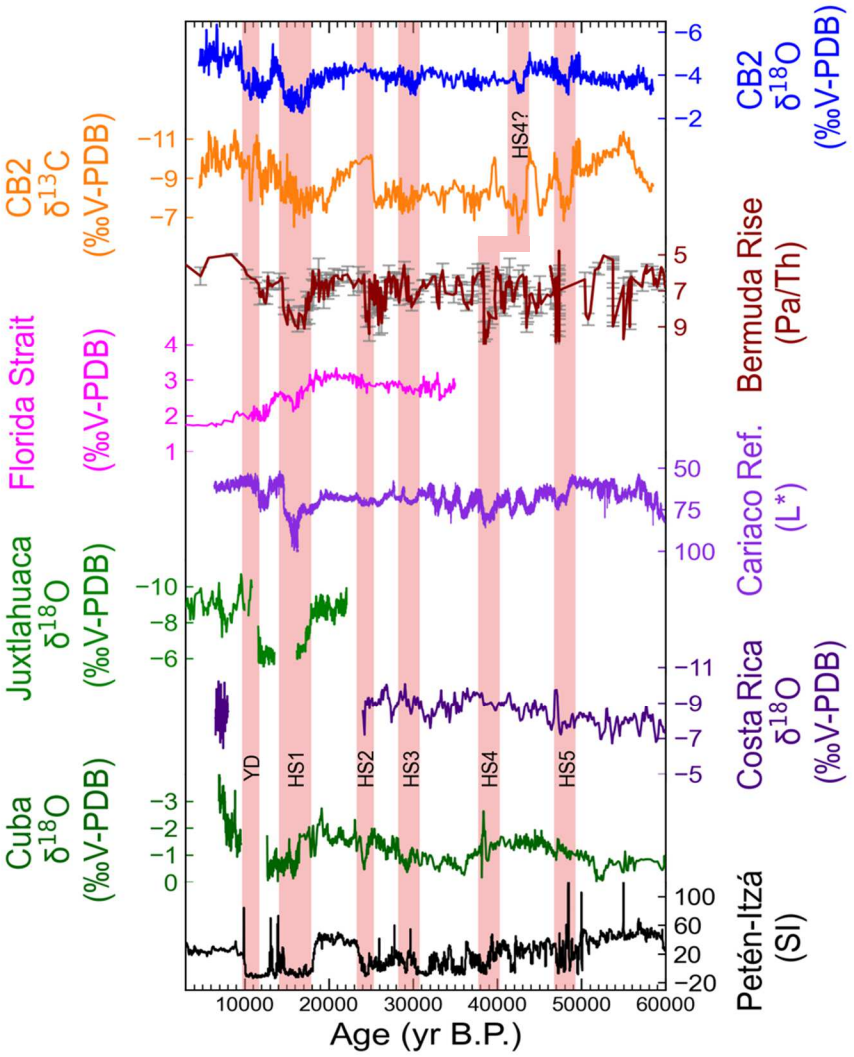

Fig. 3.5: Comparison of CB2 with other paleoclimate records. Comparison of CB2 $\delta^{13}O$ (blue) and $\delta^{13}C$ (orange) to Pa/Th ratios (burgundy; 46) with Florida Strait gulf stream circulation (magenta; Lynch-Stieglitz et al., 2014), Cariaco Basin reflectance (purple; Guatemala (Deplazes *et al.*, 2013)(Escobar *et al.*, 2012), Juxtlahuaca (light green, Lachniet et al., 2013), Costa Rica (blue; Lachniet, 2009), Cuba (dark green; (Warken *et al.*, 2019) and Lake Petén-Itzá (black; Escobar et al., 2012).

contrast to other proxy records from Lake Péten Itzá, Guatemala (Escobar *et al.*, 2012; Hodell *et al.*, 2008), Santo Tomás Cave, Cuba (Warken *et al.*, 2019), and Terciopelo Cave, Costa Rica (Lachniet *et al.*, 2009), which all show the expected response of drying during HS 2 (Fig. 3.5). While the CB2 response could potentially reflect a highly localized signal or be impacted by non-climatic proxy controls, the clear covariation between $\delta^{13}C$ and Mg/Ca during this event does suggest it was characterized by increased water balance. There are three potential mechanisms we consider that could explain the wetter conditions in NE Mexico during HS 2, which occurs around the time of the Last Glacial Maximum: 1) Increased winter precipitation derived from the Pacific winter storm track during the LGM, 2) A weaker HS 2 event which NE Mexico hydroclimate is more sensitive to than other regions, and/or 3) increased water balance due to colder temperatures during HS 2 and the LGM.

An intensified Pacific winter storm track during the Last Glacial Maximum has been frequently evoked to explain increased precipitation across Southern USA and Northern Mexico, but the spatial extent of the winter storm track has been previously disputed (Bradbury, 1997; Metcalfe *et al.*, 2000). Speleothem $\delta^{18}O$ demonstrates no change in precipitation amount during HS 2 while both $\delta^{13}C$ and Mg/Ca ratios (Fig. 3.2) suggest anomalous increases in local water balance, compared to earlier glacial conditions. Furthermore, precipitation sourced from the Pacific would have an isotopic composition heavily depleted in ^{18}O due to the moisture's distance and terrain traversed (Dansgaard, 1964), which is not observed in CB2 $\delta^{18}O$ during this time period. Additionally, some of the best performing PMIP3 models (Chevalier *et al.*, 2017) show an increase in the magnitude of the CLLJ (Appendix A, Fig. S3.4) but no increase in winter precipitation during the LGM (Appendix A, Fig. S3.5). Therefore, we suggest there was no

contribution of rainfall from an enhanced winter storm track in NE Mexico during HS 2 or the LGM.

There is still some debate about whether HS 2 resulted in a full AMOC shutdown. Higher Pa/Th ratios in North Atlantic sediment cores are traditionally interpreted to be reflective of a weakened AMOC (Lynch-Stieglitz *et al.*, 2014). However, increases in opal flux as noted during HS 2 and HS 3 could also contribute to higher Pa/Th ratios (Lynch-Stieglitz *et al.*, 2014). Additionally, oxygen isotopes from benthic foraminifera in cores from the Caribbean suggest changes in oceanic circulation during HS 2 were lower in magnitude compared to those during HS 1 and the YD (Lynch-Stieglitz *et al.*, 2014). An incomplete shutdown in the western gulf stream, as potentially indicated from Caribbean benthic foraminifera, would have helped mitigate SST cooling, weakening the precipitation response in NE Mexico. This idea is further supported from SSTs from the Gulf of Mexico, the North Atlantic and the Caribbean, that show elevated temperatures compared to other Heinrich Stadials. We suggest our site is more sensitive to changes in Heinrich Stadial strength than other records of Mesoamerica because Cueva Bonita is located at the divergence of predicted precipitation $\delta^{18}O$ change (Fig. 3.4d), where weaker Heinrich Stadials could result in no change, or even a slight positive excursion in precipitation $\delta^{18}O$. Therefore, the lack of response of CB2 $\delta^{18}O$ to HS 2 in our proxy record lends further, concrete support to the possibility that HS 2 may have been weaker than other Heinrich Stadials.

Finally, we suggest wetter conditions during HS 2 and the LGM are primarily driven by decreased temperature at our study site, with no change in precipitation amount. While this is evident in the response of CB2 proxies, it is also supported by PMIP3 data. For instance, increased local water balance is observed in elevated soil moisture content in the LGM, compared to both the Mid-Holocene and Pre-Industrial period (Fig. 3.6). This is likely driven by

a reduction in evapotranspiration, linked to increased cloudiness (Bush *et al.*, 2009), reduced land temperatures (Lachniet & Vazquez-Selem, 2005), or changes in relative humidity over land (Bush & Philander, 1999). While evaluating the exact mechanism of increased local water balance is beyond the scope of this paper, our record is consistent with PMIP3 data and recent modeling studies (Lowry & Morrill, 2019) demonstrating high lake stands in Mexico and Central America (Escobar *et al.*, 2012) may have been driven by decreased ET.

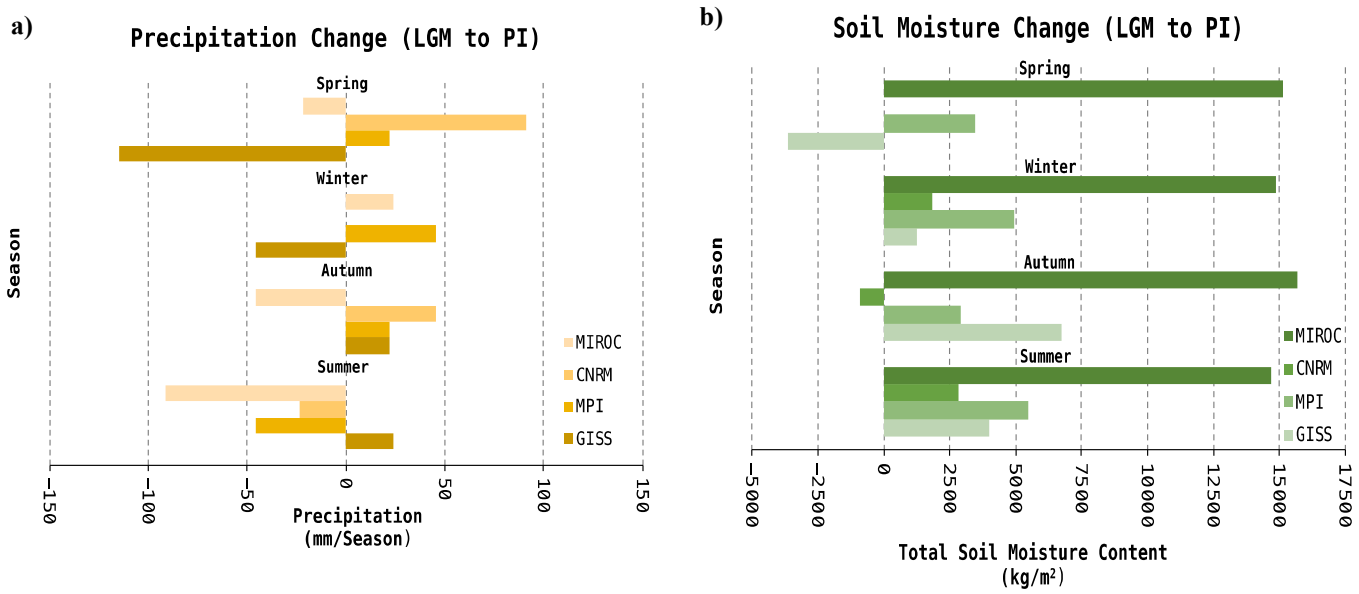

Fig. 3.6: Precipitation and soil-moisture in the Pre-Industrial and Last Glacial Maximum. (a) Comparison of LGM precipitation and **(b)** soil moisture during the LGM and Pre-industrial for 4 of the best performing PMIP3 models during Spring (MAM), Winter (DJF), Autumn (SON) and Summer (JJA) averaged over 22°N-24°N and 98°W-100°W. It is unclear if precipitation increased or decreased during the LGM compared to PI. However, all models show increases in total soil moisture, suggestive of decreased evaporation during the LGM.

3.6 Conclusion

We have presented the first multi-proxy speleothem record from NE Mexico, that highlights millennial and orbital scale hydroclimate variability from 4.6 to 58.5 ka. In contrast to other speleothem records from tropical and monsoon regions, we find no strong evidence for a direct insolation control on regional hydroclimate. We show instead that glacial-interglacial variations are closely linked to Atlantic SST variations on orbital timescales. We find dry

conditions in NE Mexico during the Younger Dryas and HS 1, 3, 4, and 5, and use climate model simulations to demonstrate that this response is driven by cool Atlantic and Caribbean SSTs rather than by a weakening of the CLLJ, as previously thought. Notably, we find evidence for increased local water balance during HS 2 and the LGM, which likely reflects a combination of a relatively weaker Heinrich Stadial 2 and reduced evapotranspiration at our study site.

Our record demonstrates that precipitation in NE Mexico is more sensitive to changes in SSTs, likely via relative humidity, orographic cooling and/or vertical convection, than to the strength of the CLLJ, highlighting the thermodynamic response may be more important than the dynamic response in driving precipitation change in response to external forcing and internal climate variability. Furthermore, through comparison with other records and with climate model simulations, we find a uniform drying across Mesoamerica in response to cool SSTs during Heinrich stadials, suggesting that all of Mexico may experience similar hydroclimate shifts in response to future climate forcing.

3.7 References

Aggarwal, P. K., Fröhlich, K., Kulkarni, K. M., & Gourcy, L. L. (2004). Stable isotope evidence for moisture sources in the asian summer monsoon under present and past climate regimes. *Geophysical Research Letters*, *31*(8). doi: 10.1029/2004GL019911

Aggarwal, P. K., Romatschke, U., Araguas-Araguas, L., Belachew, D., Longstaae, F. J., Berg, P., … Funk, A. (2016). *Proportions of convective and stratiform precipitation revealed in water isotope ratios*. doi: 10.1038/NGEO2739

Araguás-Araguás, L., Froehlich, K., & Rozanski, K. (1998). Stable isotope composition of precipitation over southeast Asia. *Journal of Geophysical Research: Atmospheres*, *103*(D22), 28721–28742. doi: 10.1029/98JD02582

Ashouri, H., Hsu, K.-L., Sorooshian, S., Braithwaite, D. K., Knapp, K. R., Cecil, L. D., … Prat, O. P. (2015). PERSIANN-CDR: Daily Precipitation Climate Data Record from Multisatellite Observations for Hydrological and Climate Studies. *Bulletin of the American Meteorological Society*, *96*(1), 69–83. doi: 10.1175/BAMS-D-13-00068.1

Ayalon, A., Bar-Matthews, M., & Sass, E. (1998). Rainfall-recharge relationships within a karstic terrain in the Eastern Mediterranean semi-arid region, Israel: δ 18O and δD characteristics. *Journal of Hydrology*, *207*(1–2), 18–31. doi: 10.1016/S0022-1694(98)00119-X

Bajo, P., Borsato, A., Drysdale, R., Hua, Q., Frisia, S., Zanchetta, G., … Woodhead, J. (2017). Stalagmite carbon isotopes and dead carbon proportion (DCP) in a near-closed-system situation: An interplay between sulphuric and carbonic acid dissolution. *Geochimica et Cosmochimica Acta*, *210*, 208–227. doi: 10.1016/j.gca.2017.04.038

Baker, A., & Bradley, C. (2009). *Modern stalagmite δ 18 O: Instrumental calibration and forward modelling*. doi: 10.1016/j.gloplacha.2009.05.002

Baker, A., Ito, E., Smart, P. L., & McEwan, R. F. (1997). Elevated and variable values of 13C in speleothems in a British cave system. *Chemical Geology*, *136*(3–4), 263–270. doi: 10.1016/S0009-2541(96)00129-5

Baker, A., Smith, C., Jex, C., Fairchild, I., Genty, D., & Fuller, L. (2008). Annually laminated speleothems: a review. *International Journal of Speleology*, *37*(3), 4. doi: http://dx.doi.org/10.5038/1827-806X.37.3.4

Baldini, J. U. L., McDermott, F., Hoffmann, D. L., Richards, D. A., & Clipson, N. (2008). Very high-frequency and seasonal cave atmosphere PCO2 variability: Implications for stalagmite growth and oxygen isotope-based paleoclimate records. *Earth and Planetary Science Letters*, *272*(1–2), 118–129. doi: 10.1016/J.EPSL.2008.04.031

Beck, J. W., Richards, D. A., Edwards, R. L., Silverman, B. W., Smart, P. L., Donahue, D. J., … Biddulph, D. (2001). Extremely large variations of atmospheric 14C concentration during the last glacial period. *Science*, *292*(5526), 2453–2458. doi: 10.1126/science.1056649

Bereiter, B., Eggleston, S., Schmitt, J., Nehrbass-Ahles, C., Stocker, T. F., Fischer, H., … Chappellaz, J. (2015). Revision of the EPICA Dome C CO2 record from 800 to 600-kyr before present. *Geophysical Research Letters*, *42*(2), 542–549. doi: 10.1002/2014GL061957

Bernal, J. P., Lachniet, M., McCulloch, M., Mortimer, G., Morales, P., & Cienfuegos, E. (2011). A speleothem record of Holocene climate variability from southwestern Mexico. *Quaternary Research*, *75*(01), 104–113. doi: 10.1016/j.yqres.2010.09.002

Bhattacharya, T., & Chiang, J. C. H. (2014). Spatial variability and mechanisms underlying El

Niño-induced droughts in Mexico. *Climate Dynamics*, *43*(12), 3309–3326. doi: 10.1007/s00382-014-2106-8

Bhattacharya, T., Chiang, J. C. H., & Cheng, W. (2017). Ocean-atmosphere dynamics linked to 800–1050 CE drying in mesoamerica. *Quaternary Science Reviews*, *169*, 263–277. doi: 10.1016/j.quascirev.2017.06.005

Bhattacharya, T., & Coats, S. (2020). Atlantic-Pacific Gradients Drive Last Millennium Hydroclimate Variability in Mesoamerica. *Geophysical Research Letters*, *47*(13), e2020GL088061. doi: 10.1029/2020GL088061

Bony, S., Risi, C., & Vimeux, F. (2008). Influence of convective processes on the isotopic composition (δ18O and δD) of precipitation and water vapor in the tropics: 1. Radiative-convective equilibrium and Tropical Ocean–Global Atmosphere–Coupled Ocean-Atmosphere Response Experiment (TOGA-COARE) simulations. *Journal of Geophysical Research: Atmospheres*, *113*(D19), 19305. doi: 10.1029/2008JD009942

Borsato, A., Johnston, V. E., Frisia, S., Miorandi, R., Corradini, F., Au, (A, & Borsato,). (2016). Temperature and altitudinal influence on karst dripwater chemistry: Implications for regional-scale palaeoclimate reconstructions from speleothems Cosmogenic Cl-36 in speleothems as a potential solar proxy View project OLOAMBIENT View project Temperature and altitudinal influence on karst dripwater chemistry: Implications for regional-scale palaeoclimate reconstructions from speleothems. *Geochimica et Cosmochimica Acta*, *177*, 275–297. doi: 10.1016/j.gca.2015.11.043

Bradley, C., Baker, A., Jex, C. N., & Leng, M. J. (2010). Hydrological uncertainties in the modelling of cave drip-water δ18O and the implications for stalagmite palaeoclimate reconstructions. *Quaternary Science Reviews*, *29*(17–18), 2201–2214. doi: 10.1016/j.quascirev.2010.05.017

Breitenbach, S. F. M., Adkins, J. F., Meyer, H., Marwan, N., Kumar, K. K., & Haug, G. H. (2010). Strong influence of water vapor source dynamics on stable isotopes in precipitation observed in Southern Meghalaya, NE India. *Earth and Planetary Science Letters*, *292*(1–2), 212–220. doi: 10.1016/j.epsl.2010.01.038

Breitenbach, S. F. M., Rehfeld, K., Goswami, B., Baldini, J. U. L., Ridley, H. E., Kennett, D. J., … Marwan, N. (2012). Constructing proxy records from age models (COPRA). *Climate of the Past*, *8*(5), 1765–1779. doi: 10.5194/cp-8-1765-2012

Burns, S. J., Godfrey, L. R., Faina, P., Mcgee, D., Hardt, B., Ranivoharimanana, L., & Randrianasy, J. (2016). *Rapid human-induced landscape transformation in Madagascar at the end of the first millennium of the Common Era*. doi: 10.1016/j.quascirev.2016.01.007

Cai, Y., Fung, I. Y., Edwards, R. L., An, Z., Cheng, H., Lee, J. E., … Chiang, J. C. H. (2015). Variability of stalagmite-inferred Indian monsoon precipitation over the past 252,000 y. *Proceedings of the National Academy of Sciences of the United States of America*, *112*(10), 2954–2959. doi: 10.1073/pnas.1424035112

Cai, Z., & Tian, L. (2016). Atmospheric controls on seasonal and interannual variations in the precipitation isotope in the East Asian Monsoon region. *Journal of Climate*, *29*(4), 1339–1352. doi: 10.1175/JCLI-D-15-0363.1

Caley, T., Roche, D. M., & Renssen, H. (2014). Orbital Asian summer monsoon dynamics revealed using an isotope-enabled global climate model. *Nature Communications*, *5*(1), 1–6. doi: 10.1038/ncomms6371

Chávez-Lara, C. M., Holtvoeth, J., Roy, P. D., & Pancost, R. D. (2019). Lipid biomarkers in lacustrine sediments of subtropical northeastern Mexico and inferred ecosystem changes

during the late Pleistocene and Holocene. *Palaeogeography, Palaeoclimatology, Palaeoecology*, *535*. doi: 10.1016/j.palaeo.2019.109343

Chen, Z., Auler, A. S., Bakalowicz, M., Drew, D., Griger, F., Hartmann, J., … Goldscheider, N. (2017). The World Karst Aquifer Mapping project: concept, mapping procedure and map of Europe. *Hydrogeology Journal 2017 25:3*, *25*(3), 771–785. doi: 10.1007/S10040-016-1519-3

Cheng, H., Edwards, R. L., Sinha, A., Spötl, C., Yi, L., Chen, S., … Zhang, H. (2016). The Asian monsoon over the past 640,000 years and ice age terminations. *Nature*, *534*(7609), 640–646. doi: 10.1038/nature18591

Cheng, H., Lawrence Edwards, R., Shen, C. C., Polyak, V. J., Asmerom, Y., Woodhead, J., … Calvin Alexander, E. (2013). Improvements in 230Th dating, 230Th and 234U half-life values, and U-Th isotopic measurements by multi-collector inductively coupled plasma mass spectrometry. *Earth and Planetary Science Letters*, *371–372*, 82–91. doi: 10.1016/j.epsl.2013.04.006

Clemens, S. C., Prell, W. L., & Sun, Y. (2010). Orbital-scale timing and mechanisms driving Late Pleistocene Indo-Asian summer monsoons: Reinterpreting cave speleothem δ18O. *Paleoceanography*, *25*(4). doi: 10.1029/2010PA001926

Cross, M. (2015). PySPLIT: Package for the Generation, Analysis, and Visualization of HYSPLIT Air Parcel Trajectories. In *PROC*. Retrieved from https://www.youtube.com/watch?v=2mzhTC4Kp-Y

Cuthbert, M. O., Baker, A., Jex, C. N., Graham, P. W., Treble, P. C., Andersen, M. S., & Ian Acworth, R. (2014). Drip water isotopes in semi-arid karst: Implications for speleothem paleoclimatology. *Earth and Planetary Science Letters*, *395*, 194–204. doi: 10.1016/j.epsl.2014.03.034

Daëron, M., Drysdale, R. N., Peral, M., Huyghe, D., Blamart, D., Coplen, T. B., … Zanchetta, G. (2019). Most Earth-surface calcites precipitate out of isotopic equilibrium. *Nature Communications*, *10*(1), 1–7. doi: 10.1038/s41467-019-08336-5

Dansgaard, W. (1964). Stable isotopes in precipitation. *Tellus*, *16*(4), 436–468. doi: 10.3402/tellusa.v16i4.8993

Day, C. C., & Henderson, G. M. (2013). Controls on trace-element partitioning in cave-analogue calcite. *Geochimica et Cosmochimica Acta*, *120*, 612–627. doi: 10.1016/j.gca.2013.05.044

Dayem, K. E., Molnar, P., Battisti, D. S., & Roe, G. H. (2010). Lessons learned from oxygen isotopes in modern precipitation applied to interpretation of speleothem records of paleoclimate from eastern Asia. *Earth and Planetary Science Letters*, *295*(1–2), 219–230. doi: 10.1016/j.epsl.2010.04.003

Dee, S., Emile-Geay, J., Evans, M. N., Allam, A., Steig, E. J., & Thompson, D. M. (2015). PRYSM: An open-source framework for PRoxY System Modeling, with applications to oxygen-isotope systems. *Journal of Advances in Modeling Earth Systems*, *7*(3), 1220–1247. doi: 10.1002/2015MS000447

Deininger, M., Fohlmeister, J., Scholz, D., & Mangini, A. (2012). Isotope disequilibrium effects: The influence of evaporation and ventilation effects on the carbon and oxygen isotope composition of speleothems - A model approach. *Geochimica et Cosmochimica Acta*, *96*, 57–79. doi: 10.1016/j.gca.2012.08.013

Deininger, M., & Scholz, D. (2019). ISOLUTION 1.0: an ISOtope evoLUTION model describing the stable oxygen (δ18O) and carbon (δ13C) isotope values of speleothems. *International Journal of Speleology*, *48*(1), 21–32. doi: 10.5038/1827-806X.48.1.2219

Denniston, R. F., Houts, A. N., Asmerom, Y., Wanamaker, A. D., Haws, J. A., Polyak, V. J., … Bicho, N. F. (2018). A stalagmite test of North Atlantic SST and Iberian hydroclimate linkages over the last two glacial cycles. *Climate of the Past*, *14*(12), 1893–1913. doi: 10.5194/cp-14-1893-2018

Deplazes, G., Lückge, A., Peterson, L. C., Timmermann, A., Hamann, Y., Hughen, K. A., … Haug, G. H. (2013). Links between tropical rainfall and North Atlantic climate during the last glacial period. *Nature Geoscience*, *6*(3), 213–217. doi: 10.1038/ngeo1712

Dietzel, M., Tang, J., Leis, A., & Köhler, S. J. (2009). Oxygen isotopic fractionation during inorganic calcite precipitation - Effects of temperature, precipitation rate and pH. *Chemical Geology*, *268*(1–2), 107–115. doi: 10.1016/j.chemgeo.2009.07.015

Dorale, J. A. (1998). Climate and Vegetation History of the Midcontinent from 75 kyr to 25 kyr. A Speleothem Record from Crevice Cave, Missouri, USA. *Science*, *282*(5395), 1871–1874. doi: 10.1126/science.282.5395.1871

Dorale, J. A., & Liu, Z. (2009). Limitations of hendy test criteria in judging the paleoclimatic suitability of speleothems and the need for replication. In *Journal of Cave and Karst Studies* (Vol. 71). doi: PNR61

Dreybrodt, W., & Deininger, M. (2014). The impact of evaporation to the isotope composition of DIC in calcite precipitating water films in equilibrium and kinetic fractionation models. *Geochimica et Cosmochimica Acta*, *125*, 433–439. doi: 10.1016/j.gca.2013.10.004

Drysdale, R., Zanchetta, G., Hellstrom, J., Maas, R., Fallick, A., Pickett, M., … Piccini, L. (2006). Late Holocene drought responsible for the collapse of Old World civilizations is recorded in an Italian cave flowstone. *Geology*, *34*(2), 101–104. doi: 10.1130/G22103.1

Dubois, N., Kienast, M., Kienast, S., Normandeau, C., Calvert, S. E., Herbert, T. D., & Mix, A. (2011). Millennial-scale variations in hydrography and biogeochemistry in the Eastern Equatorial Pacific over the last 100 kyr. *Quaternary Science Reviews*, *30*(1–2), 210–223. doi: 10.1016/j.quascirev.2010.10.012

Dunning, N. P., Beach, T. P., & Luzzadder-Beach, S. (2012). Kax and kol: Collapse and resilience in lowland Maya civilization. *Proceedings of the National Academy of Sciences*, *109*(10), 3652–3657. doi: 10.1073/PNAS.1114838109

Dykoski, C. A., Lawrence Edwards, R., Cheng, H., Yuan, D., Cai, Y., Zhang, M., … Boyle, E. (2005). *A high-resolution, absolute-dated Holocene and deglacial Asian monsoon record from Dongge Cave, China*. doi: 10.1016/j.epsl.2005.01.036

Escobar, J., Hodell, D. A., Brenner, M., Curtis, J. H., Gilli, A., Mueller, A. D., … Guilderson, T. P. (2012). A ~43-ka record of paleoenvironmental change in the Central American lowlands inferred from stable isotopes of lacustrine ostracods. *Quaternary Science Reviews*, *37*, 92–104. doi: 10.1016/j.quascirev.2012.01.020

Fairchild, I., Baker, A., Borsato, A., & Frisia, S. (2001). Annual to sub-annual resolution of multiple trace-element trends in speleothems. *Article in Journal of the Geological Society*. doi: 10.1144/jgs.158.5.831

Fairchild, I. J., Smith, C. L., Baker, A., Fuller, L., Spötl, C., Mattey, D., … E.I.M.F. (2006). Modification and preservation of environmental signals in speleothems. *Earth-Science Reviews*, *75*(1–4), 105–153. doi: 10.1016/J.EARSCIREV.2005.08.003

Fairchild, I. J., & Treble, P. C. (2009). Trace elements in speleothems as recorders of environmental change. *Quaternary Science Reviews*, *28*(5–6), 449–468. doi: 10.1016/j.quascirev.2008.11.007

Feng, S., Krueger, A. B., & Oppenheimer, M. (2010). Linkages among climate change, crop

yields and Mexico-US cross-border migration. *Proceedings of the National Academy of Sciences of the United States of America*, *107*(32), 14257–14262. doi: 10.1073/pnas.1002632107

Feng, W., Banner, J. L., Guilfoyle, A. L., Musgrove, M. L., & James, E. W. (2012). Oxygen isotopic fractionation between drip water and speleothem calcite: A 10-year monitoring study, central Texas, USA. *Chemical Geology*, *304–305*, 53–67. doi: 10.1016/j.chemgeo.2012.02.004

Feng, W., Casteel, R. C., Banner, J. L., & Heinze-Fry, A. (2013). *Oxygen isotope variations in rainfall, drip-water and speleothem calcite from a well-ventilated cave in Texas, USA: Assessing a new speleothem temperature proxy*. doi: 10.1016/j.gca.2013.11.039

Fetter, C. W. (2014). Applied hydrogeology. 4th. In *Pearson*. Retrieved from http://sutlib2.sut.ac.th/sut_contents/H109081.pdf

Fohlmeister, J., Kromer, B., & Mangini, A. (2011). The influence of soil organic matter age spectrum on the reconstruction of atmospheric 14C levels via stalagmites. *Radiocarbon*, *53*(1), 99–115. doi: 10.1017/S003382220003438X

Fohlmeister, J., Voarintsoa, N. R. G., Lechleitner, F. A., Boyd, M., Brandtstätter, S., Jacobson, M. J., & Oster, J. L. (2020). Main controls on the stable carbon isotope composition of speleothems. *Geochimica et Cosmochimica Acta*, *279*, 67–87. doi: 10.1016/j.gca.2020.03.042

Ford, D. C. (2000). Deep phreatic caves and groundwater systems of the Sierra de El Abra, Mexico. *Speleogenesis: Evolution of Karst Aquifers: Huntsville, Alabama, National Speleological*, 325–331.

Frappier, A. B., Pyburn, J., Pinkey-Drobnis, A. D., Wang, X., Corbett, D. R., & Dahlin, B. H. (2014). Two millennia of tropical cyclone-induced mud layers in a northern Yucatán stalagmite: Multiple overlapping climatic hazards during the Maya Terminal Classic "megadroughts." *Geophysical Research Letters*, *41*(14), 5148–5157. doi: 10.1002/2014GL059882

Frappier, A. B., Sahagian, D., Carpenter, S. J., González, L. A., & Frappier, B. R. (2007). Stalagmite stable isotope record of recent tropic cyclone events. *Geology*, *35*(2), 111–114. doi: 10.1130/G23145A.1

Freitas, C. R. De, Littlbjohn, R. N., Clarkson, T. S., & Kristament, I. S. (1982). Cave climate: Assessment of airflow and ventilation. *Journal of Climatology*, *2*(4), 383–397. doi: 10.1002/JOC.3370020408

Frisia, S., Borsato, A., Fairchild, I. J., McDermott, F., & Selmo, E. M. (2002). Aragonite-calcite relationships in speleothems (Grotte de Clamouse, France): Environment, fabrics, and carbonate geochemistry. *Journal of Sedimentary Research*, *72*(5), 687–699. doi: 10.1306/020702720687

Frisia, S., Fairchild, I. J., Fohlmeister, J., Miorandi, R., Spötl, C., & Borsato, A. (2011). Carbon mass-balance modelling and carbon isotope exchange processes in dynamic caves. *Geochimica et Cosmochimica Acta*, *75*(2), 380–400. doi: 10.1016/J.GCA.2010.10.021

Frumkin, A., & Stein, M. (2004). The Sahara–East Mediterranean dust and climate connection revealed by strontium and uranium isotopes in a Jerusalem speleothem. *Earth and Planetary Science Letters*, *217*(3–4), 451–464. doi: 10.1016/S0012-821X(03)00589-2

Gabitov, R. I., & Watson, E. B. (2006). Partitioning of strontium between calcite and fluid. *Geochemistry, Geophysics, Geosystems*, *7*(11). doi: 10.1029/2005GC001216

Galy, V., François, L., France-Lanord, C., Faure, P., Kudrass, H., Palhol, F., & Singh, S. K.

(2008). C4 plants decline in the Himalayan basin since the Last Glacial Maximum. *Quaternary Science Reviews*, *27*(13–14), 1396–1409. doi: 10.1016/J.QUASCIREV.2008.04.005

Gary, M. S. J. (2006). *Volcanogenic karstification of Sistema Zacatón, Mexico*. 79–89. doi: 10.1130/2006.2404(08)

Genty, D., & Massault, M. (1997). Bomb14C recorded in laminated speleothems: Calculation of dead carbon proportion. *Radiocarbon*, *39*(1), 33–48. doi: 10.1017/S0033822200040881

Genty, D., Massault, M., Gilmour, M., Baker, A., Verheyden, S., & Kepens, E. (1999). Calculation of past dead carbon proportion and variability by the comparison of AMS 14C and TIMS U/Th ages on two Holocene stalagmites. *Radiocarbon*, *41*(3), 251–270. doi: 10.1017/S003382220005712X

Gill, R. B., Mayewski, P. A., Nyberg, J., Haug, G. H., & Peterson, L. C. (2007). Drought and the maya collapse. *Ancient Mesoamerica*, *18*(2), 283–302. doi: 10.1017/S0956536107000193

Giorgetta, M. A., Jungclaus, J., Reick, C. H., Legutke, S., Bader, J., Böttinger, M., … Stevens, B. (2013). Climate and carbon cycle changes from 1850 to 2100 in MPI-ESM simulations for the Coupled Model Intercomparison Project phase 5. *Journal of Advances in Modeling Earth Systems*, *5*(3), 572–597. doi: 10.1002/jame.20038

Goede, A., McCulloch, M., McDermott, F., & Hawkesworth, C. (1998). Aeolian contribution to strontium and strontium isotope variations in a Tasmanian speleothem. *Chemical Geology*, *149*(1–2), 37–50. doi: 10.1016/S0009-2541(98)00035-7

Goldsmith, G. R., Allen, S. T., Braun, S., Engbersen, N., González-Quijano, C. R., Kirchner, J. W., & Siegwolf, R. T. W. (2019). Spatial variation in throughfall, soil, and plant water isotopes in a temperate forest. *Ecohydrology*, *12*(2), e2059. doi: 10.1002/ECO.2059

Gram, W. K., & Faaborg, J. (1997). The Distribution of Neotropical Migrant Birds Wintering in the El Cielo Biosphere Reserve, Tamaulipas, Mexico. *The Condor*, *99*(3), 658–670. doi: 10.2307/1370478

Griffiths, M. L., Drysdale, R. N., Vonhof, H. B., Gagan, M. K., Zhao, J. xin, Ayliffe, L. K., … Suwargadi, B. W. (2010). Younger Dryas-Holocene temperature and rainfall history of southern Indonesia from δ18O in speleothem calcite and fluid inclusions. *Earth and Planetary Science Letters*, *295*(1–2), 30–36. doi: 10.1016/j.epsl.2010.03.018

Griffiths, M. L., Fohlmeister, J., Drysdale, R. N., Hua, Q., Johnson, K. R., Hellstrom, J. C., … Zhao, J. x. (2012). Hydrological control of the dead carbon fraction in a Holocene tropical speleothem. *Quaternary Geochronology*, *14*, 81–93. doi: 10.1016/J.QUAGEO.2012.04.001

Griffiths, M. L., Johnson, K. R., Pausata, F. S. R., White, J. C., Henderson, G. M., Wood, C. T., … Sekhon, N. (2020). End of Green Sahara amplified mid- to late Holocene megadroughts in mainland Southeast Asia. *Nature Communications*, *11*(1), 4204. doi: 10.1038/s41467-020-17927-6

Griffiths, M. L., Kimbrough, A. K., Gagan, M. K., Drysdale, R. N., Cole, J. E., Johnson, K. R., … Hantoro, W. S. (2016). Western Pacific hydroclimate linked to global climate variability over the past two millennia. *Nature Communications*, *7*. doi: 10.1038/ncomms11719

Gutiérrez-García, G., Beramendi-Orosco, L. E., & Johnson, K. R. (2020). Climate-growth relationships of Pinus pseudostrobus from a tropical mountain cloud forest in northeast Mexico. *Dendrochronologia*, *64*, 125749. doi: 10.1016/j.dendro.2020.125749

Harman, C. J. (2015). Time-variable transit time distributions and transport: Theory and application to storage-dependent transport of chloride in a watershed. *Water Resources Research*, *51*(1), 1–30. doi: 10.1002/2014WR015707

Hartland, A., Fairchild, I. J., Lead, J. R., Borsato, A., Baker, A., Frisia, S., & Baalousha, M. (2012). From soil to cave: Transport of trace metals by natural organic matter in karst dripwaters. *Chemical Geology*, *304–305*, 68–82. doi: 10.1016/J.CHEMGEO.2012.01.032

Hartland, A., & Zitoun, R. (2018). Transition metal availability to speleothems controlled by organic binding ligands. *Geochem. Persp. Let*, *8*, 22–25. doi: 10.7185/geochemlet.1824

Hellstrom, J. (2006). U–Th dating of speleothems with high initial 230Th using stratigraphical constraint. *Quaternary Geochronology*, *1*(4), 289–295. doi: 10.1016/J.QUAGEO.2007.01.004

Hendy, C. H. (1971). *The isotopic geochemistry of speleothems-I. The calculation of the effects of different modes of formation on the isotopic composition of speleothems and their applicability as palaeoclimatic indicators* * (Vol. 35). Pergamon Press. Printed in Northern Ireland. Retrieved from Pergamon Press. Printed in Northern Ireland website: https://ac.els-cdn.com/001670377190127X/1-s2.0-001670377190127X-main.pdf?_tid=9d24d077-1c6a-4651-b253-c15525034ea9&acdnat=1549696557_a9657fa3d144aca8ac631b95b8603c45

Hodge, E., McDonald, J., Fischer, M., Redwood, D., Hual, Q., Levchenko, V., … Fink, D. (2011). Using the 14C bomb pulse to date young speleothems. In *Radiocarbon* (Vol. 53). doi: 10.1017/S0033822200056605

Hoggarth, J. A., Restall, M., Wood, J. W., & Kennett, D. J. (2017). Drought and its demographic effects in the maya lowlands. *Current Anthropology*, *58*(1), 82–113. doi: 10.1086/690046

Hu, C., Henderson, G. M., Huang, J., Xie, S., Sun, Y., & Johnson, K. R. (2008). Quantification of Holocene Asian monsoon rainfall from spatially separated cave records. *Earth and Planetary Science Letters*, *266*(3–4), 221–232. doi: 10.1016/j.epsl.2007.10.015

Hua, Q., Cook, D., Fohlmeister, J., Penny, D., Bishop, P., & Buckman, S. (2017). Radiocarbon Dating of a Speleothem Record of Paleoclimate for Angkor, Cambodia. *Radiocarbon*, *59*(6), 1873–1890. doi: 10.1017/RDC.2017.115

Huang, Y., Fairchild, I. J., Borsato, A., Frisia, S., Cassidy, N. J., McDermott, F., & Hawkesworth, C. J. (2001). Seasonal variations in Sr, Mg and P in modern speleothems (Grotta di Ernesto, Italy). *Chemical Geology*, *175*(3–4), 429–448. doi: 10.1016/S0009-2541(00)00337-5

Jaffey, A. H., Flynn, K. F., Glendenin, L. E., Bentley, W. C., & Essling, A. M. (1971). Precision measurement of half-lives and specific activities of U235 and U238. *Physical Review C*, *4*(5), 1889–1906. doi: 10.1103/PhysRevC.4.1889

James, E. W., Banner, J. L., & Hardt, B. (2015). A global model for cave ventilation and seasonal bias in speleothem paleoclimate records. *Geochemistry, Geophysics, Geosystems*, *16*(4), 1044–1051. doi: 10.1002/2014GC005658

John Bierhorst. (1992). *History and Mythology of the Aztecs: The Codex Chimalpopoca - Google Books*. Retrieved from https://books.google.com/books?hl=en&lr=&id=xErlvmBuakoC&oi=fnd&pg=PA1&dq=Bierhorst,+J.,+Ed.,+Trans.,+1992:+History+and+Mythology+of+the+Aztecs:+The+Codex+Chimalpopoca.+University+of+Arizona+Press,+238+pp.&ots=BuLIKOxdw9&sig=mGh1x__1DElEzd_sP_U_UY0BStU#v=

Johnson, K. R., Hu, C., Belshaw, N. S., & Henderson, G. M. (2006). Seasonal trace-element and stable-isotope variations in a Chinese speleothem: The potential for high-resolution paleomonsoon reconstruction. *Earth and Planetary Science Letters*, *244*(1–2), 394–407. doi: 10.1016/j.epsl.2006.01.064

Johnson, R. (2011). Immigration as a Response Variable to Climate Change from Mexico into

the United States. In *Journal of Alternative Perspectives in the Social Sciences* (Vol. 3).
Kennett, D. J., Breitenbach, S. F. M., Aquino, V. V., Asmerom, Y., Awe, J., Baldini, J. U. L., … Haug, G. H. (2012). Development and disintegration of maya political systems in response to climate change. *Science*, *338*(6108), 788–791. doi: 10.1126/science.1226299
Kim, S. T., & O'Neil, J. R. (1997). Equilibrium and nonequilibrium oxygen isotope effects in synthetic carbonates. *Geochimica et Cosmochimica Acta*, *61*(16), 3461–3475. doi: 10.1016/S0016-7037(97)00169-5
Knutti, R., & Sedláček, J. (2013). Robustness and uncertainties in the new CMIP5 climate model projections. *Nature Climate Change*, *3*(4), 369–373. doi: 10.1038/nclimate1716
Konecky, B. L., Noone, D. C., & Cobb, K. M. (2019). The Influence of Competing Hydroclimate Processes on Stable Isotope Ratios in Tropical Rainfall. *Geophysical Research Letters*, *46*(3), 1622–1633. doi: 10.1029/2018GL080188
Kovacs, S. E., Reinhardt, E. G., Stastna, M., Coutino, A., Werner, C., Collins, S. V., … Le Maillot, C. (2017). Hurricane Ingrid and Tropical Storm Hanna's effects on the salinity of the coastal aquifer, Quintana Roo, Mexico. *Journal of Hydrology*, *551*, 703–714. doi: 10.1016/J.JHYDROL.2017.02.024
Kovaltsov, G. A., Mishev, A., & Usoskin, I. G. (2012). A new model of cosmogenic production of radiocarbon 14C in the atmosphere. *Earth and Planetary Science Letters*, *337–338*, 114–120. doi: 10.1016/j.epsl.2012.05.036
Kurczyn, J. A., Appendini, C. M., Beier, E., Sosa-López, A., López-González, J., & Posada-Vanegas, G. (2021). Oceanic and atmospheric impact of central American cold surges (Nortes) in the Gulf of Mexico. *International Journal of Climatology*, *41*(S1), E1450–E1468. doi: 10.1002/joc.6779
Kurita, N., Ichiyanagi, K., Matsumoto, J., Yamanaka, M. D., & Ohata, T. (2009). The relationship between the isotopic content of precipitation and the precipitation amount in tropical regions. *Journal of Geochemical Exploration*, *102*(3), 113–122. doi: 10.1016/J.GEXPLO.2009.03.002
Lachniet, M. S. (2009). Climatic and environmental controls on speleothem oxygen-isotope values. *Quaternary Science Reviews*, *28*(5–6), 412–432. doi: 10.1016/j.quascirev.2008.10.021
Lachniet, M. S., Asmerom, Y., Bernal, J. P., Polyak, V. J., & Vazquez-Selem, L. (2013). Orbital pacing and ocean circulation-induced collapses of the Mesoamerican monsoon over the past 22,000 y. *Proceedings of the National Academy of Sciences of the United States of America*, *110*(23), 9255–9260. doi: 10.1073/pnas.1222804110
Lachniet, M. S., Asmerom, Y., Polyak, V., & Bernal, J. P. (2017). Two millennia of Mesoamerican monsoon variability driven by Pacific and Atlantic synergistic forcing. *Quaternary Science Reviews*, *155*, 100–113. doi: 10.1016/j.quascirev.2016.11.012
Lachniet, M. S., Bernal, J. P., Asmerom, Y., Polyak, V., & Piperno, D. (2012). A 2400 yr Mesoamerican rainfall reconstruction links climate and cultural change. *Geology*, *40*(3), 259–262. doi: 10.1130/G32471.1
Lachniet, M. S., Burns, S. J., Piperno, D. R., Asmerom, Y., Polyak, V. J., Moy, C. M., & Christenson, K. (2004). A 1500-year El Niño/Southern Oscillation and rainfall history for the Isthmus of Panama from speleothem calcite. *Journal of Geophysical Research D: Atmospheres*, *109*(20), 20117. doi: 10.1029/2004JD004694
Lachniet, M. S., & Patterson, W. P. (2009). Oxygen isotope values of precipitation and surface waters in northern Central America (Belize and Guatemala) are dominated by temperature

and amount effects. *Earth and Planetary Science Letters*, *284*(3–4), 435–446. doi: 10.1016/J.EPSL.2009.05.010

Lachniet, M. S., Patterson, W. P., Burns, S., Asmerom, Y., & Polyak, V. (2007). Caribbean and Pacific moisture sources on the Isthmus of Panama revealed from stalagmite and surface water δ18O gradients. *Geophysical Research Letters*, *34*(1). doi: 10.1029/2006GL028469

Landsea, C. W., & Franklin, J. L. (2013). Atlantic Hurricane Database Uncertainty and Presentation of a New Database Format. *Monthly Weather Review*, *141*(10), 3576–3592. doi: 10.1175/MWR-D-12-00254.1

Lases-Hernández, F., Medina-Elizalde, M., & Benoit Frappier, A. (2020). Drip water δ18O variability in the northeastern Yucatán Peninsula, Mexico: Implications for tropical cyclone detection and rainfall reconstruction from speleothems. *Geochimica et Cosmochimica Acta*, *285*, 237–256. doi: 10.1016/J.GCA.2020.07.008

Lawrence Edwards, R., Chen, J. H., & Wasserburg, G. J. (1987). 238U234U230Th232Th systematics and the precise measurement of time over the past 500,000 years. *Earth and Planetary Science Letters*, *81*(2–3), 175–192. doi: 10.1016/0012-821X(87)90154-3

Lea, D. W., Pak, D. K., Peterson, L. C., & Hughen, K. A. (2003). Synchroneity of tropical and high-latitude Atlantic temperatures over the last glacial termination. *Science*, *301*(5638), 1361–1364. doi: 10.1126/science.1088470

Lentz, D. L., Dunning, N. P., Scarborough, V. L., & Grazioso, L. (2018). Imperial resource management at the ancient Maya city of Tikal: A resilience model of sustainability and collapse. *Journal of Anthropological Archaeology*, *52*, 113–122. doi: 10.1016/J.JAA.2018.08.005

Lewis, S. C., LeGrande, A. N., Kelley, M., & Schmidt, G. A. (2010). Water vapour source impacts on oxygen isotope variability in tropical precipitation during Heinrich events. *Climate of the Past* , 87–133. doi: 10.5194/cpd-6-87-2010

Liu, W. J., Li, P. J., Li, H. M., & Duan, W. P. (2006). Estimation of evaporation rate from soil surface using stable isotopic composition of throughfall and stream water in a tropical seasonal rain forest in Xishuangbanna, China. *Acta Ecologica Sinica*, *26*(5), 1303–1311. doi: 10.1016/s1872-2032(06)60022-x

Lynch-Stieglitz, J., Schmidt, M. W., Gene Henry, L., Curry, W. B., Skinner, L. C., Mulitza, S., … Chang, P. (2014). Muted change in Atlantic overturning circulation over some glacial-aged Heinrich events. *Nature Geoscience*, *7*(2), 144–150. doi: 10.1038/ngeo2045

Lyu, Y., Luo, W., Wang, Y., Zeng, G., Wang, Y., Cheng, A., … Wang, S. (2020). *Impacts of cave ventilation on drip water δ 13 C DIC and its paleoclimate implication*. doi: 10.1016/j.quaint.2020.03.050

Magaña, V. O., Vázquez, J. L., Pérez, J. L., & Pérez, J. B. (2003). Impact of El Niño on precipitation in Mexico . *Geofísica Internacional* , *42*(3), 313–330. Retrieved from http://www.redalyc.org/articulo.oa?id=56842304

Marks, G. S. (2020). Investigating Mexican paleoclimate with precisely dated speleothems. In *Investigating Mexican paleoclimate with precisely dated speleothems*. Massachusetts Institute of Technology. doi: 10.1575/1912/26101

Martín-Chivelet, J., Belén Muñoz-García, M., Cruz, J. A., Ortega, A. I., Turrero, M. J., & Jones, B. (2017). *Speleothem Architectural Analysis: Integrated approach for stalagmite-based paleoclimate research*. doi: 10.1016/j.sedgeo.2017.03.003

McDermott, F. (2004). Palaeo-climate reconstruction from stable isotope variations in speleothems: a review. *Quaternary Science Reviews*, *23*(7–8), 901–918. doi:

10.1016/J.QUASCIREV.2003.06.021
Medina-Elizalde, M., Burns, S. J., Lea, D. W., Asmerom, Y., von Gunten, L., Polyak, V., … Karmalkar, A. (2010a). High resolution stalagmite climate record from the Yucatán Peninsula spanning the Maya terminal classic period. *Earth and Planetary Science Letters*, *298*(1–2), 255–262. doi: 10.1016/J.EPSL.2010.08.016
Medina-Elizalde, M., Burns, S. J., Lea, D. W., Asmerom, Y., von Gunten, L., Polyak, V., … Karmalkar, A. (2010b). High resolution stalagmite climate record from the Yucatán Peninsula spanning the Maya terminal classic period. *Earth and Planetary Science Letters*, *298*(1–2), 255–262. doi: 10.1016/j.epsl.2010.08.016
Medina-Elizalde, M., Burns, S. J., Polanco-Martínez, J. M., Beach, T., Lases-Hernández, F., Shen, C. C., & Wang, H. C. (2016). High-resolution speleothem record of precipitation from the Yucatan Peninsula spanning the Maya Preclassic Period. *Global and Planetary Change*, *138*, 93–102. doi: 10.1016/j.gloplacha.2015.10.003
Medina-Elizalde, M., & Rohling, E. J. (2012). Collapse of Classic Maya Civilization Related to Modest Reduction in Precipitation. *Science* . doi: 10.1126/science.1216629
Méndez, M., & Magaña, V. (2010). Regional aspects of prolonged meteorological droughts over Mexico and central America. *Journal of Climate*, *23*(5), 1175–1188. doi: 10.1175/2009JCLI3080.1
Mestas-Nuñez, A. M., Enfield, D. B., & Zhang, C. (2007). Water vapor fluxes over the Intra-Americas Sea: Seasonal and interannual variability and associations with rainfall. *Journal of Climate*, *20*(9), 1910–1922. doi: 10.1175/JCLI4096.1
Meyer, K. W., Feng, W., Breecker, D. O., Banner, J. L., & Guilfoyle, A. (2014). Interpretation of speleothem calcite δ13C variations: Evidence from monitoring soil CO2, drip water, and modern speleothem calcite in central Texas. *Geochimica et Cosmochimica Acta*, *142*, 281–298. doi: 10.1016/j.gca.2014.07.027
Mickler, P. J., Banner, J. L., Stern, L., Asmerom, Y., Edwards, R. L., & Ito, E. (2004). Stable isotope variations in modern tropical speleothems: Evaluating equilibrium vs. kinetic isotope effects. *Geochimica et Cosmochimica Acta*, *68*(21), 4381–4393. doi: 10.1016/j.gca.2004.02.012
Mickler, P. J., Carlson, P., Banner, J. L., Breecker, D. O., Stern, L., & Guilfoyle, A. (2019). Quantifying carbon isotope disequilibrium during in-cave evolution of drip water along discreet flow paths. *Geochimica et Cosmochimica Acta*, *244*, 182–196. doi: 10.1016/j.gca.2018.09.027
Mickler, P. J., Stern, L. A., & Banner, J. L. (2006). Large kinetic isotope effects in modern speleothems. *GSA Bulletin*, *118*(1–2), 65–81. doi: 10.1130/B25698.1
Mischel, S. A., Scholz, D., & Spötl, C. (2015). δ18O values of cave drip water: a promising proxy for the reconstruction of the North Atlantic Oscillation? *Climate Dynamics*, *45*(11–12), 3035–3050. doi: 10.1007/s00382-015-2521-5
Moreau-Le Golvan, Y., Michelot, J. L., & Boisson, J. Y. (1997). Stable isotope contents of porewater in a claystone formation (Tournemire, France): Assessment of the extraction technique and preliminary results. *Applied Geochemistry*, *12*(6), 739–745. doi: 10.1016/S0883-2927(97)00044-9
Morse, J. W., & Bender, M. L. (1990). Partition coefficients in calcite: Examination of factors influencing the validity of experimental results and their application to natural systems. *Chemical Geology*, *82*(C), 265–277. doi: 10.1016/0009-2541(90)90085-L
Mühlinghaus, C., Scholz, D., & Mangini, A. (2007). Modelling stalagmite growth and δ13C as a

function of drip interval and temperature>. *Geochimica et Cosmochimica Acta*, *71*(11), 2780–2790. doi: 10.1016/j.gca.2007.03.018
Mühlinghaus, C., Scholz, D., & Mangini, A. (2009). Modelling fractionation of stable isotopes in stalagmites. *Geochimica et Cosmochimica Acta*, *73*(24), 7275–7289. doi: 10.1016/j.gca.2009.09.010
Murray-Tortarolo, G. N., & Salgado, M. M. (2021). Drought as a driver of Mexico-US migration. *Climatic Change*, *164*(3–4), 1–11. doi: 10.1007/s10584-021-03030-2
Nguyen, P., Shearer, E. J., Tran, H., Ombadi, M., Hayatbini, N., Palacios, T., … Sorooshian, S. (2019). The CHRS data portal, an easily accessible public repository for PERSIANN global satellite precipitation data. *Scientific Data*, *6*(1), 1–10. doi: 10.1038/sdata.2018.296
Noronha, A. L., Johnson, K. R., Southon, J. R., Hu, C., Ruan, J., & McCabe-Glynn, S. (2015). Radiocarbon evidence for decomposition of aged organic matter in the vadose zone as the main source of speleothem carbon. *Quaternary Science Reviews*, *127*, 37–47. doi: 10.1016/J.QUASCIREV.2015.05.021
Oerter, E., Finstad, K., Schaefer, J., Goldsmith, G. R., Dawson, T., & Amundson, R. (2014). Oxygen isotope fractionation effects in soil water via interaction with cations (Mg, Ca, K, Na) adsorbed to phyllosilicate clay minerals. *Journal of Hydrology*, *515*, 1–9. doi: 10.1016/j.jhydrol.2014.04.029
Osácar, M. C., Sancho, C., Muñoz, A., Moreno, A., Bartolomé, M., Pérez, C., … Stoll, H. (2017). δ13C and Mg/Ca dripwater response to environmental conditions in the Ortigosa caves (La Rioja, Spain). *Geogaceta*, *61*, 175–178.
Osorio-Osorio, J. A., Astudillo-Sánchez, C. C., Villanueva-Díaz, J., Soria-Díaz, L., & Vargas-Tristán, V. (2020). Historical precipitation reconstruction of el cielo biosphere reserve, Mexico, using taxodium mucronatum (Cupressaceae) annual growth rings. *Revista de Biologia Tropical*, *68*(3), 818–832. doi: 10.15517/RBT.V68I3.39624
Oster, J. L., Montañez, I. P., Guilderson, T. P., Sharp, W. D., & Banner, J. L. (2010). Modeling speleothem δ13C variability in a central Sierra Nevada cave using 14C and 87Sr/86Sr. *Geochimica et Cosmochimica Acta*, *74*(18), 5228–5242. doi: 10.1016/j.gca.2010.06.030
Palmer, M. V., & Palmer, A. N. (2012). Petrographic and isotopic evidence for late-stage processes in sulfuric acid caves of the Guadalupe Mountains, New Mexico, USA. *International Journal of Speleology*, *41*(2), 231–250. doi: 10.5038/1827-806X.41.2.10
Pausata, F. S. R., Battisti, D. S., Nisancioglu, K. H., & Bitz, C. M. (2011). Chinese stalagmite δ 18 O controlled by changes in the indian monsoon during a simulated heinrich event. *Nature Geoscience*, *4*(7), 474–480. doi: 10.1038/ngeo1169
Pavia, E. G., Graef, F., & Reyes, J. (2006). PDO–ENSO Effects in the Climate of Mexico. *Journal of Climate*, *19*(24), 6433–6438. doi: 10.1175/JCLI4045.1
Pérez Quezadas, J., Cortés Silva, A., Inguaggiato, S., del Rocío Salas Ortega, M., Cervantes Pérez, J., & Heilweil, V. M. (2015). Meteoric isotopic gradient on the windward side of the sierra madre oriental area, Veracruz - Mexico. *Geofisica Internacional*, *54*(3), 267–276. doi: 10.1016/j.gi.2015.04.021
Quezadas, J. P., Adams, D., Sánchez Murillo, R., Lagunes, A. J., & Rodríguez Castañeda, J. L. (2021). Isotopic variability (δ18O, δ2H and d-excess) during rainfall events of the north American monsoon across the Sonora River Basin, Mexico. *Journal of South American Earth Sciences*, *105*, 102928. doi: 10.1016/j.jsames.2020.102928
Quiroz-Jiménez, J. D., Roy, P. D., Beramendi-Orosco, L. E., Lozano-García, S., & Vázquez-Selem, L. (2018). Orbital-scale droughts in central-northern Mexico during the late

Quaternary and comparison with other subtropical and tropical records. *Geological Journal*, *53*(1), 230–242. doi: 10.1002/gj.2888

Rasmussen, S. O., Andersen, K. K., Svensson, A. M., Steffensen, J. P., Vinther, B. M., Clausen, H. B., … Ruth, U. (2006). A new Greenland ice core chronology for the last glacial termination. *Journal of Geophysical Research Atmospheres*, *111*(6), D06102. doi: 10.1029/2005JD006079

Reimer, P. J., Bard, E., Bayliss, A., Beck, J. W., Blackwell, P. G., Ramsey, C. B., … van der Plicht, J. (2013). Selection and Treatment of Data for Radiocarbon Calibration: An Update to the International Calibration (IntCal) Criteria. *Radiocarbon*, *55*(4), 1923–1945. doi: 10.2458/azu_js_rc.55.16955

Riechelmann, D. F. C., Deininger, M., Scholz, D., Riechelmann, S., Schröder-Ritzrau, A., Spötl, C., … Immenhauser, A. (2013). Disequilibrium carbon and oxygen isotope fractionation in recent cave calcite: Comparison of cave precipitates and model data. *Geochimica et Cosmochimica Acta*, *103*, 232–244. doi: 10.1016/j.gca.2012.11.002

Riechelmann, D. F. C., Schröder-Ritzrau, A., Scholz, D., Fohlmeister, J., Spötl, C., Richter, D. K., & Mangini, A. (2011). Monitoring Bunker Cave (NW Germany): A prerequisite to interpret geochemical proxy data of speleothems from this site. *Journal of Hydrology*, *409*(3–4), 682–695. doi: 10.1016/J.JHYDROL.2011.08.068

Risi, C., Bony, S., & Vimeux, F. (2008). Influence of convective processes on the isotopic composition (δ^{18} O and δ D) of precipitation and water vapor in the tropics: 2. Physical interpretation of the amount effect. *Journal of Geophysical Research*, *113*(D19), D19306. doi: 10.1029/2008JD009943

Rivera-Rivera, D. M., Chidambaram, S., Tirumalesh, K., Escobedo-Urias, D. C., Sujitha, S. B., Rodriguez-Espinosa, P. F., … Jonathan, M. P. (2021). Stable isotopic (δ2H, δ18O) monograms of winter precipitation events and hydro-climatic dynamics in Central Mexico. *Atmospheric Research*, *261*, 105744. doi: 10.1016/j.atmosres.2021.105744

Roy, P. D., Quiroz-Jiménez, J. D., Pérez-Cruz, L. L., Lozano-García, S., Metcalfe, S. E., Lozano-Santacruz, R., … Romero, F. M. (2013a). Late Quaternary paleohydrological conditions in the drylands of northern Mexico: A summer precipitation proxy record of the last 80 cal ka BP. *Quaternary Science Reviews*, *78*, 342–354. doi: 10.1016/j.quascirev.2012.11.020

Roy, P. D., Rivero-Navarette, A., Lopez-Balbiaux, N., Pérez-Cruz, L. L., Metcalfe, S. E., Sankar, G. M., & Sánchez-Zavala, J. L. (2013b). A record of Holocene summer-season palaeohydrological changes from the southern margin of Chihuahua Desert (Mexico) and possible forcings. *The Holocene*, *23*(8), 1105–1114. doi: 10.1177/0959683613483619

Roy, P. D., Rivero-Navarrete, A., Sánchez-Zavala, J. L., Beramendi-Orosco, L. E., Muthu-Sankar, G., & Lozano-Santacruz, R. (2016). Atlantic Ocean modulated hydroclimate of the subtropical northeastern Mexico since the last glacial maximum and comparison with the southern US. *Earth and Planetary Science Letters*, *434*, 141–150. doi: 10.1016/j.epsl.2015.11.048

Roy, P. D., Vera-Vera, G., Sánchez-Zavala, J. L., Shanahan, T. M., Quiroz-Jiménez, J. D., Curtis, J. H., … Muthusankar, G. (2020). Depositional histories of vegetation and rainfall intensity in Sierra Madre Oriental Mountains (northeast Mexico) since the late Last Glacial. *Global and Planetary Change*, *187*(July 2019), 103136. doi: 10.1016/j.gloplacha.2020.103136

Rudzka, D., McDermott, F., Baldini, L. M., Fleitmann, D., Moreno, A., & Stoll, H. (2011). The

coupled δ13C-radiocarbon systematics of three Late Glacial/early Holocene speleothems; insights into soil and cave processes at climatic transitions. *Geochimica et Cosmochimica Acta*, *75*(15), 4321–4339. doi: 10.1016/j.gca.2011.05.022

Salinas-Rodríguez, M. M., Estrada-Castillón, E., & Illarreal-Quintanilla, J. A. (2017). Endemic vascular plants of the sierra madre oriental, Mexico. *Phytotaxa*, *328*(1), 1–52. doi: 10.11646/PHYTOTAXA.328.1.1

Sánchez-Murillo, R., Birkel, C., Welsh, K., Esquivel-Hernández, G., Corrales-Salazar, J., Boll, J., … Araguás-Araguás, L. J. (2016). Key drivers controlling stable isotope variations in daily precipitation of Costa Rica: Caribbean Sea versus Eastern Pacific Ocean moisture sources. *Quaternary Science Reviews*, *131*, 250–261. doi: 10.1016/J.QUASCIREV.2015.08.028

Sánchez-Murillo, R., Esquivel-Hernández, G., Welsh, K., Brooks, E. S., Boll, J., Alfaro-Solís, R., … Valdés-González, J. (2013). Spatial and Temporal Variation of Stable Isotopes in Precipitation across Costa Rica: An Analysis of Historic GNIP Records. *Open Journal of Modern Hydrology*, *3*(4), 226–240. doi: 10.4236/OJMH.2013.34027

Schmidt, M. W., Spero, H. J., & Lea, D. W. (2004). Links between salinity variation in the Caribbean and North Atlantic thermohaline circulation. *Nature*, *428*(6979), 160–163. doi: 10.1038/nature02346

Schwarcz, H. P., Harmon, R. S., Thompson, P., & Ford, D. C. (1976). Stable isotope studies of fluid inclusions in speleothems and their paleoclimatic significance. *Geochimica et Cosmochimica Acta*, *40*(6), 657–665. doi: 10.1016/0016-7037(76)90111-3

Seager, R., Ting, M., Davis, M., & Stahle, D. W. (2009). Mexican drought: an observational modeling and tree ring study of variability and climate change. In *Atmósfera* (Vol. 22). Retrieved from http://ingrid.ldeo.columbia.edu/SOURCES/UNAM/

Shen, C.-C., Lin, K., Duan, W., Jiang, X., Partin, J. W., Edwards, R. L., … Tan, M. (2013). Testing the annual nature of speleothem banding. *Scientific Reports 2013 3:1*, *3*(1), 1–5. doi: 10.1038/srep02633

Shultz, J. M., Berg, R. C., Kossin, J. P., Burkle Jr, F., Maggioni, A., Pinilla Escobar, V. A., … Galea, S. (2021). Convergence of climate-driven hurricanes and COVID-19: The impact of 2020 hurricanes Eta and Iota on Nicaragua. *The Journal of Climate Change and Health*, *3*, 100019. doi: 10.1016/j.joclim.2021.100019

Sinclair, D. J., Banner, J. L., Taylor, F. W., Partin, J., Jenson, J., Mylroie, J., … Miklavič, B. (2012). Magnesium and strontium systematics in tropical speleothems from the Western Pacific. *Chemical Geology*, *294–295*, 1–17. doi: 10.1016/J.CHEMGEO.2011.10.008

Smith, C. L., Fairchild, I. J., Spötl, C., Frisia, S., Borsato, A., Moreton, S. G., & Wynn, P. M. (2009). Chronology building using objective identification of annual signals in trace element profiles of stalagmites. *Quaternary Geochronology*, *4*(1), 11–21. doi: 10.1016/j.quageo.2008.06.005

Southon, J., Noronha, A. L., Cheng, H., Edwards, R. L., & Wang, Y. (2012). A high-resolution record of atmospheric 14C based on Hulu Cave speleothem H82. *Quaternary Science Reviews*, *33*, 32–41. doi: 10.1016/j.quascirev.2011.11.022

Spötl, C., Fairchild, I. J., & Tooth, A. F. (2005). Cave air control on dripwater geochemistry, Obir Caves (Austria): Implications for speleothem deposition in dynamically ventilated caves. *Geochimica et Cosmochimica Acta*, *69*(10), 2451–2468. doi: 10.1016/J.GCA.2004.12.009

Spötl, C., Mangini, A., & Richards, D. A. (2006). Chronology and paleoenvironment of Marine

Isotope Stage 3 from two high-elevation speleothems, Austrian Alps. *Quaternary Science Reviews*, *25*(9–10), 1127–1136. doi: 10.1016/j.quascirev.2005.10.006
Sprenger, M., Leistert, H., Gimbel, K., & Weiler, M. (2016). Illuminating hydrological processes at the soil-vegetation-atmosphere interface with water stable isotopes. *Reviews of Geophysics*, *54*(3), 674–704. doi: 10.1002/2015RG000515
Sprenger, M., Tetzlaff, D., Buttle, J., Laudon, H., Leistert, H., Mitchell, C. P. J., … Soulsby, C. (2018). Measuring and Modeling Stable Isotopes of Mobile and Bulk Soil Water. *Vadose Zone Journal*, *17*(1), 170149. doi: 10.2136/vzj2017.08.0149
Stahle, D. W., Burnette, D. J., Villanueva, J., Cerano, J., Fye, F. K., Griffin, R. D., … Wolff, K. P. (2012). Tree-ring analysis of ancient baldcypress trees and subfossil wood. *Quaternary Science Reviews*, *34*, 1–15. doi: 10.1016/J.QUASCIREV.2011.11.005
Stahle, D. W., Cook, E. R., Burnette, D. J., Villanueva, J., Cerano, J., Burns, J. N., … Howard, I. M. (2016, October 1). The Mexican Drought Atlas: Tree-ring reconstructions of the soil moisture balance during the late pre-Hispanic, colonial, and modern eras. *Quaternary Science Reviews*, Vol. 149, pp. 34–60. Pergamon. doi: 10.1016/j.quascirev.2016.06.018
Stein, A. F., Draxler, R. R., Rolph, G. D., Stunder, B. J. B., Cohen, M. D., & Ngan, F. (2015, December 1). Noaa's hysplit atmospheric transport and dispersion modeling system. *Bulletin of the American Meteorological Society*, Vol. 96, pp. 2059–2077. American Meteorological Society. doi: 10.1175/BAMS-D-14-00110.1
Stoll, H. M., Müller, W., & Prieto, M. (2012). I-STAL, a model for interpretation of Mg/Ca, Sr/Ca and Ba/Ca variations in speleothems and its forward and inverse application on seasonal to millennial scales. *Geochemistry, Geophysics, Geosystems*, *13*(9). doi: 10.1029/2012GC004183
Tooth, A. F., & Fairchild, I. J. (2003). Soil and karst aquifer hydrological controls on the geochemical evolution of speleothem-forming drip waters, Crag Cave, southwest Ireland. *Journal of Hydrology*, *273*(1–4), 51–68. doi: 10.1016/S0022-1694(02)00349-9
Treble, P. C., Fairchild, I. J., Griffiths, A., Baker, A., Meredith, K. T., Wood, A., & McGuire, E. (2015). Impacts of cave air ventilation and in-cave prior calcite precipitation on Golgotha Cave dripwater chemistry, southwest Australia. *Quaternary Science Reviews*, *127*, 61–72. doi: 10.1016/j.quascirev.2015.06.001
Treble, P., Shelley, J. M. G., & Chappell, J. (2003). Comparison of high resolution sub-annual records of trace elements in a modern (1911–1992) speleothem with instrumental climate data from southwest Australia. *Earth and Planetary Science Letters*, *216*(1–2), 141–153. doi: 10.1016/S0012-821X(03)00504-1
U.S. Customs and Border Protection. (2021). US Border Patrol Apprehensions Southwest land Border Encounters per year. *U.S. Customs and Border ProtectionU.S. Customs and Border Protection*. Retrieved from https://www.cbp.gov/newsroom/stats/southwest-land-border-encounters
Villanueva-Diaz, J., Stahle, D. W., Luckman, B. H., Cerano-Paredes, J., Therrell, M. D., Cleaveland, M. K., & Cornejo-Oviedo, E. (2007). Winter-spring precipitation reconstructions from tree rings for northeast Mexico. *Climatic Change*, *83*(1–2), 117–131. doi: 10.1007/s10584-006-9144-0
Vuille, M., & Werner, M. (2005). Stable isotopes in precipitation recording South American summer monsoon and ENSO variability: Observations and model results. *Climate Dynamics*, *25*(4), 401–413. doi: 10.1007/s00382-005-0049-9
Waelbroeck, C., Labeyrie, L., Michel, E., Duplessy, J. C., Mcmanus, J. F., Lambeck, K., …

Labracherie, M. (2002). Sea-level and deep water temperature changes derived from benthic foraminifera isotopic records. In *Quaternary Science Reviews* (Vol. 21).

Wagner, J. D. M., Cole, J. E., Beck, J. W., Patchett, P. J., Henderson, G. M., & Barnett, H. R. (2010). Moisture variability in the southwestern United States linked to abrupt glacial climate change. *Nature Geoscience*, *3*(2), 110–113. doi: 10.1038/ngeo707

Wang, C., Enfield, D. B., Lee, S. K., & Landsea, C. W. (2006). Influences of the Atlantic warm pool on western hemisphere summer rainfall and Atlantic hurricanes. *Journal of Climate*, *19*(12), 3011–3028. doi: 10.1175/JCLI3770.1

Wang, C., Liu, H., Lee, S. K., & Atlas, R. (2011). Impact of the Atlantic warm pool on United States landfalling hurricanes. *Geophysical Research Letters*, *38*(19), n/a-n/a. doi: 10.1029/2011GL049265

Wang, Y., Cheng, H., Edwards, R. L., Kong, X., Shao, X., Chen, S., … An, Z. (2008). Millennial- and orbital-scale changes in the East Asian monsoon over the past 224,000 years. *Nature*, *451*(7182), 1090–1093. doi: 10.1038/nature06692

Wang, Y. J., Cheng, H., Edwards, R. L., An, Z. S., Wu, J. Y., Shen, C. C., & Dorale, J. A. (2001). A high-resolution absolute-dated late Pleistocene Monsoon record from Hulu Cave, China. *Science (New York, N.Y.)*, *294*(5550), 2345–2348. doi: 10.1126/science.1064618

Warken, S. F., Scholz, D., Spötl, C., Jochum, K. P., Pajón, J. M., Bahr, A., & Mangini, A. (2019). Caribbean hydroclimate and vegetation history across the last glacial period. *Quaternary Science Reviews*, *218*, 75–90. doi: 10.1016/j.quascirev.2019.06.019

Webster, J. W., Brook, G. A., Railsback, L. B., Cheng, H., Edwards, R. L., Alexander, C., & Reeder, P. P. (2007). Stalagmite evidence from Belize indicating significant droughts at the time of Preclassic Abandonment, the Maya Hiatus, and the Classic Maya collapse. *Palaeogeography, Palaeoclimatology, Palaeoecology*, *250*(1–4), 1–17. doi: 10.1016/j.palaeo.2007.02.022

Williams, P. W., King, D. N. T., Zhao, J. X., & Collerson, K. D. (2005). Late Pleistocene to Holocene composite speleothem 18O and 13C chronologies from South Island, New Zealand - Did a global Younger Dryas really exist? *Earth and Planetary Science Letters*, *230*(3–4), 301–317. doi: 10.1016/j.epsl.2004.10.024

Wong, C. I., Banner, J. L., & Musgrove, M. L. (2011). Seasonal dripwater Mg/Ca and Sr/Ca variations driven by cave ventilation: Implications for and modeling of speleothem paleoclimate records. *Geochimica et Cosmochimica Acta*, *75*(12), 3514–3529. doi: 10.1016/j.gca.2011.03.025

Wong, C. I., Banner, J. L., & Musgrove, M. L. (2015). Holocene climate variability in Texas, USA: An integration of existing paleoclimate data and modeling with a new, high-resolution speleothem record. *Quaternary Science Reviews*, *127*, 155–173. doi: 10.1016/j.quascirev.2015.06.023

Woodhead, J., Reisz, R., Fox, D., Drysdale, R., Hellstrom, J., Maas, R., … Edwards, R. L. (2010). Speleothem climate records from deep time? Exploring the potential with an example from the Permian. *Geology*, *38*(5), 455–458. doi: 10.1130/G30354.1

Yadava, M. G., & Ramesh, R. (2005). Monsoon reconstruction from radiocarbon dated tropical Indian speleothems. *Holocene*, *15*(1), 48–59. doi: 10.1191/0959683605h1783rp

Yang, H., Johnson, K. R., Griffiths, M. L., & Yoshimura, K. (2016). Interannual controls on oxygen isotope variability in Asian monsoon precipitation and implications for paleoclimate reconstructions. *Journal of Geophysical Research*, *121*(14), 8410–8428. doi: 10.1002/2015JD024683

Zhang, H., Griffiths, M. L., Chiang, J. C. H., Kong, W., Wu, S., Atwood, A., … Xie, S. (2018). East Asian hydroclimate modulated by the position of the westerlies during Termination I. *Science*, *362*(6414), 580–583. doi: 10.1126/science.aat9393

Zhang, P., Cheng, H., Edwards, R. L., Chen, F., Wang, Y., Yang, X., … Johnson, K. R. (2008). A test of climate, sun, and culture relationships from an 1810-year Chinese cave record. *Science*, *322*(5903), 940–942. doi: 10.1126/science.1163965

Ziegler, M., Nürnberg, D., Karas, C., Tiedemann, R., & Lourens, L. J. (2008). Persistent summer expansion of the Atlantic Warm Pool during glacial abrupt cold events. *Nature Geoscience*, *1*(9), 601–605. doi: 10.1038/ngeo277

3.8 Appendix A

This Appendix includes:

Supplementary methods
Fig. S3.1: Comparison of raw CB2 δ18O with mean-seawater subtracted CB2 $\delta^{18}O$.
Fig. S3.2: Modern precipitation patterns of NE Mexico.
Fig. S3.3: CB2 $\delta^{18}O$ compared to various seasons of insolation.
Fig. S3.4: Summer and winter low level winds during the Last Glacial Maximum, Mid-Holocene and Pre-Industrial Period.
Fig. S3.5: Summer and winter precipitation during the Last Glacial Maximum, Mid-Holocene and Pre-Industrial Period.
Table S3.1: Uranium-thorium data for Stalagmite CB2

Supplementary methods: Speleothem sample CB2

Stalagmite CB2 was collected on a slope approximately 30 meters from the cave entrance on a second level, approximately 15 meters below the first level. Stalagmite CB2 was inactive when collected, but drip water was collected from around the sample in spring 2016 and 2017. CB2 is a 78 cm long stalagmite composed of translucent grey and beige calcite. No acicular patterns were detected by hand lens, and XRD analysis conducted at ~ 15cm intervals showed CB2 is 100% calcite. CB2 exhibits a predominantly aggregational stratigraphic stacking pattern as well as a globular morphostratigraphic units throughout, suggesting relatively consistent drip rates and calcite saturation (Martín-Chivelet *et al.*, 2017). The speleothem sampled is 100% calcite and temperatures remain relatively constant throughout time, therefore we assume $\delta^{18}O$ variations are dominantly driven by changes in precipitation $\delta^{18}O$.

Supplementary methods: Interpretation of geochemical proxies

During periods of reduced local water balance (i.e. reduced water in the critical zone, P-ET), Prior Calcite Precipitation is enhanced due to an increase in air-filled voids on the cave-ceiling, in the epikarst, and overlying soil (Johnson *et al.*, 2006). Air-filled voids have reduced

pCO_2 in comparison to infiltrating water, which enhances CO_2 degassing and the precipitation of calcite (Borsato *et al.*, 2016). Enhanced CO_2 degassing leads to the preferential loss of ^{12}C in the percolating waters, increasing the $\delta^{13}C$ values in the remaining solution and speleothem. Additionally, when calcite precipitates it preferentially uptakes Ca^{2+} leaving the remaining solution and speleothem enriched in the divalent ions (Mg^{2+}, Sr^{2+}, Ba^{2+}). Therefore, we interpret the covariation in $\delta^{13}C$ and Mg/Ca in our record to be reflective of prior calcite precipitation, primarily controlled by local water balance, not necessary precipitation amount. It is important to note during the transition out of the Pleistocene the increasing trend in Mg/Ca is anomalous compared to $\delta^{13}C$ ($r = 0.14$, $p = 0.04$) and $\delta^{18}O$, suggesting trace elements do not match our other proxies on orbital timescales.

Mg/Ca values diverge from the stable isotope record during the glacial-interglacial transition, with an increase from mean glacial concentrations of 30 mmol/mol to Holocene concentrations of ~40 mmol/mol (Fig. 2). The increase in Mg/Ca ratios could be reflective of dryer conditions during the Holocene, however, we interpret the rise in Mg/Ca ratios as a result of non-hydrologic controls on speleothem trace element ratios. During the glacial, we find overall agreement between Mg/Ca and $\delta^{13}C$, indicative that hydrologically sensitive PCP is likely an important controlling mechanism especially on millennial timescales. The divergence between these proxies during the deglacial and Holocene, however, may be explained by the competing influence of temperatures on Mg partitioning into calcite. Cave temperatures are reflective of mean annual surface temperatures (Dorale, 1998), therefore as temperatures increased from the glacial through mid-Holocene the temperature dependent partition coefficient for Mg was likely affected (Stoll *et al.*, 2012). If we assume a 5°C interglacial-glacial

temperature correction for Mg/Ca, modeling studies demonstrate this change could impart up to a 23% increase in Mg/Ca (Stoll *et al.*, 2012), consistent with the observed shift in CB2.

Supplementary methods: Correction for Seawater $\delta^{18}O$

The ultimate moisture source of any precipitation is seawater. In order to correct precipitation for glacial-interglacial shifts in $\delta^{18}O_{sw}$, we subtracted interpolated $\delta^{18}O_{sw}$ values (Waelbroeck *et al.*, 2002) from CB2 data (Fig. S3.1). This ultimately decreases glacial-interglacial $\delta^{18}O_{speleothem}$ values but does not play a huge role in mitigating or amplifying millennial scale variability.

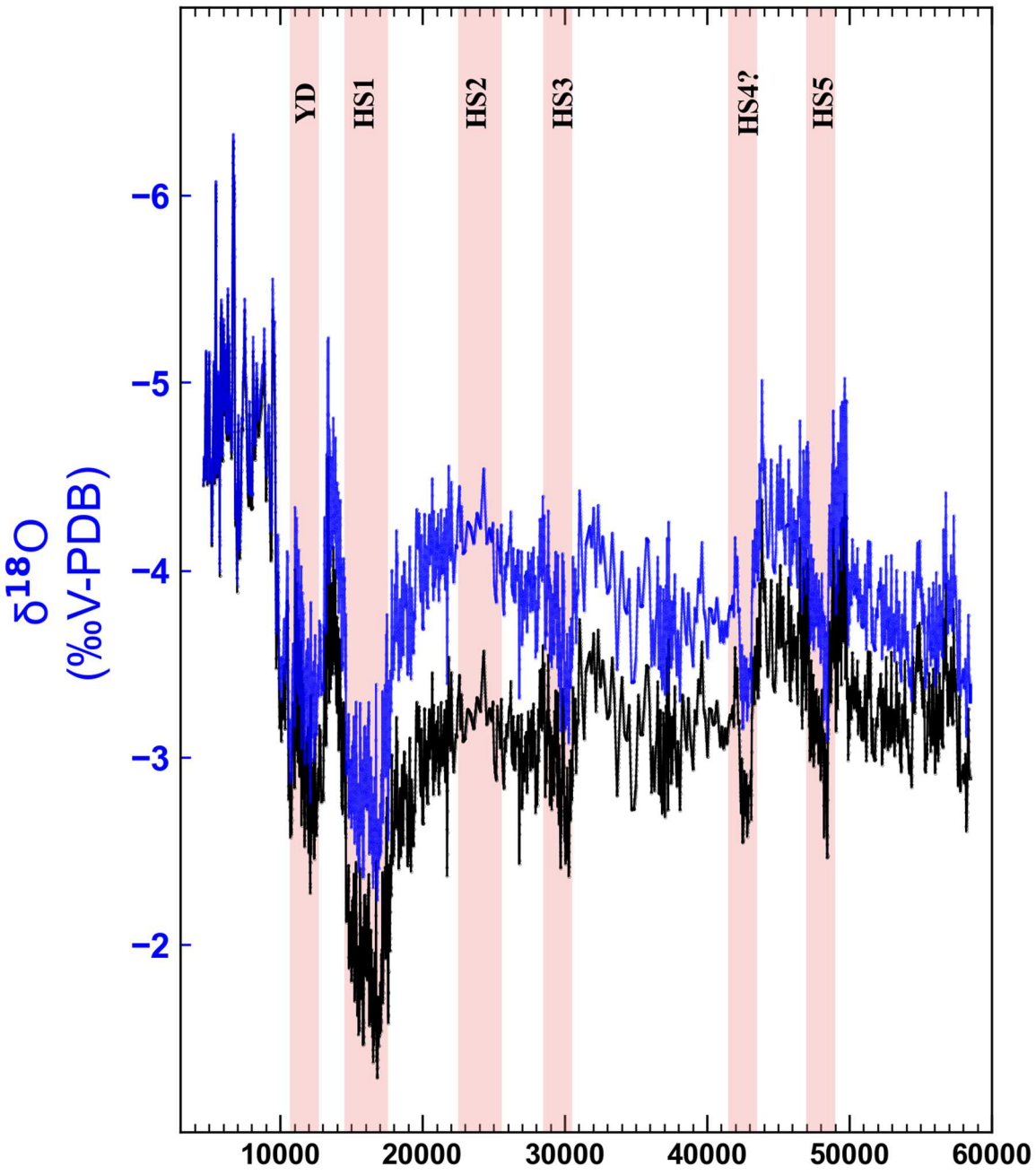

Fig. S3.1: Comparison of raw CB2 $\delta^{18}O$ with mean-seawater subtracted CB2 $\delta^{18}O$. Mean seawater interglacial-glacial $\delta^{18}O$ from Waelbroeck et al. (2002) subtracted from raw CB2 $\delta^{18}O_{speleothem}$ shown in black, to yield corrected CB2 $\delta^{18}O_{speleothem}$ shown in blue. Corrected $\delta^{18}O_{speleothem}$ was used in all figures, and all other speleothem records used for comparison were also corrected using values from Waelbroeck et al. (2002). Correcting our record for changes in mean seawater $\delta^{18}O$ does not affect the magnitude of change in millennial scale events. Furthermore, changes in $\delta^{18}O_{seawater}$ during the Holocene were minimal, reflected in the overlap of corrected (blue) and uncorrected (black) values.

A)

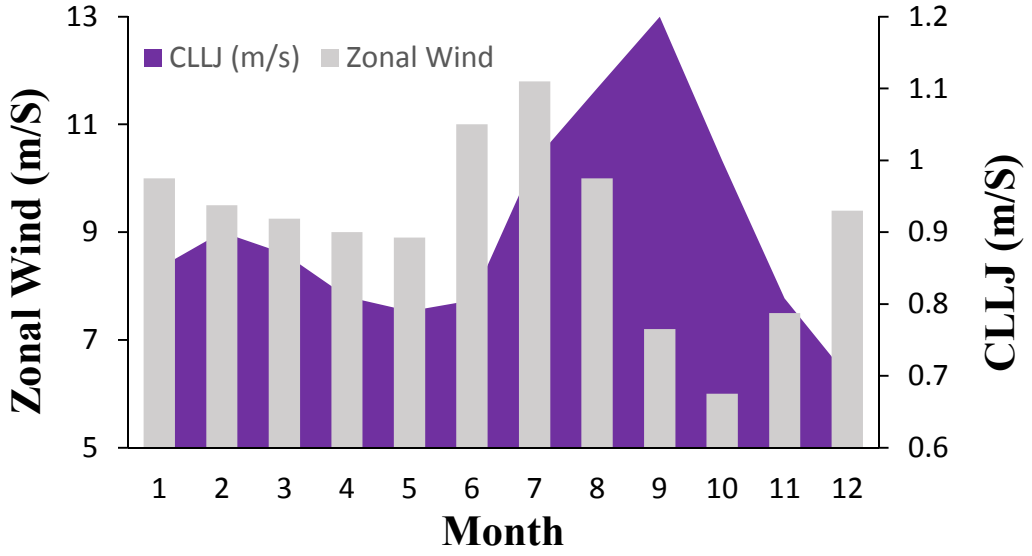

B)

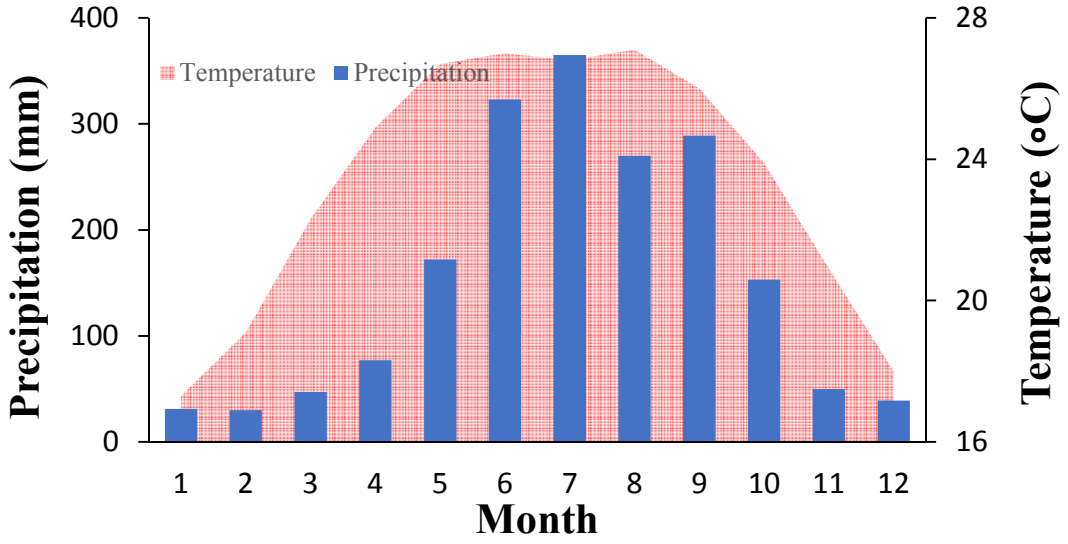

Fig. S3.2: Modern precipitation and wind patterns of NE Mexico. A) Monthly average precipitation and temperature above cave site from www.weatherbase.com. **B)** Monthly average zonal winds in the Caribbean Basin and strength of Caribbean Low-Level Jet (Mestas-Nuñez *et al.*, 2007).

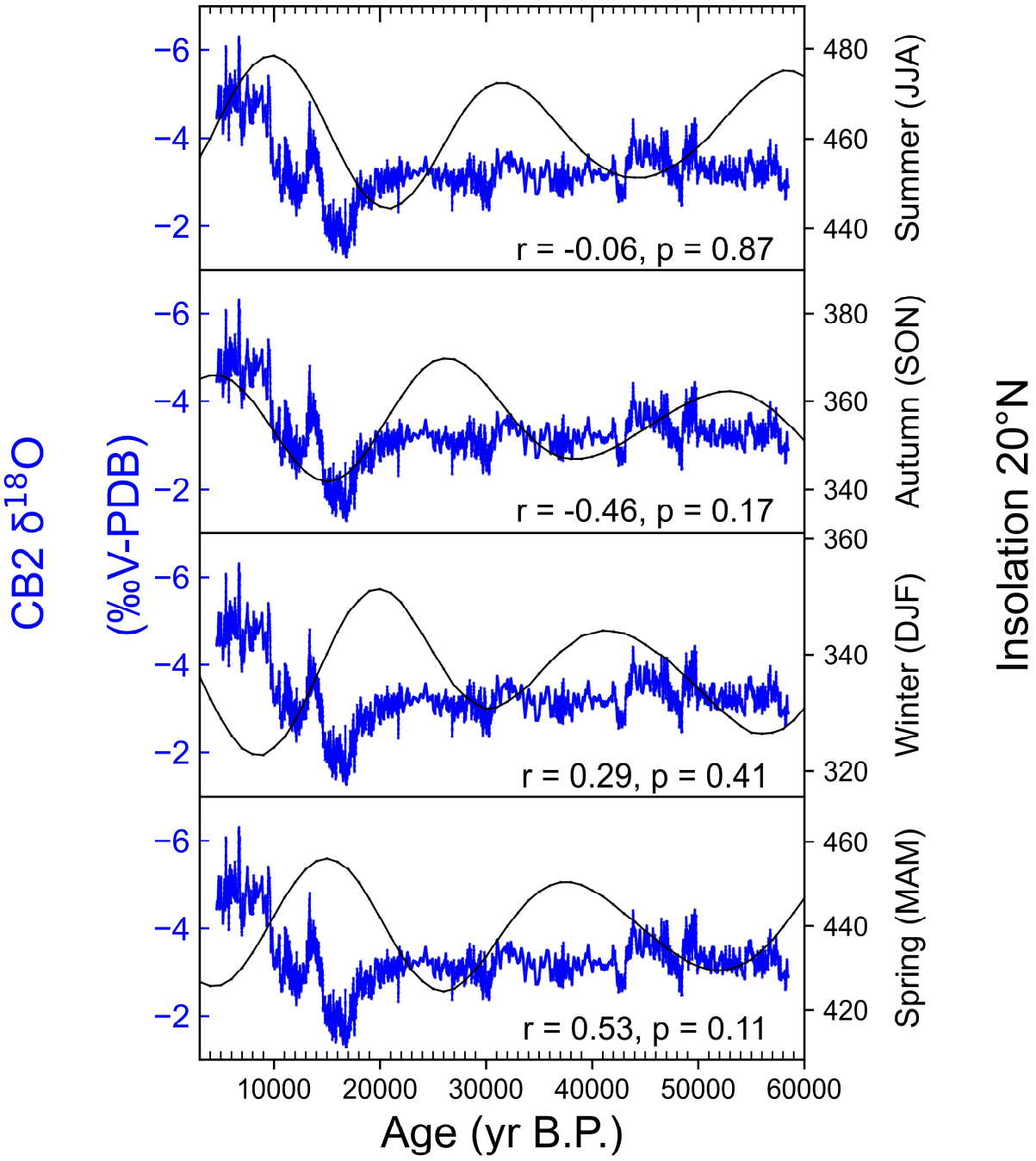

Fig. S3: CB2 $\delta^{18}O$ (blue) compared to various seasons of insolation. While autumn and summer insolation appear to have a strong negative correlation to CB2 $\delta^{18}O$ (positive correlation to rainfall) over the Pleistocene – Holocene transition, this co-variation does not continue over the late Pleistocene. We also do not see a significant correlation to Winter (DJF) or Spring (MAM) insolation.

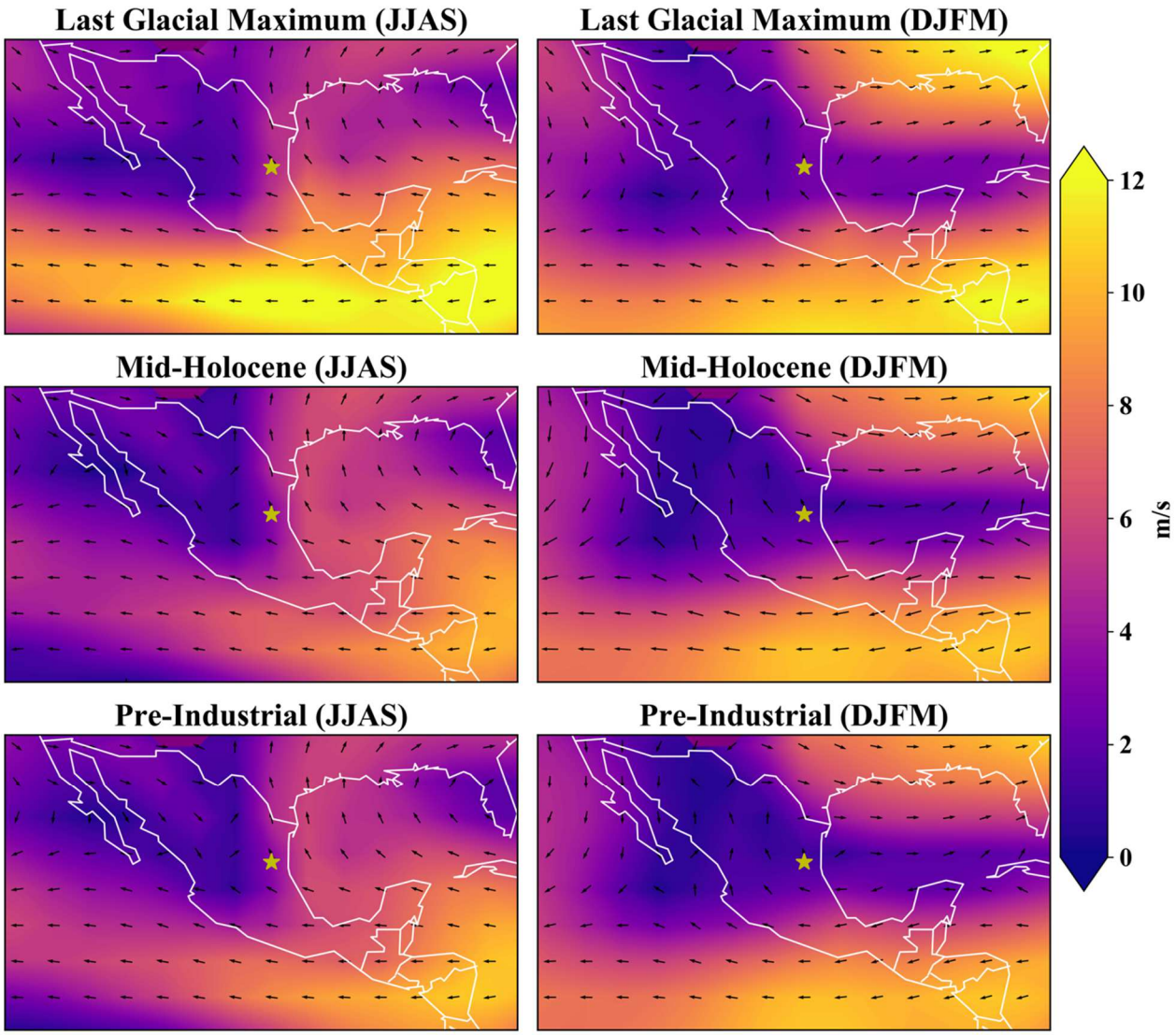

Fig. S3.4: Summer and winter low level winds. Summer (left) and winter (right) low-level wind direction and magnitude during the LGM (top), Mid-Holocene (mid) and Pre-Industrial (bottom) time periods from the NASA model GISS-E2-R (Braconnot et al., 2012). The magnitude is illustrated by color, direction is indicated by arrow. Winds were noticeably stronger during the Last Glacial Maximum (top), indicated by yellow, however, there is no major changes in in wind direction with respect to the Mid-Holocene or Pre-Industrial period that would suggest an increased proportion of rainfall from the Pacific.

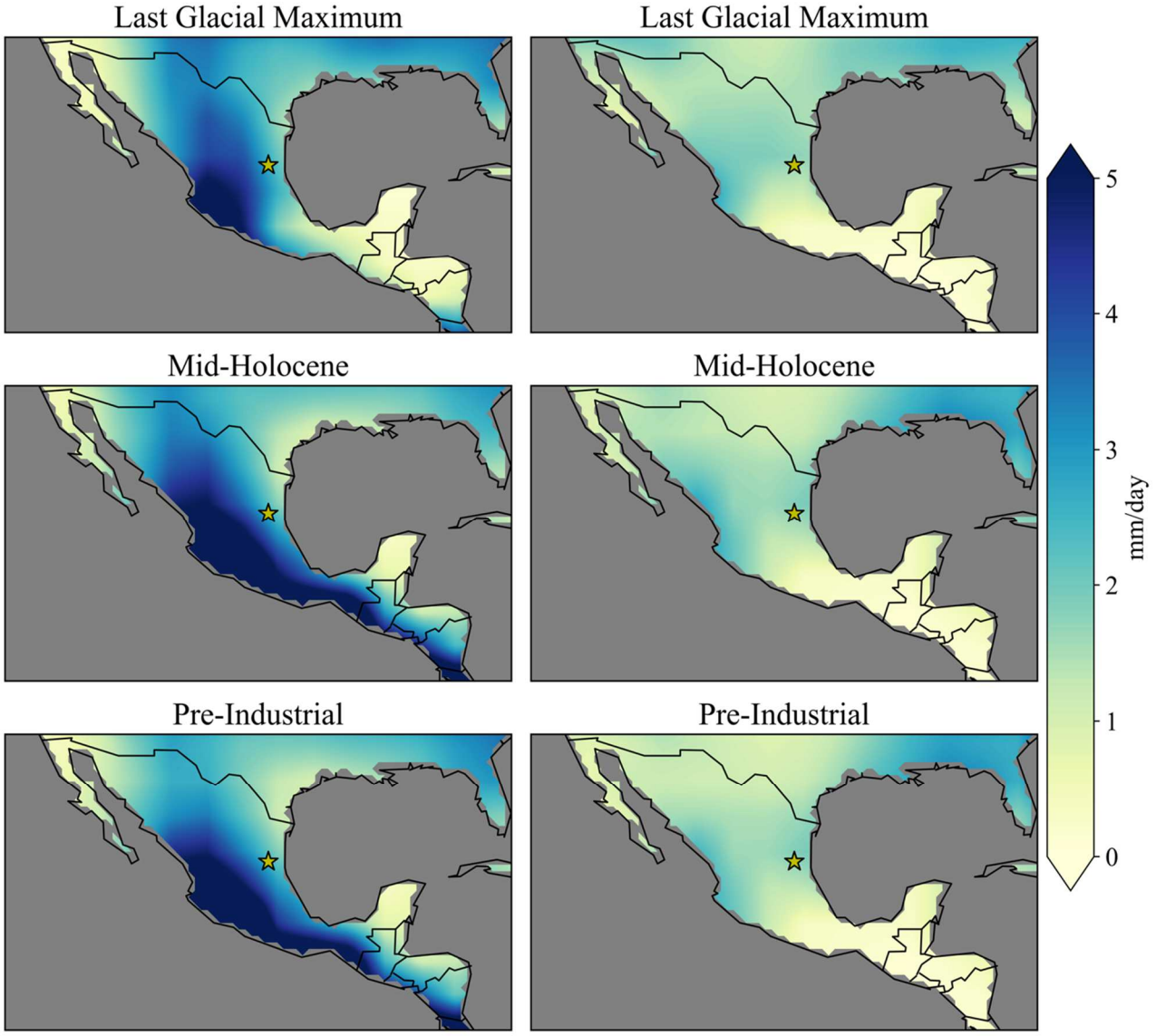

Fig. S3.5: Summer and winter precipitation. Precipitation results from PMIP3 Model GISS-E2-R (Braconnot et al., 2012). Summer (left) and winter (right) precipitation during the LGM (top), Mid-Holocene (mid) and Pre-Industrial (bottom) time periods. The model demonstrates increased precipitation throughout time (LGM<MI<PI), however, summer remains the wet season throughout all time periods.

Table S2.1: Uranium-thorium data for Stalagmite CB2

Depth (mm)	^{238}U (ng/g)	^{232}Th (ng/g)	$\delta^{234}U$ (‰)	($^{232}Th/^{238}U$) (Activity)	$^{230}Th/^{232}Th$ ppm atomic	Uncorrected Age (yr)	Corrected age (yr)	$\delta^{234}Uinit$ (‰)
3	39 ± 1	3639 ± 95	132 ± 2	0.1115 ± 0.0069	19.1 ± 1.2	11298 ± 742	5187 ± 1399	134 ± 2
14	38 ± 1	87 ± 2	128 ± 3	0.0584 ± 0.0012	406.9 ± 10.2	5801 ± 133	5587 ± 136	130 ± 3
27	45 ± 1	159 ± 4	129 ± 2	0.0611 ± 0.0019	271.9 ± 9.2	6057 ± 203	5761 ± 207	131 ± 2
45	52 ± 1	7262 ± 146	146 ± 2	0.1529 ± 0.0036	17.5 ± 0.4	15565 ± 395	6428 ± 1848	149 ± 2
85	63 ± 1	70 ± 2	174 ± 2	0.1144 ± 0.0006	1648.9 ± 33.3	11154 ± 63	11019 ± 64	179 ± 2
90	59 ± 1	156 ± 3	225 ± 3	0.1219 ± 0.0006	735.6 ± 7.5	11402 ± 68	11180 ± 74	232 ± 3
118	52 ± 1	360 ± 7	191 ± 3	0.1255 ± 0.0006	290.9 ± 1.7	12111 ± 68	11629 ± 104	197 ± 3
149	51 ± 1	368 ± 8	200 ± 2	0.1361 ± 0.0009	296.8 ± 2.8	13079 ± 91	12576 ± 123	208 ± 2
158	51 ± 1	130 ± 3	213 ± 2	0.1401 ± 0.0008	874.6 ± 11.6	13331 ± 85	13113 ± 90	221 ± 2
179	50 ± 1	276 ± 6	236 ± 2	0.1482 ± 0.0007	423.4 ± 2.9	13882 ± 70	13492 ± 93	245 ± 2
203	41 ± 1	88 ± 2	240 ± 2	0.1529 ± 0.0007	1124.2 ± 16.9	14300 ± 74	14106 ± 78	250 ± 2
235	47 ± 1	166 ± 4	230 ± 2	0.1623 ± 0.0008	730.4 ± 7.2	15373 ± 87	15100 ± 95	240 ± 2
314	22 ± 1	109 ± 3	415 ± 2	0.2211 ± 0.0011	699.6 ± 11.3	18370 ± 103	18051 ± 114	437 ± 2
344	22 ± 1	609 ± 12	447 ± 2	0.2649 ± 0.0017	154.2 ± 1	21825 ± 153	20414 ± 299	474 ± 2
376	30 ± 1	130 ± 3	355 ± 3	0.2601 ± 0.0013	945.3 ± 10.1	23029 ± 138	22733 ± 144	378 ± 3
382	22 ± 1	140 ± 3	386 ± 2	0.2903 ± 0.0017	727.3 ± 8.6	25342 ± 175	24950 ± 185	415 ± 2
413	18 ± 1	171 ± 4	378 ± 6	0.3171 ± 0.0021	528.3 ± 4.8	28166 ± 249	27610 ± 265	409 ± 6
447	27 ± 1	952 ± 19	398 ± 2	0.3521 ± 0.002	157.6 ± 1	31187 ± 212	29320 ± 405	433 ± 2
483	39 ± 1	327 ± 7	330 ± 2	0.3341 ± 0.0016	628 ± 3.9	31160 ± 178	30642 ± 198	360 ± 2
507	29 ± 1	3827 ± 77	313 ± 4	0.4449 ± 0.0065	53.4 ± 0.8	44348 ± 806	36973 ± 1654	348 ± 5
533	36 ± 1	2619 ± 53	318 ± 2	0.4241 ± 0.0026	92.6 ± 0.6	41621 ± 309	37618 ± 824	354 ± 2
556	34 ± 1	7114 ± 144	313 ± 2	0.5263 ± 0.0074	39.5 ± 0.6	54588 ± 977	42665 ± 2592	354 ± 3
577	24 ± 1	2209 ± 44	298 ± 2	0.4789 ± 0.0034	81.6 ± 0.6	49253 ± 446	44048 ± 1098	338 ± 3
582	26 ± 1	3505 ± 70	297 ± 3	0.5013 ± 0.0039	60.1 ± 0.5	52171 ± 533	44738 ± 1549	338 ± 3
603	34 ± 1	1364 ± 28	270 ± 5	0.4674 ± 0.0044	183.3 ± 1.7	49166 ± 620	46843 ± 755	308 ± 5
624	28 ± 1	2793 ± 56	263 ± 2	0.4901 ± 0.0029	79.4 ± 0.5	52548 ± 406	46916 ± 1163	300 ± 2
662	30 ± 1	2723 ± 55	254 ± 2	0.5019 ± 0.0031	87.6 ± 0.6	54687 ± 448	49427 ± 1109	292 ± 2
666	36 ± 1	2122 ± 43	238 ± 2	0.4819 ± 0.0025	129 ± 0.7	52811 ± 365	49339 ± 753	274 ± 2
690	40 ± 1	1006 ± 20	286 ± 2	0.5011 ± 0.0019	316.1 ± 1.3	52770 ± 280	51328 ± 384	330 ± 2
709	49 ± 1	1377 ± 28	274 ± 2	0.5106 ± 0.0033	289.2 ± 1.9	54704 ± 459	53094 ± 546	318 ± 3
730	44 ± 1	921 ± 19	240 ± 5	0.5071 ± 0.0037	388.5 ± 3	56215 ± 603	54974 ± 641	281 ± 6
754	34 ± 1	8140 ± 163	270 ± 1	0.6207 ± 0.0046	40.8 ± 0.3	71084 ± 733	56987 ± 2962	318 ± 3
774	31 ± 1	4339 ± 88	361 ± 3	0.6268 ± 0.0053	70.5 ± 0.6	65165 ± 750	57731 ± 1638	426 ± 4

All reported errors are 2σ. Errors for ^{238}U and ^{232}Th concentrations are estimated to be ±1% due to uncertainties in spike concentration; analytical uncertainties are smaller. Corrected ages are corrected for initial ^{230}Th assuming an initial $^{230}Th/^{232}Th$ of 10.5 ± 2 ppm. Decay constants for ^{230}Th and ^{234}U are from Cheng et al. (2013) decay constant for ^{238}U is 1.55125 x 10^{-10} yr^{-1} (Jaffey *et al.*, 1971).

Chapter 4: Northeast Mexico precipitation primarily controlled by Atlantic SSTs

Adapted from:
Kevin T. Wright, Kathleen R. Johnson, Tripti Bhattacharya, Gabriela Serrato Marks, David McGee, Dillon Elsbury, Yannick Peings, Jean-Louis Lacaille-Muzquiz, Gianna Lum, Laura Beramendi-Orosco, Northeast Mexico precipitation primarily controlled by Atlantic SSTs. (in prep) Science.

4.1 Abstract

Reconstructing hydroclimate over the Common Era is essential for understanding the dominant mechanisms of precipitation change and improving climate model projections, which currently suggest Northeast Mexico will become drier in the future. Tree-ring reconstructions have suggested Pacific sea surface temperatures (SST) strongly influence Northern Mexico precipitation variability. However, tree ring records tend to reflect winter-spring rainfall, and thus may not accurately record total annual precipitation. We demonstrate using the first multiproxy speleothem record spanning the last millennium that mean annual rainfall in Northeast Mexico is more heavily influenced by Atlantic SST variability, further confirmed by forced SST atmospheric global circulation model simulations. We suggest precipitation in Northern Mexico may increase in response to future warming, in contrast to current model predictions.

4.2 Introduction

Recent droughts in Mexico have led to significant economic crises, national food shortages and mass migrations, greatly impacting over 127 million people. Unfortunately, climate models suggest anthropogenic carbon emissions are likely to increase the frequency and intensity of droughts in the future. However, climate models have been shown to inaccurately capture present and past rainfall throughout most of Mexico and Central America, exhibiting particularly

poor skill in modeling natural internal climate variability (Hidalgo *et al.*, 2013). Additionally, a growing body of paleoclimate records from the Northern Tropics imply future droughts may not be as dire as model predictions, as the region may receive increased precipitation in response to a warmer climate (He & Soden, 2017; Sachs *et al.*, 2009), though it is unclear if increased precipitation will extend to Northern Mexico. Paleoclimate constraints on the response of regional precipitation to internal climate variability and external forcing is of utmost importance for evaluating climate models and mitigating the impacts of future rainfall change, yet few records exist in Northern Mexico.

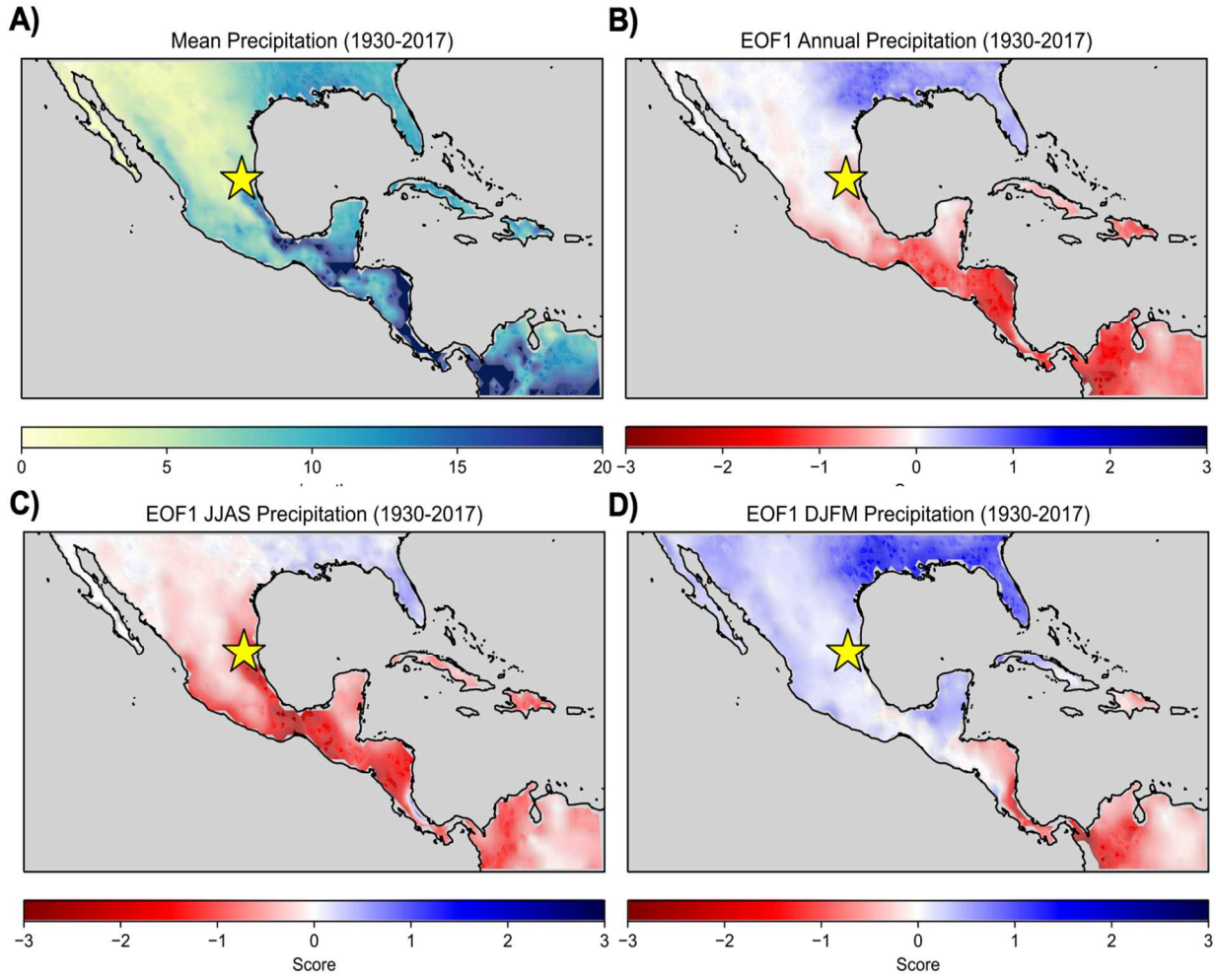

Fig. 4.1: Precipitation patterns in Mexico. A) Mean precipitation over Mexico, Central America, and the Circum-Caribbean region. **B)** EOF1 of mean annual precipitation. **C)** EOF1 of mean summer (JJAS) precipitation. **D)** EOF1 of mean winter (DJFM) precipitation.

Tree ring records suggest interannual to multidecadal hydroclimate variability in Mexico is dominated by changes in Eastern Equatorial Pacific (EEP) SSTs, dominantly associated with the El Niño Southern Oscillation (ENSO) and to a lesser magnitude, the lower frequency Pacific Decadal Oscillation (PDO). Warm EEP SSTs are thought to drive a dipole precipitation pattern, with wet conditions in Northern Mexico and dry conditions in Southern Mexico. While drying in Southern Mexico in response to a warmer EEP SSTs have been confirmed with paleoclimate records and modeling studies (Bhattacharya & Coats, 2020), increased precipitation in Northeast Mexico remains poorly constrained, with weaker than expected or inconsistent correlations in both instrumental and tree ring data (Gutiérrez-García *et al.*, 2020; Stahle *et al.*, 2016; Villanueva-Diaz *et al.*, 2007). Surprisingly, the role of SSTs in the Tropical North Atlantic, the dominant source of moisture for Mexico, remains enigmatic and could obscure the effect of Pacific SSTs. For instance, a positive phase of the Atlantic Multidecadal Variability (AMV) has been invoked to explain broad drying in Northeast Mexico (Stahle *et al.*, 2016) but instrumental data (Curtis, 2008) and tree ring records from nearby Texas (Gray *et al.*, 2004), as well as records of runoff and precipitation on millennial to orbital scales from Northeast Mexico (Roy *et al.*, 2016, 2020) suggest warmer Atlantic SSTs may drive the opposite response, with regional increases in precipitation. Speleothem records from Northern Mexico covering the more recent past (Common Era) can provide an additional, robust record of past hydroclimate variability to help clarify the role of Atlantic versus Pacific SSTs on regional precipitation, but none exist in the region.

To address this gap, we have developed the first continuous inter-annually resolved stalagmite record (CB4) of hydroclimate covering the last millennium utilizing four geochemical proxies: stable oxygen isotopes ($\delta^{18}O$), carbon isotopes ($\delta^{13}C$), trace elements (Mg/Ca), and dead

carbon proportion (DCP, ^{14}C). The sample was retrieved from Cueva Bonita (23°N, 99°W; 1071 m above sea level) located in the northern-most tropical rainforest on the windward side of the Sierra Madre Oriental in the Northeast state of Tamaulipas (Fig. 4.1, fig. S4.1, supplementary materials). The stalagmite age model is constrained by 19 U-Th dates and fluorescent layer counting (Appendix B, fig. S4.2), and extends from 833 CE to 2017 CE, when the sample was collected (supplementary materials). Previous research has often interpreted $\delta^{18}O$ as a proxy for weighted mean annual precipitation amount (Baker *et al.*, 2020), which we also demonstrate is the predominant influence of $\delta^{18}O$ at Cueva Bonita (Appendix B, fig. S4.3). However, a growing number of studies have shown that $\delta^{13}C$, Mg/Ca, and dead carbon proportion (DCP) are also potentially reliable proxies for local water balance (Griffiths *et al.*, 2020b), improving our interpretation of hydroclimate when combined with speleothem $\delta^{18}O$ (see Appendix B).

4.3 Methods

4.3.1 Chronology

The CB4 stalagmite was cut, polished and sampled for 21 U-Th dates along its vertical growth axis using a Dremel hand drill with a diamond dental bur. The CB4 sample has uranium concentrations ranging from 37 to 160 ng/g (Table S4.1). Calcite powder samples weighing 250-300 mg were prepared at Massachusetts Institute of Technology following methods similar to Edwards et al., (1987) (Lawrence Edwards *et al.*, 1987). Powders were dissolved in nitric acid and spiked with a ^{229}Th – ^{233}U – ^{236}U tracer, followed by separation of U and Th by iron co-precipitation and elution in columns with AG1-X8 resin. The U and Th fractions were analyzed using a Nu Plasma II-ES multi-collector inductively coupled plasma mass spectrometer (MC-ICP-MS) equipped with an Aridus 2 desolvating nebulizer, following methods described in Burns et al. (2016) (Burns *et al.*, 2016). The corrected ages were calculated using an initial

$^{230}Th/^{232}Th$ value of 9.8 ± 4.9 ppm to correct for detrital ^{230}Th. The 9.8 ppm initial Th correction value was determined by testing dates corrected with different initial ^{230}Th corrections for stratigraphic order following methods laid out by Hellstrom et al. (2006) and matching the ages with the radiocarbon bomb peak depth. The uncertainty of 4.9 ppm was scaled proportionally to the normal ± 50% correction (4.4 ± 2.2 ppm). U-Th ages were combined with fluorescent layer counting to decrease uncertainty. The 95% confidence interval for the age-depth model was constructed using 2000 Monte-Carlo simulations through the age-depth modeling software COPRA (Breitenbach *et al.*, 2012).

4.3.2 Stable Isotope and Trace Element Analysis

CB4 was micro-sampled for both stable isotope and trace element analyses using a Sherline micromill at 250 μm increments to a depth of 1 mm, producing 400 samples. The powder for CB4 was collected, weighed out to 40 - 80 μg and analyzed on a Kiel IV Carbonate Preparation Device coupled to a Thermo Scientific Delta V-IRMS at the UC Irvine Center for Isotope Tracers in Earth Sciences (CITIES) following methods described by McCabe-Glynn et al. (2013) to determine $\delta^{18}O$ and $\delta^{13}C$ (McCabe-Glynn *et al.*, 2013). Every 32 samples of unknown composition were analyzed with 14 standards which included a mix of NBS-18, IAEA-CO-1, and an in-house standard. The analytical precision for $\delta^{18}O$ and $\delta^{13}C$ is 0.08‰ and 0.05‰, respectively.

For trace element analysis, 20 - 60 μg calcite powder samples were dissolved in 500 μL of a double distilled 2% nitric acid solution. The samples were analyzed using a Nu Instruments Attom High Resolution Inductively Coupled Plasma Mass Spectrometer (HR-ICP-MS) at the CITIES laboratory. Mg/Ca ratios were calculated from the intensity ratios using a bracketing technique with five standards of known concentration and an internal standard (Ge) added to all

samples to correct for instrumental drift. Trace element analysis of CB4 serves to complement the interpretation of speleothem $\delta^{18}O$ and $\delta^{13}C$; therefore, a lower-resolution (multi-decadal to centennial) analysis was conducted over the complete record by analyzing every other sample (200 total). For plotting/aesthetic purposes, CB2 Mg/Ca, $\delta^{18}O$ and $\delta^{13}C$ were smoothed using a moving average. The pandas function DataFrame.rolling().mean()was utilized to smooth the data for plotting only, with the size of the moving window set to 4. The full data set reported in the supplementary materials is unsmoothed.

4.3.3 Forced SST Model Simulations

We utilize an atmospheric global circulation model (WACCM) with a prescribed warming and/or cooling in the Atlantic or Pacific basins (Elsbury *et al.*, 2019). We use a 200-yr mean control run subtracted from a 200-year prescribed SST experiment to demonstrate the net change in precipitation in response to SST-forcing. Dissimilar to future climate projections which exhibit a large range of inter-model discrepancy and precipitation variability, these models are tuned for modern-day conditions and have been shown to match observational records reasonably well (Elsbury *et al.*, 2019).

4.4 Results

4.4.1 Study Site

Sample CB4 was retrieved from a terminal room at the rear of Cueva Bonita (23°N, 99°W; 1071 m above sea level). The cave is located in the northern-most tropical rainforest in the highlands of the Sierra Madre Oriental in the state of Tamaulipas, Mexico (Fig. 4.1). Regional climate is characterized by warm-wet summers and cool-dry winters, with precipitation maximums in June, July and September. The wet season is initiated in June with an intensification of the Caribbean Low-Level Jet in response to a northward shift of the ITCZ and

an amplification of the North Atlantic Subtropical High (Wang & Lee, 2007b). Precipitation during August is generally reduced in comparison to other summer wet months due to a period of intense heat and aridity frequently described as *La Canícula,* a known phenomenon in much of Mesoamerica. Although the winter is predominantly dry in comparison to summer months, roughly 10% of annual precipitation can be attributed to short winter cold front storms (Gutiérrez-García *et al.*, 2020). These winter storms are known as *Nortes* and occur roughly 20 times a year during the months of November through March (Kurczyn *et al.*, 2021; Schultz *et al.*, 1998).

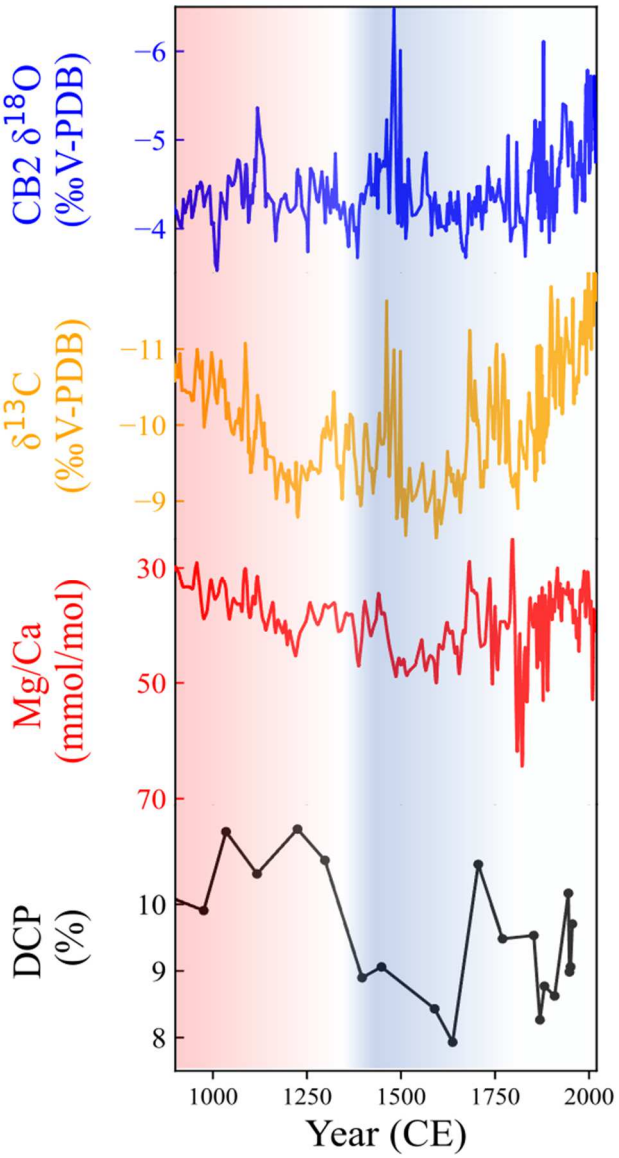

Fig. 4.2: Results of CB4 geochemical proxies. Speleothem δ18O, δ13C, Mg/Ca ratios and DCP over the last millennium. Speleothem δ18O and δ13C have an average resolution of 3 years, Mg/Ca ratios have an average resolution of 6 years, and DCP has an 83 year average. Results of CB4 proxies show a similar response on multi-decadal to centennial timescales. Compared to δ18O, proxies show a moderate to strong correlation on multidecadal timescales (δ13C $r = 0.56$, $p < 0.05$; Mg/Ca $r = 0.29$, $p < 0.05$). Shading in red presents the Medieval Warm Period, shading in blue represents the Little Ice Age.

Empirical orthogonal functions (EOF) investigation of re-analysis precipitation data from 1930-2017 (Willmott & Matsura, 2001) suggests precipitation in NE Mexico is out-of-phase with much of southern Mesoamerica during winter (Fig 4.1b), but in-

phase for summer and annual precipitation (Fig, 4.1c-d). Summer and annual precipitation likely exhibit the same spatial pattern because summer accounts for ~70% of total annual rainfall. However, it is unclear if these spatial patterns are accurate representations of rainfall, as EOF1 explains a relatively low percentage of the total variance (16%, 20% and 16% for annual, summer, winter, respectively, Appendix B, fig. S4.1). Additionally, interpretations are limited due to few precipitation stations before 1950 and a financial crisis in the 1980s, which also disrupted data collection. Therefore, the addition of paleoclimate records can assist in a more robust interpretation, but, EOFs at least suggest the spatial response of precipitation in winter and summer may be different.

4.4.2 Chronology

CB4 is a 17 cm-long, candle-shaped stalagmite that is translucent grey and beige in color (Appendix B, fig. S4.2). The sample was confirmed to be 100% calcite by X-ray diffraction analysis performed at roughly 5 cm intervals (n = 3). The growth history for CB4 is constrained by 21 U-Th dates analyzed by MC-ICP-MS (Appendix B, fig. S4.2, and SI Table 1) and thin section fluorescent layer-counting via microscope and UV light excitation. The sample was actively growing when collected (2017) confirmed by radiometric measurements and new calcite growth observed on the speleothem scar in subsequent years. U-Th ages range from 78 ± 96 to 2119 ± 162 years before present, however, this study focused on the top 100 mm of the sample with an oldest date of 1189 ± 154 (where present is 1950 CE) because of a growth hiatus. Two ages were identified to be outliers based on low probability of fit for age models (Appendix B, Fig. S4.2). The average uncertainty is 14 years, but the top of the sample has less uncertainty (average top 25 mm uncertainty = 1 year) compared to the bottom of the sample (average bottom 25 mm uncertainty = 37 years). Larger errors near the bottom of the sample are the product of

larger uncertainties in the U-Th ages and compounding errors of layer counting. The CB4 growth rate was relatively constant, averaging 90 μm/year. The temporal resolution varies with growth rate, but the average resolution is 2.8 years over the last millennium.

4.4.3 Geochemical Proxies

We utilize four hydroclimate proxies in this study: $\delta^{18}O$, $\delta^{13}C$, Mg/Ca, and Dead Carbon Proportion (DCP, ^{14}C). Similar to previous work from Cueva Bonita, we interpret $\delta^{18}O$ to be reflective of precipitation amount while we believe $\delta^{13}C$ and Mg/Ca are reflective of prior calcite precipitation, which increases with decreased local water balance (i.e. ET). We interpret DCP, previously unstudied at this cave, to reflect the amount of closed- versus open-system bedrock dissolution. Open- versus closed-system dissolution varies with hydrology and regulates the amount of dissolved inorganic carbon (DIC) sourced from the soil and epikarst (open) versus DIC sourced from bedrock (closed). Generally, closed-system dissolution occurs when conditions are wet (Griffiths *et al.*, 2012, 2020a).

Speleothem $\delta^{18}O$ values experience several significant shifts to more positive values, with the highest recorded value over the last millennium of -3.53‰ occurring at 1011 CE. These excursions represent droughts transpiring on interannual to decadal timescales. Speleothem $\delta^{18}O$ progressively moves towards more negative values during the late 15th century, eventually reaching the lowest levels recorded in CB4 of -6.53‰ (VDPB) at 1483 CE. This transition represents a multi-decadal to centennial long period of pluvial conditions. Speleothem $\delta^{18}O$ then rapidly shifts to more positive values indicating drier conditions at 1600 CE. Overall, there is a decreasing trend of $\delta^{18}O$ values from the onset of the industrial period (1800) to present, suggesting progressively wetter conditions over the last two centuries. However, the last 200

years are also punctuated with severe droughts, as noted by a high $\delta^{18}O$ value of 3.94‰ at 1894 CE.

These precipitation patterns are generally reflected in records of local water balance as recorded by Mg/Ca, $\delta^{13}C$ and DCP, albeit with some minor differences. A noticeable divergence is the increasing trend near the end of the Medieval Warm Period, where the increasing trend is not observed in speleothem $\delta^{18}O$. We interpret this to reflect multi-century long decreased local water balance from elevated temperatures and enhanced evapotranspiration (ET). Enhanced temperatures and ET are known to have occurred over much of North America during this time period (Mann et al., 2009). Interestingly, the highest trace element ratio (123 mmol/mol) recorded in CB4 does not occur during the Medieval Warm Period or the Little Ice Age. Trace element ratios suggest one of the most severe droughts may have occurred in the more recent past at 1882 CE. DCP responds differently in comparison to other proxies during the MWP. However, the temporal resolution (83 years) likely inhibits the ability to fully capture the interannual to decadal variability encapsulated in the other proxies. DCP does, however, nicely capture the drought at 1600 CE.

4.5 Discussion

The multi-proxy CB4 record details substantial decadal to centennial scale hydroclimate variability over the last millennium. The most striking centennial-scale feature of this record is the extremely low speleothem $\delta^{18}O$ values of -6.5‰ at ~1490 CE (Fig. 4.2), which is also supported by very low $\delta^{13}C$ values (-11‰) and Mg/Ca ratios (38 mmol/mol) near the same time. Increased precipitation during the 15th century has been suggested as a dominant driver of population expansion at major archaeological sites, including Tenochtitlan in the Basin of Mexico, and has thus been referred to as the Aztec Pluvial (Sanders *et al.*, 1979). Stahle et al.

(2016) provided evidence that the Aztec Pluvial could be a major wet period over the Common Era, but lacked older tree ring records to confirm the magnitude and spatial extent of increased precipitation. Our record confirms through multiple geochemical proxies that the Aztec Pluvial represented the wettest conditions in Northeast Mexico over the last millennium. Speleothem $\delta^{18}O$ from Juxtlahuaca cave also show increased precipitation during this interval (Lachniet *et al.*, 2017), suggesting the Aztec Pluvial impacted at least Northeast, Central and Southwest Mexico, if not the entire country. While a strengthening of the North American Monsoon has been invoked to explain increased precipitation in Southwest and Central Mexico, NE Mexico is outside the monsoon's dominant core region and is therefore unlikely to receive monsoonal precipitation. A comparison of Cueva Bonita $\delta^{18}O$ to Eastern and Tropical North Atlantic SSTs instead suggests the 15th century pluvial period was likely forced by anomalously warm Atlantic SSTs (Appendix B, fig. S4.4-4.5). Warmer SSTs are known to increase precipitation through increased boundary layer moisture and are favorable to larger magnitude and more frequent hurricanes in Central America and Southern Mexico (Wang & Lee, 2007b). Our results suggest this wetting effect may extend farther north than previously thought.

Notably, the CB4 record also indicates a pattern of decreasing $\delta^{18}O$ values (from -3.5‰ to -6.7‰) beginning near the start of the pre-industrial period, around 1830. This trend is also supported by a shift towards more negative $\delta^{13}C$ values (-8.9‰ to -13‰) and decreased Mg/Ca ratios (54 to 28 mmol/mol), suggesting an increase in both regional and localized precipitation with anthropogenic warming. The decreasing trend of $\delta^{18}O$ and $\delta^{13}C$ appears to be in response to Atlantic warming, as Pacific warming is delayed until the early- to mid-20th century (Appendix B, fig. S4.5). Interestingly, this trend towards wetter conditions is not obvious in Mexican tree rings (Stahle *et al.*, 2016), but is evident in historical precipitation records, satellite data and re-

analysis data from Central Mexico (Martinez-Lopez *et al.*, 2018), suggesting precipitation increases may occur only in summer. Although our record does not possess sub-annual

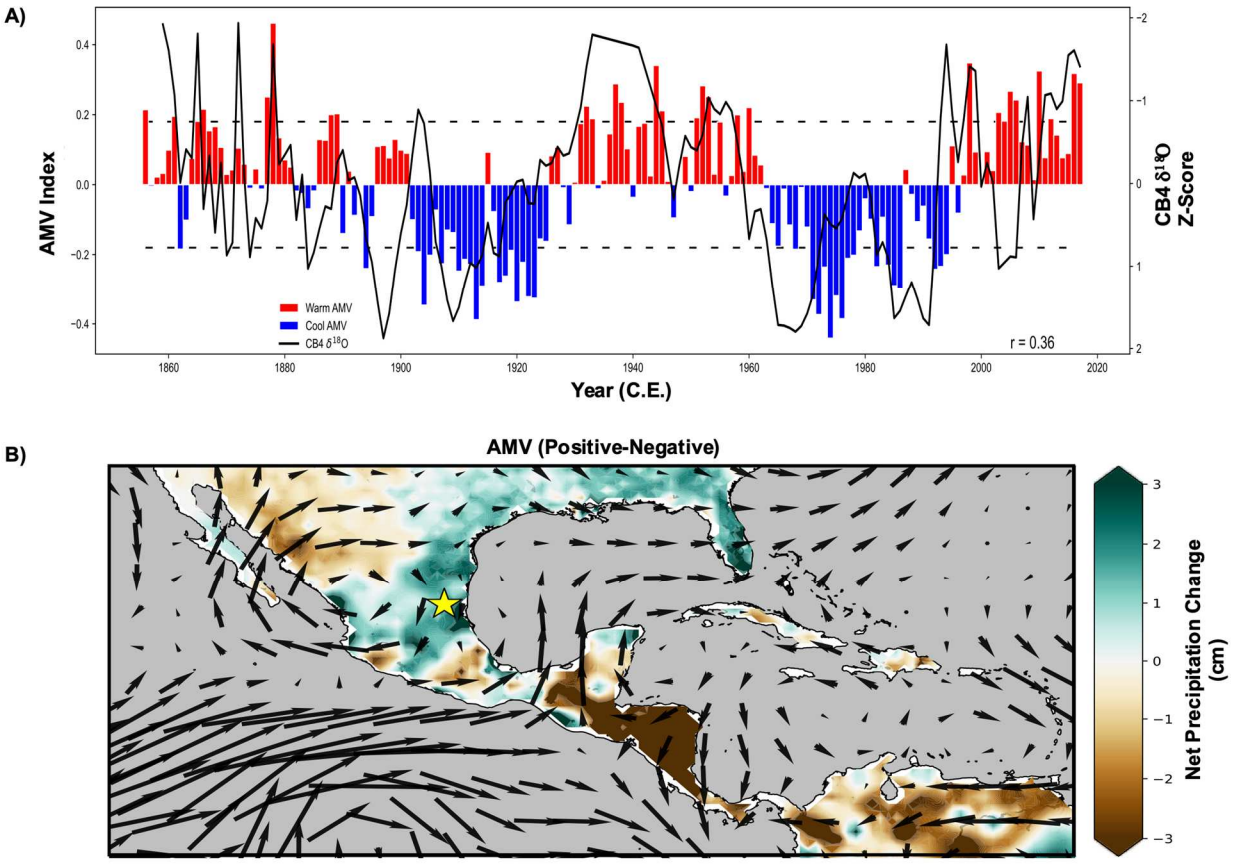

Fig. 4.3: Comparison of AMV to CB4, precipitation and low-level winds. A) Both records are detrended to account for the impact of anthropogenic warming on Atlantic SSTs. The $\delta^{18}O$ appears to correspond strongly to the AMV Index over the last ~150 years, capturing both extended periods of positive phases (1920-1960, 2000-2020+) and extended negative phases (1900-1920, 1960-2000). Surprisingly, CB4 even captures some the short-term variability (1860-1900). **B)** Comparison of AMV phases (positive minus negative) on mean low-level winds and precipitation. A positive phase leads to increased precipitation in NE Mexico but drying in NW and Southern Mexico.

resolution to verify, we suggest the wetting trend may be driven by more extreme pluvial climate events in the later summer months, such as tropical storms and hurricanes, that are becoming both more frequent (Bhatia *et al.*, 2019) and decaying more slowly on land (Li & Chakraborty, 2020).

The strong positive correlation of NE Mexico rainfall to Atlantic SSTs is surprising, considering tree ring records have provided robust evidence of spatially widespread drying in response to positive phases of the AMO (Stahle *et al.*, 2016). However, our record demonstrates a strong positive correlation to Atlantic SSTs not only on centennial timescales but on multidecadal timescales as well. This is evident in a direct comparison of proxies over the last ~800 years (Appendix B, fig. S4.4-4.5), wavelet power spectrum analysis demonstrating a periodicity of 66 years for $\delta^{18}O$ and 55 years for $\delta^{13}C$ (Appendix B, fig. S4.6), which is close to the previously suggested periodicity of 65 years for the AMV (Schlesinger & Ramankutty, 1994), and a direct comparison of the AMV index to CB4 $\delta^{18}O$ over the last century (Appendix B, Fig. 3a). Previous reconstructions of runoff in NE Mexico speculated the AMV likely altered regional hydroclimate in the early Holocene and Late-Pleistocene (Roy *et al.*, 2016), but did not retain the temporal resolution required to verify. Our record provides the first multiproxy evidence of the role of AMV on NE Mexico precipitation over the last millennium.

Interestingly, CB4 proxies not only contrast tree ring interpretations of the role of Atlantic SSTs, but speleothem $\delta^{18}O$, $\delta^{13}C$, and Mg/Ca ratios also record wetter conditions during periods of cool Eastern Pacific SSTs, a response also reflected in additional speleothem records from Southern Mexico and Central America (Lachniet *et al.*, 2017, 2004). The similarity in speleothem records suggests the dipole precipitation pattern over the last millennium is more complicated than previously thought. Modern instrumental data also suggests precipitation is mostly in-phase during seasonal (summer) and annual timescales, only showing a strong dipole precipitation pattern for winter rainfall (Fig. 4.1). While changes in winter-spring soil moisture, as typically recorded by tree ring chronologies, are closely linked to changes in early summer soil moisture, they can be poorly correlated with late summer and autumn rainfall (St. George *et*

al., 2010; Stahle *et al.*, 2016). We therefore suggest the discrepancies between the speleothem data presented here and previous tree ring-based interpretations are potentially driven by the seasonal bias of tree rings to record winter-spring and early summer precipitation. While analysis of instrumental data supports this notion, with a positive phase of the AMV leading to increased precipitation in NE Mexico (Fig. 4.3B), historical rainfall is complicated as it is also impacted by Pacific variability.

Therefore, to test the seasonality and spatial pattern of rainfall in response to SST variability, we utilized a state-of-the-art global atmospheric circulation climate model with prescribed SST warming and/or cooling. Control runs have been shown to reliably capture global patterns of observational precipitation and low-level winds (Elsbury *et al.*, 2019), and a comparison to observational data suggests this is also the case for Mexico and Central America (Appendix B, fig. S4.7-4.8). While our analysis includes a full range of forced-SST conditions, the natural environment on interannual to decadal timescales is most likely to exhibit an Atlantic-Pacific out-of-phase warming or cooling via changes in the strength of the Walker Circulation (Fosu *et al.*, 2020), and are therefore the focus of this discussion.

During summer, in response to a warm Pacific and cold Atlantic, precipitation decreases across almost all of Mexico and Central America (Fig. 4.4). Anomalous convection in the Pacific in response to warmer conditions has previously been attributed to drying via an enhanced Walker Circulation, which is also simulated in this study (Appendix B, fig. S4.9-4.10). This results in a southward migration of the Atlantic ITCZ and stronger easterly trade winds (Bhattacharya *et al.*, 2017; Bhattacharya & Coats, 2020; Chiang & Sobel, 2002; Giannini *et al.*, 2001, 2000). While the contraction of the ITCZ is known to decrease precipitation in Southern Mexico and Central America (Asmerom *et al.*, 2020), stronger easterly trade winds are thought

to increase precipitation in Northern Mexico via an intensification of easterlies and the Caribbean Low-Level Jet (CLLJ) (Wang & Lee, 2007a). Although low-level wind anomalies in model simulations correctly replicate the intensification of the CLLJ (Fig. 4.4), models demonstrate this instead leads to decreased precipitation over much of Mexico. This response is also replicated when SST conditions are reversed, which drives a weakening of the CLLJ and increased precipitation. While on longer, orbital to interannual timescales, a stronger CLLJ has been attributed to drier conditions in NE Mexico by cooling Atlantic SSTs via an enhanced wind-evaporation-SST feedback loop (Wright et al., in review), this experiment utilizes prescribed SSTs and we therefore cannot attribute observed precipitation changes to this mechanism. We instead suggest that warmer Atlantic SSTs lead to a reduction in the strength of the CLLJ and, consequently, vertical wind shear. This reduction can be amplified by cooler Pacific SSTs (Fig. 4.4), but still occurs when the Pacific is also warm (S11). The reduced vertical wind shear fosters the formation of deep convective rainfall. While ACGM cannot simulate extreme pluvial events, we suggest the reduction in vertical wind shear will likely increase the frequency and magnitude of tropical storms and hurricanes, as has been shown in previous work (Wang & Lee, 2007a)

Another notable result of the fixed SST simulations is the contrasting response of precipitation throughout most of Mexico during summer and winter (Fig. 4.4, Appendix B fig. S4.11). The only region that appears to respond consistently in both seasons is Northwest Mexico, which is strongly influenced by the North American Monsoon and is likely to be more sensitive to variability in Pacific SSTs. In response to a warm Pacific/cold Atlantic, winter precipitation throughout much of Mexico slightly increases. Increased winter precipitation in Northwest and Central Mexico has been attributed to a strengthening of North Pacific storm-

track extending further south and west in response to anomalous Rossby waves (Seager & Hoerling, 2014). While this is not likely to drive increased precipitation in NE Mexico (Wright et al., in review), anomalous northerly low-level winds could drive more frequent and intensified cold fronts from the North, increasing light, low-intensity rainfall to the region (Fig 4.4). This appears to be an important control of winter precipitation, as a reversal of the wind patterns under opposing SST conditions drives a reduction in regional precipitation. Winter simulations

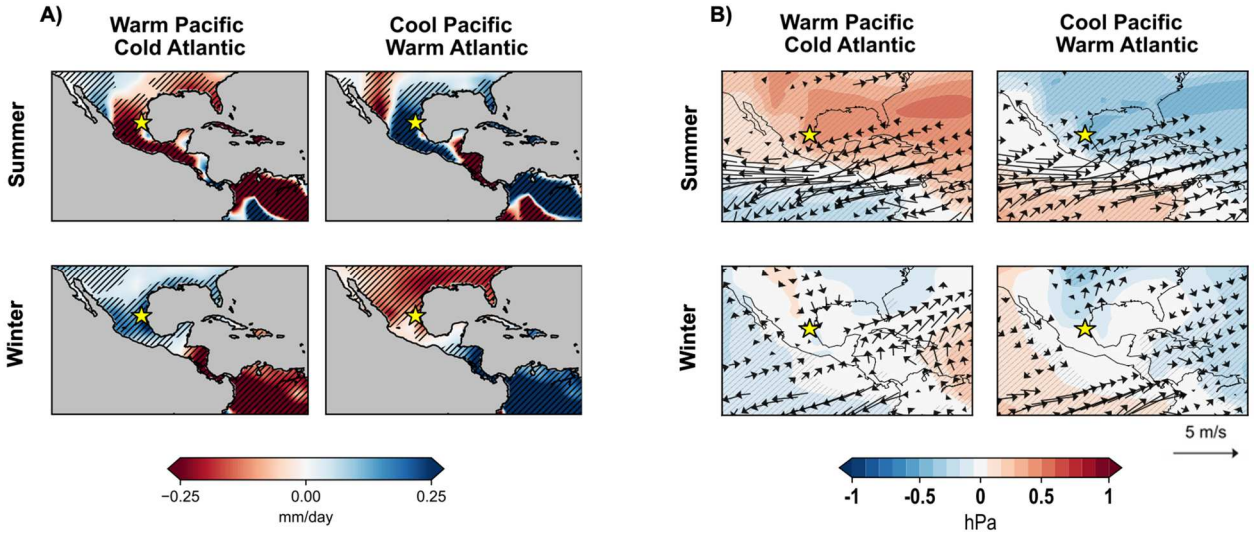

Fig. 4.4: Precipitation, sea level pressure, and low-level winds in response to forced SSTs. A) Results of net precipitation change in response to forced SST simulations. Statistically significant changes (90% CI) are shaded by the hatching. B) Results of anomalous low-level wind patterns and sea level pressure (SLP) in response to forced SST simulations. Changes in SLPs are indicated by color, statistically significant changes are indicated by hatching. Only statistically significant low-level winds are plotted. Cueva Bonita indicated by the star.

of rainfall support tree ring interpretations of 1) an out-of-phase dipole spatial pattern and 2) a dominant role of Pacific SSTs in controlling regional precipitation. However, winter precipitation only accounts for a small fraction of total annual rainfall, with winter contributing less than 7% of annual rainfall in NE Mexico. We therefore suggest Atlantic SSTs are much more important in controlling precipitation in the region.

4.6 Conclusion

The new CB4 speleothem record from NE Mexico highlights the precipitation dipole pattern is far more spatially complex in Mexico than previously thought (Appendix B, fig. S4.12-13). We suggest previous reconstructions of the dipole pattern may have utilized tree rings that potentially bias winter-spring rainfall (Stahle *et al.*, 2020, 2016), minimizing the role of the Atlantic in modulating summer precipitation throughout most of the region. While variability in Pacific SSTs can still play a secondary role in regulating precipitation, mainly by controlling the amount of winter precipitation and summer vertical wind shear in the Tropical North Atlantic, we suggest this has the opposite effect on NE Mexico rainfall than previously thought. We suggest warmer Pacific SSTs predominantly drive decreased precipitation over the region.

This work also demonstrates the fate of precipitation in Northeast Mexico lies in the future of the Tropical North Atlantic SSTs. If anthropogenic carbon emissions continue to warm the Tropical Atlantic, the observed trend of increased precipitation in NE Mexico over the industrial period is likely to continue.

4.7 References

Asmerom, Y., Baldini, J. U. L., Prufer, K. M., Polyak, V. J., Ridley, H. E., Aquino, V. V, … Kennett, D. J. (2020). Intertropical convergence zone variability in the Neotropics during the Common Era. *Science Advances*, *6*(7), 3644–3658. doi: 10.1126/sciadv.aax3644

Baker, A., Berthelin, R., Cuthbert, M. O., Treble, P. C., Hartmann, A., & KSS Cave Studies Team, T. (2020). Rainfall recharge thresholds in a subtropical climate determined using a regional cave drip water monitoring network. *Journal of Hydrology*, *587*, 125001. doi: 10.1016/j.jhydrol.2020.125001

Bhatia, K. T., Vecchi, G. A., Knutson, T. R., Murakami, H., Kossin, J., Dixon, K. W., & Whitlock, C. E. (2019). Recent increases in tropical cyclone intensification rates. *Nature Communications*, *10*(1), 1–9. doi: 10.1038/s41467-019-08471-z

Bhattacharya, T., Chiang, J. C. H., & Cheng, W. (2017). Ocean-atmosphere dynamics linked to 800–1050 CE drying in mesoamerica. *Quaternary Science Reviews*, *169*, 263–277. doi: 10.1016/j.quascirev.2017.06.005

Bhattacharya, T., & Coats, S. (2020). Atlantic-Pacific Gradients Drive Last Millennium Hydroclimate Variability in Mesoamerica. *Geophysical Research Letters*, *47*(13), e2020GL088061. doi: 10.1029/2020GL088061

Breitenbach, S. F. M., Rehfeld, K., Goswami, B., Baldini, J. U. L., Ridley, H. E., Kennett, D. J., … Marwan, N. (2012). Constructing proxy records from age models (COPRA). *Climate of the Past*, *8*(5), 1765–1779. doi: 10.5194/cp-8-1765-2012

Burns, S. J., Godfrey, L. R., Faina, P., Mcgee, D., Hardt, B., Ranivoharimanana, L., & Randrianasy, J. (2016). *Rapid human-induced landscape transformation in Madagascar at the end of the first millennium of the Common Era*. doi: 10.1016/j.quascirev.2016.01.007

Chiang, J. C. H., & Sobel, A. H. (2002). Tropical tropospheric temperature variations caused by ENSO and their influence on the remote tropical climate. *Journal of Climate*, *15*(18), 2616–2631. doi: 10.1175/1520-0442(2002)015<2616:TTTVCB>2.0.CO;2

Curtis, S. (2008). The Atlantic multidecadal oscillation and extreme daily precipitation over the US and Mexico during the hurricane season. *Climate Dynamics*, *30*(4), 343–351. doi: 10.1007/s00382-007-0295-0

Elsbury, D., Peings, Y., Saint-Martin, D., Douville, H., & Magnusdottir, G. (2019). The atmospheric response to positive IPV, positive AMV, and their combination in boreal winter. *Journal of Climate*, *32*(14), 4193–4213. doi: 10.1175/JCLI-D-18-0422.1

Fosu, B., He, J., & Liguori, G. (2020). Equatorial Pacific Warming Attenuated by SST Warming Patterns in the Tropical Atlantic and Indian Oceans. *Geophysical Research Letters*, *47*(18), e2020GL088231. doi: 10.1029/2020GL088231

Giannini, A., Chiang, J. C. H., Cane, M. A., Kushnir, Y., & Seager, R. (2001). The ENSO teleconnection to the Tropical Atlantic Ocean: Contributions of the remote and local SSTs to rainfall variability in the Tropical Americas. *Journal of Climate*, *14*(24), 4530–4544. doi: 10.1175/1520-0442(2001)014<4530:TETTTT>2.0.CO;2

Giannini, A., Kushnir, Y., & Cane, M. A. (2000). Interannual variability of Caribbean rainfall, ENSO, and the Atlantic Ocean. *Journal of Climate*, *13*(2), 297–311. doi: 10.1175/1520-0442(2000)013<0297:IVOCRE>2.0.CO;2

Gray, S. T., Graumlich, L. J., Betancourt, J. L., & Pederson, G. T. (2004). A tree-ring based reconstruction of the Atlantic Multidecadal Oscillation since 1567 A.D. *Geophysical Research Letters*, *31*(12), n/a-n/a. doi: 10.1029/2004GL019932

Griffiths, M. L., Fohlmeister, J., Drysdale, R. N., Hua, Q., Johnson, K. R., Hellstrom, J. C., … Zhao, J. x. (2012). Hydrological control of the dead carbon fraction in a Holocene tropical speleothem. *Quaternary Geochronology*, *14*, 81–93. doi: 10.1016/j.quageo.2012.04.001

Griffiths, M. L., Johnson, K. R., Pausata, F. S. R., White, J. C., Henderson, G. M., Wood, C. T., … Sekhon, N. (2020a). End of Green Sahara amplified mid- to late Holocene megadroughts in mainland Southeast Asia. *Nature Communications 2020 11:1*, *11*(1), 1–12. doi: 10.1038/s41467-020-17927-6

Griffiths, M. L., Johnson, K. R., Pausata, F. S. R., White, J. C., Henderson, G. M., Wood, C. T., … Sekhon, N. (2020b). End of Green Sahara amplified mid- to late Holocene megadroughts in mainland Southeast Asia. *Nature Communications*, *11*(1), 4204. doi: 10.1038/s41467-020-17927-6

Gutiérrez-García, G., Beramendi-Orosco, L. E., & Johnson, K. R. (2020). Climate-growth relationships of Pinus pseudostrobus from a tropical mountain cloud forest in northeast Mexico. *Dendrochronologia*, *64*, 125749. doi: 10.1016/j.dendro.2020.125749

He, J., & Soden, B. J. (2017). A re-examination of the projected subtropical precipitation decline. *Nature Climate Change*, *7*(1), 53–57. doi: 10.1038/nclimate3157

Hidalgo, H. G., Amador, J. A., Alfaro, E. J., & Quesada, B. (2013). Hydrological climate change projections for Central America. *Journal of Hydrology*, *495*, 94–112. doi: 10.1016/j.jhydrol.2013.05.004

Kurczyn, J. A., Appendini, C. M., Beier, E., Sosa-López, A., López-González, J., & Posada-Vanegas, G. (2021). Oceanic and atmospheric impact of central American cold surges (Nortes) in the Gulf of Mexico. *International Journal of Climatology*, *41*(S1), E1450–E1468. doi: 10.1002/joc.6779

Lachniet, M. S., Asmerom, Y., Polyak, V., & Bernal, J. P. (2017). Two millennia of Mesoamerican monsoon variability driven by Pacific and Atlantic synergistic forcing. *Quaternary Science Reviews*, *155*, 100–113. doi: 10.1016/j.quascirev.2016.11.012

Lachniet, M. S., Burns, S. J., Piperno, D. R., Asmerom, Y., Polyak, V. J., Moy, C. M., & Christenson, K. (2004). A 1500-year El Niño/Southern Oscillation and rainfall history for the Isthmus of Panama from speleothem calcite. *Journal of Geophysical Research D: Atmospheres*, *109*(20), 20117. doi: 10.1029/2004JD004694

Lawrence Edwards, R., Chen, J. H., & Wasserburg, G. J. (1987). 238U234U230Th232Th systematics and the precise measurement of time over the past 500,000 years. *Earth and Planetary Science Letters*, *81*(2–3), 175–192. doi: 10.1016/0012-821X(87)90154-3

Li, L., & Chakraborty, P. (2020). Slower decay of landfalling hurricanes in a warming world. *Nature*, *587*(7833), 230–234. doi: 10.1038/s41586-020-2867-7

Martinez-Lopez, B., Quintanar, A. I., Cabos-Narvaez, W. D., Gay-Garcia, C., & Sein, D. V. (2018). Nonlinear Trends and Nonstationary Oscillations as Extracted From Annual Accumulated Precipitation at Mexico City. *Earth and Space Science*, *5*(9), 473–485. doi: 10.1029/2018EA000395

McCabe-Glynn, S., Johnson, K. R., Strong, C., Berkelhammer, M., Sinha, A., Cheng, H., & Edwards, R. L. (2013). Variable North Pacific influence on drought in southwestern North America since AD 854. *Nature Geoscience*, *6*(8), 617–621. doi: 10.1038/ngeo1862

Roy, P. D., Rivero-Navarrete, A., Sánchez-Zavala, J. L., Beramendi-Orosco, L. E., Muthu-Sankar, G., & Lozano-Santacruz, R. (2016). Atlantic Ocean modulated hydroclimate of the subtropical northeastern Mexico since the last glacial maximum and comparison with the southern US. *Earth and Planetary Science Letters*, *434*, 141–150. doi:

10.1016/j.epsl.2015.11.048
Roy, P. D., Vera-Vera, G., Sánchez-Zavala, J. L., Shanahan, T. M., Quiroz-Jiménez, J. D., Curtis, J. H., … Muthusankar, G. (2020). Depositional histories of vegetation and rainfall intensity in Sierra Madre Oriental Mountains (northeast Mexico) since the late Last Glacial. *Global and Planetary Change*, *187*(July 2019), 103136. doi: 10.1016/j.gloplacha.2020.103136
Sachs, J. P., Sachse, D., Smittenberg, R. H., Zhang, Z., Battisti, D. S., & Golubic, S. (2009). Southward movement of the Pacific intertropical convergence zone AD 1400-1850. *Nature Geoscience*, *2*(7), 519–525. doi: 10.1038/ngeo554
Sanders, W. T., Parsons, J. R., & Santley, R. S. (1979). The Basin of Mexico: Ecological Processes in the Evolution of a Civilization. *Academic Press*, 561.
Schlesinger, M. E., & Ramankutty, N. (1994). An oscillation in the global climate system of period 65-70 years. *Nature*, *367*(6465), 723–726. doi: 10.1038/367723a0
Schultz, D. M., Bracken, W. E., & Bosart, L. F. (1998). Planetary- and synoptic-scale signatures associated with Central American cold surges. *Monthly Weather Review*, *126*(1), 5–27. doi: 10.1175/1520-0493(1998)126<0005:PASSSA>2.0.CO;2
Seager, R., & Hoerling, M. (2014). Atmosphere and ocean origins of North American droughts. *Journal of Climate*, *27*(12), 4581–4606. doi: 10.1175/JCLI-D-13-00329.1
St. George, S., Meko, D. M., & Cook, E. R. (2010). The seasonality of precipitation signals embedded within the North American Drought Atlas. *Holocene*, *20*(6), 983–988. doi: 10.1177/0959683610365937
Stahle, D. W., Cook, E. R., Burnette, D. J., Torbenson, M. C. A., Howard, I. M., Griffin, D., … Crawford, C. J. (2020). Dynamics, Variability, and Change in Seasonal Precipitation Reconstructions for North America. *Journal of Climate*, *33*(8), 3173–3195. doi: 10.1175/JCLI-D-19-0270.1
Stahle, D. W., Cook, E. R., Burnette, D. J., Villanueva, J., Cerano, J., Burns, J. N., … Howard, I. M. (2016, October 1). The Mexican Drought Atlas: Tree-ring reconstructions of the soil moisture balance during the late pre-Hispanic, colonial, and modern eras. *Quaternary Science Reviews*, Vol. 149, pp. 34–60. Pergamon. doi: 10.1016/j.quascirev.2016.06.018
Villanueva-Diaz, J., Stahle, D. W., Luckman, B. H., Cerano-Paredes, J., Therrell, M. D., Cleaveland, M. K., … Cornejo-Oviedo, E. (2007). Winter-spring precipitation reconstructions from tree rings for northeast Mexico the Tropical Rainfall Index) indicated long-term instability of the Pacific equa-torial teleconnection. Atmospheric circulation systems coming from higher latitudes (cold. *Climatic Change*, *83*, 117–131. doi: 10.1007/s10584-006-9144-0
Wang, C., & Lee, S. (2007a). Atlantic warm pool, Caribbean low-level jet, and their potential impact on Atlantic hurricanes. *Geophysical Research Letters*, *34*(2), L02703. doi: 10.1029/2006GL028579
Wang, C., & Lee, S. K. (2007b). Atlantic warm pool, Caribbean low-level jet, and their potential impact on Atlantic hurricanes. *Geophysical Research Letters*, *34*(2), L02703. doi: 10.1029/2006GL028579
Willmott, C. J., & Matsura, K. (2001). *Terrestrial air temperature and precipitation: Monthly and annual time series (1950–1999)*. Retrieved from http://climate.geog.udel.edu/~climate/html_pages/Global2011/README.GlobalTsP2011.html

4.8 Appendix B

This Appendix file includes:

Supplementary Text
Figs. S1 to S13
Tables S1 to S2

Calculation and interpretation of DCP

In order to calculate Dead Carbon Proportion (DCP), we first solved for initial stalagmite activity ($a^{14}C_{initial}$) by correcting for radioactive decay in the measured activity ($a^{14}C_{measured}$) (Eq. 1 Genty & Massault, 1997).

$$a^{14}C_{initial} = \frac{a^{14}C_{measured}}{\exp[\frac{-\ln(2)}{5730} * t]} \quad \text{Eq. 1}$$

However, this produces an initial activity ratio which is not corrected for atmospheric activity, which can vary through time due to solar wind activity, the solar magnetic field, and the Earth's magnetic field (*51*). Therefore, we utilized the combined U-Th and fluorescent layer produced age model to estimate the time of deposition at each radiocarbon depth. We utilized age model estimated age of deposition to determine the atmospheric activity ($a^{14}C_{atmosphere}$) using IntCal3, which is a record of atmospheric radiocarbon, to solve for DCP (Eq. 2; (*50*, *52*)).

$$DCP = \left[1 - \left(\frac{a^{14}C_{initial}}{a^{14}C_{atmosphere}}\right)\right] * 100\% \quad \text{Eq. 2}$$

Variable DCP measurements, such as those measured in sample CB4, have been shown in previous speleothem studies to be indicative of hydrological changes above the cave (*53–55*).

The exact mechanism of varying DCP is site specific but changes are commonly driven by the response of soil organic matter and open versus closed system bedrock dissolution (*54*, *56*). A fully open dissolution system occurs when conditions are dry and cave drip water dissolved inorganic carbon (DIC) in the epikarst is in complete isotopic equilibrium with modern ^{14}C values. In this scenario, the DCP would be equal to 0% (*57*). Alternatively, closed system dissolution occurs when conditions are wet, and water in the voids and fractures of the epikarst are in isotopic exchange with both the atmosphere and the bedrock. Therefore, the upper limit of DCP in a completely closed system would be 50% (*53*, *55*, *57*). Of course, most DCP values in natural cave systems are somewhere between these extremes, with caves demonstrating an average DCP of 15 ± 5% (*58*). The average CB4 DCP values fall within this range and are 10.2%.

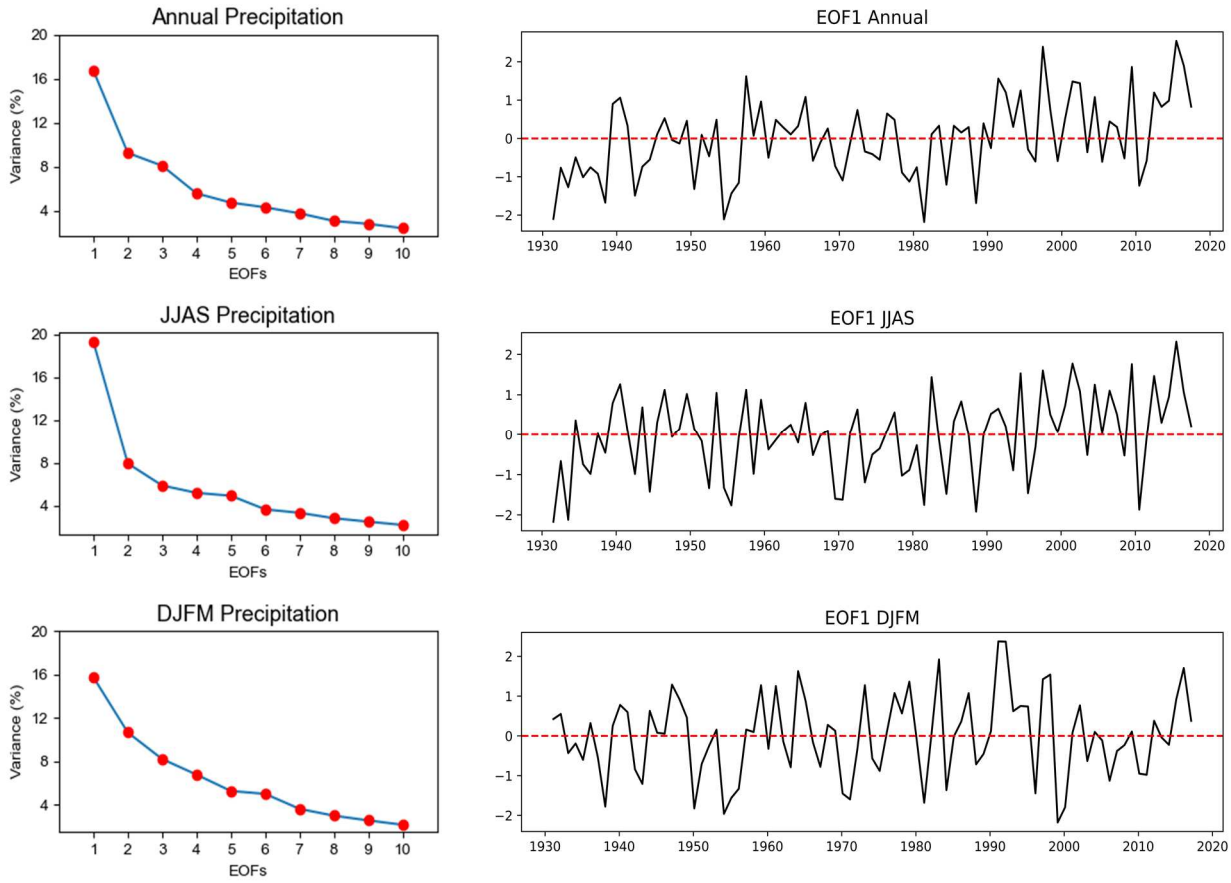

Fig. S4.1 Variance explained by the first 10 EOFs.
(Left) Variance explained by the first 10 EOFs and PCs of precipitation from 1930-2017 for Annual (top left), Summer (middle left) and Winter (bottom left). We only selected EOF 1 for annual, summer and winter which represents the greatest amount of variance, and is displayed over time from 1930-2017 on the right.

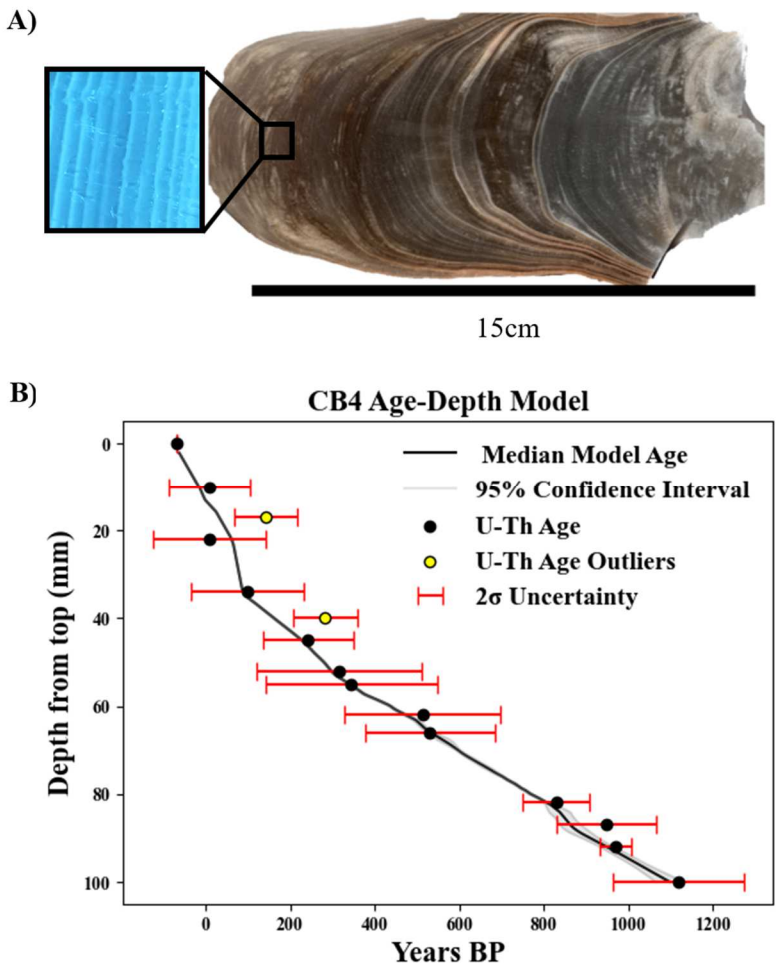

Fig. S4.2: Speleothem sample CB4 and U-Th age model.
A) Speleothem sample CB4 is roughly 15cm long, exhibits visible laminae to the visible eye and fluorescence laminae under microscope with UV light excitation. Fluorescence laminae are annual and likely driven by seasonal input of fulvic and humic acid brought down to the cave during the initiation of the wet season. B) Age model for sample CB4. The age model was constructed using 13 U-Th dates and layer counting of the top 100mm input to the COPRA age modeling software (Breitenbach et al., 2012) parameterized with 2,000 Monte-Carlo simulations.

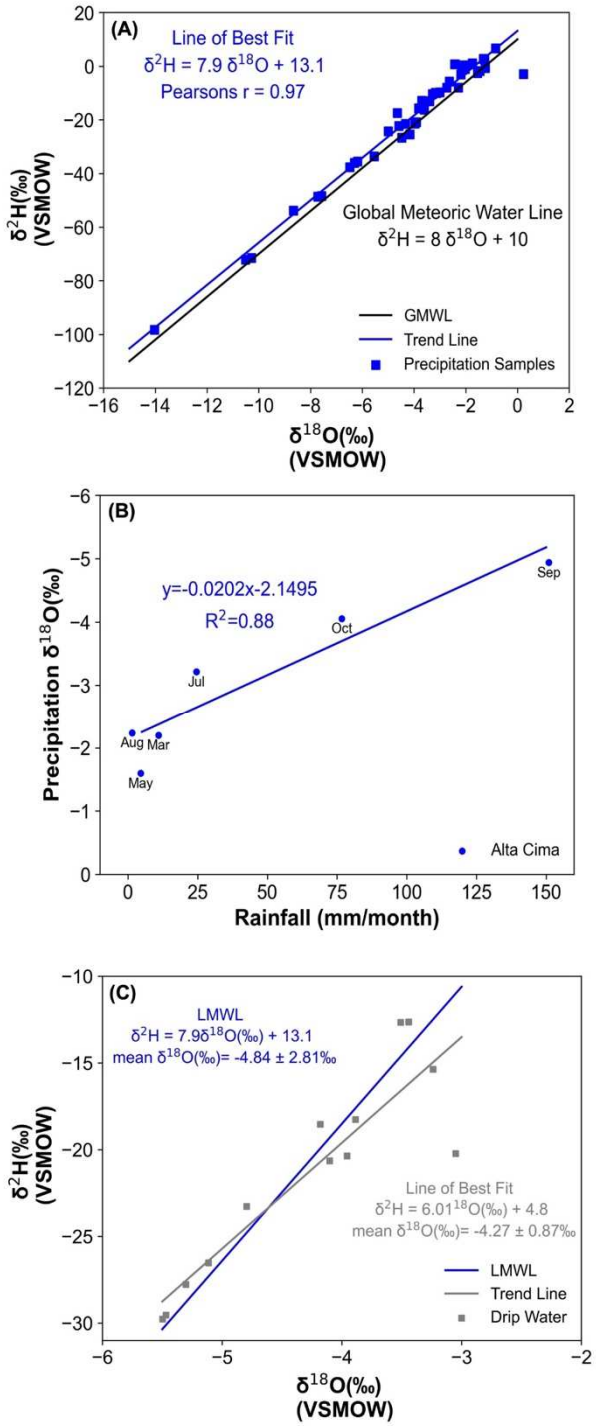

Fig. S4.3: Precipitation and drip water $\delta^{18}O$.
Figure adapted from Wright et al. (in review), demonstrating precipitation samples collected above the cave exhibit limited evaporation (top), a strong relationship between precipitation $\delta^{18}O$ and precipitation amount (middle), and drip water $\delta^{18}O$ does not strongly deviate from precipitation $\delta^{18}O$. This suggests calcite $\delta^{18}O$ is reflective of precipitation amount.

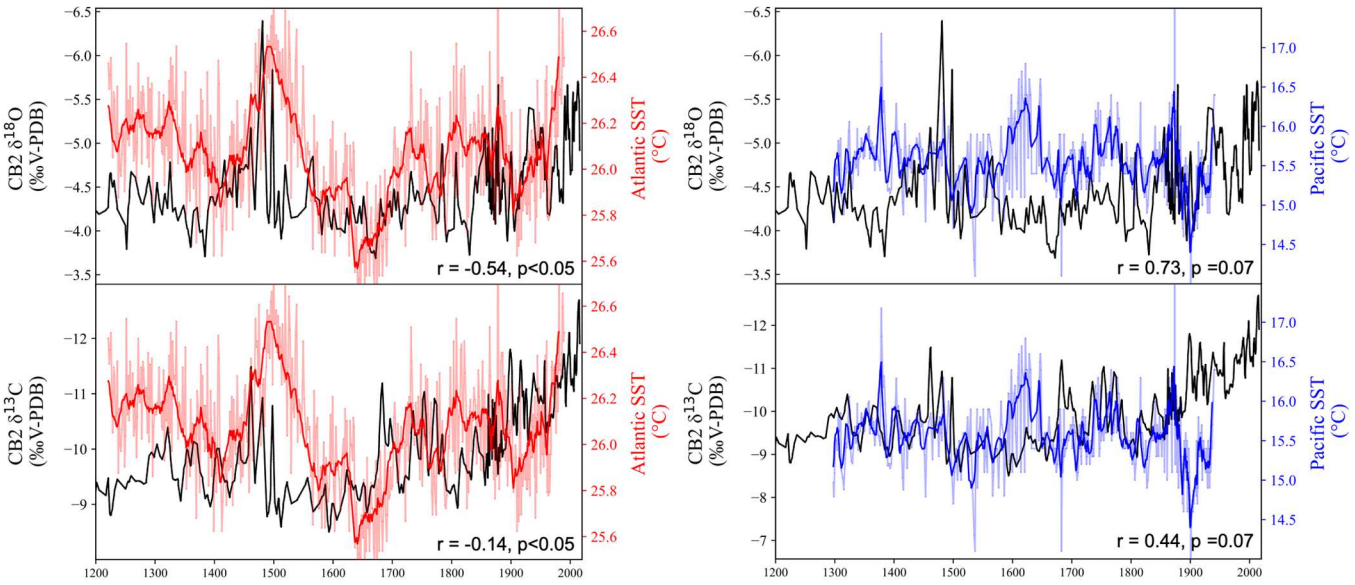

Fig. S4.4: Comparison of CB4 $\delta^{18}O$ and $\delta^{13}C$ to Atlantic and Pacific SSTs.
CB4 $\delta^{18}O$ (top) and $\delta^{13}C$ (bottom) compared to SST records from the Caribbean Sea (left) (Black et al., 2007), which we interpret to broadly reflect Western Tropical Atlantic SSTs. Pearson correlation values suggest precipitation amount ($\delta^{18}O$) is moderately correlated ($r = -0.54$, $p < 0.05$) to Atlantic SSTs and potentially weakly correlated to ($r = -0.14$, $p < 0.05$) to soil moisture. Reconstruction of Eastern Pacific SSTs, from the Santa Barbara Basin, are not significantly correlated ($p=0.07$) to $\delta^{18}O$ or $\delta^{13}C$ over the last 800 years (Schimmelmann et al., 2013). Atlantic SSTs capture both the negative $\delta^{18}O$ and $\delta^{13}C$ at the end of the 15th century and over the industrial period. The SST records utilized in this study were selected due to their high temporal resolution.

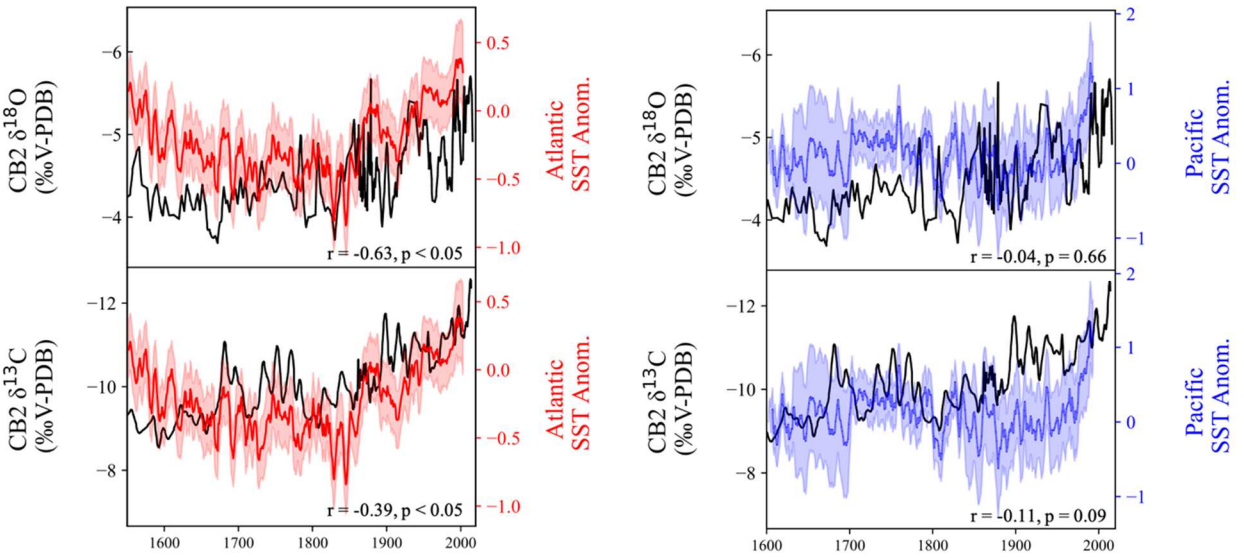

Fig. S4.5: Comparison of CB4 $\delta^{18}O$ and $\delta^{13}C$ to coral-based Atlantic and Pacific SSTs. CB4 stable isotopes compared to coral-based SST-reconstructions in the Western Tropical Atlantic (left) and Eastern Tropical Pacific (right) over the last 400 years (Tierney et al., 2015). The correlation of CB4 $\delta^{18}O$ to Western Tropical Atlantic SSTs is amplified in comparison to records from the Cariaco Basin, with a moderate to strong negative correlation of $\delta^{18}O$ ($r = -0.63$, $p < 0.05$) and $\delta^{13}C$ ($r = -0.39$, $p < 0.05$) (Tierney et al., 2015). We demonstrate no significant correlation of $\delta^{18}O$ ($r = -0.04$, $p = 0.66$) or $\delta^{13}C$ ($r = -0.11$, $p = 0.09$) to Eastern Tropical Pacific SST reconstructions (Tierney et al., 2015).

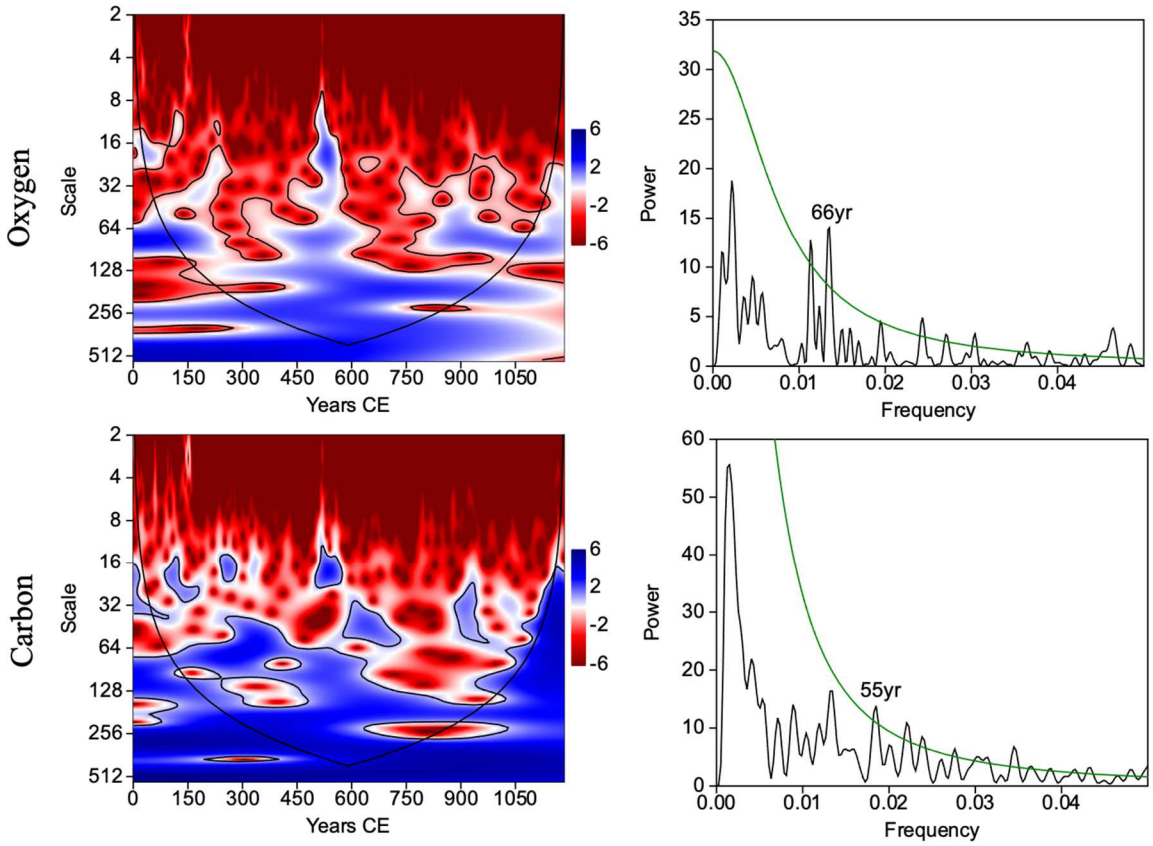

Fig. S4.6: Morlet wavelet and REDFIT spectral analysis.
PAST (*29*) Morlet wavelet and REDFIT spectral analysis (*30*) of CB4 $\delta^{18}O$ and $\delta^{13}C$. The $\delta^{18}O$ and $\delta^{13}C$ wavelet transform from ranging from deep blue (strong) to red (weak). Black lines indicate the cone of influence and the 95% significance level and the cone of influence. The black lines of the spectral analysis indicate the power spectrum. The green lines represents the 95% confidence limits relative to the red-noise spectrum.

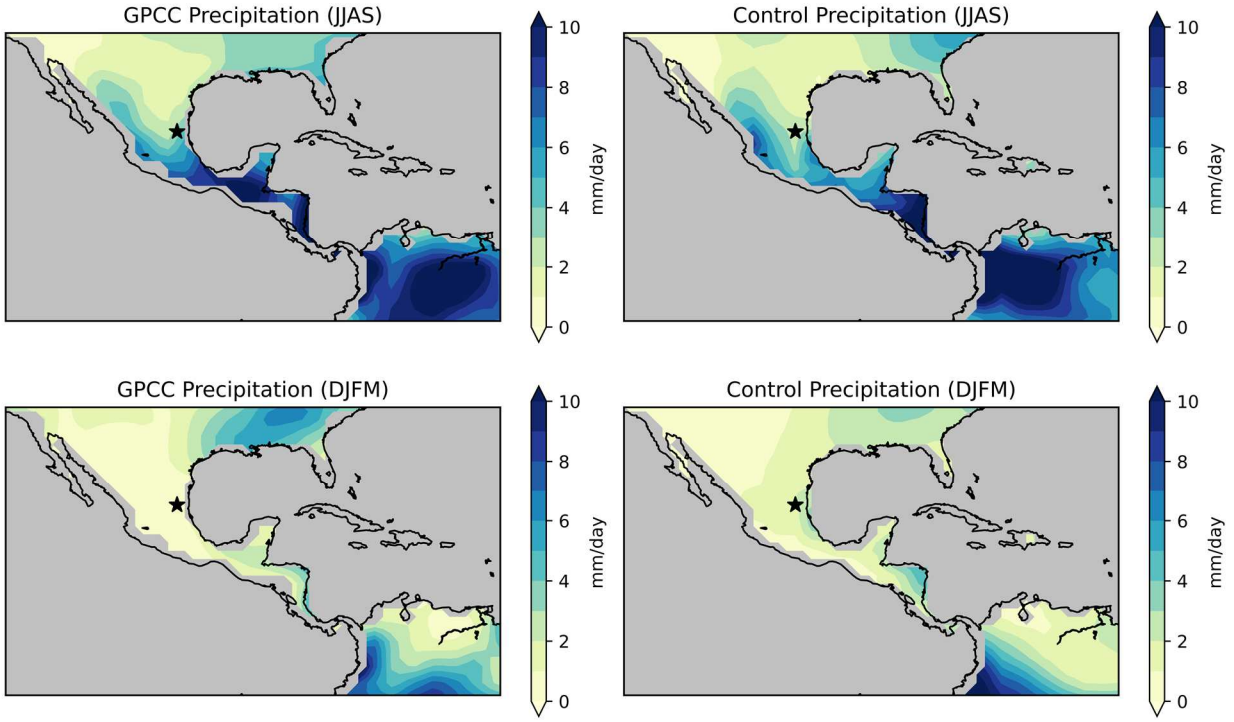

Fig. S4.7: Comparison of GPCC and control precipitation.
Comparison of GPCC precipitation (left) versus the control run (right) of this study in both summer (top) and winter (bottom). The control run captures most, if not all, the spatial precipitation pattern in Mesoamerica and does especially well in Northern Mexico.

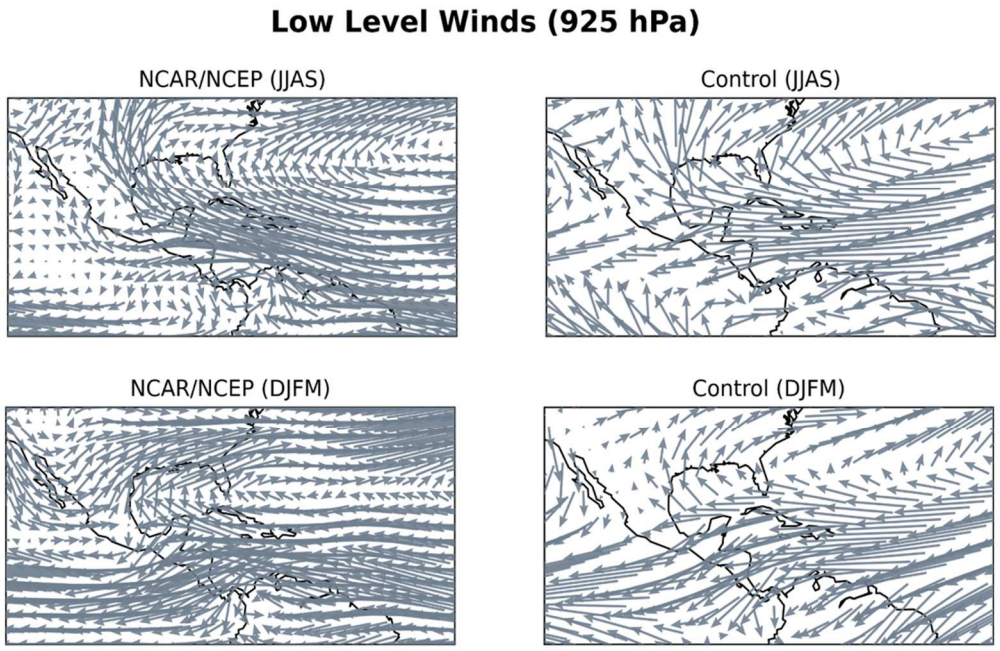

Fig. S4.8: Comparison of low-level winds between NCAR/NCEP and control-run. Comparison of NCAR/NCEP low-level (925 hpa) winds (left) to control-run low-level winds (right). The control run captures seasonal differences between the CLLJ, with a strengthening of the southeasterly winds during summer. However, the control run produces slightly stronger cross-isthmus transport than observations.

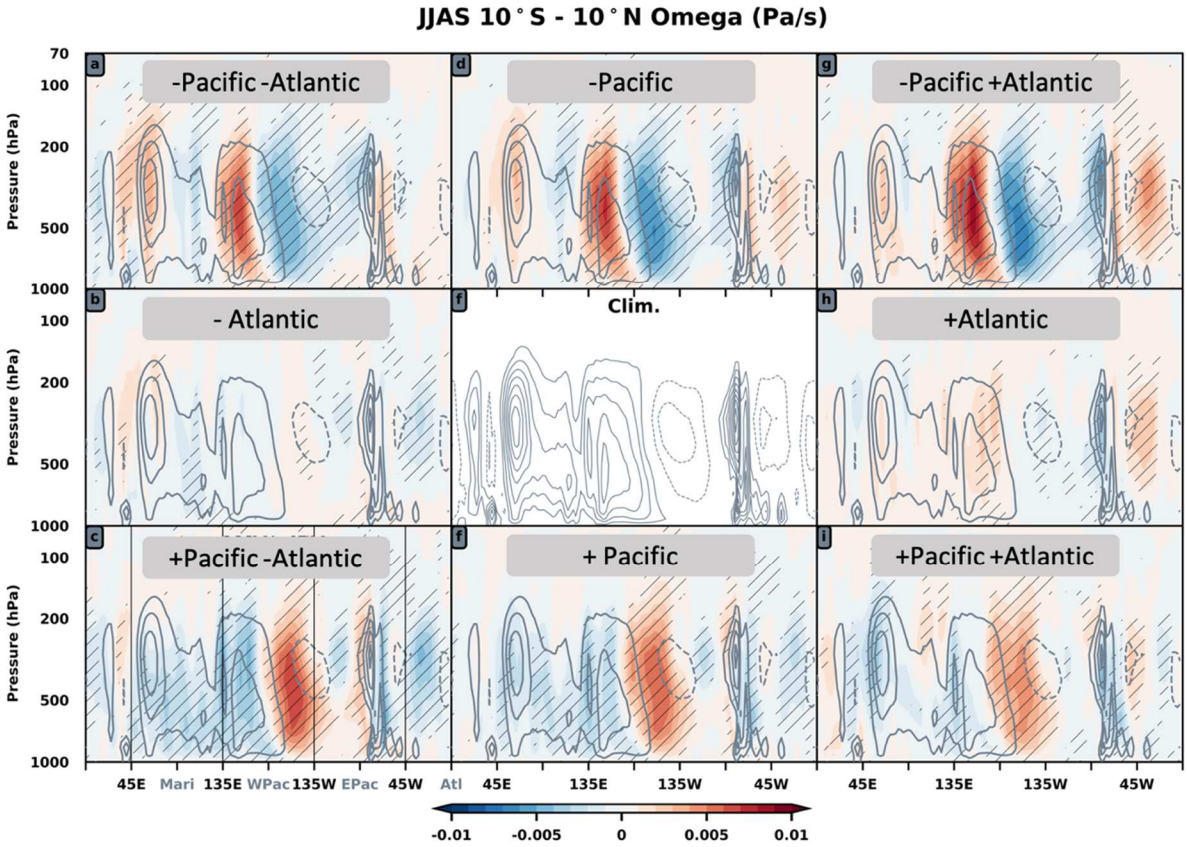

Fig. S4.9: Summer vertical velocity in the troposphere.
Net change in vertical velocity in the troposphere during summer (JJAS). Red indicates convection, blue indicates subsidence. Shading indicates statistically significant changes. The grey contour represents normal climatology. An intensification of the Walker Circulation is noted during warm Pacific conditions.

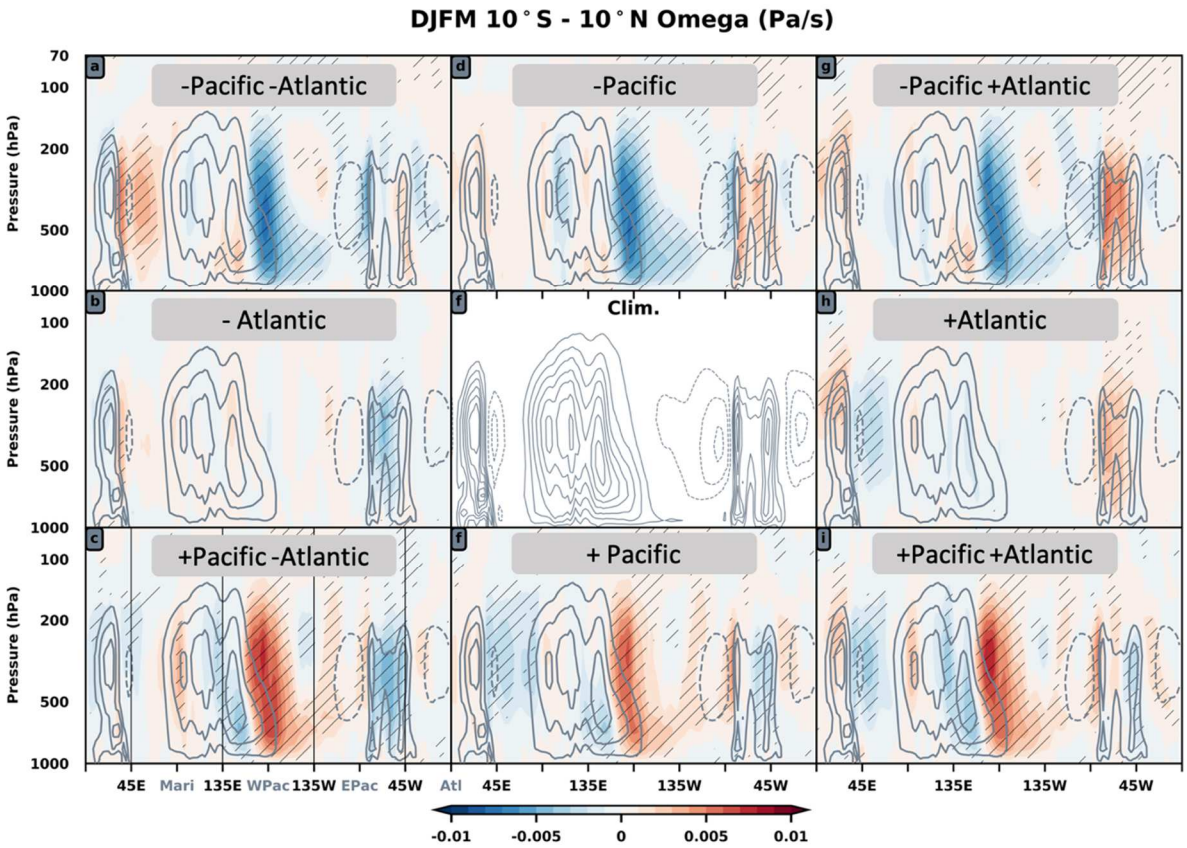

Fig. S4.10: Winter vertical velocity in the troposphere.
Net change in vertical velocity in the troposphere during winter (DJFM). Red indicates convection, blue indicates subsidence. Shading indicates statistically significant changes. The grey contour represents normal climatology. An intensification of the Walker Circulation is noted during warm Pacific conditions.

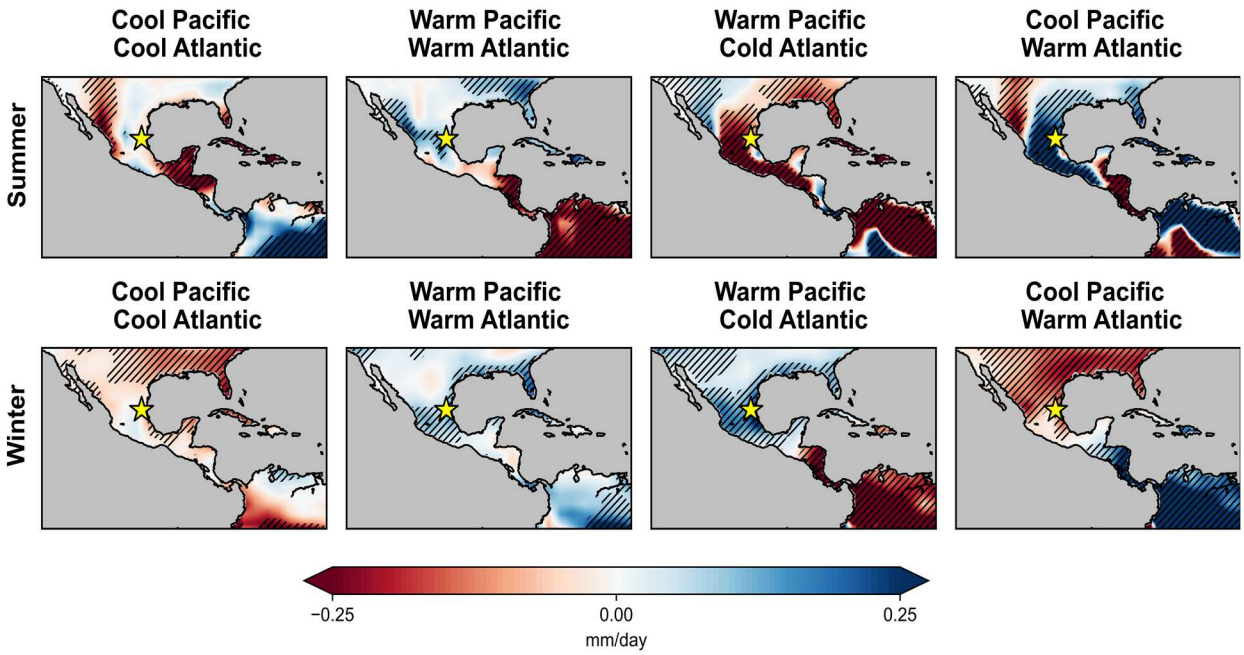

Fig. S4.11: Change in precipitation in response to various forced-SSTs.
Combined influence of in-phase (i.e. warm Pacific, warm Atlantic) and out-of-phase (i.e. warm Pacific, cool Atlantic) SST forcing during boreal summer (top) and winter (bottom). The wettest and driest conditions during summer in NE Mexico occur when there is asymmetric heating in the oceanic basins, with a warm Pacific and cold Atlantic producing dry conditions and a cool Pacific and warm Atlantic producing the wettest conditions. An out-of-phase precipitation pattern in Mesoamerica (i.e. wet north, dry south) is most noticeable during winter, but much more spatially complex during summer.

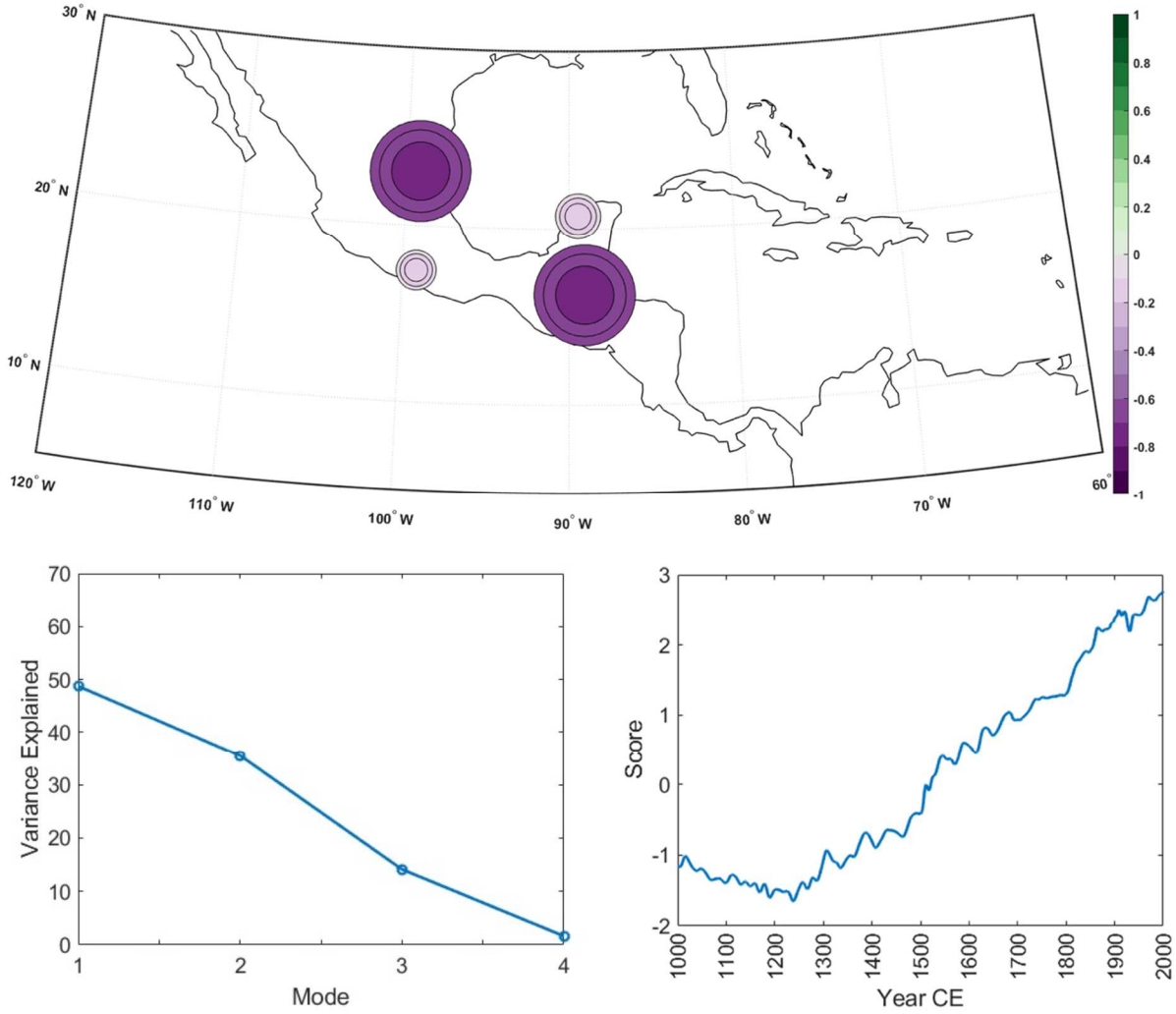

Fig. S4.12: Leading mode of speleothem hydroclimate proxies.
The leading modes of Mexican speleothem hydroclimate proxies from our site (CB4), SW Mexico (Lachniet et al., 2012), the Yucatan Peninsula (Medina-Elizalde et al., 2010) and Belize (Kennett et al., 2012). Additional records from Mesoamerica and Cuba were not included due to low temporal resolution or different time periods covered. The top figure demonstrates the leading spatiotemporal pattern of speleothem $\delta^{18}O$, with the size representing the median loading strength and color representing the sign and strength of the median. The innermost circle represents the median, the lower 95% confidence interval is indicated by middle circle and the upper 95% confidence interval is indicated by the outer circle. Bottom left demonstrates that EOF1 explains 50% of the variance. Bottom right demonstrates the composite EOF 1 plotted over time. This analysis was conducted following methods described by Bhattacharya & Coates (2020).

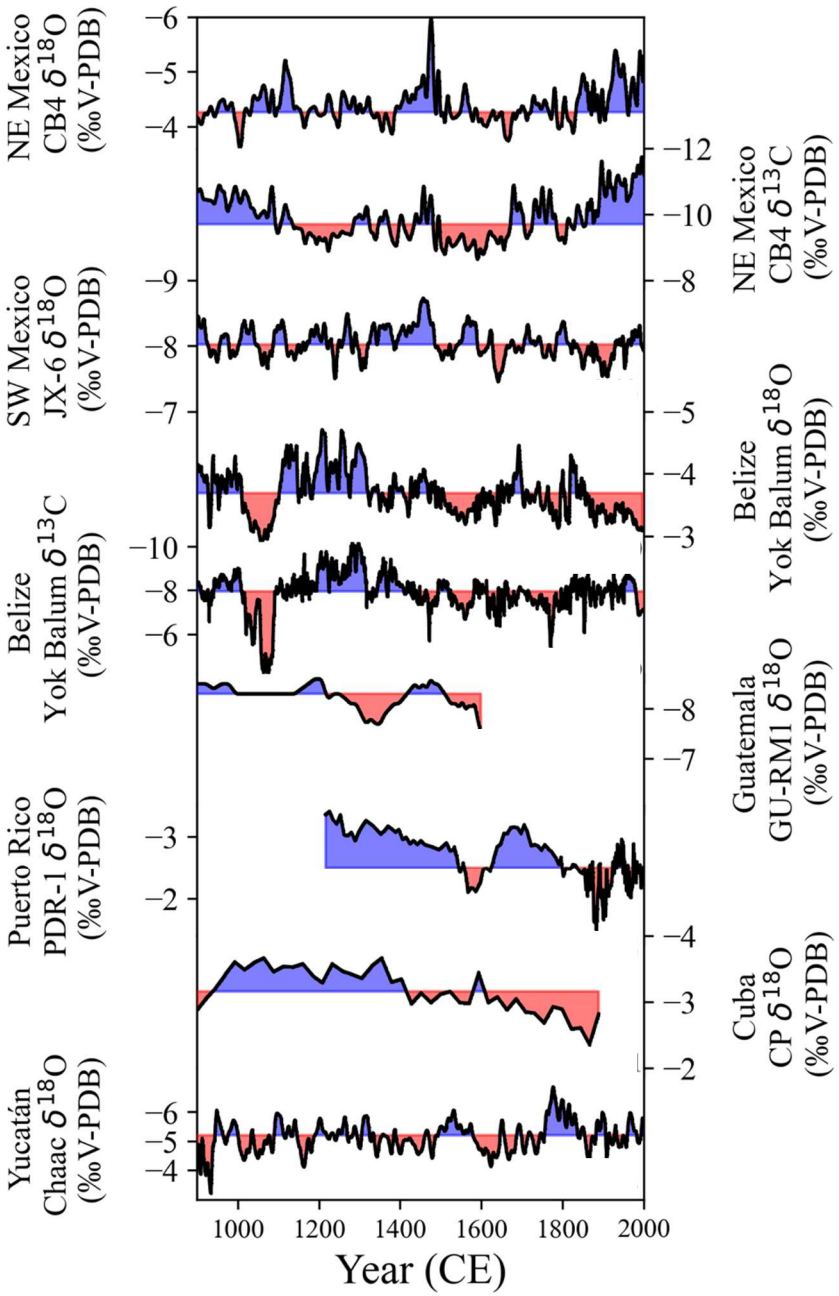

Fig. S4.13: Comparison of last millennium speleothem records from Mesoamerica. CB4 $\delta^{18}O$ and $\delta^{13}C$ compared to other speleothem records from SW Mexico (Lachniet et al., 2012), Belize (Kennett et al., 2012), Guatemala (Winter et al., 2020), Puerto Rico (Winter et al., 2011), Cuba (Fensterer eet al., 2013) and the Yucatan (Medina-Elizalde et al., 2010). Red and blue indicate below or above mean $\delta^{18}O$ and $\delta^{13}C$ values for each individual record, respectively.

Depth (mm)	^{238}U (ng/g)	^{232}Th (ng/g)	$\delta^{234}U$ (‰)	$^{230}Th/^{238}U$ (activity)	$^{230}Th/^{232}Th$ (ppm atomic)	Uncorrected Age (yr)	Corrected Age (yr)	$\delta^{234}U_{init}$ (‰)
10	52 ± 1	165 ± 3	119 ± 2	0.0028 ± 0.0001	14 ± 1	269 ± 10	78 ± 96	119 ± 2
17	65 ± 1	149 ± 3	116 ± 3	0.0036 ± 0.0003	25 ± 2	351 ± 26	212 ± 74	116 ± 3
22	55 ± 1	247 ± 5	136 ± 3	0.0036 ± 0.0001	13 ± 1	346 ± 12	79 ± 134	136 ± 3
34	54 ± 1	239 ± 5	137 ± 1	0.0045 ± 0.0001	16 ± 1	432 ± 11	169 ± 132	137 ± 1
40	58 ± 1	140 ± 3	161 ± 2	0.0052 ± 0.0003	34 ± 2	493 ± 27	353 ± 75	161 ± 2
45	53 ± 1	189 ± 4	139 ± 2	0.0055 ± 0.0001	24 ± 1	524 ± 13	313 ± 106	140 ± 2
52	48 ± 1	320 ± 6	159 ± 5	0.0082 ± 0.0004	20 ± 1	771 ± 38	386 ± 196	159 ± 6
55	37 ± 1	251 ± 5	141 ± 2	0.0085 ± 0.0002	20 ± 1	819 ± 22	415 ± 203	141 ± 3
62	41 ± 1	257 ± 5	175 ± 2	0.0102 ± 0.0004	25 ± 1	949 ± 33	584 ± 185	176 ± 2
66	43 ± 1	223 ± 5	161 ± 2	0.0096 ± 0.0002	29 ± 1	904 ± 23	601 ± 153	161 ± 2
82	49 ± 1	126 ± 3	186 ± 2	0.0113 ± 0.0003	70 ± 2	1048 ± 28	900 ± 79	187 ± 2
87	50 ± 1	199 ± 4	157 ± 1	0.0132 ± 0.0002	53 ± 1	1251 ± 21	1019 ± 118	158 ± 2
92	62 ± 1	69 ± 2	159 ± 2	0.0117 ± 0.0002	165 ± 3	1107 ± 20	1041 ± 38	159 ± 2
100	160 ± 3	1213 ± 25	695 ± 7	0.023 ± 0.0005	48 ± 1	1491 ± 32	1189 ± 154	697 ± 7
103	36 ± 1	54 ± 1	245 ± 1	0.0185 ± 0.0003	196 ± 3	1632 ± 24	1550 ± 47	246 ± 2
111	31 ± 1	175 ± 4	202 ± 2	0.0233 ± 0.0006	65 ± 2	2132 ± 51	1811 ± 168	203 ± 2
122	38 ± 1	60 ± 1	201 ± 3	0.0212 ± 0.0005	212 ± 6	1942 ± 50	1853 ± 67	202 ± 3
130	40 ± 1	91 ± 2	205 ± 3	0.0229 ± 0.0006	160 ± 4	2092 ± 53	1965 ± 83	206 ± 3
139	48 ± 1	259 ± 5	208 ± 16	0.0248 ± 0.0003	73 ± 1	2261 ± 41	1959 ± 156	209 ± 17
144	44 ± 1	187 ± 4	202 ± 1	0.0238 ± 0.0005	90 ± 2	2178 ± 45	1941 ± 127	204 ± 2
167	41 ± 1	226 ± 5	173 ± 2	0.0259 ± 0.0004	75 ± 1	2433 ± 40	2119 ± 162	174 ± 2

All reported errors are 2σ. Errors for ^{238}U and ^{232}Th concentrations are estimated to be ±1% due to uncertainties in spike concentration; analytical uncertainties are smaller. Corrected ages are corrected for initial ^{230}Th assuming an initial $^{230}Th/^{232}Th$ of 9.8 ± 4.9 ppm. Decay constants for ^{230}Th and ^{234}U are from Cheng et al. (2013) decay constant for ^{238}U is 1.55125 x 10^{-10} yr^{-1} (Jaffey et al., 1971).

Table S4.1: Uranium-thorium data for Stalagmite CB4

Results of 19 U-Th dates demonstrate there is at least one major growth hiatus between 1189 Years B.P. and 1550 Years B.P. We therefore chose to focus on analyzing the top 100 mm of the sample.

Depth (mm)	Age Model Date	Radiocarbon label	Fraction Modern	Uncertainty	d14c spel	a14c measured	a14c measured uncertainty	IntCal (years BP)	IntCal D14C (per mil)	a14c atm	a14c initial	DCP
10.5	62	Mexico_CB4_7	0.8843	0.0015	-115.7	88.43	0.0015	25	-13.3	98.67	89.0963	9.7
11.5	66	Mexico_CB4_8	0.8901	0.0014	-109.9	89.01	0.0014			98.67	89.7260	9.1
12	69	Mexico_CB4_9	0.8906	0.0014	-109.4	89.06	0.0014			98.67	89.8025	9.0
12.5	72	Mexico_CB4_10	0.8787	0.0016	-122.9	87.87	0.0016			98.67	88.6361	10.2
17	109	Mexico_CB4_13	0.8898	0.0014	-108.8	88.98	0.1395			98.67	90.1630	8.6
22	136	Mexico_CB4_14	0.8855	0.0014	-115.9	88.55	0.1384			98.67	90.0188	8.8
28	148	Mexico_CB4_15	0.8903	0.0016	-108.1	89.03	0.1619			98.8	90.6364	8.3
34	164	Mexico_CB4_16	0.8867	0.0014	-113.3	88.67	0.1393	115	-0.2	99.98	90.4477	9.5
40	247	Mexico_CB4_17	0.8868	0.0016	-113.2	88.52	0.1591			100.76	91.2054	9.5
45	312	Mexico_CB4_18	0.8738	0.0014	-126.2	87.38	0.1369	260	15	101.5	90.7445	10.6
52	380	Mexico_CB4_19	0.8779	0.0014	-122.1	87.79	0.1398	330	-1.7	99.83	91.9154	7.9
55	428	Mexico_CB4_20	0.8714	0.0014	-128.6	87.14	0.1359	360	2.2	100.22	91.7732	8.4
62	569	Mexico_CB4_21	0.8492	0.0015	-150.8	84.92	0.1492	530	0.3	100.03	90.9672	9.1
66	620	Mexico_CB4_22	0.8419	0.0014	-158.1	84.19	0.1413	545	-3.8	99.62	90.7504	8.9
72	719	Mexico_CB4_23	0.8189	0.0013	-181.1	81.89	0.1281			99.24	89.3351	10.0
76	792	Mexico_CB4_24	0.8075	0.0013	-192.5	80.75	0.1263			98.86	88.8691	10.1
82	900	Mexico_CB4_25	0.7909	0.0014	-209.1	79.09	0.1389	845	-15.2	98.48	88.1842	10.5
87	982	Mexico_CB4_26	0.7762	0.0012	-223.8	77.62	0.1217	965	-16.8	98.32	87.4136	11.1
92	1041	Mexico_CB4_27	0.7792	0.0013	-220.8	77.92	0.1278	985	-19	98.1	88.3765	9.9
100	1189	Mexico_CB4_28	0.7681	0.0012	-232.0	76.80	0.1205	1130	-12.1	98.79	88.6769	10.2

Table S4.2: Results of radiocarbon dates and the calculation of DCP.
DCP was calculated using the age provided by the age model and corrected for atmospheric fluctuations.

Chapter 5: Conclusions

5.1 Summary of Work

The collection of studies presented here serves to reconstruct the hydroclimate in Northeast Mexico on interannual to orbital timescales over the Holocene and Pleistocene epochs. This dissertation also incorporates climate model data to develop, and test, hypotheses on the mechanisms driving precipitation variability on these timescales. Consequently, this work provides the timing, magnitude, and underlying causes of precipitation change in response to past climate variability.

Chapter 2 presents the first precipitation $\delta^{18}O$ data from Northeast Mexico, combined with modeling and cave monitoring data, to access how overlying climate, groundwater mixing, and in-cave processes may alter geochemical proxies in speleothems from Cueva Bonita. HYSPLIT wind-trajectory analysis demonstrate minimal moisture source variability in precipitation at the study site, with almost all precipitation-yielding air trajectories coming from the Caribbean Sea and Gulf of Mexico. An analysis of precipitation $\delta^{18}O$ and precipitation amount from a nearby weather station demonstrates precipitation amount strongly controls the oxygen isotope composition of rainfall above the cave. By measuring drip water $\delta^{18}O$, we demonstrate groundwater mixing and evaporation in the soil zone and epikarst may slightly alter the $\delta^{18}O$ values. However, the response of drip water $\delta^{18}O$ to these processes is minimal, compared to the range of variability we demonstrate in response to changing precipitation amount. Using a proxy system model, we demonstrate that calcite precipitated in isotopic equilibrium from drip waters despite seasonal and interannual variability of cave air pCO_2, drip

rate and relative humidity. This work suggests calcite $\delta^{18}O$ is reflective of precipitation $\delta^{18}O$, and thus of precipitation amount, and is a suitable to reconstruct past changes in hydroclimate.

Chapter 3 presents the first stable isotope ($\delta^{13}C$, $\delta^{18}O$) and trace element (Mg/Ca) speleothem record from Northeast Mexico, recording millennial and orbital-scale hydroclimate variability over the Holocene and Late-Pleistocene. By extending the paleoclimate record by an additional ~30 ka in NE Mexico, we demonstrate precipitation is not strongly controlled by direct changes in insolation. We rather suggest that hydroclimate in Northeast Mexico is much more sensitive to changes in regional SST variations, which is further evidenced by dry conditions in NE Mexico during the Younger Dryas and Heinrich Stadials 1, 3, 4, and 5. By utilizing paleoclimate model simulations we isolate cooler Atlantic SSTs as the dominant mechanism for drying during Heinrich Stadials, rather than a reduction in the magnitude of Caribbean Low-Level Jet, as previously theorized. This study also provides additional evidence that Heinrich Stadial 2 was relatively weaker than other Heinrich Stadials, as indicated by no reduction in precipitation amount and an increase in local water balance demonstrated by speleothem $\delta^{13}C$ and Mg/Ca abundances. We attribute increased local water balance during the Last Glacial Maximum to reduced evapotranspiration at our study site. The record presented in this chapter exhibits similar variability to records from southern Mexico and Central America, suggesting changes in SSTs affects precipitation throughout this region similarly. This suggests the region may respond similarly in response to external forcings, such as anthropogenic-driven CO_2 emissions, and internal climate variability.

Chapter 4 presents the first high-resolution speleothem record from Northeast Mexico spanning the last millennium, a period of utmost importance for the testing of climate models and identifying internal climate variability. In this multi-proxy ($\delta^{13}C$, $\delta^{18}O$, Mg/Ca, ^{14}C) record,

we demonstrate that precipitation in NE Mexico is strongly influenced by Atlantic SST variability on centennial to decadal timescales. This work contrasts previous interpretations from tree rings that identified Pacific SST variability as the dominant forcing of precipitation, with minimal influence by Atlantic SSTs. We demonstrate using forced-SST climate models, that previous tree ring interpretations likely biased winter-spring precipitation responses, and do not accurately capture the response to changes in total annual precipitation. Climate models also reinforce the findings in Chapter 3, confirming a strengthened Caribbean Low-Level Jet decreases precipitation in Northeast Mexico. We suggest decreased vertical wind shear, in response to weakened easterly low-level winds, lead to deeper convection and increased frequency of tropical storms and hurricanes. We attribute the increased frequency of hurricanes to the observed wetting trend in NE Mexico over the industrial era. While this trend in precipitation may continue in response to future warming, in contrast to current model predictions, the increased frequency of hurricanes may lead to structural destruction, devastation of crops and cause substantial loss of life as it has the recent past, further fueling the displacement of the Mexican people.

5.2 Uncertainties and Future directions

Chapter 2 highlights the importance of constraining the controls of geochemical proxies before reconstructing past climate variability. The precipitation data collected as part of this chapter, suggests $\delta^{18}O$ is reflective of a regional precipitation amount effect, at least near Cueva Bonita. However, it is unclear to what extent this phenomenon encompasses the broader region of Northeast Mexico, including more semi-arid regions on the leeward side of the Sierra Madre Oriental. This is crucial for the interpretation of future speleothem samples which have been collected from this region, but not included in this thesis. Future work should also incorporate

the roughly 100 cave drip water and precipitation samples collected during the last several years, and currently being analyzed at Chapman University. At Cueva Bonita, future work should focus on determining the transit time and seasonal variability in $\delta^{18}O$ and soil-derived elements in both drip waters and glass captured calcite. Fieldwork should particularly be conducted in summer or early-autumn to better constrain the seasonality of the cave. Recording variability on these timescales will be essential for the reconstruction of sub-seasonal climate variability, including extreme precipitation events such as hurricanes and tropical storms. Furthermore, the role of cave variability on $\delta^{13}C$ should be constrained. Specifically, drip water samples should be analyzed for $\delta^{13}C$ which can then be used as input to proxy system models to quantitively evaluate the role of drip water variability, pCO_2 variability and changes in relative humidity on $\delta^{13}C$.

Chapter 3 demonstrated precipitation and local water balance variability from the Pleistocene – Holocene transition and during multiple Heinrich Stadials. We proposed insolation was not an important driver of climate variability on orbital timescales. This interpretation would be strengthened by additional paleoclimate records from the region covering both the interglacial-glacial transition and over the late-Pleistocene during earlier minima and maxima in Northern Hemisphere Summer Insolation. Work from Chapter 3 also demonstrated a drying response to abrupt North Atlantic cooling events in both paleoclimate and paleo-tuned climate models. While additional records and comparisons between additional models can help confirm and support these findings, the mechanisms driving increased water balance during Heinrich Stadial 2 remains elusive. We have proposed two hypothesis that could result in wetter conditions: decreased evapotranspiration, and/or a weaker Tropical North Atlantic cooling compared to other Heinrich Stadials. While initial analysis of paleoclimate models supports the

interpretation of decreased evapotranspiration, a more rigorous analysis could potentially highlight if increased cloudiness, decreased temperatures or decreased relative humidity drive the hypothesized decreased evapotranspiration. Importantly, future paleoclimate model analysis could employ PMIP4 models which are based upon the better performing and newly released CMIP6 models, not readily available during the original time of analysis. To test the second hypothesis of a weaker or less intense Heinrich Stadial 2, additional reconstructions of North Atlantic circulation from ocean sediment cores utilizing benthic foraminifera $\delta^{18}O$, or other proxies not sensitive to higher opal flux, are required.

In chapter 4, we present the first speleothem record spanning the last millennium from NE Mexico and demonstrate Atlantic SSTs primarily drive hydroclimate variability in the region. Most importantly, we demonstrate the region has become more wet as Atlantic SSTs increase over the industrial period. Through prescribed-SST climate models we demonstrate warm Atlantic SSTs likely drive increase precipitation from a decrease in the magnitude of the Caribbean Low-Level Jet, which drives a decrease in the vertical wind shear leading to the formation of deep-convective storms and hurricanes. However, it is uncertain how well the prescribed-SST models accurately capture the low-level wind patterns. Also, the current temporal resolution of the sample (2.8 years) does not allow for sub-seasonal reconstruction of these extreme pluvial events. Providing a seasonal to sub-seasonal record of climate over the last millennium is of incredible importance for constraining future projections of precipitation in response to both El Niño Southern Oscillation and the frequency of tropical storms and hurricanes. To accomplish this goal, future work should center on the timing of the response of cave drip water $\delta^{18}O$ and both soil and bedrock derived trace element concentrations at Cueva

Bonita as hydrological mixing and a long transit time could blur these chemical signatures inhibiting their ability to reconstruct paleoclimate on such short timescales.